Innovative approaches in the characterization of xenobiotic metabolizing enzymes of the nasal tissues : from the animal to human tissue engineering

Jeanne Mérignac-Lacombe

THESE DE DOCTORAT DE L'ETABLISSEMENT UNIVERSITE BOURGOGNE FRANCHE-COMTE

PREPAREE AU CENTRE DES SCIENCES DU GOÛT ET DE L'ALIMENTATION

Ecole doctorale n°554

Ecole doctorale Environnement-Santé

Doctorat de Biochimie, Biologie Moléculaire

Par

Mme. Jeanne Mérignac-Lacombe

Approches innovantes dans la caractérisation des enzymes du métabolisme des xénobiotiques dans les muqueuses nasales : du modèle animal à l'ingénierie tissulaire

Innovative approaches in the characterization of xenobiotic metabolizing enzymes of the nasal tissues: from the animal to human tissue engineering

Thèse présentée et soutenue à Dijon, le 10 Avril 2024

Composition du Jury :

Pr. NEIERS, Fabrice	Professeur des Universités, Université de Bourgogne	Président du jury
PD Dr Med. ICKRATH, Pascal	Praticien hospitalier, University Hospital Wuerzburg	Rapporteur
Dr. DESSEYN, Jean-Luc	Chargé de recherche, Inserm / Univ. Lille / CHU Lille	Rapporteur
PD Dr Med. HACKENBERG, Stephan	Praticien hospitalier, University Hospital Wuerzburg	Examinateur
Dr. MEUNIER, Nicolas	Directeur de recherche, INRAE Jouy-en-Josas	Examinateur
Pr. HEYDEL, Jean-Marie	Professeur des Universités, directeur de recherche, Université de Bourgogne	Directeur de thèse
Dr. STEINKE, Maria	Directrice de recherche, University Hospital Wuerzburg	Codirectrice de thèse

Université Bourgogne Franche-Comté
32, avenue de l'Observatoire
25000 Besançon

Titre : Approches innovantes dans la caractérisation des EMX/EMO dans les tissus nasaux : du modèle animal à l'ingénierie tissulaire

Mots clés : métabolisme des xénobiotiques/odorants, voies respiratoires, ingénierie tissulaire, 3R, olfaction

Résumé : La sensibilité de notre odorat dépend des enzymes du métabolisme des xénobiotiques (EMX). Non seulement les EMX détoxifient la muqueuse nasale mais elles arrêtent aussi le signal olfactif pour en permettre la détection d'un nouveau. Parfois appelées enzymes du métabolisme des odorants (EMO), certaines participent aussi à la genèse de nouveaux métabolites odorants. L'objectif de cette thèse était d'étudier les EMX nasales en utilisant deux modèles innovants respectant au mieux les principes éthiques des 3R (Remplacement, Réduction, Raffinement des expérimentations animales). Alors que les explants olfactifs de rat montrent leurs limites pour étudier la régulation génique des EMX nasales, le modèle tissulaire respiratoire humain est un outil *in vitro* prometteur pour étudier le métabolisme des odorants. Ces modèles issus de l'ingénierie tissulaire expriment environ 80 isoformes d'EMX et de transporteurs d'efflux. Bien qu'aucune des molécules testées n'ait impacté la régulation génique de certaines EMX exprimées par le modèle tissulaire, les EMX du modèle sont capables de métaboliser des odorants tels que le benzaldéhyde et la 3,4-hexanedione. Pour conclure, la création et l'adaptation de méthodes durant cette thèse permet maintenant d'étudier la contribution de l'épithélium respiratoire humain dans le métabolisme des odorants. Ces travaux montrent l'implication des tissus respiratoires dans le métabolisme des odorants chez l'humain, tout en contribuant à réduire l'expérimentation animale.

Title: Innovative approaches in the characterization of XME/OME in nasal tissues: from the animal to human tissue engineering

Keywords: odorant/xenobiotic metabolism, airways, tissue engineering, 3R, olfaction

Abstract: Our sensitive olfaction relies on Xenobiotic Metabolizing Enzymes (XMEs) that protect the nasal tissue from potentially harmful volatile compounds, but also quickly terminate the olfactory signal to prepare olfactory receptors to detect new odorant stimuli. Some of them also generate metabolites that participate in the odorant signal, hence their other name Odorant Metabolizing Enzymes (OMEs). The objective of this thesis was to study the nasal XMEs using two innovative models that aim to comply as much as possible with the 3R principles (Replacement, Reduction, and Refinement of animal experiments). While expression, human nasal respiratory mucosa tissue models were promising *in vitro* tools for the odorant metabolism field. These models express around 80 XME variants and efflux transporters. Selected XME genes were not regulated by the compounds chosen for the thesis. However, they were able to metabolize odorants, such as benzaldehyde and 3,4-hexanedione. Overall, protocols were created and adapted to use tissue models to study the implication of the respiratory epithelium in odorant metabolism in humans. This work provides novel knowledge on the involvement of the human respiratory tissue in odorant

rat olfactory explants showed some limitations in investigating XME gene metabolism and contributes to the reduction of animal experiments.

ACKNOWLEDGMENTS

I extend my heartfelt appreciation to Jean-Luc Desseyn and Pascale Ickrath, who kindly accepted to be my thesis referees, to Stephan Hackenberg, and Nicolas Meunier for evaluating my work, and to Fabrice Neiers for presiding this jury.

My sincere gratitude goes to Lionel Bretillon and Loïc Briand, successive directors of the Center for Taste and Feeding Behavior of Dijon, France (UMR Centre des Sciences du Goût et de l'Alimentation), for giving me the opportunity to do a PhD in your laboratory, and to Prof. Dr. Jürgen Groll from the Chair of Tissue Engineering and Regenerative Medicine of Würzburg, Germany (Lehrstuhl für Tissue Engineering und Regenerative Medizin), for welcoming me as a guest in your laboratory for two years.

I am immensely grateful to Francis Canon, Fabrice Neiers, and Jean-Marie Heydel, for having at some point sailed the ship of our research team with dedication. I am proud to have been part of such a living team.

I owe a debt of gratitude to my mentors and supervisors, Jean-Marie Heydel (you have so many hats that you deserve these second thanks) and Maria Steinke, for their invaluable guidance and encouragement that shaped my journey. Jean-Marie, thank you for believing in me, for being a listener and a protective figure especially when I needed it the most. You showed me there was strength in asking for help, and while all your advice helped me tremendously to complete this program, I will keep this particular one in mind forever. May your ideas never run dry! Maria, I have been very lucky to have you as my co-supervisor. You were curious and available since the beginning, and have always guided me with kindness. Thank you for always pushing me and teaching me, for these delicious shared meals, and for making my stay in Germany a wonderful experience! You two are so different yet a perfectly complementary team when it comes to supervising a project as rich in ups and downs as a Ph.D. Thank you for bringing me to those amazing international congresses, and for expanding my world. It was a privilege being mentored by you and I will look up to you both wherever my path leads me.

Special thanks to my collaborators from the Chair of Aroma and Smell Research of Erlangen, Germany (Lehrstuhl für Aroma- und Geruchsforschung), Andrea Büttner, Helene Loos, and Nicole Kornbausch, who contributed their expertise to make odorant metabolism studies on the human 3D model possible, as well as Valentin Boichot and Rinu Sivarajan for their contribution to the paper. I am grateful we published together. My thanks also go to my colleagues Fabrice Neiers, Mathieu Schwarz, Franck Menetrier, Nicolas Poirier, Catherine Potin, Christine Belloir, from Dijon, and Heike Oberwinkler, Renate Bausch, Totta Ehret-Kasemo, Stephan Hackenberg, Agmal Scherzad Tobias Weigel from Würzburg, for their support all along my thesis, and without whom these experiments could not have been done. Many thanks go to Enisa Aruci for all her advice on how to do RT-qPCR she earned from hard-learned experience, and to Remy Renaud and Manon Biehlmann for their expertise in odorant molecules and GC-MS.

I would like to express my appreciation to Claire Rosnoblet, who gave me the privilege to teach biochemistry to bachelor students during the first year of my Ph.D. It was a wonderful and challenging experience; I hope they obtained their degree.

To my cherished co-workers and friends who made each day brighter with their presence, technical and emotional support, and sometimes delicious cakes and specialties. Many thanks to, from Dijon: Remy Reynaud for the spot-on gaming recommendations, Manon Biehlmann and Valentin Boichot for the running motivation (I quit, but don't worry I swim instead), Lucie Moitrier and Patoche for their laughs and good mood, Margot Glaz for sharing her favorite artists, Vincent Tolassy, and Elodie Gonis for their kindness, help, and for bringing life to the "fly lab", Jean-Baptiste Bizeau for openly liking dinosaurs (they're so cool), and form Würzburg: Rinu Sivarajan for your friendship, mentoring, and all the songs that will be forever stuck in my head, Niklas Pallmann for crafting with me the best PhD hat ever, Christina Popp for your coffee and your warmth, Philipp Ockermann for the PhD therapy sessions, Jihyoung Choi for the amazing authentic *Boricha* (many thanks to your grandma), Ives Bernardelli de Matos for the comics recommendation and for almost breaking your back when moving my washing machine, Dalia Madhy Samir Ahmed for the sunshine you bring in every room you enter, Sara Giddins for the shopping sprees, Fabiola Walz for the chess games, the honey, and the wonderful concert, Laura Lechner for instantly making my mood brighter

with your stories, Jana Keller for all your tips about organization. Thank you Sooraj for always being there whenever there was a poster to print (or re-print) urgently, you saved Rinu and I's congresses. It's difficult to be concise and select only a few moments of what we all shared. Some of you may have eluded my memory when I wrote these lines, but please know I have many warm memories of shared meals, coffee, pretzels, and chitchat between doors. Thank you for having been an integral part of my life during the three years of this academic journey, and friends I hope to keep. I wish you luck and success in all your projects.

To the whole Martin family and friends of the family, thank you so much for transforming Würzburg into a home for me. I cherish the Christmas choral, the bonfires, the birthday parties, the game nights, the super-duper home-made advent calendar. Especially Insa and Kili, thank you for being the best flatmates ever and for opening your family to me. Thank you, Joey, for being an *abuela* and making sure I was fed, it was an honor to be your guest for Thanksgiving. I think you and I have the same relationship with food: cooking it and sharing it is the way we care for people.

My long-time friends, thank you for being my pillars of strength when I disappeared to do a PhD. Laetitia, I hope you know you're my number one choice whenever I need help moving my life to another country, although next time I won't give you the keys to the truck to save its bodywork. Remember, all the roads lead to *Ausfahrt*. Thank you for having opened your door to me every time I needed to go back to Dijon. Thank you, Maud, and Ludivine, for always reaching out whenever I was losing touch with my life. It saddens me that I haven't been present for some major events in your life. We were the weird kids, I think we turned out quite okay! Thank you, Marie and Manon, for eloping with me to Annecy to eat the most decadent fondue. Rémi, Audrey, I wish you all the best in your marriage and I hope to build a nest as warm and welcoming as yours, so that I can, in turn, share my bread, my games, and my comfort as you did with me for all these years.

Last but not least, my deepest gratitude goes to my family for their boundless love. To Romain, for being always there, for lending me more shoulders to cry than I can count, and for putting me back into the ring with a pat on the shoulder and plasters on my wounds. To my mother and brother, who did not always get what I was doing but were

proud anyway. Who I forced to read so many sciency things in English and who will have once again to go through it to read these lines. Who helped me move away and back and showed me every day that no matter where I go, I have a home to bounce back.

I do not forget that a work like this is made possible by connecting with people from every horizon and background. Science was never meant to be researched alone. Thank you, everyone, for every piece of the puzzle you brought me.

SUMMARY

TABLES

FIGURES

ABBREVIATIONS

ACTB: actin beta

ADH: alcohol dehydrogenase

AECGM: airway epithelial cell growth medium

AhR: aryl hydrocarbon receptor

AKR: aldoketo reductase

ALDH: aldehyde dehydrogenase

B2M: Beta 2 microglobulin

BAX: Bcl2 X-associated protein

Bcl2: B-cell lymphoma 2

CASP3: caspase 3

CDKN1B: cyclin dependent kinase inhibitor 1B

CK18: cytokeratin 18

CK5: cytokeratin 5

CT: cycle threshold

CYP: cytochrome P450

DAB; 3,3'-Diaminobenzidine

DCXR: Dicarbonyl and L-xylulose reductase

DMEM: Dulbecco's modified Eagle medium

DMSO: dimethyl sulfoxide

DPBS: Dulbecco's Phosphate Buffered Saline, Modified

RNA : ribonucleic acid

RPL30: Homo sapiens ribosomal protein L30

RT-qPCR: Reverse transcription-quantitative polymerase chain reaction

EI-MS: electron impact mode for mass spectra

GST: glutathione transferase

HAF: hypoxia-associated factor

HNEC: human nasal epithelial cells

HPRT: hypoxanthine-guanine phosphoribosyltransferase

IF: Immunofluorescence

KET: ketakonazole

m/z: mass by charge ration

MTBE: tert-butyl methyl ether

MTT: 3-(4,5-dimethylthiazol-2-yl)-2,5-diphenyl tetrazolium bromide

MUC5AC: mucin 5AC

MUC5B: mucin 5B

NADPH: nicotinamide adenine dinucleotide phosphate hydrogen

NEM: N-ethylmaleimide

nFb: nasal fibroblasts

Nrf2: nuclear factor erythroid 2–related factor 2

PPARG: peroxisome proliferator activated receptor gamma

RIN: RNA integrity number

scRNA-seq: single-cell RNA sequencing

TIC: total ion chromatogram

XME/OME: xenobiotic/odorant metabolizing enzyme (EMX and OME in French)

COMMUNICATIONS

Poster presentation:

J. Mérignac-Lacombe, R. Sivarajan, K. Berg, H. Oberwinkler, A.-E. Saliba, T. Ehret Kasemo, A. Scherzad, F. Neiers, F. Erhard, M. Steinke, S. Hackenberg, J.-M. Heydel, Investigating Odorant Metabolizing Capacity in a Human Respiratory Tissue Model, (2023). AChemS 2023, Bonita Springs, Florida, USA.

Book chapter:

F. Neiers, **J. Mérignac-Lacombe**, J.-M. Heydel, Odorant metabolizing enzymes in the peripheral olfactory process, in: C. Guichard, Elisabeth; Salles (Ed.), Flavor From Food to Behav. Wellbeing Heal., 2nd editio, Elsevier Science, 2022: pp. 127–147.

Review:

N. Kornbausch, **J. Mérignac-Lacombe**, F. Neiers, T. Thomas-Danguin, J.-M. Heydel, M. Steinke, S. Hackenberg, H.M. Loos, Perspectives on Nasal Odorant Metabolism Research, J. Agric. Food Chem. 71 (2023) 16488–16492. https://doi.org/10.1021/ACS.JAFC.3C04662.

Original article:

J. Mérignac-Lacombe, N. Kornbausch, R. Sivarajan, V. Boichot, K. Berg, H. Oberwinkler, A.-E. Saliba, H.M. Loos, T.E. Kasemo, A. Scherzad, J. Bodem, A. Buettner, F. Neiers, F. Erhard, S. Hackenberg, J.-M. Heydel, M. Steinke, Characterization of a human respiratory mucosa model to study odorant metabolism, under revision at the Journal of Agricultural and Food Chemistry.

Prizes:

Laureate of the First-Year PhD Student Bursary from GIRACT (11th edition, in 2021)

Finalist of the Don Tucker Memorial Award (AchemS 2023)

INTRODUCTION AND OBJECTIVES

Can you buy and wear a social status? Well, books are judged by their covers, and people by their odor, so perfume may help!

Survival of species depends on the ability of individuals to avoid danger, find nutrients, and pass on their genes. The sense of smell, or olfaction, dictates the behavior of a lot of terrestrial species. Invertebrates widely use chemosensory cues to detect threats, find appealing food (Zjacic and Scholz, 2022), but also communicate as it is the case for social insects like ants (Kannan et al., 2022). Decoding the olfactory signals of pheromones from body fluids organizes social networks and mating behavior of a lot of species to the point that supplementary olfactory structures are dedicated to these sensory cues (Tirindelli, 2021). We humans only have vestigial versions of these organs and rely more on visual and auditory cues, which participate in the general idea that humans have a poor sense of smell. Since Antiquity, Western culture has been at best overlooking olfaction, and at worst considered it impure, degrading, and animal by a long line of philosophers from Plato, Aristotle, to Descartes, Kant, and Hegel. The psychoanalyst Freud theorized that repressing animal instincts like smell and sexuality, among other things, is what allowed the rise of civilization (Le Guérer, 2017).

Despite their desire to separate us from our nose and our mammalian nature, odors have always been intimately linked to human societies. The first objects related to perfumes and cosmetics belonged to the Mesopotamians. The Egyptians burned incense for their gods and royal families. In the Middle Ages, regardless of the civilization, perfumes were used in sacred contexts, but also in medicine, and for cosmetics and culinary purposes. For a long time, Western doctors accused foul odors of propagating diseases and treated them with perfumes (Le Guérer, 2017; Schwarcz, 2017). Malodorous persons are regarded negatively and reciprocally, a person viewed negatively and/or low on the social hierarchy will most likely be associated with stench (Candau, 2015). On the opposite side, the fragrance industry spread quickly from the XVIth century and exploded in France in the XVIIth. The French city of Grasse, famous for its delicate scented gloves liked by Catherine de' Medici, switched its specialty from

tannery to perfumery and became an international pole of perfumery. It is nowadays still its principal industry and a museum is dedicated to this odorant saga[1].

In the 80's, the books of Annick Le Guérer (*Les pouvoirs de l'odeur*), Alain Corbin (*Le miasme et la Jonquille*), Pierro Camporesi (*Les effluves du temps jadis*) and the famous novel *Perfume* (*Das Parfum: Die Geschichte eines Mörders*) of Patrick Süskind lit up the interest of the scientific community for olfaction and in 2004, Linda Buck and Richard Axel won the Nobel prize of physiology and medicine for their work on olfactory mechanisms. The sense of smell encompasses a succession of events starting when volatile odorant compounds enter the nasal cavity and travel to a particular area called the olfactory epithelium. This tissue contains neurons specialized in the recognition of these compounds – the olfactory sensory neurons that harbor olfactory receptors – and sends signals to the brain to be interpreted. Our brain then decodes the signal and associate an identity to the odor, as well as a valence (like, dislike), emotions, memories, and will use other sensory information to localize the odor and perhaps its source.

The performance of our sense of smell relies on the olfactory system's ability to stay sensitive to new odorant stimuli; the tissue is equipped with a system that successfully allows the odorant compounds to interact with the olfactory receptors, but also maintains the olfactory receptors in optimal conditions. Since our olfactory environment is prone to rapid changes in terms of quality (different odors) and quantity (does it smell more or less than before?), the signal must be terminated quickly and the tissue cleared of the "old" odorant compounds to prepare the olfactory receptors to new interactions. This is the job of olfactory peri-receptor events. Among these events, biotransformation enzymes called Xenobiotic Metabolizing Enzymes (XMEs), or Odorant-Metabolizing Enzymes (OMEs) when their study concerns odorant as substrates, participate actively to (i) the termination the olfactory signal through a quick nasal clearance of odorant molecules (Heydel et al., 2019a; Legendre et al., 2014; Robert-Hazotte et al., 2019a); and to (ii) the modulation of the olfactory signal by synthetizing odorant metabolites (Hanser et al., 2017; Ijichi et al., 2019; Robert-Hazotte et al., 2019b; Thiebaud et al.,

[1] https://www.museesdegrasse.com/en

2013). Consequently, every aspect of their regulation can potentially influence the olfactory perception.

The aim of this PhD thesis is to characterize the expression, regulation, and functionality of nasal XME using innovative approaches.

In this thesis work, I made the deliberate choice to follow as much as possible the principle of the 3R (replacement, reduction, and refinement) by favoring models that are not live animals and exploring *ex vivo* and *in vitro* alternatives, while keeping in mind the thematic around nasal XMEs. This project has been made possible thanks to a partnership between the Center for Taste and Feeding Behavior (CSGA, France), and the Chair of Tissue Engineering and Regenerative Medicine (TERM, Germany), which specialize in olfactory events in animal models, and tissue engineering, respectively, with the help of the other partners of the NAOMI consortium (Nasal Odorant Metabolites). I also wanted to purely focus on olfaction and physiological olfactory events, which means that odorant substances were used at low concentrations and the different tissue models were exposed to them for a relatively short time. I set the bar at 2 hours maximum, which could be the duration of a meal or any social event where the sense of smell could be solicited (to evaluate food, or judge and interact with a person). In the next part, the state of the art will place the scientific context of this thesis work. The technical details will then be explicated in the material and method part. Following this, I chose to present the results and discussion in two parts: one for each model I explored. Indeed, I started at the CSGA, where I familiarized myself with the rat olfactory mucosa *ex vivo* tissue and the exploration of nasal XME gene expression, which is a model well established in Prof. Jean-Marie Heydel's team. I then seized the opportunity given by the TERM to adapt these skills to explore the human nasal respiratory tissue model developed by Dr. Maria Steinke's team, and characterize the expression and functionality the nasal XMEs expressed by the tissue model. A conclusion and perspective will finish the story and suggest possible follow-up projects, followed by a short summary of the thesis in French.

STATE OF THE ART

1. Physiology of mammalian olfaction

Although the witty Cyrano de Bergerac describes his nose as a peninsular protuberance in the middle of his face – among other colorful metaphors – its greatness actually resides in what is hidden behind.

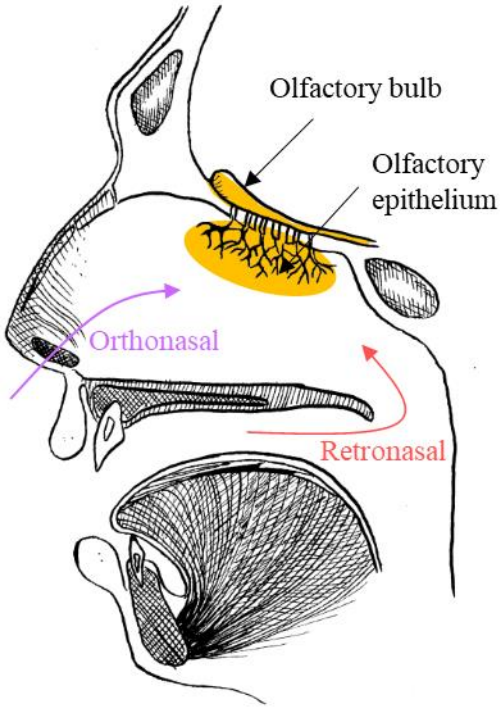

***Figure 1**: Orthonasal and retronasal routes by which odorants reach the olfactory mucosa. Original illustration.*

What we call the nose in mammals are two paired cavities that open from the nostrils, on the anterior nares, to the rhinopharynx, on the posterior nares. We are able to smell thanks to a neuroepithelium that "recognizes" volatile odorants, and that is located, in humans, on the roof of the nasal cavities. Odorants reach this particular tissue through two routes, as demonstrated in Figure 1: (1) the orthonasal pathway, through the nostrils, that can be assimilated to odors we smell in the ambient air, and (2) the retronasal pathway, by which odorants and aromas released from food by mastication reach the olfactory epithelium and participate in the flavor of food (Bojanowski and Hummel, 2012; Negoias et al., 2008; Rozin, 1982).

The following part will present the anatomy of these cavities, the structure of this neuroepithelium, and the mechanisms involved in the recognition of odorants.

1.1. Anatomy of the human nasal cavity

Main structures of the human nasal cavity

Each nasal cavity is delimited on the bottom side by the maxillary bone and the palatal bone, on the external lateral side by the maxillary bone, the ethmoid bone, and the nasal turbinate, on the internal lateral side by the septum, and on the top side by the nasal

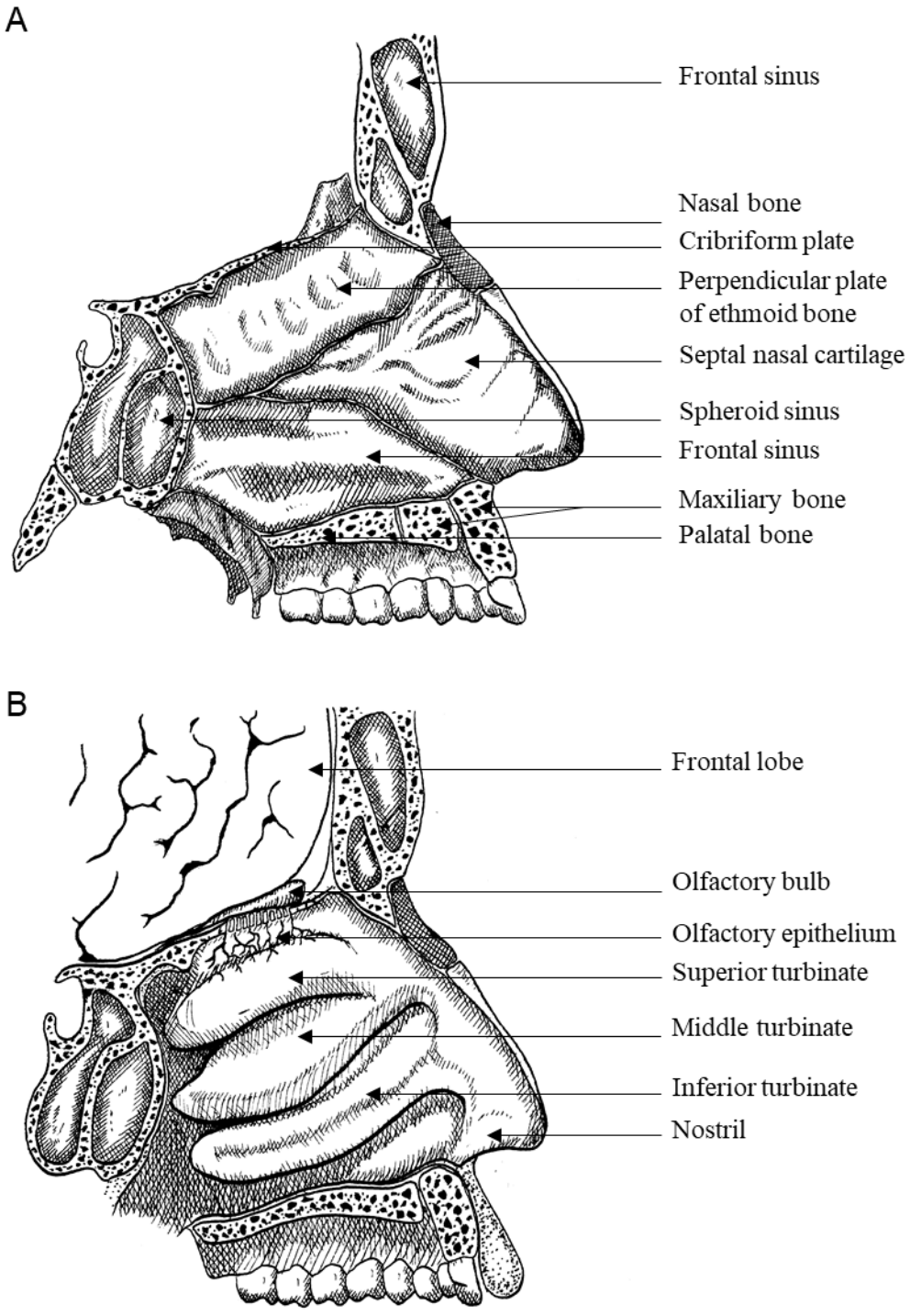

***Figure 2**: Sagittal section of the human nasal cavity presenting the main bones and cartilages. (A) Internal lateral side of the human nasal cavity. (B) External lateral side of the human nasal cavity. Original illustration.*

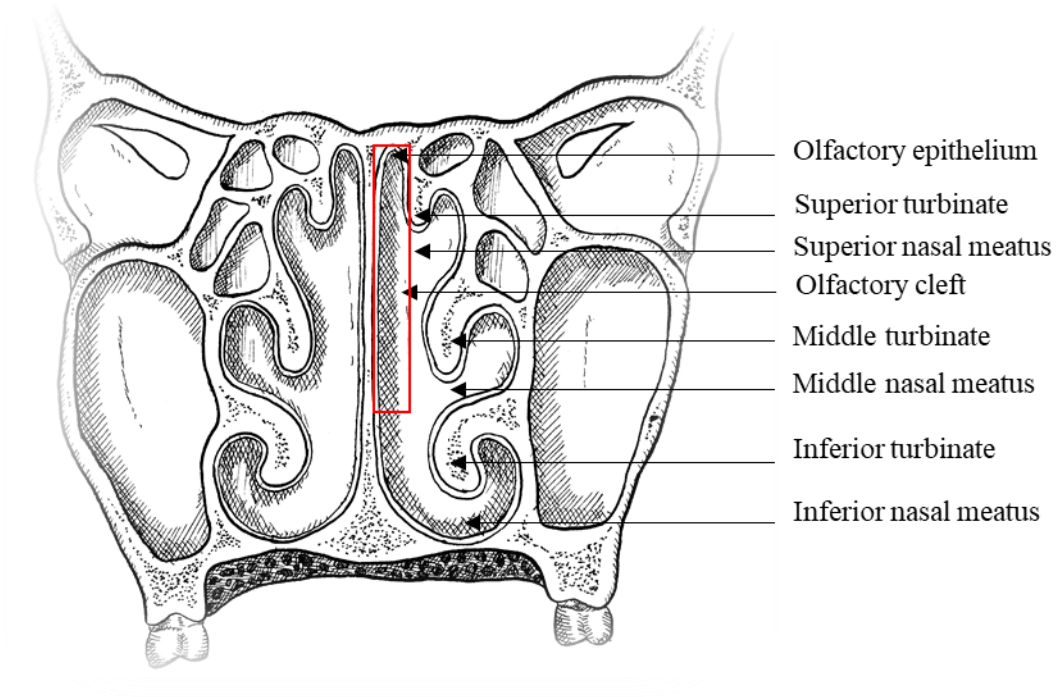

***Figure 3**: Coronal section of the human nasal cavity. Original illustration.*

bone and the ethmoid bone (Patel and Pinto, 2014). Figure 2 illustrates these different bones from a sagittal view, whereas a coronal view is presented in Figure 3. Turbinates are thin slats of bones that circumvolute within the nasal cavity, which increases the surface contact with the air up to 150 to 200 cm² (Harkema et al., 2006).

The nasal mucosa

The nasal mucosa can be split into four types of epithelia: squamous, transitional, respiratory, and olfactory epithelia. The squamous epithelium, similar to the skin, is located in the nasal vestibule, while the respiratory epithelium, a ciliated pseudostratified columnar epithelium, lines the majority of the human nasal cavity. Transitional epithelium, a non-ciliated columnar epithelium, makes the junction between these two epithelia, and the olfactory epithelium is usually restricted in the dorsoposterior part of the nasal cavity, near the cribriform plate (Harkema et al., 2006).

Olfactory epithelium will be addressed in a more detailed way in part 1.3.; as for the nasal respiratory epithelium, structure of this epithelium is shown in Figure 4. It is made of 3 main cell types: differentiated multiciliated cells, goblet cells that produce a mucus layer sitting on top the epithelium, and progenitor cells lying on the basement

membrane, called basal cells (Uraih and Maronpot, 1990). Other cell types such as brush cells and non-ciliated cells were described as well in rats (Alvites et al., 2018).

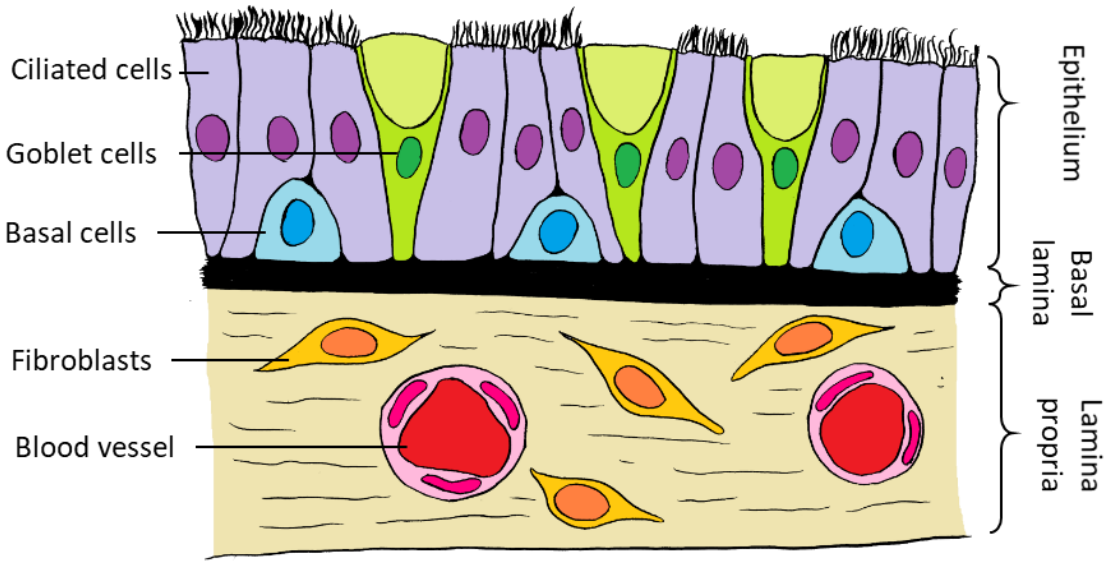

***Figure 4**: Schematic drawings of the nasal respiratory mucosa, depicting the three main cell-types found in the respiratory epithelium: ciliated cells, goblet cells, and basal cells. The epithelium lies on a conjunctive tissue irrigated with blood vessels. Original illustration.*

Role of the nasal mucosa

The nasal epithelium lies on a highly vascularized connective tissue that covers the nasal cavity including the turbinates. As a consequence, the nasal cavity is well-equipped to filtrate, humidify, and warm the inhaled air before it reaches the lower airways, and impact the airflow (Harkema et al., 2006; Kia'i and Bajaj, 2022; Pérez-Mota et al., 2018). In humans, the filtering properties of the nasal cavities is facilitated by the presence of thick hairs at the vestibule that mechanically filtrate particles to some extent. While nasal hair filters particles superior to 5 µm such as pollen (Swift and Kesavanathan, 1996), particles above 3 µm accumulates in the anterior nares, particles between 0.5 µm and 3 µm are filtered by the nasal mucosa: trapped in the nasal mucus, the ciliary beating at the surface of the nasal epithelium pushes it into the nasopharynx to be evacuated in the esophagus. Under 0.5 µm, the nose poorly filters the particles that usually end up in the lower airways (Kia'i and Bajaj, 2022; Schwab and Zenkel, 1998). Density and length of nasal hair impact the filtration of particles (Scott et al., 1978): the bushiest the nostrils, the better! This hair coverage varies among the population, and a higher risk of developing seasonal rhinitis was associated with less nasal hair (Ozturk et al., 2011).

The vestibule, and then the turbinates, form intricate conduits through which the air passes. Depending on the rate of the inspiration, these conduits can generate turbulence in the air flow, which enhance the contact of the air with the nasal mucosa. It can vary in shape depending on phenotype and on pathologies such as polyps, which can impact the airflow reaching the olfactory cleft (Sicard and Frank-Ito, 2021; Zhao et al., 2004).

1.2. Anatomy of the rat nasal cavity

Main structures of the rat nasal cavity

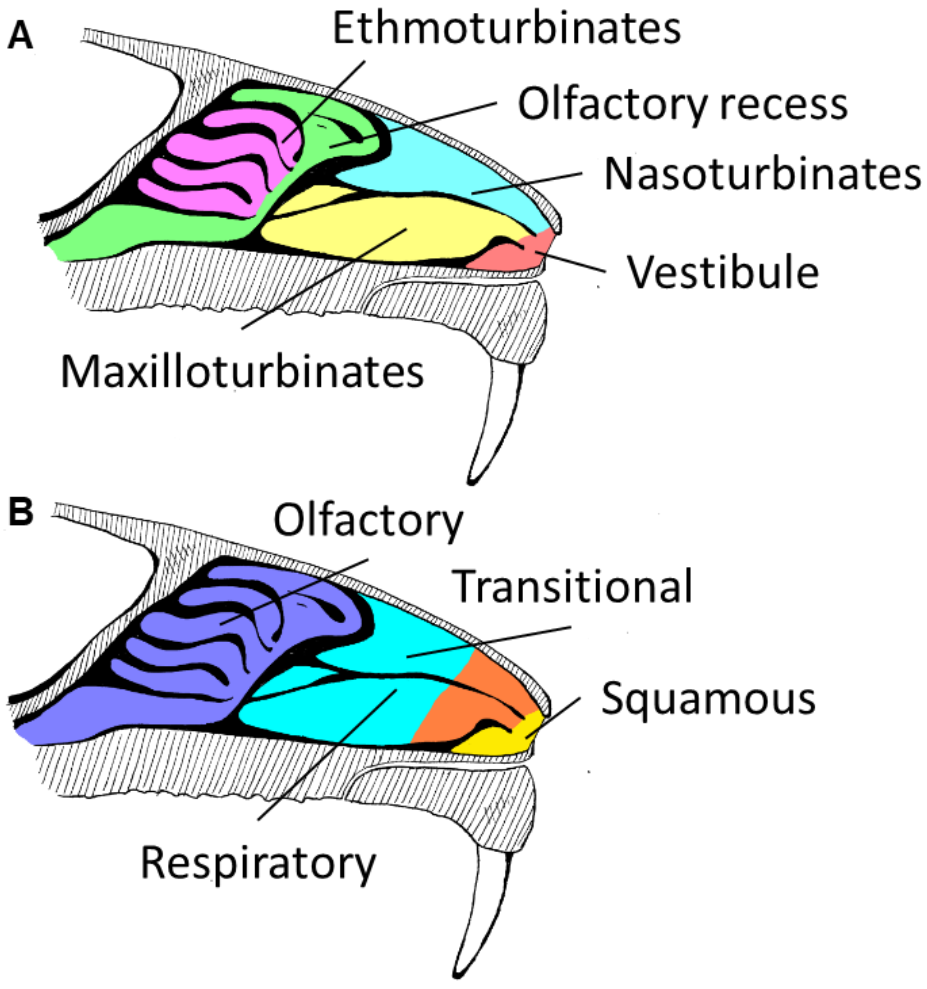

***Figure 5**: Anatomy of the rat nasal cavity. (A) Schematic representation of the nasal cavity of a rodent and relative position of the nasal vestibule, nasoturbinates, maxilloturbinates and ethmoturbinates. (B) Distribution of the different types of epithelium within the nasal cavity of rodents. Original illustration inspired from Alvites et al., 2018.*

Contrarily to humans, rats are obligatory nose-breathers, meaning the upper airways reach the epiglottis in the nasopharynx and not in the oropharynx. Hence, rats can swallow food while breathing and sniffing. It was thought that this separation did not allow retronasal olfaction since the exhaled air does not go through the oropharynx

where food aromas are released, but retronasal olfaction in rats has been demonstrated (Gautam and Verhagen, 2012). However, as mammals, humans and rats share some similarities regarding the structure of the nasal cavity. Like humans, the rat nose is composed of two nasal cavities separated by the septum. In rats, the osseous part of the septum meets the ethmoid bone on the caudal part of the nasal cavities, the vomer bone in the ventral part, and the frontal and nasal bones of the dorsal side of the cavities. The two cavities are not completely separated from each other as an opening is present in the septum near the vomer. Like humans, rat nasal cavities open at the nostril on a nasal vestibule, but then the structure of the nasal cavities differs in a more complex construction of turbinates than the human nasal cavities. Figure 5A summarizes the different parts of the rat nasal cavity. After the nasal vestibule, the nasal chamber opens to the nasal concha or turbinates, that can be differentiated into the nasoturbinates on the dorsal side and the maxilloturbinates on the ventral side (Alvites et al., 2018).

The nasal mucosa: particularities of the rat

Like humans, the turbinates are covered with nasal respiratory mucosa that condition and filter the air, while the anterior opening of the nasal cavity is first covered with squamous epithelium at the nares, then with transitional epithelium. Nasal respiratory mucosa covers 47% of the rat nasal cavity. The rat olfactory tissue can be distinguished from the respiratory tissue thanks to its yellow color. It lies on a defined structure called the ethmoid labyrinth emerging from the ethmoid bones, called ethmoturbinates (Figure 5B). The air flow can be directed either toward the nasopharynx or the olfactory recess depending on the state of “swell bodies”. Collapsed, these prominences direct the flow bellow the maxilloturbinates; distended, the air goes toward the nasoturbinates and can reach the olfactory tissue (Alvites et al., 2018).

1.3. Chemosensory systems

The chemosensory system comprises the olfactory epithelium in the nasal cavity, a neuroepithelium containing olfactory sensory neurons expressing olfactory receptors (OR) that binds odorants, and the central nervous system pathways associated. Smelling begins right in the nasal cavity, where odorants have to travel to the olfactory tissue, solubilize in the mucus layer, and binds to the OR. In humans, the olfactory mucosa is around 2 to 10 cm^2 and represent 3% of the epitheliums covering the nasal cavity

(Salazar et al., 2019). Comparatively, the olfactory mucosa makes up to 50 % of the rat nasal cavity (Alvites et al., 2018; Harkema et al., 2006; Salazar et al., 2019). The following part will focus on the anatomy and cell population of this neuro olfactory epithelium, while the next part will go in details into the odorant signal coding and decryption by the central nervous system.

Main peripheral olfactory system: the olfactory mucosa

This part refers the olfactory mucosa whose structure is common to mammals. The olfactory mucosa itself is composed of the olfactory epithelium, and its *lamina propria*. The olfactory epithelium differs from the respiratory mucosa by the presence of the Bowman's glands that emerge from the *lamina propria* and whose ducts open in the nasal cavity, olfactory sensory neurons, and a pseudostratified columnar epithelium twice as thick as the respiratory epithelium. Olfactory sensory neurons are arranged and surrounded by the differentiated epithelial cells called supporting cells or sustentacular cells. Like the respiratory epithelium, progenitor cells called basal cells are present at the basal side of the olfactory epithelium. Nuclei of these cell types align from sustentacular cells on the apical side, to mature olfactory sensory neurons, then immature olfactory sensory neurons, followed by basal cells at the basal side (Alvites et al., 2018; Neiers et al., 2022). Figure 6 summarizes this organization.

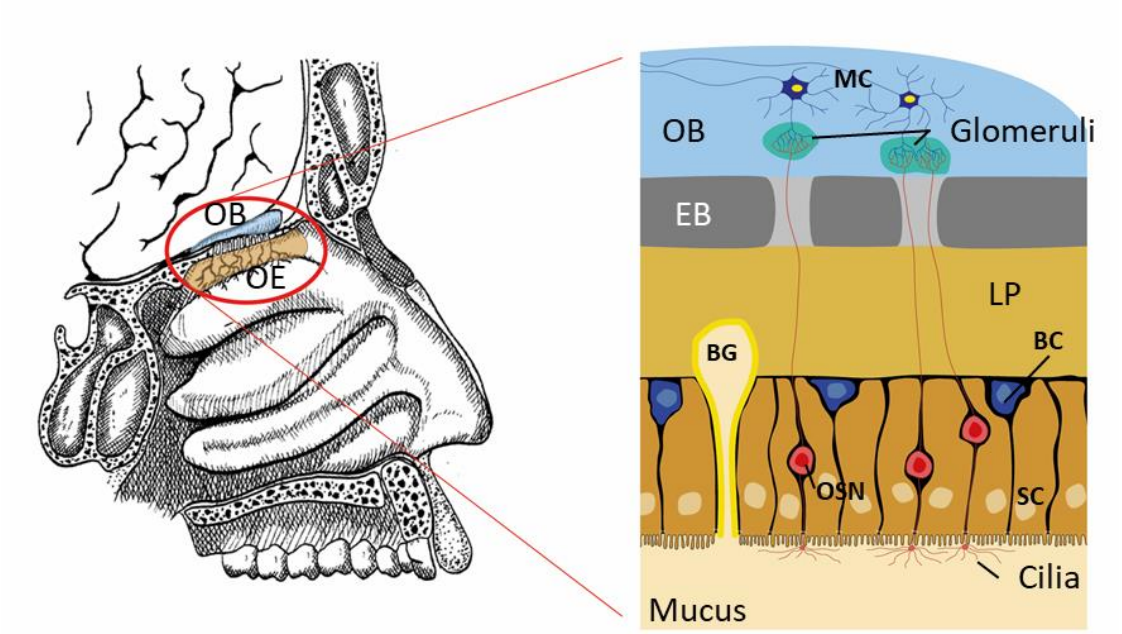

***Figure 6**: Structure and localization of the olfactory mucosa. OE: olfactory epithelium, EB: ethmoid bone, BG: Bowman's glands, SC: sustentacular cells, BC: basal cells, OSN: olfactory sensory neurons, LP:* lamina propria*, MC: mitral cells, OB: olfactory bulb. Original illustration inspired from Neiers et al., 2022.*

Olfactory sensory neurons

Olfactory sensory neurons are bipolar sensory neurons that differentiate from the basal cells (Hill et al., 2004). They are the only neurons directly at the contact with the external environment and the central nervous system, which makes them a gateway to the brain for infections and xenobiotics (Minn et al., 2002).

Each cell extends a unique dendrite that extends at the epithelial surface while the axon projects through the ethmoid bone to the olfactory bulb. The dendrite ends on a tumescence at the surface, called the olfactory knob or olfactory vesicle, from which between 10 to 15 cilia radially extend in the mucus. These cilia measure around 50 µm length and 0.1 to 0.3 µm diameters, and form a dense mesh that maximizes the surface of contact with odorants. Cilia of olfactory sensory neurons differs from the kinocilia described in the respiratory epithelium: they are larger and do not contribute to any ciliary beating as they lack dynein, a protein essential for motility (Menco, 1980; Sankaran et al., 2012). These cilia bear the olfactory receptors (OR) that "recognize" the odorant by acting like receptors that, upon activation, leads to chemical reactions that transmit the signal to the central nervous system to be decoded (Menco et al., 1992). Interestingly, each olfactory sensory neurons only harbor one type of OR recognizing one type of "odotope" (Malnic et al., 1999), much like a particular lymphocyte B produces an antibody that recognizes one epitope. The axon projected by each olfactory sensory neurons is thin and non-myelinated (Hill et al., 2004). They form bundles helped by ensheating cells to form the olfactory nerve (Lledo et al., 2005) that cross the *lamina propria* and the ethmoid bone to connect with second-order neurons called mitral cells and tufted cells in the olfactory bulb, which is a pair organ: one in the left hemisphere, the other in the right hemisphere (Pinching and Powell, 1971).

Sustentacular cells

Sustentacular cells are non-neuronal cells that proliferate at a very slow rate (Graziadei, 1973). They are also called support cells as they provide the neuroepithelium mechanical and metabolic support to the olfactory sensory neurons, like a neuroglia would do in the brain. Their columnar, elongated shaped is responsible for the thickness of the olfactory epithelium. The oval nuclei are aligned closed to the apical side (Menco, 1980). Besides the mechanical support, sustentacular cells provide a detoxification system to the olfactory tissue (Chen et al., 1992) and contribute to the phagocytosis of

dead cells (Suzuki et al., 1995). The microvilli present on the apical side intertwine with the olfactory cilia, but tight junction separates them from the olfactory sensory neurons and maintain a strict physical barrier between the external environment and the mucosa. By doing so, they maintain the polarity of the olfactory sensory neurons (de Lorenzo, 1957; Moran et al., 1982; Tang et al., 2009). As for the metabolic support, these cells possess numerous organelles such as mitochondria. They also contribute to the composition of the mucus by regulating the ionic concentration of this fluid, which affects the interaction between odorants and the OR (Harkema et al., 2006; Morrison and Costanzo, 1992).

Basal cells

Basal cells can be separated into two populations: globose basal cells and horizontal basal cells, that sits on the basal side of the epithelium (Alvites et al., 2018). They are the stem cells of the olfactory mucosa from which sustentacular cells and olfactory sensory neurons originate (Graziadei and Graziadei, 1985; Monti Graziadei and Graziadei, 1979); more precisely, globose basal cells are thought to be the olfactory sensory neurons progenitors, while horizontal basal cells are more pluripotent and can differentiate into globose basal cells, sustentacular cells, but also Bowman's glands and ducts. However, this strict separation is questioned as horizontal basal cells were also able to differentiate into all the cell types composing the olfactory epithelium (Iwai et al., 2008). Horizontal basal cells share similarities with the basal cells of the respiratory mucosa (Caggiano et al., 1994; Goldstein and Schwob, 1996), especially regarding keratin content that gives them a darker color. Horizontal basal cells are directly at the contact with the basal lamina and do not proliferate much in basal conditions, whereas globose basal cells, which are rounds, small, and with a clear cytoplasm, have a higher proliferation rate (Huard and Schwob, 1995).

As the olfactory mucosa is perpetually exposed to the external environment, it is also exposed to potentially harmful components. However, the tissue is not defenseless and can recover after injury. The epithelium is able to reconstitute and olfactory sensory neurons regenerate and reinnervate the olfactory bulb up to some extent, which is a spectacular phenomenon in the mammalian physiology, all thanks to the basal progenitors (Schwob, 2002). For example, infection with SARS-COV-2 in the Syrian

golden Hamster induced the destruction of the olfactory epithelium. However, this destruction allows the system to fight off the infection by recruiting immune cells, and the tissue regenerates within 14 days (Bryche et al., 2020). In humans, olfactory sensory neurons regenerates from basal cells every 30 to 120 days from basal cells (Crews and Hunter, 1994; Shepherd, 2010), and regeneration of olfactory sensory neurons is thought to be essentially helped by inflammatory signals (Bauer et al., 2003). In general, basal cells respond to neuronal death, olfactory nerve injury, exposure to aggressive toxicant and bulbectomy by increasing their proliferation, which highlights again the resilience of this tissue (Harkema and Morgan, 1996). Basal cells can start responding the day of the injury, and new olfactory sensory neurons start to appear three to four days after the injury. Within eight to ten days they are mature and functional again (Schwob, 2002).

However, this regenerative power has limits. For example, olfaction impairment has been linked with the degree of head injuries: the more severe the injury, the higher risk of olfaction impairment. This impairment can be caused by a blockage in the airways, of brain injuries located in the structures involved in olfaction, which is not related to the regenerative power of basal cells. However, the choc can also disrupt the olfactory nerve and depending on severe is the disconnection between olfactory sensory neurons and the olfactory bulb, the reinnervation might be impossible to operate. This type of trauma can occur even with mild head choc like a ground-level fall, or even with any other choc inducing contra-coup forces that can move the brain and stretch or shear the rather fragile olfactory nerve (Howell et al., 2018; Yousem et al., 1996).

Bowman's glands

Bowman's glands are nested in the lamina propria whose ducts emerge at the surface of the epithelium. These acini measure from 20 to 40 µm diameter secrete the olfactory mucus that covers the olfactory epithelium. The olfactory mucus is 3 to 50 µm thick depending on the species and contains ions, mucopolysaccharides, mucins and other proteins (Getchell and Getchell, 1990). It protects the olfactory mucosa, keeps it moist, and controls the biodisponibility of generally hydrophobic odorants to reach the olfactory receptors by concentrating or diluting them (Morrison and Costanzo, 1992). Among the proteins secreted in the mucus are Odorant Binding Proteins (OBP) (Vidic et

al., 2008), that can bind odorants, and xenobiotic metabolizing enzymes (XMEs) (Débat et al., 2007; Harkema et al., 2006; Nagashima and Touhara, 2010). These proteins also control the biodisponibility of odorants for olfactory receptors and thus modulate the olfactory signal. As such, they are part of the "perireceptor events" that will be developed in part 2.

The central nervous system parts of olfaction

When odorants bind OR, a series of chemical reactions transmit the signal from the olfactory sensory neurons to the central nervous system structures responsible for integrating and decoding the odorant signal. While the precise chemical reactions of the odorant signal and the odorant coding will have a part of its own further down, it is interesting to now understand the brains structures that will decode and integrate this signal. As described before, the olfactory sensory neurons project through the ethmoid bone to connect with mitral cells and tufted cells in neuronal organizations called glomeruli (singular: glomerulus) in the olfactory bulb (see Figure 6). There are around 5600 glomeruli in the human olfactory bulbs, and 4200 in the rat's (Maresh et al., 2008; Royet et al., 1998), and each glomerulus groups olfactory sensory neurons expressing the same OR. This strict separation and organization of the signal depending on the OR activated by the odorant stimuli allows to code the olfactory signal in a way the brain

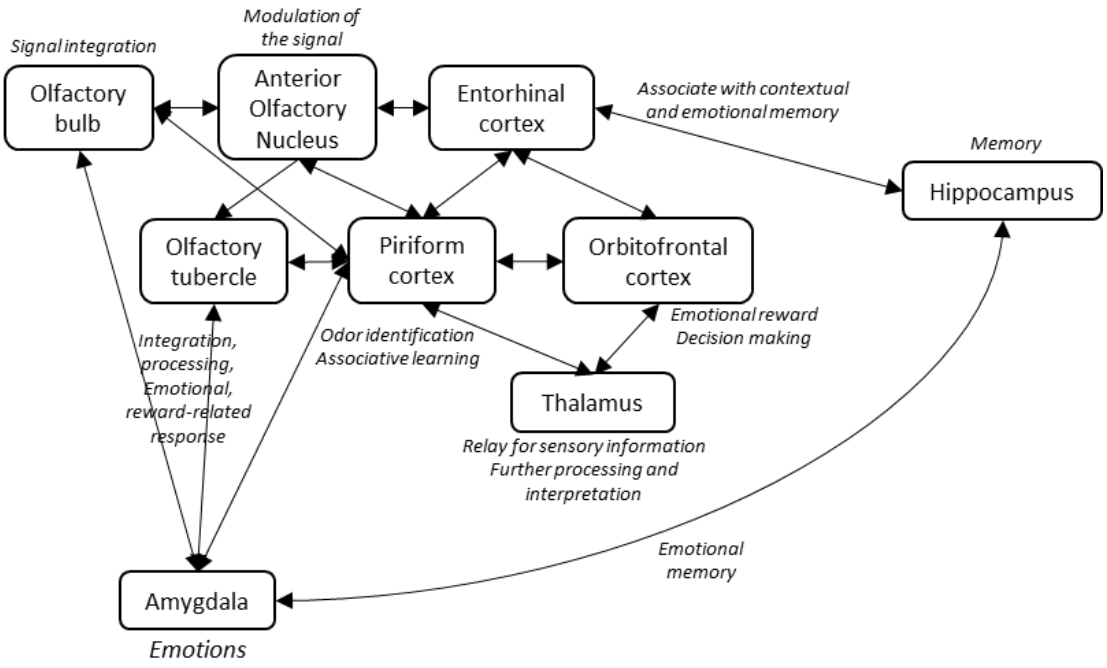

***Figure 7**: Simplified organization of the main cerebral structures involved in the odorant signal processing. (a) Medial pathway. (b) Lateral pathway. Original illustration.*

can decrypt it. To put it differently, odorant stimuli activate specific patterns of glomeruli in a dynamic way. The olfactory bulb axons, forming a structure called the olfactory peduncle, transmit the message to olfactory cortices that then identify the nature of the successive stimuli (Smith and Bhatnagar, 2019). Figure 7 shows a simplified organization of the neuronal structures involved in the treatment of the olfactory signal.

The primary olfactory cortex is an ensemble of different regions of the brain receiving signals from the olfactory bulb. It comprises the anterior olfactory nucleus, the piriform cortex, the olfactory tubercle, the amygdala, and the entorhinal cortex – although the most devoted neuroanatomists would complete this definition by adding other less-known structures, that the present author encourages the readers to discover in the following review (Cleland and Linster, 2019). Contrarily to the other senses, the olfactory cortex primarily connects with structures of the limbic system (the amygdala, center of the emotions and behavior, and the hippocampus, center of the memory), which make the olfactory signal treatment mostly unconscious and emotionally related at its early stages (Catani et al., 2013). This is the reason of the “Proust Madeleine effect”, which describes how scents trigger strong emotional autobiographical memories (de Bruijn and Bender, 2018). For other senses, the relay is first made via the thalamus that relays and compute information to higher cognitive areas for multisensorial analysis. The thalamus is later involved in the odorant signal process, as we still have a conscious perception of odors.

The anterior olfactory nucleus is a relatively ignored structure that is often described as a “hub” between the olfactory bulb and the piriform cortex and is sometimes skipped to the benefit of the piriform cortex. The anterior olfactory nucleus is a multimodal and complex structure that modulates, refines, and enhances some specific features of the signal sent from the olfactory bulb via the medial pathway before sending it to higher centers, and connects the olfactory cortices from the right and left hemispheres. Specialists of the anterior olfactory nucleus suggest that the structure is actively involved in the olfactory coding via its link with the olfactory bulb, which activates specific patterns of neurons inside the nucleus. The fact that tufted cells mostly project to the anterior olfactory nucleus and not in the piriform cortex is another argument of its defender to call it the “principal higher-order olfactory structure” (Brunjes et al.,

2005). The piriform cortex has been described as the larger and principal olfactory cortical area, at the crossroad between the olfactory bulb via the lateral pathway, and higher centers. However, focusing on its size does not do justice to the complex associative nature of this cortex. Indeed, it receives inputs from the olfactory bulb, the orbitofrontal cortex, the anterior olfactory nucleus, the amygdaloid structures, etc. (Brunjes et al., 2005; Haberly and Bower, 1989). The piriform cortex is also involved in the odor coding circuitry in collaboration with the olfactory bulb, the anterior olfactory nucleus, the lateral entorhinal cortex, the cortical amygdala, and the olfactory tubercle. By associating information from all these cerebral structures, the piriform cortex contributes to odor identification, odor intensity, odor valence (attraction or aversion, influenced by odor learning and memory), and is involved in associative learning related to smell (Blazing and Franks, 2020). The olfactory tubercle connects with the anterior olfactory nucleus, the piriform cortex, and the amygdala. It is thought to be responsible to quickly encode the valence of odorant cues, especially reward-related odorant cues (Gadziola et al., 2015). As mentioned before, the limbic system, including parts of the amygdala, is involved in the treatment of the olfactory signal. This gives a strong connection between smell and emotions. The amygdala is usually involved in innate behavior in response to olfactory cues (Mori and Sakano, 2021). Lastly, the entorhinal cortex transfers information to the hippocampus, the memory center. By associating contextual (notably spatial) and emotional information, it contributes to smell related and emotional related memories (Leitner et al., 2016).

From this “primary” olfactory cortices, the signal is transferred to higher-order cognitive areas, notably the orbitofrontal cortex. This structure projects to the anterior cingulate cortex, place of cognitive processes capable of word-level descriptions. The orbitofrontal cortex is not a region specific to olfaction: it can integrate taste signal and is responsible for the acquired associated between taste and smell in flavor perception. As such, it also modulates reward value. Other sensory cues can be integrated as well, and it contributes to the control the appetite, the liking of the food, etc. In associated with the anterior cingulate cortex, a hedonic map is thus drawn. Higher cognitive areas are then responsible for a learned-based behavior (Rolls, 2019).

It is worthy to note that most of these regions project back to their afferences, and that the olfactory cortices also communicate with the hypothalamus, a zone that notably controls food intake (Gascuel et al., 2012).

Accessory olfactory organs

Also called the Jacobson organ after the Danish surgeon that described it first (Jacobson, 1813), the vomeronasal organ (VNO) is one of the accessory olfactory tissues found in most amniote, with exceptions: in humans, it develops in the embryo then regresses, and its functionality in our specie is disputed (Dénes et al., 2015; Meredith, 2001; Stoyanov et al., 2018). The remaining structure lacks the neuronal connection found in species with a functional VNO, and the presence of the structure itself is strongly debated as it varies among individuals (Salazar et al., 2019). It is a pair of blind-ending tubular cavities opening rostrally in the nasal cavity or into the incisive duct, depending on species (Adams, 1992). Concerning rats, it opens at the incisive duct in the oral cavity and communicate with the nasal cavity through the palatine fissure. The conduit follows the vomer and the nasal septum (Alvites et al., 2018). The VNO tissue has a structure similar to other olfactory sensory tissues, which sensory neurons connected to the olfactory bulb, sustentacular cells and basal cells (Adams, 1992). It is thought to be involved in the pheromonal communication within the species, particularly for sexual behavior and for marking territories (Alvites et al., 2018), and that its disappearance from the human physiology could be linked to the predominance of vision and language in human social behavior, which would give less space to hormonal and pheromone-related sexual behavior (Swaney and Keverne, 2009).

Aside from the VNO, two other olfactory subsystems are present and mostly relevant for rodents: the septal organ of Masera and the septal organ of Grüneberg. In humans, these organs are almost non-existent .

The septal organ of Masera is a neuroolfactory mucosa found at the nasal septum in rodents, rabbits and marsupials (Giannetti et al., 1995; Miragall et al., 1984). In rats, it forms patches near the septal window. The septal organ of Masera is thought to contribute to the detection of odorants, especially odorants relevant to alert functions but without discriminating them (Storan and Key, 2006).

Lastly, the septal organ of Grüneberg is a group of olfactory neurons located inside the nostrils of some species including rats and mice (Storan and Key, 2006). In rats, it is isolated from the nasal cavity by a keratinized epithelium. Its function is believed to be related to panic and freezing behaviors in response to specific pheromones (Alvites et al., 2018; Brechbühl et al., 2014, 2013).

Trigeminal perceptions

Trigeminal perception depends on the fifth cranial nerve, also called trigeminal nerve. The nerve divides into three main branches: the ophthalmic branch (V1), the maxillary branch (V2), and the mandibular branch (V3). V1 and V2 are purely sensory nerves, while V3 also possess motor properties. Roughly, V1 innervate the eye region, the nose is served by V1 and V2, and V3 innervates the mouth, especially the bottom region (Bathla and Hegde, 2013). Trigeminal – or somatosensory – perceptions complete the triad of chemoperception formed by the olfactory and gustatory systems. It notably adds intensity, warmth, coldness, and pain dimensions to the overall flavor perception. It is thought that the main purpose of the olfactory system is to detect harmful volatile molecule – due to their nature or their concentration – by stopping the inhaling reflex to protect the mucosa (Hummel and Livermore, 2002). Few molecules stimulate exclusively the olfactory or the trigeminal system; while the olfactory system discriminates the molecules, the trigeminal stimulation allow to perceive irritating molecules such as carbon dioxide and ammonia and to localize the origin of the odor (Bensafi et al., 2008; Han et al., 2018; Kleemann et al., 2009).

Common examples of these perceptions in the everyday life: temperature receptor agonists like menthol and eucalyptol confer to some products of coolness or freshness, while cinnamaldehyde is perceived warm (Filiou et al., 2015). On the oral side, mustard enthusiasts know well the irritating effect of allyl isothiocyanate when it activates the TRPA1 and the tears associated. As the trigeminal nerve links the mouth, nose and eyes, it is the reason why mustard makes you cry! Spicy food adepts are also familiar with the burning sensation caused by capsaicin through trigeminal warm thermoreceptor TRPV1 and nociceptors activation (Frasnelli et al., 2011; Leijon et al., 2019).

Interestingly, we actually perceive and evaluate the airflow in the nasal cavities thanks to the trigeminal perception of the nasal mucosa cooling due to the conductive heat

transfer to the inhaled air, notably through TRPM8. This receptor sends a message to the respiratory center, which then impact the respiratory cycle. The process has been nicely reviewed by Sozansky and Houser, and notably explain the temporary relief we feel when, congested, we inhale an activator of TRPM8 like menthol (Sozansky and Houser, 2014).

People suffering from anosmia usually still perceive trigeminal stimuli and are still able to discriminate odorant molecules through trigeminal perception: menthol and cineol as the cool and fresh perception, and ethanol. Although it is far from perfect, it shows again the participation of the trigeminal system to an odor quality (Doty et al., 1978; Laska et al., 1997).

1.4. Olfactory signaling

Behavior such as sniffing benefits the interaction between volatile odorant and the olfactory mucosa and thus serves odorant recognition. Sniffing is an essential part of olfaction as it forces the air to reach the olfactory mucosa and activates the olfactory bulb (Ishikawa et al., 2009; Le Magnen, 1944; Mainland and Sobel, 2006), and a quite recent study showed that it is always trade-off between a quick odorant recognition, enabled by and increased frequency of sniffing, and a good odorant signal amplitude, enabled by a slow sniff (Spencer et al., 2021). The following part will describe in detail the genesis of the odorant signal. By now the general anatomy the peripheric and central structures involved in olfaction has already been unveiled; this part focuses on mechanisms happening on the cellular level.

The binding of the odorant molecule and the OR is the first step of the odorant signal, which then triggers a chain of molecular signaling within the olfactory sensory neurons. As mentioned before, the signal is then coded by the olfactory bulb, among other central nervous olfactory areas, in a way that discriminates finely the odorant molecules.

Olfactory receptors

The olfactory receptors gene family was characterized in 1991 by Linda Buck and Richard Axel, who in 2004 share the Nobel Prize in Physiology and Medicine for this (Buck and Axel, 1991). Aside from OR, other receptor families contribute to the mammalian olfaction: vomeronasal receptors V1R and V2R, trace amine-associated receptors (TAAR), and formyl peptide receptors (FPR) (Liberles, 2015). The OR gene family is

usually large and is highly variable in size depending on the species. For example, around 800 OR genes were identified in the human genome, but only a 380 OR genes code for OR proteins, and the human genome contains 6 TAAR and one V1R (Rodriguez et al., 2000). In comparison, the rat genome possess approximately 1430 OR protein coding genes, 240 V1R, 120 V2R, and 7 FPR (Ache and Young, 2005; Liberles et al., 2009; Niimura et al., 2014; Young et al., 2005). In humans, OR genes are scattered in the whole genome except chromosome 20 and the Y chromosome, and OR genes are concentrated in chromosome 11. OR genes closed to each other usually share higher similarities than with OR genes located further. This supports the idea that OR genes increased via repeated tandem gene duplication, although the puzzle was mixed during the evolution due to chromosomal rearrangements. In addition to the number of OR protein coding genes, the high OR gene polymorphism must be considered to grasp the huge interindividual variability there is concerning the sense of smell. Moreover, some person, consciously or not, are specifically anosmia to certain odorant molecule. For example, the pig pheromone androstenone can be either perceived as an unpleasant sweaty urinous odor, as a pleasant sweet floral odor, or completely odorless (Niimura, 2009). As previously mentioned, each olfactory sensory neuron expresses only one type of olfactory receptor, which is named allelic competition for transcriptional dominance. Briefly, when olfactory sensory neurons are maturing, several multichromosomal enhancer hubs compete with each other to transcribe a single OR. One of them win and stay euchromatic, meaning the chromatin stays in a relaxed state and functional, while the other hubs condense in heterochromatin and lose their functionality. The competition between hubs is played with three main “rules”. First, transcription of OR strengthen its hub by recruiting enhancers, which in turn enhance the OR transcription. Secondly, transcript OR inhibit the transcription of competing ORs. In time, the equilibrium between the different hubs/OR breaks in favor of one. Thirdly, the transcribed OR stabilize the favors hub, and becomes the single OR type expressed by the mature olfactory sensory neurons. Pourmorady and colleagues investigated this mechanisms and suggest OR mRNA, on top of coding for an OR protein, can also contribute to the nuclear architecture that favor one OR over the others (Pourmorady et al., 2024).

The OR gene family codes for olfactory receptors that makes up to 5 % of the entire proteome in mammals (Niimura, 2009). They are G-coupled receptors (GTP binding proteins), and belong to the rhodopsin-like GPCR superfamily. They all share a structure organised with 7 hydrophobic transmembrane domains (TM) in α-helix structures, an extracellular N-terminus and a short intracellular C-terminus. The transmembrane domains are linked with three external (EL) and three internal loops (IL). Additionally,

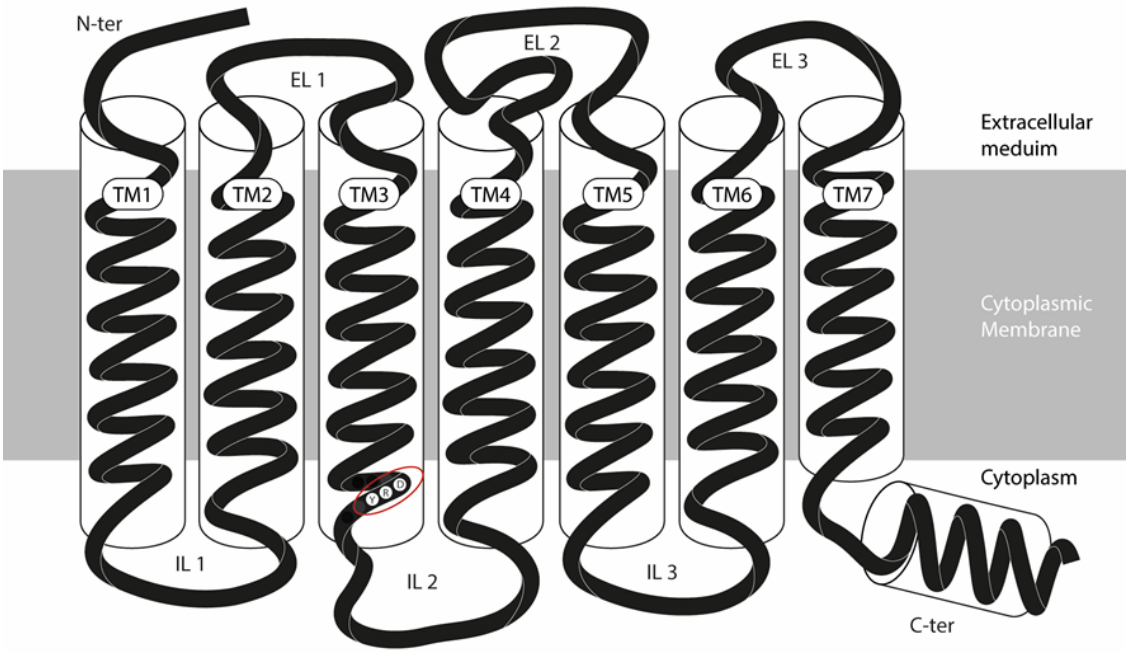

***Figure 8**: Trans-membrane representation of an odorant receptor. TM: transmembrane domain, EL: external loop, IL: internal loop. The DRY amino acids between TM3 and IL2 are characteristic of GPCR. Original illustration.*

olfactory receptors share conserved sequences whose amino-acids are circled in red in Figure 8. More particularly, the aspartate-arginine-tyrosine sequence (DRY) between the TM3 and the IL2, which is characteristic of the GPCRs. While TM1, TM2, and TM7 are conserved, hyper-variable regions of around 20 amino-acids in TM3, TM4, and TM5 contribute to the binding-specificity of olfactory receptors for specific odorants. N-terminal and C-terminal regions also contribute to this binding-specificity. Olfactory receptors interact with heteromeric G-protein (named G_{olf}), composed of the α and a βγ subunits. In basal conditions, G_{olf} is bound to guanosine diphosphate (GDP). More specific features of the 3D structure of olfactory receptors can be found in Sharma and colleague's review (Glezer and Malnic, 2019; Sharma et al., 2018).

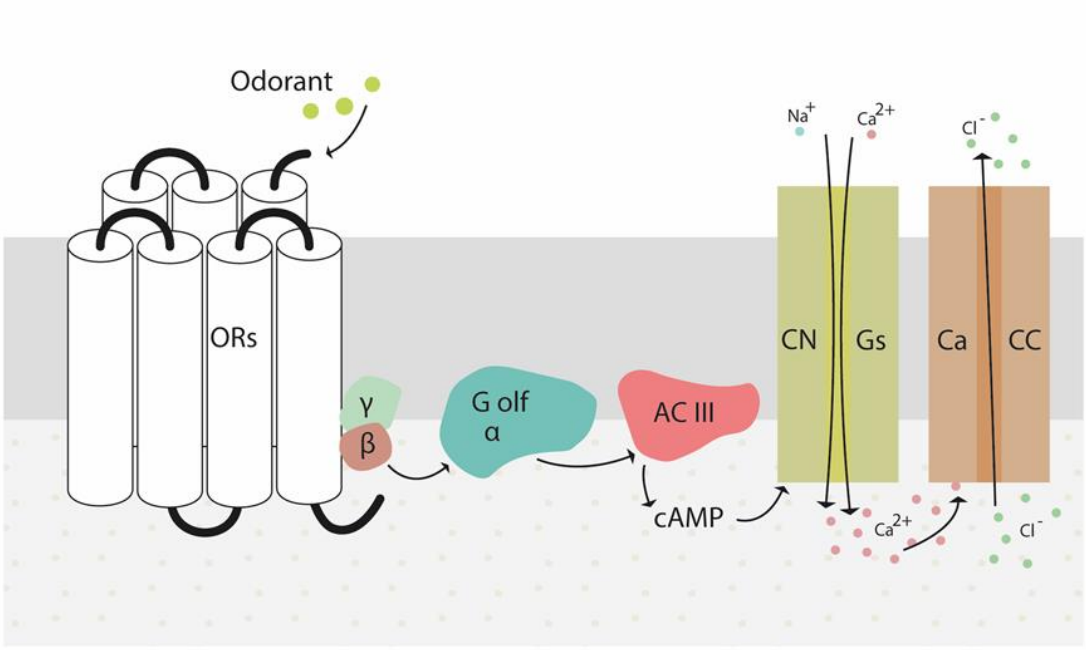

***Figure 9**: Intracellular signaling in response to an odorant binding an olfactory receptor. Original illustration inspired from Neiers et al., 2022.*

The odorant signal is triggered by the odorant binding an olfactory receptor. In response, the α subunit of G_{olf} exchange GDP for GTP (guanosine triphosphate) and dissociate from the βγ subunit, as shown in Figure 9. The GTP- α- G_{olf} then activates adenylyl cyclase III (ACIII), an enzyme converting adenosine triphosphate (ATP) into cyclic adenosine monophosphate (cAMP). Increased intracellular levels of cAMP is a message for the cyclic nucleotide-gated (CNG) channels to open. Opened CNGs allow the influx of sodium (Na^+) and calcium (Ca^{2+}) ions. Ca^{2+} is a secondary messenger and activates chloride channels (CaCCs), allowing the chlorine ions Cl^- to exit the cilia lumen, notably with the help of NA^+-K^+-$2Cl^-$ cotransporter NKCC-1. The chlorine efflux generates a depolarization of the neuron membrane that is transmitted in the form of an action potential from the olfactory cilia to the axon. This state of depolarization is transient: Ca^{2+} ions also binds to calmodulin (CaM) that activates phosphodiesterase (PDE) and calmodulin kinase II (CaMKII). In turn, PDE and CaMKII inhibit ACIII. In the meantime, levels of cAMP decrease in the cilia lumen, and Na^+Ca^{2+} transporters lower the intracellular levels of Ca^{2+}, ending the cycle and leaving the cilia ready for another odorant binding the receptor (Elsaesser and Paysan, 2005; Sharma et al., 2018). Another alternative pathway to ACIII/cAMP to raise intracellular Ca^{2+} levels using inositol 1,4,5-triphosphate has also been suggested recently. This pathway would be involved in response to some unpleasant odors, although it is not entirely understood (Elsaesser and Paysan, 2005).

Odor coding

Olfactory sensory neurons expressing only one type of OR per cell allows the olfactory system to discriminate the molecules triggering the olfactory signal. Malnic and colleagues published in 1999 a paper showing that different odorants could trigger responses in the same OR, and that different OR can respond to the same odorant. The team found that carboxylic acids and alcohols sharing the same number of carbons were discriminated by activating different sets of OR, and consequently activating a specific pattern of glomeruli (Malnic et al., 1999). This is the basis and the power of what the olfaction field call combinatorial coding: odorant molecules bind to a specific set of OR, each set, or pattern, being specific for a particular molecule at a given concentration. Analysis of the odor identity and intensity is then done on the set of OR activated at a given time-point, rather than one OR being equal to one odor. Indeed, although the number of OR genes and their polymorphism generate a neuroepithelium capable of binding a fair number of molecules, the variety of odorant molecules is infinitesimally bigger than the number of OR types expressed even in species expressing the highest numbers of OR. By activating several OR at the same time, molecules are then assigned a code written from a pool of around 800 OR – the present number considers that each of the almost 400 OR protein-coding genes can be expressed with the two alleles the human genome allows. The combination of OR activated also changes depending on the concentration of the odorant molecule, which allows the appreciation of intensity on top of identifying the molecule (Kurian et al., 2021; Touhara, 2002). By analogy, a simple digicode using digits from 0 to 9 allows for approximately 10^8 different codes of varying lengths when each digit can only be used once. With 800 “characters”, the order of magnitude of all the combinatorial possibilities rises to 800^{10}, a fairly correct number for humans to discriminate the volatile molecules of their environment. Another layer of complexity can be added to this mechanism: in odorant mixtures, the antagonism mechanism of odorant molecules for olfactory receptors have been evidenced. In simple terms, some odorants are able to bind an olfactory receptor without activating it. This prevents potential agonist odorants of the mixture to bind and activate the olfactory receptor, which *in fine* changes the set of activated glomeruli, thus impacting the olfactory perception (Oka et al., 2004; Pfister et al., 2020).

The dominant theory considers this combinatorial code to depend of the shape/structure of the molecules. Different odorant molecules would then be able to activate the same OR by sharing similar functional groups among their structure. Also called “odotopes”, from the word “epitopes” that designate molecular patterns recognized by antibodies, the nature of these pattern would then be reflected by the combination of OR activated by the molecule. However, it fails to predict the perceived odor based on the shape of the molecule. Sell published a nice review on the topic, showing effects of functional groups, isomers, hydrophobic residue, saturations, etc. in the perceived odor. The chosen examples illustrate how what’s true for some molecules isn’t for others, and that similar structures do not always equate with similar odor quality, among other examples (Sell, 2007). Turin contested the odotope theory and suggested OR could recognize vibration signature instead of shapes/functional groups (Turin, 2002; Turin and Yoshii, 2003), although it does not reach the scientific consensus and has been disproved since (Block et al., 2015).

Understanding the sense of smell is still a hot topic nowadays as a great challenge for the field is to identify ligands for these receptors, as well as deciphering what conditions the scent of a molecule.

2. Peri-receptors events and odorant metabolism

As mentioned in part 1, the nasal cavity filters and warms the inhaled air, solubilizing a part of the volatile compounds it transports in the nasal mucus. This phenomenon allows the tissue to detoxify potentially harmful components thanks to XME expressed in the tissue and present in the mucus. Nasal XME were indeed localized in sustentacular cells and Bowman’s glands (Bogdanffy, 1990; Getchell et al., 1993), but also in olfactory sensory neurons (Heydel et al., 2001; Mayer et al., 2007, 2009; Neiers et al., 2021) and in olfactory mucus (Bogdanffy, 1990; Débat et al., 2007; Nagashima and Touhara, 2010).

However, odorant molecules are also xenobiotics and have to solubilize in the mucus in order to reach the olfactory receptors. Their journey in the nasal mucus and their interaction with macromolecules thus condition their availability for OR, and so far, two phenomena were described: (1) odorant molecules can be metabolized by the nasal XME, and (2) they can bind proteins solubilized in the mucus called Odorant Binding

Proteins (OBP), and sometimes XME as some variants can transport ligands without metabolizing them (Listowsky et al., 1988; Zucker et al., 1995).

These phenomena impact the odorant signal before it begins and are called peri-receptor events (Getchell et al., 1984; Heydel et al., 2013; Pelosi, 1996).

2.1. Odorant metabolism

Xenobiotic Metabolizing Enzymes (XMEs)

The term *xenobiotics* refers to man-made or natural chemicals that are not found in a defined organism. This includes a huge variety of compounds found in drugs, food, cosmetics, air, textiles, and the list goes on. Living organisms are therefore constantly exposed to an infinite number of foreign substances through the skin, the respiratory and the gastrointestinal tracts. Although altogether different in terms of structures and chemical families, it is generally accepted that a majority of these compounds are lipophilic and therefore not stopped by cellular membranes, which is often toxic. Most species have developed a detoxifying system composed of a network of xenobiotic metabolizing enzymes (XMEs) that limit this toxicity. Interestingly, these enzymes are also involved in physiological metabolism. The liver is an example of an XMEs enriched tissue, responsible for detoxicating any xenobiotic brought via the bloodstream, as well as being on actor in the enterohepatic cycle of bile salts (Grant, 1991). More interestingly in the context of this thesis, the olfactory mucosa is also really well-equipped with XMEs, which makes this tissue able to metabolize volatile xenobiotic including odorants (Gervasi et al., 1991; Heydel et al., 2019a; Longo et al., 1991).

These enzymes are classified into 2 categories depending on their reaction type, and completed by a third step involving efflux transporters. The joint action of phase I and phase II XME render xenobiotics more hydrophile and easier to excrete via bile, sweat, urine, feces and mucus, while efflux transporters export xenobiotics and their metabolites out of the cellular compartment. Mechanisms of biotransformation have been reviewed before (Hodgson, 2010), but some details about enzymatic actions and families of the 3 categories are given in the next paragraphs for a better comprehension.

Phase I

Phase I, also known as oxidation phase, aims to increase the water solubility and the reactivity of the xenobiotics to promote their excretion and/or their conjugation with

polar groups by phase II enzymes. Interestingly, phase I reactions can sometimes activate the biological activity of a compound, instead of inactivating it. A good example is acetaminophen, also known as paracetamol, which is primarily metabolized by the microsomal monooxygenase cytochrome P450 (CYP), the main variants involved being CYP2E1 and CYP3A4. The metabolite N-Acetyl-p-benzoquinone (NAPQI) is hepatotoxic when it accumulates in the liver. This metabolite is usually metabolized and inactivated by phase II enzymes, which is why we can tolerate the drug at regular concentrations (McGill and Hinson, 2020). CYP display several NADPH-dependent enzymatic reactions in their catalog, which make them reactive to a wide range of molecules. CYP are ubiquitous enzymes that can be regrouped in 781 gene families, with only 18 families found in vertebrates. Humans are equipped with these 18 families which comprise 44 subfamilies of 57 genes and 58 pseudo genes. (Esteves et al., 2021). CYP levels and activity comparable to those of the liver were found in mammalian olfactory epithelium (Dahl et al., 1982; Hadley and Dahl, 1982). So far, 33 CYPs were identified in the mammalian olfactory mucosa. CYP2A13 is notably thought to be specific to the respiratory tract (Su et al., 2000). Animal models such as rats and rabbits allowed to detected them more precisely either in the entire nasal cavity, the olfactory mucosa, or directly on olfactory cilia of olfactory sensory neurons (Heydel et al., 2019a; Hodgson, 2010; Minn et al., 2005).

CYP are not the only microsomal monooxygenase among phase I enzymes: flavin-containing monooxygenase (FMO) also require NADPH and oxygen to function, although their substrate preference is narrower than the CYP's. Five families of FMO have been discovered so far (FMO1 to FMO5), that were identified in notably in the liver, kidney, lungs, and in the olfactory epithelium as well. Variants EPH1 and EPH4 were more particularly found in the olfactory epithelium. Among their substrate are epoxides found in some xenobiotics (Gan et al., 2016; Heydel et al., 2019a; Hodgson, 2010).

Alcohol and aldehyde dehydrogenase (ADH and ALDH) are named after the substrates they oxidize in a NADPH-dependent manner into carboxylic acids (Gan et al., 2016). The most famous ones are ADH1, ADH3 and ALDH2, involved in liver alcohol detoxication (Contreras-Zentella et al., 2022; Haseba and Ohno, 2010). ALDH1A1, ALDH3A1 as well and the aldoketoreductase 1B10 (AKR1B10) were identified in the human nasal and oral

cavity and shown to metabolize some aroma compounds (Boichot et al., 2023). AKR are a family of phase I XME involved in redox biosynthesis, metabolism, and detoxification (Barski et al., 2008).

Carboxylesterase belong to the α, β-hydrolase family. Their enzymatic activity form a carboxylic acid and an alcohol by hydrolysis of carboxylic esters (Hosokawa et al., 2008, 1990; Satoh, 2002). Evidence of carboxylesterase activity was found in nasal tissues of several mammalian species including rabbit, rat, mouse, Syrian hamster, dog and human (Dahl et al., 1987; Lewis et al., 1994; Robinson et al., 2002)

Dicarbonyl/L-xylulose reductase (DCXR) is a NADPH-dependent oxidoreductase playing a role in carbohydrate metabolism and detoxifying processes, by converting L-xylulose to xylitol and reducing α-dicarbonyl compounds of endogenous and xenobiotic origin, respectively. This enzyme was discovered separately in different tissues and species: as lung dehydrogenase reductase, as sperm protein p34H in epididymis, and as α-dicarbonyl/diacetyl reductase (EC 1.1.1.5) in kidney and liver; until biomolecular analysis showed they were the same protein nowadays called DCXR (EC 1.1.1.10) (Nakagawa et al., 2002). Concerning its endogenous detoxification activity, DCXR is thought to prevent oxidative stress related advanced glycation end products accumulation in tissues such as liver and kidney and protect them from carbonyl stress (Lee et al., 2013). DCXR is also found in respiratory tissues including nasal tissues (Robert-Hazotte et al., 2019b, 2022). Among the xenobiotics metabolized by DXCR are α-diketones used as butter flavoring agents such as 2,3-pentanedione, which were investigated for their toxicity toward the respiratory tracts (Halldin et al., 2013; Hubbs et al., 2012; Kreiss et al., 2002; Van Rooy et al., 2007; Zaccone et al., 2015, 2013).

Phase II

Phase II xenobiotic metabolism is also called the conjugation phase and mainly involves transferases. They are classified in different families that each transfer specific groups on functionalized xenobiotics, and some of them have been identified in the olfactory epithelium, such as UDP-glucuronosyltransferase (UGT), sulfotransferase (SULT), and glutathione transferase (GST).

UGT are glucuronide conjugation enzymes involved in the elimination of xenobiotics, but also in different physiological metabolism pathways such as thyroid hormone

synthesis and bile acids (Jancova et al., 2010). They catalyze the conjugation of a glucuronic acid from the acid cofactor uridine-5'-diphospho-α-d-glucuronide (Testa, 2005).

There are four main families found in humans: UGT1, UGT2 (divided into subfamilies A and B), UGT3, and UGT8. While UGT1 and UGT2 are the main glucuronide conjugation enzymes, UGT8 variants are mostly involved in biosynthesis in the nervous system, and UGT3 family is thought to be part of steroid hormone biosynthesis (Strauss and FitzGerald, 2018). Some UGT variants are expressed specifically in the olfactory epithelium, the most know being UGT2A1, as well as UGT2A2 and 2B1 (Heydel et al., 2019a; Jancova et al., 2010).

SULT are able to conjugate sulfate from 3'-Phosphoadenosine-5'phosphosulfate on phenol, enol, alcohol or amine groups of small endogenic and exogenic molecules. There are four SULT families in humans: SULT1, SULT2 (divided into subfamilies A and B), SULT4, and SULT6 (Gamage et al., 2006). Depending on the family, SULT are cytosolic of in the Golgi apparatus. SULT6B1 and SULT1C1 were notably located in olfactory cilia, although they are far from restricted to the olfactory system and are found in a plethora of tissues. They are notably major enzymes in the human fetus (Heydel et al., 2019a; Jancova et al., 2010). Other hydrophilic groups can later be added to sulfo-conjugated metabolites by methyltransferase and acetyltransferase (Heydel et al., 2010).

GST are important actors in the cellular protection against reactive oxygen species-related oxidative stress (Mannervik and Danielson, 1988). They catalyze the transfer of reduced glutathione to electrophiles groups to make glutathione-conjugated metabolites. This conjugation does not always require GST but is greatly enhanced by them. Four structural families of GST have been described so far: cytosolic GST, mitochondrial GST, MAPEG (membrane-associated proteins in eicosanoid and glutathione metabolism), and Fosfomycin-resistant proteins (Board and Menon, 2013). Soluble GSTs, which are the most studied, are involved in drugs and xenobiotic metabolism, and in drug resistance (Mohana and Achary, 2017). They function as dimers and are divided into family named with letters from the Greek alphabet: Alpha, Kappa, Mu, Pi, Sigma, Theta, Zeta and Omega (Board and Menon, 2013; Wu and Dong, 2012). In humans, GSTA1 and GSTP1 were located in the nasal mucus, Bowman's glands,

sustentacular cells and basal cells, while Mu class GST were preferred in rodent olfactory mucosa (Heydel et al., 2019b, 2019a; Jancova et al., 2010; Schwartz et al., 2020).

Efflux transporters

Phase I and phase II enzymatic activities aim to render initially hydrophobic xenobiotic more hydrophilic to eliminated them. However, hydrophilic conjugated metabolites can no longer passively cross the cytoplasmic membrane and are thus transported out of the cellular compartment via efflux transporters. This step is often called the phase III of xenobiotic metabolism. The nasal mucosa is a potential route for drug delivery, and an interesting one as it allows a quick delivery that does not go through the first pass effect, a phenomenon occurring to orally taken drugs that go through a first biotransformation by XME of the liver that decreases their systemic bioavailability (Herman and Santos, 2023). However, as stated before, the nasal cavity is far from devoid of XME activity, which is why nasal XME and efflux transporters are notably studied (Oliveira et al., 2016).

Several gene superfamilies code for transmembrane transporters, of which efflux transporters are part. First, the ATP-Binding Cassette superfamily (ABC) comprise a variety of transporter families, from subfamily A to H. ABCs use ATP hydrolysis to power up substrate transport across membranes (Zhang et al., 2015). Two subfamilies are of interest in the detoxifying context: subfamily B (ABCB) and subfamily C (ABCC). ABCB gene family codes for multidrug resistance proteins (MDR), the most known example being MDR1/ABCB1, also called P-glycoprotein (P-gp). P-gp actively eliminates toxins (Ehlers et al., 2014) and is mostly known for its role in multidrug resistance of cancerous cells (Heming et al., 2022). MDR usually have a structure containing three transmembrane domains (Zhang et al., 2015). In rats, variants 1A seems to be specifically expressed in the olfactory epithelium and in the olfactory bulb, while MDR2 expression is restricted to the liver. MDR1b was found in all three tissues (Thiebaud et al., 2011). ABCC gene family codes for multidrug resistance-related proteins (MRP), whose structure differs from MDR. Indeed, MRP usually have two transmembrane domains as well as two nucleotide binding sites (Zhang et al., 2015). In rats, MRP1 and MRP5 were found in the olfactory epithelium and the olfactory bulb, while MRP2 is restricted to the liver. MRP3 was found expressed in these 3 tissues (Thiebaud et al., 2011). ABC

subfamily also contains an efflux transporter involved in drug resistance: breast cancer resistance protein (BCRP/ABCG2) (Mao and Unadkat, 2014), although to my knowledge it has not been described in the olfactory mucosa so far.

Role in the olfactory system of XME

The first suggestion of odorant metabolism in the literature was in 1950 (Kistiakowsky, 1950), which was latter followed by observation of XME activity in the olfactory tissues in the 80's (Yin et al., 2001). These works notably showed a greater CYP activity in the olfactory mucosa than in the liver that is the key organ in terms of detoxifying enzymatic activity (Dahl et al., 1982; Hadley and Dahl, 1982). Since this discovery, the presence of nasal XME activity has been explored in numerous animal models (N. Ben-Arie et al., 1993; Débat et al., 2007; Hanser et al., 2017; Lazard et al., 1991b; Nef et al., 1989; Robert-Hazotte et al., 2019b, 2019a, 2022; Schoumacker et al., 2016; Thiebaud et al., 2011). When specifically talking about XME activity toward odorants, nasal XME are sometimes called odorant metabolizing enzymes (OMEs) instead of XME (Heydel et al., 2019a). In insect models, the link between odorant metabolism and olfactory processes has been proven to be crucial for their survival, and insect XME in the olfactory context are also called odorant degrading enzymes (ODE) (Chertemps et al., 2015, 2012; Durand et al., 2012; Steiner et al., 2017). In mammals, the link between odorant metabolism and olfaction is less known, although several studies allow to attribute olfactory roles to this phenomenon.

Protective and detoxifying role

The first role of XME expressed in the nasal mucosa and nasal mucus is to protect the tissue as it is exposed to the external environment. It is especially important to protect the olfactory mucosa as olfactory sensory neurons are in direct contact with the environment of the nasal cavity through the olfactory cilia. Olfactory sensory neurons are thus a direct route between the nasal cavity and the olfactory bulb. An early example of the protective role of XME in the nasal cavity used the dog model. Indeed, a study in 1970 shows that the dog nasal cavity is able to uptake up to 99.999% of 50 ppm of inhaled sulfuric dioxide. Such compound being associated with airway oedema, it was a first hint that the nasal cavity has a protective detoxifying barrier (Brain, 1970). This study was followed by another one in 1977 showing that the frog olfactory mucosa metabolizes tritium labelled octane into the water-soluble metabolite octanol (Hornung

and Mozell, 1977). Moreover, as mentioned before, the nasal route is an interesting pathway for drug delivery. However, XME activity can impact the bioavailability of drug molecules, especially CYP enzymatic activity (Oliveira et al., 2016; Sarkar, 1992).

Termination of the olfactory signal

The first role of odorant metabolism is olfactory signal termination by enzymatic inactivation of odorant molecules. Hydrophiles metabolites are then eliminated, which leaves the space open for new odorant molecules to bind olfactory receptors. The odorant signal termination prevents olfactory receptors to be saturated and allows new signal to be detected. This is important notably to have a temporal evaluation of olfactory cues. In the 90's, odorant molecules were shown to be substrates of UGT, which played a role in odorant signal termination (Lazard et al., 1991a). At the same time, nasal GST activity toward odorant molecules was also investigated (Nissim Ben-Arie et al., 1993). Other XME have been investigated since (Heydel et al., 2013, 2010; Thiebaud et al., 2013). UGT2A1, an isoform specifically expressed in the olfactory epithelium, has been localized at the vicinity of olfactory receptors. Inhibiting UGT2A1 enzymatic activity toward the odorant substrate eugenol impact signals measured with electroolfactogram: olfactory sensory neurons response is greater when the UGT2A1 is inhibited (Neiers et al., 2021). Electroolfactograms record the electrical potential at the surface of vertebrate olfactory epithelium, which *in fine* reflects the electric activity of a population of olfactory sensory neurons in response to stimuli (Scott and Scott-Johnson, 2002). Electroolfactography has also been used in the rat model to demonstrate *in vitro* and *ex vivo* that XME metabolites, especially CYP and UGT metabolites, loose their ability to trigger olfactory sensory neurons response (Thiebaud et al., 2013). As for GST, a panel of odorant aldehyde were shown to be glucuronide conjugated by rabbit, rat and human GST (Faure et al., 2016; Heydel et al., 2019b; Legendre et al., 2014; Schwartz et al., 2020). *In vivo*, glucuronide conjugation of the mammalian pheromone by GST of the rabbit pup nasal mucus impacted the pup's behavior. Rabbit pups respond to the mammary pheromone, a scent emitted in their mother's milk. The blind and deaf pups use that pheromone to find and feed off their mother's breasts during her unique daily visit. The pups immediately respond to the scent with suction-related orocephalic movement that is essential for them to survive. When the pup's nose is gently washed to temporarily

remove the nasal mucus, pups are able to detect the pheromone at concentrations much below the usual detection threshold (Robert-Hazotte et al., 2019a).

Modulation of the olfactory signal

The second role of odorant metabolism in olfactory process is the creation of new odorant metabolites that, in turn, participate in the odorant signal. As such, odorant metabolites add new odotopes that modulates the odorant signal. Odorant metabolites can harbor the same olfactory characteristics, or different ones. Nagashima and Touhara explored in 2010 odorant metabolites in mice nasal mucus and the impact of this metabolism on the behavior of mice. The glomeruli pattern activated by odorants change depending on whether mice were treated with inhibitors or not. This effect is translated by a change in mice behavior: mice treated with inhibitors were no longer able to detect acetyl isoeugenol, an odorant associated with a reward for mice used in the study. Isoeugenol, the metabolite of acetyl isoeugenol, was in fact the odorant that mice associated with the reward. When treated with a specific enzymatic inhibitor, acetyl isoeugenol was no longer converted into isoeugenol, and the mice could no longer detect the reward-associated odorant (Nagashima and Touhara, 2010). Our team at the Center for Feeding and Taste Behavior in Dijon recently showed using rat *ex vivo* olfactory mucosa that odorant metabolite generation happens on a timescale relevant for olfactory mechanisms, under 300 msec. The odorant metabolites identified were then identified: for example, 2,3-pentanedione, which scent is described as buttery, give two metabolites with odorant properties: 2-hydroxypentan-2-one (truffle scent) and 3-hydroxypentan-2-one (herbaceous scent) (Robert-Hazotte et al., 2019b). In humans, odorant metabolites were measured in the exhaled nasal breath of volunteers after they consumed wine. The identified metabolites and their properties correlate the olfactory perception described by the volunteers, meaning these odorant metabolites participated in the overall retronasal olfactory perception of the wine (Muñoz-González et al., 2018). Odorant metabolites were also identified in the human exhaled nasal airflow after an orthonasal sampling of odorants. The team showed that the perceived odor is sometimes due to its metabolite. It is the case of 2-furfurylthiol, which has been described as having a “pungent, garlic and burnt coffee” scent. It turns out the methylated metabolite furfuryl-methylsulfide is responsible for the “pungent, garlic” aspect of the scent, not 2-furfurylthiol (Ijichi et al., 2019).

On top of odorant metabolites participating in the olfactory signal, odorant can compete for the same enzyme, which then impact odorant metabolism itself. Our research team showed in 2017 that odorant-odorant competition impacted perception and behavior, using again the rabbit pup model. Competitors of the mammary pheromone for GST were selected using *in vitro* and *ex vivo* tests. In *in vivo* tests, pups presented to a mixture of the mammary pheromone at subthreshold levels, and the best competitor, were able to detect the pheromone. By competing with the mammary pheromone for GST, the competitor inhibited the enzymatic activity of GST toward the mammary pheromone. Subsequently, the mammary pheromone accumulated around the olfactory receptor until it reached the recognition threshold (Hanser et al., 2017). This effect was also observed in humans: butanoic acid (vomit scent) compete with 2,3-pentanedione (butter scent) for DCXR. DCXR has a higher affinity toward butanoic acid than 2,3-pentanedione, and thus preferentially metabolize butanoic acid first when exposed to a mixture of both odorants, letting 2,3-pentanedione accumulated near the olfactory receptor until it reaches the detection threshold. Indeed, when presented a mixture of both the two odorants at subthreshold levels, a significant number of volunteers clearly detected 2,3-pentanedione in dynamic olfactometry studies (Robert-Hazotte et al., 2022). This particularly highlights that short exposure times with odorants at low concentrations can impact the olfactory perception.

Modulation of OMEs/regulation

So far, very little is known about the modulation of nasal XME, especially short time response in the context of an olfactory event (a rather quick exposure to odorants at low concentrations). A study done on rats at the Center for Taste and Feeding Behavior in Dijon revealed in 2010 that systemic treatment of known liver XME inducers could regulate nasal XME. Some CYP variants whose transcripts were almost absent at basal levels in the liver were induced by some of these inducers. For example, CYP1A1 and CYP1A2 were induced by aroclor and 3-methylcholanthrene, while dexamethasone induced CYP2A3 and CYP2F4. CYP3A9 was upregulated by several inducers, the most potent being dexamethasone. In the rat olfactory mucosa, these variants were detected in basal conditions, but AR was able to upregulate CYP1A1 and CYP1A2, while dexamethasone induced CYP3A1, CYP2F4 and CYP3A9. UGT2A1 was also upregulated by dexamethasone, as well as SULT1C1 and GSTM2, to only cite some variants.

Transporters were also affected by dexamethasone, notably OAT6, MDR1a, MRP1 and Nrf2. Not only inducers rise transcript levels, they also impacted the enzymatic activity of these enzymes. ALDH3 and ALDH1 responded to phenobarbital, aroclor, 3-methylcholanthrene, dexamethasone and ethoxyquin with an increased enzymatic activity (Thiebaud et al., 2010). In a more recent study on rats aiming to understand the effect of chronic stress on olfaction, mimicked by a systemic glucocorticoid treatment (dexamethasone). The treatment affected rat olfactory function, which was illustrated by reduced electrophysiological response of the olfactory mucosa to odorants. This change was accompanied with an upregulation of nuclear receptors specialized in the response to glucocorticoids (Meunier et al., 2020). Overall, several factors modulating the olfactory signal detection have been identified (Bryche et al., 2021), meaning there is room to explore the modulation of olfaction. But little to nothing is known about the potential effect of odorants in the regulation of nasal XME. In the human saliva, some ALDH and GST variants were upregulated in response to consumption of coffee and broccoli (Sreerama et al., 1995). One could imagine a similar effect of odorants in the nasal epithelium.

2.2. Other peri-receptor events: OBP

OBP are small globular soluble binding proteins of the lipocalin family that are notably abundantly found in the olfactory region. These proteins are able to bind small hydrophobic molecules like odorants, which are small volatile hydrophobic molecules of around 300 and 400 Da, but also volatile pheromones. Thus, this definition does not allow to draw a clear distinction between OBP and other lipocalins binding to other volatile cues. Indeed, OBPs were described as proteins secreted by glands of the mammalian nasal cavity and vomeronasal organ, while similar proteins of the lipocalin family have also been described in other biological fluids such as the urine, salivary, and vaginal secretion, where their role is thought to be related to pheromone-related sexual behavior in some mammalian species. OBPs were also found in the sensillar lymph of invertebrates (notably insects), which can be roughly assimilated to the mammalian nasal mucus as odorants needs to solubilize in the sensillar lymph to bind insects' olfactory receptors (Kuntová et al., 2018; Pelosi, 1994; Tegoni et al., 2000).

OBPs were discovered by Pelosi who published in 1982 his observations of a component of the cow mucosa homogenate capable of binding 2-isobutyl-3-methoxypyrazine, an odorant molecule with a bell-pepper scent (Pelosi et al., 1982). This led to the first OBP characterized from the bovine model (Bignetti et al., 1985). If we focus on the mammalian species of interest in this thesis, three rat OBPs (Briand et al., 2000) and one human OBP (Briand et al., 2002; Lacazette et al., 2000) were described so far.

OBP reversibly bind odorant molecules with an affinity around the millimolar (Briand et al., 2000). Mammalian OBPs are rather nonspecific and usually bind a broad range of odorant molecules, although when species express several variants of OBPs they tend to have their field of predilection and specialize in different odorant families (Löbel et al., 2002; Tegoni et al., 2004). As for the human hOBP2a, it seems to specialize in binding aliphatic and aromatic aldehydes, and to strongly binds to 2-isobutyl-3-methoxypyrazine (Briand et al., 2002; Tcatchoff et al., 2006).

Concerning the function of OBP, several hypotheses cohabit: their binding properties make them good odorant transporters to olfactory receptors, while helping hydrophobic odorants to solubilize in the nasal mucus. Bound to an OBP, odorants may have a longer half-life by being protected from nasal XME. They are thought to actively contribute to odorant discrimination and selectively enhance the contact of odorants with olfactory receptors. Lastly, a passive role of scavenger is attributed to them, which would prevent the saturation of olfactory receptors (Brito et al., 2016; Heydel et al., 2013; Tegoni et al., 2000; Vidic et al., 2008; Yabuki et al., 2011). The insect model *Drosophila melanogaster* allowed to observe olfactory and mating-related behavioral changes in response to the deletion of an OBP gene (Aruci, 2023; Kim and Smith, 2001; Shorter et al., 2016). In humans, gene polymorphism of the OBP is related variation in the bitter perception (Tomassini Barbarossa et al., 2017).

3. Biological models available to study odorant metabolism

Studies in the olfactory field were possible thanks to the availability of common laboratory animal models, either invertebrates like the fruit fly *Drosophila melanogaster*, or mammalian species such as rodents and rabbits. Our consortium published in 2023 a perspective paper presenting an overview of the odorant metabolism field and the tools currently available to explore it, which include organisms

used as models as well as techniques and methods available to the field (Kornbausch et al., 2023). In the present thesis, the focus is on mammalian olfaction, which is why only studies and techniques using models relevant for mammalian physiology will be presented in the next part.

3.1. Animal models: species, methods and findings

The odorant metabolism field is rather new and, in comparison with other fields, the corpus is composed of relatively few studies. Historically, the biological model of predilection is the laboratory animal, from which the first findings on nasal XME were produced. The rat (*Rattus norvegicus*) model has been a gold standard to investigate mammalian nasal XME. For example, UGT2A1 (also called the olfactory UGT) was found to be expressed in the olfactory epithelium and the olfactory bulb using *in situ* hybridization and RT-qPCR on rat tissues (Heydel et al., 2001; Lazard et al., 1991b; Leclerc et al., 2002). The UGT protein was later localized in the rat nasal cavity using immunohistochemistry (Heydel et al., 2001; Neiers et al., 2021) and electron microscopy that allowed to locate UGT2A1 presence in the sensory cilia of olfactory sensory neurons (Neiers et al., 2021). Other animal species complete the rat models: notably, UGT were immunolocalized on the bovine olfactory epithelium (*Bos taurus*), and carboxylesterase in rat, dog (*Canis lupus*), rabbit (*Oryctolagus cuniculus*), and hamsters (*Mesocricetus auratus*) nasal tissues (Dahl et al., 1987; Hadley and Dahl, 1982; Lewis et al., 1994). Various techniques allow the analysis of XME proteins: Mu class GST were identified in the rat and rabbit olfactory mucus using mass-spectrometry (MS) and Western blot (Heydel et al., 2019b; Robert-Hazotte et al., 2019a). The rat model gives easy access to olfactory tissues and its olfactory sensory neurons, which allows the generation of specific proteomes such as the rat sensory cilia proteome (Mayer et al., 2009).

Nasal XME activity has also been assessed on several animal models, thanks to *ex vivo* olfactory explants. Rabbit olfactory explants allowed to measure the metabolism of the mammalian pheromone using gas chromatography coupled with mass-spectrometry (GC-MS). In simpler terms, explants were exposed to the gaseous mammalian pheromone in a closed environment (glass vials), and at regular intervals a portion of the headspace (the air above the explants) was analyzed to measure the remaining mammalian pheromone (Hanser et al., 2017). Proton transfer reaction – mass

spectrometry (PTR-MS) enables a real-time monitoring of odorant metabolism: this technique was used on the rabbit olfactory explant to measure the metabolic capacity of the tissue with and without mucus (Robert-Hazotte et al., 2019a), and on rat olfactory explants to estimate the time-range of nasal odorant metabolism (Robert-Hazotte et al., 2019b). Enzymatic assays were also performed on olfactory tissue homogenates: glucuronidation of odorants by UGT was verified with homogenates of rat olfactory explants (Leclerc et al., 2002), and glutathione conjugation of the mammary pheromone with the rabbit olfactory tissue homogenates and nasal mucus (Legendre et al., 2014; Robert-Hazotte et al., 2019a). The method also allowed the identification of several odorant competitors of the mammary pheromone for GST (Hanser et al., 2017). Rat olfactory tissue homogenates have also been used to produce purified fractions before measuring enzymatic assays of CYP, carboxylesterase, and GST (Nissim Ben-Arie et al., 1993; Hadley and Dahl, 1982; Thiebaud et al., 2013).

Impact of odorant metabolism can be studied with animal models using several approaches: purified bovine olfactory epithelial microsomes have been used in the 90's to demonstrate that the glucuronide-conjugation of odorants attenuated adenylate cyclase activity compared to the original odorants (Lazard et al., 1991b). As explained in part 1.4, adenylate cyclase activity reflects the activation of olfactory receptors, meaning glucuronide-conjugation of odorants by UGT can terminate the odorant signal, as explained in part 2.1. This effect was later confirmed on live animals such as rats that were anesthetized to perform electroolfactograms. UGT metabolites (Leclerc et al., 2002; Neiers et al., 2021), CYP metabolites and carboxylesterase metabolites (Thiebaud et al., 2013) were tested this way. Mice (*Mus musculus*) have been used to illustrate the contribution of odorant metabolites to the olfactory signal: after having verified the conversion of odorant aldehydes into acids, and esters into alcohols by mouse nasal mucus, a behavioral analysis showed that mice were no longer able to detect a scent if this conversion was abolished by the use of an inhibitor (Nagashima and Touhara, 2010). Rabbit neonate are also a useful model to study the behavioral impact of odorant metabolism, as they respond to the mammalian pheromone with a reflex easy to quantify. The pups either detect it, which trigger the reflex, or not. Physically removing GST with a gentle mucus wash or inhibiting GST activity toward the mammary

pheromone using odorant competitors impact the detection threshold of the pheromone, which is visualized by rabbit pups having the reflex when presented with the mammary pheromone at concentrations below the usual detection threshold (Hanser et al., 2017; Robert-Hazotte et al., 2019a).

3.2. Human studies

Despite all the advantages of performing studies on animal models that allow the use of techniques and compounds that would not be ethical in humans, the human model has the great advantage to be relevant to the human biology. To apply findings obtained on animal models to human biology, comparison must be done between human and other animal species. Nasal XME expression in human tissues was verified using RT-PCR, Northern blot, and immunohistochemistry: UGT (Jedlitschky et al., 1999), GSTA1, GSTP1 (Schwartz et al., 2020), DCXR (Robert-Hazotte et al., 2022), CYP (Getchell et al., 1993), and carboxylesterase (Lewis et al., 1994) were notably identified in human tissues with these techniques. Mass-spectrometry allowed the identification of a lot of XME families expressed in human nasal tissues, mucus, and saliva (Boichot et al., 2023; Débat et al., 2007; Kao et al., 2021). Activity of the human nasal XME was also verified with similar techniques as those used in animal models: electroolfactograms can be performed in humans (Knecht and Hummel, 2004), as well as GC-MS on human nasal mucus and saliva (Ijichi et al., 2019). Human *in vivo* studies can be performed to measure odorant metabolism in the nose space and monitor it in real time using PTR-MS (Robert-Hazotte et al., 2022). Besides, metabo-headspace and PRT-MS are routine technique to analyse odorant metabolites in the food and fragrance industry (Schilling, 2009; Schilling et al., 2010). Odorant metabolism in human notably has the particularity to happen from the orthonasal pathway (Ijichi et al., 2019; Robert-Hazotte et al., 2022), but also from the retronasal pathway (Ijichi et al., 2019; Pérez-Jiménez et al., 2021; Schwartz et al., 2021a, 2021b). While the human olfactory capacities to detect odorant cues may seem pale compared to other species whose survival and sexual behaviors are strongly dictated by olfactory cues, human olfaction is particularly adapted to retronasaly discriminate and evaluate the food flavour of our hugely varied diet! Lastly, having human volunteers comes handy to perform sensory evaluation: after having been observed in animal models, the participation of odorant metabolites to the odorant signal (Ijichi et al., 2019)

and odorant-odorant competition (Robert-Hazotte et al., 2022) has been confirmed in humans.

3.3. Human *in vitro* models: from recombinant enzymes to tissue engineering

In depth characterization of XME/OMEs has been possible thanks to biochemistry methods that allows the production of pure and functional recombinant proteins. Human recombinant enzymes have hence been produced and their structure resolved using crystallography. For example, GSTA1 structure has been resolved in presence of glutathione and the primary metabolite dihydrocinnamaldehyde, showing how these actors interact (Schwartz et al., 2020). Recombinant proteins also allow enzymatic assays to attribute XME enzymatic activity toward odorant to specific XME families and variants such as UGT2A1 (Jedlitschky et al., 1999), GSTA1, GSTP1 (Schwartz et al., 2020) and DCXR (Robert-Hazotte et al., 2022). However, such *in vitro* lack the other actors or perireceptors events at play. Co expression of XME variants and OR has been used in a study to show that CYP1A2 impacts the response of an OR (MOR161-2) to acetophenone. CYP1A2 convert acetophenone to methyl salicylate, the later activating MOR161-2 much more than the parent odorant acetophenone. This illustrates again how odorant metabolism can contribute to the odorant signal (Asakawa et al., 2017). Heterologous expression of olfactory receptors can also be used to assign odorant ligands to olfactory receptors. Activation of OR in response to odorant is once again measured via the production of cAMP by adenylate cyclase (Ijichi et al., 2019). Although they serve their intended purpose, these models are also incomplete as they lack the cell populations and the structure of the different types of epithelium lining the olfactory mucosa.

While the human model allows numerous approaches to study odorant metabolism, it certainly lacks the flexibility animal models give. For example, only food grades molecules can be used with living humans, and human tissues can be challenging to obtain, particularly human olfactory tissue. Moreover, data obtained on animal models do not always translate to the human biology, and there is nowadays a real interest in enforcing the 3R (replace, reduce, refine) when it comes to animal experiments and performing ethical science (Hubrecht and Carter, 2019). Although animal models will

certainly still have their purpose and place in the odorant metabolism field, there are nowadays more and more tissue engineered human-based models that could be of use in the field, and that could fill a biological and technological gap between animal and human experiments. So far, no *in vitro* tissue models that would mimic human olfactory mucosa by including neuronal cells are available. It is possible to isolate and cultivate human olfactory stem cells, neuroblasts and olfactory neurons, but they have yet to find an interest for scientists in the odorant metabolism field (Girard et al., 2011).

However, *in vitro* tissue engineered models of different portions of the respiratory tracts are nowadays available (Yaqub et al., 2022).

Among these models are 3D tissue models highly similar to the human *in vivo* respiratory tissues (Mercier et al., 2019). An example of ready-to-use commercially available models are the ones from Epithelix (Switzerland), which reproduce respiratory epithelium from different part of the respiratory tract using human primary cells on Transwells® inserts. Their models display an air-liquid interface and recreate tissues from the upper respiratory tract, with MucilAir™ mimicking epithelium of the nasopharynx, to the lower respiratory tracts with SmallAir™ for lung models and alveoli. Co-culture with fibroblasts is also available, with epithelial cells on the apical side of Transwell® inserts and fibroblasts on the basal side. Of course research groups have been using custom models relying in the same principles: for example, tracheal and mesenchymal cells cocultures (Le Visage et al., 2004). Such models can be used to investigate molecular mechanism of cystic fibrosis (Sette et al., 2021).

Nasal epithelial models on chip can also be used via modification of Transwell® inserts to include microfluidics (Wang et al., 2014) or via NEM-on-a-chip device (Gholizadeh et al., 2021), and can be used for toxicity or drug delivery assays. Transwell® and organ-on-chips have the advantage or displaying a mature/differentiated ciliated respiratory epithelium. However, they are respiratory epithelium models and not respiratory mucosa models, as they lack the basal extracellular matrix. Human nasal organoids are usually grown on Matrigel and display ciliated cells, basal cells, goblet cells, and overall a 3D structure close to the *in-vivo* situation. They have been used for infection studies with viruses such as SARS-Cov-2 (Chiu et al., 2022), molecular mechanisms of inflammation diseases such as chronic rhinosinusitis (Ramezanpour et al., 2022) or cystic

fibrosis (Amatngalim et al., 2022; Liu et al., 2020). Although their highly differentiated phenotype is impressive, such culture system does not allow an air-liquid interface which can be incompatible for certain studies using gaseous, aerosols or particles treatments.

Last but not least, the small intestinal submucosa (SIS) scaffold-based 3D respiratory mucosa model that was developed at the Chair of Tissue Engineering and Regenerative Medicine in Würzburg, Germany, is also an air-liquid interface model. It resembles the 3D cultures obtained from Transwell® inserts, at the exception that an organic acellular matrix replaces the synthetic insert. Another difference is that the model is a co-culture of epithelial cells and migrating fibroblasts, which shows a higher *in-vivo*/*in-vitro* correlation than an epithelial monoculture on the SIS scaffold (Steinke et al., 2014). 3D models based on SIS scaffold were previously shown to be more resilient to infection studies than Transwell®-based models (Heydarian et al., 2019). Details on the obtention of such model concerning nasal respiratory epithelium are clarified in the material and method part of this report. 3D respiratory mucosa models so far were mostly used for host-pathogens interaction studies (Bianchi et al., 2021; Derakhshani et al., 2019; Kessie et al., 2021; Sivarajan et al., 2021), and ciliopathies (Pollara et al., 2022).

Respiratory tissue models are known to emit volatile compound that can be detected in the tissue headspace (Schivo et al., 2014; Yamaguchi et al., 2018), and some XME activity have even been measured in other contexts than the olfactory field (Bovard et al., 2020).

Respiratory tissues have yet to be explored in the context of odorant metabolism and olfactory function. It has been shown that both olfactory and respiratory mucus contributed to odorant metabolism in humans (Ijichi et al., 2022), which leaves the space open to explore more deeply the exact contribution of respiratory tissue.

ANIMALS, MATERIALS, AND METHODS

This part explains the different methods used to investigate XME expression, gene regulation, protein localization and/or odorant metabolism in a physiological olfactory context, and present as well the models used to do so. “Olfactory event” designates a short exposure of odorants at low concentrations, if possible using odorants on a gaseous phase. I chose to present these technical aspects in two parts: the first focuses on the rat olfactory explants model, and the second on the human nasal respiratory mucosa model. By doing so, it will sometimes be repetitive. However, these two models were used in two different laboratories, each of them having their own routine that can slightly differ from each other, and some techniques were used on one model and not the other. By sorting the techniques depending on the nature of the model used, I intend to remove any confusion on how the two models were used.

1. *Ex vivo* rat experiments

Rat olfactory explants were used *ex vivo* to investigate the expression of some XME as well as their potential regulation by odorants. As previously explained in the introduction, using thawed explant (previously frozen to be conserved) reduces the number of rats used, as the olfactory tissue can be harvested on rats used for other scientific purposes and stored at -80 °C until their use. Freshly dissected rat olfactory explants were also used: in the result part, we will see that freezing the tissue impact its response to odorant treatment and the possible readouts. Thawed tissues were previously and successfully used in Prf. Heydel’s team to study odorant metabolism, and fresh explants to perform electroolfactograms.

1.1. Animals

Dissection of rat olfactory mucosa explants

Six-week-old male Wistar rats (Janvier Labs) were housed in 3 individuals per cage and maintained on a 12-hour light/12-hour dark cycle with food and water *ad libitum.* The project received the agreement of the ethical committee: APAFIS#27695-2020101511076483 v1. Olfactory mucosae of 7-week-old rats were harvested. Briefly, rats were decapitated thanks to a rodent guillotine while being restrained in a DecapiCone (Braintree Scientific). Rats were gently encouraged to walk into the DecapiCone to prevent unnecessary stress and potential capillary rupture in the

olfactory mucosa. After the skin and the inferior jaw were removed, the skull was opened in a sagittal section thanks to firm pressure from a scalpel knife, thus exposing the olfactory mucosa. The septum was gently removed when present after the cut. The olfactory bulb was then scooped out, the ethmoid bone cut, and the olfactory mucosae freed. Thin forceps were used to gently detach the mucosa. Two hemi-mucosae were harvested for each rat (one per nostril) and were either snap-frozen together in a cryotube with liquid nitrogen or directly used for odorant exposure.

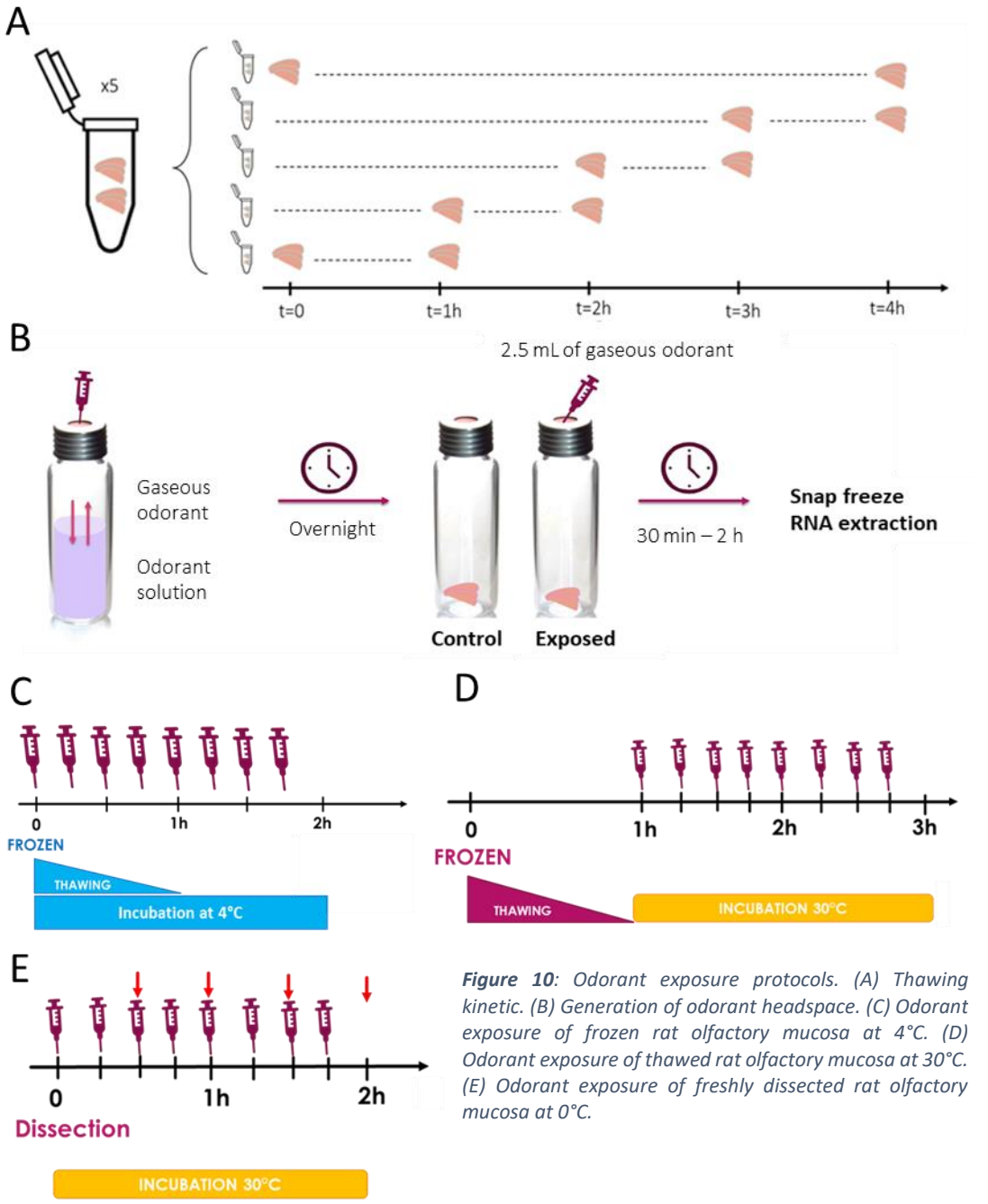

***Figure 10**: Odorant exposure protocols. (A) Thawing kinetic. (B) Generation of odorant headspace. (C) Odorant exposure of frozen rat olfactory mucosa at 4°C. (D) Odorant exposure of thawed rat olfactory mucosa at 30°C. (E) Odorant exposure of freshly dissected rat olfactory mucosa at 0°C.*

Thawing kinetic

The viability of thawed mucosae was assessed thanks to a kinetic; 5 animals were used for this experiment. Hemi-mucosae were placed individually in 1.5 mL tubes (Eppendorf) and thawed on ice for 0, 1, 2, 3, or 4 h (Figure 10A). Explants were snap-frozen in liquid nitrogen to stop any cellular process when they reached their defined time points. Total RNAs were extracted as described in the RT-qPCR part in 3.2. RNA Integrity Number (RIN) was measured using the Agilent RNA 6000 Nano Kit. RNA samples were not treated with DNase I before RT-qPCR.

1.2. Odorant exposure

Rat olfactory explants were small enough to allow gaseous odorant treatment in vials specifically used to analyse compounds in the headspace of a material (here, olfactory explants). This part describes the methods to expose the olfactory explants to odorant in a way that imitates best what happened in the rat's nose when it sniffs. The short exposure time also means that I was looking for a short-time gene regulation of XME in response to odorant molecules.

Odorant chemicals

2,3-pentanedione (W284106, Sigma Aldrich) is Food Grade, registered in the FOOD Chemical Codex, and has a purity ≥96%. Absolute ethanol 99%+ Laboratory Reagent Grade (CAS 64-17-5), was purchased from Fisher Scientific.

Gaseous odorant treatment

Rat olfactory mucosa explants were exposed to gaseous odorant generated in the headspace of 10 mL of an odorant solution via an overnight incubation. For each exposure experiment, olfactory hemi-mucosae from the same rat were separated in two glass vials. One of the hemi-mucosae was exposed while its counterpart served as a negative control (Figure 10 B), in order to erase any variation that might occur between individuals. Mucosae were either frozen directly after dissection and thawed before or during exposition (Figure 10C and 10D, respectively) or used directly after dissection (Figure 10E). More precisely, thawed mucosae were either exposed to the odorant as they thawed on ice or thawed on ice for one hour and then exposed to the odorant at 30°C. I indeed tried several modalities to optimize the protocol: I wanted to see an effect, but also preserve the tissues (and especially RNAs) from degradation. Depending on the exposure experiment, 2.5 mL of odorant headspace were injected every 15

minutes for 30 minutes, 1 hour, 1 hour and a half, or 2 hours. Once odorant exposure was done, all samples were snap-frozen in liquid nitrogen and stored at -80°C until RNA extraction.

1.3. Reverse transcription-quantitative polymerase chain reaction (RT-qPCR)

Following odorant treatment, the olfactory tissues were collected and processed to analyse short-time regulation of target XME in response to a rapid exposition with odorants at low concentrations. This required several steps: samples must be processed to isolate RNAs, then some messenger RNA expression was analysed using RT-qPCR.

Sample preparation

Total RNAs from rat olfactory samples were extracted at the CSGA using 500 µL of TRIzol reagent per hemi-mucosa (Invitrogen™ TRIzol™ Reagent, CAT 15596026, Fisher Scientific). The following steps are adapted from the fabricant's protocol: samples were individually homogenized for 2 minutes at 30 Hz with a tungsten ball in a Tissue Lyzer (QIAGEN), left for 5 minutes at room temperature, then 200 µL of chloroform were added and mixed. Samples were left for 3 minutes at room temperature, then centrifuged at 15000 *g*, 4°C, for 15 minutes. The aqueous supernatant was then taken in a new tube with 500 µL of isopropanol. After 10 minutes at room temperature, samples were centrifuged again for 10 minutes at 15000 *g*, 4°C. Supernatants were discarded and RNAs were washed twice using the following steps: RNAs were mixed with 500 µL of ethanol 75%, left for 4 minutes at room temperature, then centrifuged for 5 minutes at 15000 *g*, 4°C. Supernatants were discarded after each wash. Pellets were then left to dry for 5 minutes and then resuspended in 200 µL nuclease-free water (DEPC-treated, ThermoFisher Scientific). RNAs were quantified with a NanoDrop One (ThermoFisher Scientific) and diluted to 250 ng/µL, then stored at -80°C. Before cDNA synthesis, RNA integrity was controlled with agarose electrophoresis. Gels were prepared in TAE 1X buffer (prepared from Tris-acetate-EDTA 50X buffer, Fisher Scientific) with a ratio of 100 mL TAE for 1 g of agarose powder (Sigma Aldrich) and 2 µL of ethidium bromide (Thermo Scientific). For each sample, 500 µg of RNA were prepared in a DNA gel Loading Dye 6X (R0611 ThermoFisher Scientific) and deionized water for a final volume of 6 µL. Samples migrated 30 to 45 minutes at 90 V in the TAE buffer. RNAs were treated by DNase I (Ref 18047019, ThermoFisher Scientific), according to the

fabricant's protocol, unless told otherwise in the "results" part. cDNA synthesis was performed using the iScript™ cDNA Synthesis Kit (rxns #1708891, Bio-Rad) on 1 µg of RNAs, according to the fabricant's protocol, then stored at 4°C until PCR experiments.

RT-qPCR

PCR experiments were performed on a ViiA7 Real-Time PCR System (Applied Biosystem) on 384 well PCR plates using the Takyon™ Low ROX SYBR 2X MasterMix dTTP blue kit (Cat UF-LSMT-B0701, Eurogentec). The PCR protocol was adapted to save products: 5 µL of Takyon Master Mix, 1 µL of primers diluted to 1/50, and 4 µL of cDNA diluted to 1/5 were added per well. PCR experiments were performed following the fabricant's regular protocol: 3 minutes at 95°C for Takyon activation, then 40 cycles (10 seconds of denaturation at 95°C, 60 seconds of annealing/extension at 60°C).

The primers used are: *Adh1*: forward 5'-CAACCCTCAAGACTACACCAAACCC-3', reverse 5'-ACCCCGACAATGACGCTTACAC-3'; *Aldh2*: forward 5'-GTGTTCGGAGACGTCAAAGA-3', reverse 5'-GCAGAGCTTGGGACAGGTAA-3'; *Dcxr*: forward 5'-ACAGGTTGTGGCGGTGAGT-3', reverse 5'-TTGCTTAGGGCCTGTTCTGT-3'; *Cyp2e1*: forward 5'-TCTGCTCCTGTCTGCTATTCTGC-3', reverse 5'-GGATACTGCCAAAGCCAACTGTG-3'; *c-fos*: forward 5'-ACGACCATGATGTTCTCGGG-3', reverse 5'-TCTGCGCAAAAGTCCTGTGT-3'; *Sart1* (HAF): forward 5'-CTGTTAAGAAAGAGGCGGGC-3', reverse 5'-TCCCGTAGTTCTTCACGCTG-3'; *Bax*: forward 5'-AGGGTTTCATCCAGGATCGAGC, reverse 5'-ATCGCCAATTCGCCTGAGACAC-3'; *Bcl2*: forward 5'-AGCGTCAACAGGGAGATGTCAC-3', reverse 5'-AGTTCCACAAAGGCATCCCAGC-3'; *Casp3* (intronic sequence): forward 5'-TCTGCTGCTTTCGCGCTTTC-3', reverse 5'-TTCTCTGCCTTCAGTGCTTGCC-3'; *Actb*: forward 5'-GGAGATTACTGCCCTGGCTCCTA-3', reverse 5'-GACTCATCGTACTCCTGCTTGCTG-3'; *B2m*: forward 5'-ACATCCTGGCTCACACTGAA-3', reverse 5'-ATGTCTCGGTCCCAGGTG-3'; *Cdkn1b*: forward 5'-TGGTGGACCAAATGCCTGACTC-3', reverse 5'-CTGTTGGCCCTTTTGTTTTGCG-3'; *Rpl30*: forward 5'-CGCCAACAACTGTCCAGCTTTG-3', reverse 5'-ATTTTCCACACGCTGTGCCC-3'; and *ubc*: forward 5'-ACAGGCAAGACCATCACTCTGG-3', reverse 5'-AAGACACCTCCCCATCAAACCC-3'.

PCR analysis

Results were extracted from QuantStudio™ Real-Time PCR software to an Excel table. Amplification data were read thanks to the Linreg software, which determined

baselines, corrected CT (cycle threshold), and provided PCR efficiency per well. The expression ratio R of genes of interest for each condition was then calculated as follows, according to Ganger's work (Ganger et al., 2017):

1- **CT_w** calculation, which corresponds to the CT pondered by the PCR efficiency (E)

$$1.\ CT_w = CT \times \log_{10}(E)$$

2- **ΔCT_w** calculation, which is the normalization by reference genes

$$2.\ \Delta CT_w = CT_{w\ target} - Mean\ (CT_{w\ reference\ genes})$$

3- **$\Delta\Delta CT_w$** calculation, to compare gene expression differences between control and treated conditions for each rat.

$$3.\ \Delta\Delta CT_w = \Delta CT_{w\ control} - \Delta CT_{w\ exposed}$$

4- **$\Delta\Delta CT_w$ Mean** calculation

5- **T-test**: the experimental mean is compared to a theoretical mean of 0

6- Calculation of **R** (expression ratio)

$$6.\ R = 10^{-(\Delta\Delta CT_w)}$$

After primer validation, all reference genes were thoroughly tested on samples representing (control and treated) using PCR. PCR results were then analyzed through RefFinder (Xie et al., 2012), an online tool that regroups four methods to identify the most suitable reference genes.

2. *In vitro* human experiments

In a second time, I focused on a human-based model of the nasal respiratory mucosa. While it is not an olfactory tissue, it lines a huge majority of the human nasal cavity and thus is at the contact with odorants before the molecules reach the human olfactory tissues. First, the method to generate these tissues is explained. This type of tissue models recreates the structure of the respiratory mucosa, but were so far never used to study perireceptor events, contrarily to the rat olfactory explants. It was thus necessary to characterize first the model in terms of XME expressed in the tissue models: this was done using single-cell RNA sequencing (to explore any XME isoform the model might express) and RT-qPCR (to confirm the expression of some XME targets). The protein counterpart of some XME targets was investigated using histology, more precisely immunofluorescence that nicely show where the enzymes are present in the tissue models. Like for the rat olfactory explants, the short-time regulation of target XME in response to a short exposure to odorants at low concentration was investigated using RT-qPCR. And lastly, to study odorant metabolism by the tissue models, two different techniques were optimized. The first one used tissue model's homogenates, which was less complicated to optimize as it was already performed on the rat olfactory explant for studies not related to this Ph.D thesis. The method allowed to investigate whether the XME enzymes detected by immunofluorescence were indeed functional and metabolized odorant substrates. And the second method, which took longer to optimize but is now ready to use in further studies, measures the odorant metabolites released in the headspace of the tissue models when they are exposed to odorants. It conserves the structure of the tissue model, notably the air-liquid interface that imitates so well the human *in vivo* respiratory mucosa, and recreate what might happen in the human nasal cavity when odorants are inhaled. In summary, studying the odorant metabolism with this model aims to understand if and how the human respiratory mucosa can participate in the odorant metabolism that affect the olfactory perception. Metaphorically speaking, odorant metabolism has been so far centred on olfactory tissue, and I aim to investigate whether the respiratory suburbs could also be involved.

2.1. Human respiratory mucosa 3D cell culture model generation

Building the human nasal respiratory tissue models requires nasal epithelial cells as well as fibroblasts. Here, these two cell types come from biopsies and must then be isolated before building the models.

All cell culture media were supplemented with Penicillin/Streptomycin (P4333, Sigma Aldrich, Germany). AECGM (Airway Epithelial Cell Growth Medium, defined, Cat PB-C-MH-350-0099, PELOBIOTECH GmbH, Germany) was supplemented with the corresponding supplement kit sold with the bottles, without gentamycin. DMEM (Dulbecco's Modified Eagle Medium (1X), high glucose, GlutaMAX™, HEPES, ref 32430-027, ThermoFisher Scientific, Germany) was supplemented with 10% FCS (Foetal Calf Serum, PAN biotech, Germany).

Primary cells isolation

Human nasal epithelial cells (HNEC) and nasal fibroblasts (nFb) were isolated from biopsies from donors undergoing functional sinus surgery or by brush biopsies. Surgery and tissue collection were performed at the Department of Otorhinolaryngology, Plastic, Aesthetic, and Reconstructive Head and Neck Surgery of the University Hospital Würzburg by trained otolaryngologists. Written informed consent was obtained beforehand, and the studies were approved by the institutional ethics committees on human research of the Julius-Maximilians-University Würzburg (votes 182/10, 179/17 and 116/17). In this part, all further cell culture and incubations were performed at 37 °C with 5 % CO_2.

For surgical biopsies, tissues were cut into pieces (about 1 mm diameter) in sterile Petri dishes, then cultured for around 10 days with AECGM until HNEC growing out of the biopsy pieces reached 80% to 90% confluence. Cells were then frozen: cells were briefly washed with DPBS (Dulbecco's Phosphate Buffered Saline, Modified, without calcium chloride and magnesium chloride, liquid, sterile-filtered, suitable for cell culture, D8537, Sigma-Aldrich, Germany) then detached with a 5-minutes with trypsin 1X (0.5% Trypsin-EDTA (10X), no phenol red, Gibco, Cat 15400054, ThermoFisher Scientific, Germany). Trypsin was then deactivated with DMEM and cells were centrifuged for 5 minutes at 1200 rpm, room temperature. Supernatants were discarded, and cells were then resuspended in FCS + 10% DMSO (Dimethyl sulfoxide, D8418-100ML, Sigma Aldrich,

Germany), frozen, and kept in liquid nitrogen (~10^6 cells/mL/vial) until models were built. The remaining pieces of biopsy were digested with collagenase 1X for 20 minutes

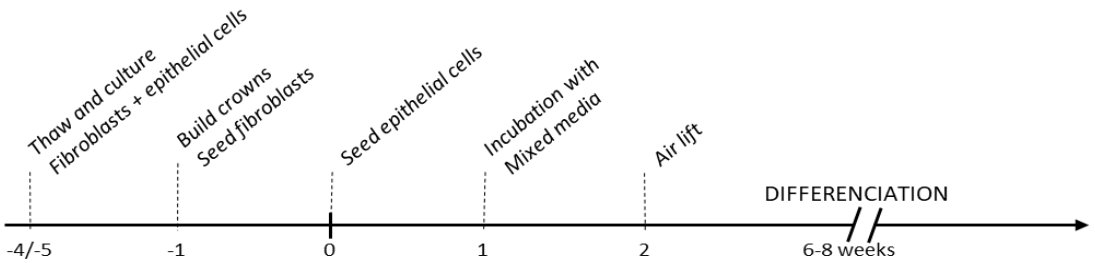

***Figure 11**: 3D human nasal respiratory mucosa generation timeline. Cells (fibroblasts and epithelial cells) were thawed up to 5 days before seeding cells, and scaffold inserted inside crowns a day prior epithelial cells seeding. Seeding epithelial cells marked day 0 of 3D models. Crowns were differentiating for 6 to 8 weeks before being treated with odorants.*

then suspended in DMEM and cultured for around 10 days in a sterile Petri dish until nFb growing out of them reached 80% to 90% confluence. Fibroblasts were then frozen following the same steps the epithelial cell went through.

***Table 1**: Donor's information*

Sex	Age
Female	25
Female	27
Female	34
Female	36
Female	38
Female	42
Female	70
Female	80
Male	24
Male	30
Male	31
Male	35
Male	40
Male	40
Male	45
Male	45
Male	45
Male	47
Male	50
Male	57
Male	60
Male	60
Male	63
Male	63
Male	68
Male	71

Concerning brush biopsies, brushes were "washed" out of trapped epithelial cells in AECGM. Culture media now containing HNEC was cultured in a T25 flask (600950-collagen type 1 CELLCOAT, Greiner Bio-one) until the generation of the model and cultured until differentiation. HNEC and nFb – donor matched when possible, as no nFb can be isolated from brush biopsies – were thawed quickly and cultures in T75 flasks (90076 TPP for fibroblasts; 659850-collagen type 1 CELLCOAT, Greiner Bio-one for epithelial cells) with hAEC and DMEM media, respectively, until 80% to 90% confluence was reached. In the meantime, scaffolds that will serve as the matrix for 3D models were fixed between two sterile tailored metal or plastic rings called cell crowns, one pair equalling one model. This scaffold consists of the small-intestinal submucosa (SIS) of pig jejunum prepared routinely in the lab (Schweinlin et al., 2017). Animal research was performed according to the German law and institutional guidelines approved by the

Ethics Committee of the District of Unterfranken, Würzburg, Germany (approval number 55.2-2532-2-256). Cell crowns were then incubated with 2 mL DMEM per crown in 6 well plates for at least 2h, then seeded with 50,000 fibroblasts per crown and incubated overnight. The next day, which is day 0 of the 3D model, crowns were seeded with 250,000 nasal epithelial cells per crown and incubated overnight with 500µL of AECGM per crown of the apical side. On day 1, crowns were incubated with 500µL of mixed media (50% AECGM and 50% DMEM). Airlift was performed on day 2, and models were kept in culture until they were differentiated and used. Differentiation took between 6 and 8 weeks of culture, with media change (mixed media) performed every 2 to 3 days (see Figure 11). Passage number did not exceed 10 for fibroblasts, and 2 for epithelial cells. A mucus wash was performed every week using 200 µL of warm DPBS per crown. The differentiation stage was followed by the visual presence of mucus (brilliant surface, sticky film being aspired during mucus wash) and cilia (at the microscope). Age and sex of the donors are summarized in Table 1.

2.2. Odorant exposure

As explained, tissue models were exposed to odorant in conditions as close as possible to an olfactory event: a brief (maximum 2 h) exposure to lowly concentrated odorant (overall, a few ppm, maximum 250 ppm, which would already be perceived as a strong and almost disagreeable odor *in vivo*). This was true for most experiments except for odorant metabolism experiments performed using tissue model's homogenates, where the aim was to primarily verify that it was possible to perform odorant metabolism studies by verifying that the enzymes were active towards odorant substrates. Tissue models do not fit the vials used with the rat olfactory explants: I had to imagine other ways to introduce odorants: I first nebulized odorant solutions to imitate aerosols. In a second time, I also directly treated the models with an odorant solution, to obtain more readouts with the models. Gaseous treatment would require more time to imagine and optimize an appropriate protocol.

Compounds

The following chemicals (2,3-pentanedione, 3,4-hexanedione, 4-hydroxy-3-hexanone, benzaldehyde, benzyl alcohol, benzoic acid, methanol, tert-butyl methyl ether (MTBE), ketoconazole (KET), N-ethylmaleimide (NEM), pentanoic acid, citral, benomyl, disodium

sulfate and human albumin), were purchased from Merck (Sigma-Aldrich). Ethanol was purchased from Carl Roth, and Dexamethasone from Thermofisher Scientific, the NADPH-regenerating kit (500x Glucose-6-phosphate dehydrogenase, 400 units/mL), assay buffer I (25 mL), and assay buffer II (25 mL, Lot: GR3406548-6, Abcam) were purchased from Fisher Scientific (Thermo Fisher Scientific). Depending on the experiments, odorant solutions were prepared differently. For odorant exposure and XME gene regulation experiments, ethanol and 2,3-pentanedione were diluted in demineralized water + 1% NaCl 0.9% for nebulization experiments. Concerning direct liquid treatment of odorants, the diluent was only sterile water. Dexamethasone was diluted in DMSO at 20mM, then 5 µL/mL if this stock solution was diluted in water to obtain a final concentration of 100µM. For odorant metabolism experiments on 3D model homogenates, the odorants (3,4-hexanedione and benzaldehyde) were diluted in ethanol [50% (v/v)] to obtain a 5,000 ppm odorant solution, as were the inhibitors benomyl (2.5 µmol/L), citral (400 nmol/L), KET (1 mmol/L), to produce the desired concentrations. NEM and pentanoic acid were diluted in H_2O to gain a concentration of 10 mmol/L and 9 mmol/L, as was human albumin (104 mg/mL).

Odorant nebulization

As the human 3D cell culture model demands more space and a sterile environment, using the headspace to perform the odorant exposure in glass vials was not an option. The choice was made to substitute headspace odorant exposure with odorant aerosol treatment using a VitroCell Cloud device to treat cell cultures. Briefly, the base block allows cell inserts to be in contact with a 37°C heated medium, while the Cloud aerosol chamber contains the cloud formed after the nebulization of liquids. On top of the chamber, the Aeroneb nebulizer applies an electric current to a mesh with defined pores. Ions in the liquid then allow it to be nebulized through the membrane. The control to verify the good functioning of the Aeroneb device is realized by nebulizing 200 µL of sodium chloride (NaCl) 0.9%, which should form a cloud in approximately 30 seconds.

For each odorant exposure, 200 µL of odorant solutions were nebulized. Five minutes after the nebulization all of the cloud dropped and inserts were put back in their plate with fresh culture medium. Optimization of odorant solutions for ideal nebulization is shown in the results part.

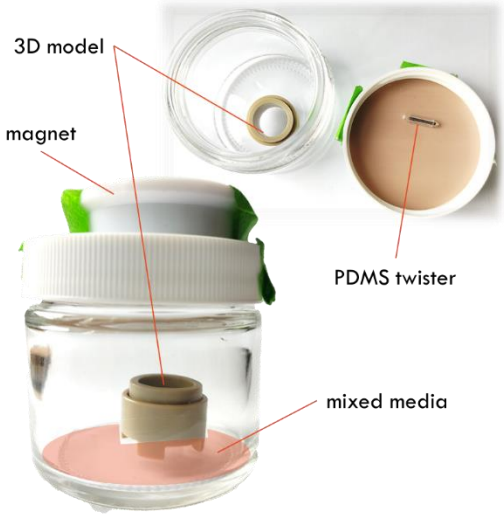

***Figure 12**: Experimental set-up for odorant treatment and capture of compounds in the headspace. Jars allowed a closed environment for the twisters to only capture compounds in the headspace of treated or untreated models. Culture medium was placed at the bottom of the jars to incubate cell crowns in the best possible conditions.*

Direct liquid treatment – odorant metabolism

In order to get more readouts from 3D models, a protocol from Yamaguchi's team was adapted to the 3D model to measure odorant metabolites, and collect samples for PCR and histology experiments (Yamaguchi et al., 2018). Crowns were individually placed in jars (Environmental Express APC3130 Straight-Side Glass Jar, Level 3, Clear, 60 mL, Cole-Parmer Instruments, Germany) containing 4 mL of mixed media. Twisters (PDMS-coated GERSTEL Twisters, 011222-001-00, WICOM GmbH, Germany) were magnetically attached to the lid (see Figure 12) in order to be exposed to the crown headspace. As soon as crowns were treated with 200 µL of the solutions, jars were closed and incubated 2 h at 37°C with 5% CO_2. Twister were then removed from lids, put back in their individual storage bottles and kept at -80°C until analysis at the Lehrstuhl für Aroma- und Geruchsforschung (Henkestr. 9, 91054 Erlangen, Germany). Mucus and culture media were sampled and stored at -80°C until analysis at the Centre for Taste and Feeding Behavior (CSGA) in Dijon. Fate of crowns then depended on the experimental plan and were either fixed for histological purpose or lysed for RNA extraction.

2.3. MTT test

When using compounds, toxicity is a matter of concentrations. The rule is the same with odorant molecules: the aim was to use concentrations that would not be toxic for the tissue. This was verified by using the MTT test, which assesses cell metabolic activity using colorimetry that is supposed to reflect cellular viability. Briefly, NADP(H)-dependent oxidoreductases reduce yellow tetrazolium dye MTT (3-(4,5-dimethylthiazol-2-yl)-2,5-diphenyltetrazolium bromide) into insoluble purple formazan. To perform this test, crowns were previously treated with odorants as per described in the odorant exposure part, and incubated for 2 h at 37°C with 5% CO_2. Odorant solutions and media

were rinsed away using DPBS, then crowns were incubated in the mixed culture media containing 1 mg/mL of MTT for 3 h, both on basal side and apical side. MTT-media mixture was then washed away using DPBS. Remaining scaffolds were then taken out of crowns and individually incubated at room temperature un 15 mL tubes (Falcon) containing 6 mL of 0.04 N HCl + isopropanol. The later solutions solubilize formazan crystals within a few hours. Once all the color is washed away, scaffolds were removed from tubes, and levels of 0.04 N HCl + isopropanol solvent were evened. Solutions were diluted if necessary, and absorbance at λ=570 nm was then measured at the TECAN reader (TECAN infiniteM200, TECAN, Switzerland). Blanks containing only the solvent were also measured. All measures were normalized by subtracting blank values. For each donor, cell viability was calculated using the following equation:

$$Cell\ viability = \left(\frac{treatment}{control}\right) x100$$

2.4.RTq-PCR

Like with the rat olfactory explants, target XME gene expression and regulation in response to odorant substrates were investigated using RT-qPCR. Samples were prepared to isolate RNAs with a different method. Both methods (TRIzol reagent or the kit) isolate total RNA; while the first is longer, it is easily adaptable to a lot of tissue. The kits are quicker but usually adapted to some sample types (bone, cells, soft tissue, etc.). Kits are also more expensive than the method using TRIzol reagent.

Sample preparation

Total RNAs were extracted using the E.Z.N.A.® Total RNA Kit II (SKU: R6934-01, Omega BIO-TEK, USA). RNAs were resuspended in DNase-free water provided by the kit, then quantified using the TECAN reader (TECAN infiniteM200, TECAN, Switzerland). cDNAs synthesis and PCR were performed according to the protocol described for rat experiments, but using a Biorad thermocycler (CFX96 Touch Real-Time PCR Detection System, Biorad, Germany). The primers used are: *DCXR*: forward 5'-CCGAGTGAATGCAGTAAAC-3', reverse 5'-TTCGGTTCAGCATAGTCTTG-3'; *ALDH1A1*: forward 5'-CCAAAGACATTGATAAAGCCATAA-3', reverse 5'-CACGCCATAGCAATTCACC-3'; *ALDH3A1*: forward 5'-TACCGGGAGAGGCTGTGTCA-3', reverse 5'-GTAGGCGTTCCATTCATTCTTGTG-3'; *AKR1B10*: forward 5'-CCTGTAACGTGTTGCAATCCTC-3', reverse 5'-CAGCACCTCGATTCTCGTCT-3'; *GSTP1*:

forward 5'-TATGGGAAGGACCAGCAGGA-3', reverse 5'-CATCCTTGCCCGCCTCATAG-3'; *GSTA1*: forward 5'-CAGGACGGTGACAGCGTTTAAC-3', reverse 5'-CATTCTGCCCCGTGCATTGAAG-3'; *GSTO1*: forward 5'-AAGGCCAAGGGAATCAGGCAT-3', reverse 5'-TGCCACCAAAGAAGGTCGTC-3'; *GSTO2*: forward 5'-CAATCCTGGTCCGGTTGCC-3', reverse 5'-CCCGAGAGTAGGAGCGGT-3'; *AhR*: forward 5'-GCCGGTGCAGAAAACAGTAA-3', reverse 5'-ATCTTGTGGGAAAGGCAGCA-3'; *NFE2L2* (Nrf2): forward 5'-AGGTTGCCCACATTCCCAAA-3', reverse 5'-ACGTAGCCGAAGAAACCTCA-3'; *NR1C3* (PPARG): forward 5'-CCAGAAGCCTGCATTTCTGC-3', reverse 5'-GTGTCAACCATGGTCATTTCGTT-3'; *B2M*: forward 5'-TGCCGTGTGAACCATGTGA-3', reverse 5'-CGGCATCTTCAAACCTCCAT-3'; and *HPRT*: forward 5'-TGAGGATTTGGAAAGGGTGT-3', reverse 5'-TCCCATCTCCTTCATCACATC-3'.

PCR analysis

Results (cycle threshold data) were extracted from Biorad CFX Manager software to an excel table. Efficiencies were calculated for each primer pair using the slope created by CT obtained from series dilution. Reference genes were chosen with the same method described in the rat experiment part. Concerning human experiments, B2M and HPRT were the most stable and consequently were chosen as reference genes.

2.5.Single-cell RNA sequencing (scRNA-seq)

ScRNA-seq dataset was used here to investigate any XME isoform that could be expressed by the tissue model. It was for sure quicker to browse the dataset than to blindly do RTq-PCR without knowing whether negative results (no amplification) was due to the target gene not being expressed, or to the primers tested not being optimal to amplify the messenger RNAs.

ScRNA-seq was performed on the 3D human nasal respiratory mucosa model by Dr. Rinu Sivarajan, then PhD student at the TERM. Dr. Sivarajan kindly provided access to the scRNA-seq data base for my own project. Briefly, models from 3 different donors were cultured until differentiation, then cells were separated from one-another using an enzymatic cocktail. For each donor, four individual tissue models were pooled. After cell to cell dissociation, cell viability was above 85 %. Samples were then sent and sequenced at the Helmholtz Institute for RNA-based Infection Research, Würzburg (Dr. Fabian Imdahl, under the supervision of Prof. Antoine Emmanuel Saliba). Samples were

processed on a 10x Genomic chips, processed according to the GEM Single Cell 3' Reagent Kits v3.1 user guide. The generated libraries were sequenced on a NovaSeq 6000 platform at 50,000 reads per cell. Data were clustered and analyzed to build the database at the Institute of Virology and Immunobiology, Würzburg University (Kevin Berg, under the supervision of Pr. Florian Erhard). Briefly, the data set was processed, after mapping, in R (v. 4.1.2 (R Core Team, 2018)). QC, Normalization, Donor demultiplexing (Core unit). To annotate the cell types, the IntegrateData function of the Seurat package (v. 4.3 (Butler et al., 2018; Hao et al., 2023, 2021; Satija et al., 2015; Stuart et al., 2019)) was used with standard parameters to integrate the data into a single cell atlas of the human healthy airways (Deprez et al., 2020), using the nasal and proximal airways data from the atlas, and calculated the nearest neighbor graph (k = 50). Subsequently, all unannotated cells were labelled according to the most prevalent cell type in their nearest neighborhood. Finally, the data set was extracted from the atlas and removed all cells of cell types with less than 50 specimens. The UMAP, Violin and Feature Plots were created with the Seurat package. From the scRNA-seq, I extracted information on phase I and phase II enzymes, as well as phase III transporters. Information of genes with a mean value <0.010 are not listed.

2.6. Histology

Histology experiments aimed to characterize and verify the structure of the individual models (as depending on donors, cell do not always differentiate), but also the characterize the presence and localization of target XME on the protein level.

Sample fixation, embedding, and cutting

Tissues were washed both on apical and basal side using DPBS, then fixated by incubating the crowns 1h at room temperature with ROTI®Histofix 4 % Formaldehyde (Carl Roth, Germany) both on apical and basal side. The next day, scaffold were removed from crowns and embedded in paraffin in a Microm STP 120 Spin Tissue Processor (Thermo Fisher Scientific, Germany), using the following protocol Table 2:

***Table 2**: Embedding protocol.*

Washing step	Purified water, 1h
Ascending alcohol series *H_2O removal*	Ethanol 50%, 1h
	Ethanol 70%, 1h
	Ethanol 80%, 1h
	Ethanol 96%, 1h

	Isopropanol 1, 1h Isopropanol 2, 1h
Alcohol removal	1:2 isopropanol-xylol mixture, 1h Xylene 1, 1h Xylene 2, 1h
Paraffin embedding	Paraffin 1, 1.5h Paraffin 2, 5h

Models were then molded in paraffin blocks, then cut into 4 µm sections with a rotative microtome (HistoCORE AUTOCUT, Leica). Sections were recovered with polysine-coated glass slides then dried overnight at 37°C.

Immunostaining

Prior to any immunostaining, sections went through the following protocol Table 3:

***Table 3**: Histology hydration, unmasking and blocking steps. The following steps are common between DAB and immunofluorescence staining.*

Melting paraffin	60°C, 5-10 minutes
Paraffin removal	Xylol, 5 min, X2
Xylol removal *Followed by ethanol removal* *Then rehydration*	Ethanol 96%, dip 3 times, X2 Ethanol 70%, dip 3 times Ethanol 50%, dip 3 times Deionized Water, until the next step
Unmasking epitope	10 minutes in the steamer Buffer used: Citrate buffer (pH6) or ETDA buffer (pH9) depending on primary antibodies
Cooling in washing buffer	0.5% Tween in PBS, until next step
Fat pen circling	
Unmasking intracellular antigens	3 minutes 0.2% Triton X-100 in PBS
Washing buffer	2X 3minutes
Blocking	BSA, 45minutes to an 1h
Washing buffer	2x 3minutes

Sections were then incubated with primary antibodies diluted in antibody dilution buffer (AL120R500, DCS Innovative Diagnostik-System, Germany) overnight at 4°C. Primary antibodies are detailed in Table 4:

***Table 4**: Primary antibodies dilutions and references.*

Target	Specie	Reference	Dilution
DCXR	Rabbit	Abcam ab154290	1:10000 (DAB) 1:3000 (IF)
GSTP1	Rabbit	Abcam ab138491	1:500 (DAB) 1:1000 (IF)
GSTA1	Rabbit	Abcam ab180650	1:1000
GSTO2	Rabbit	Abcam ab129106	1:1000
AKR1B10	Rabbit	ThermoFisher Sc PA522036	1:3000
ALDH1A1	Mouse	Santa-Cruz sc-374149	1:3000 (DAB) 1:1000 (IF)

ALDH3A1	Mouse	Santa-Cruz sc-376089	1:1000 (DAB) 1:500 (IF)
CK18	Rabbit	Novus Biologicals NBP2-67370	1:200
CK18	Mouse	Dako M7010	1:50
CK5/6	Mouse	Dako M7237	1:200
MUC5B	Rabbit	Sigma Aldrich HPA008246	1:100
MUC5AC	Mouse	ThermoFisher Sc MA138223	1:1000
Vimentin	Rabbit	Abcam ab925447	1:1000
Acetylated tubulin	Mouse	Sigma Aldrich T7451	1:1000

Following primary antibodies incubation, sections were washed 2x3 minutes in 0.5% Tween in PBS before DAB staining or immunofluorescence staining.

DAB staining

Though overall the immunofluorescence staining was the preferred method as it allows double staining (target XME and a cellular marker), DAB staining was most of the time used first to investigate whether there was a signal or not (reflecting the presence or absence of target XME on the protein level), and avoid wasting precious fluorophore-conjugated secondary antibodies. Besides, DAB (3,3'-Diaminobenzidine) is commonly used as a chromogen in immunohistochemical staining. Oxidized by HRP (Horseradish peroxidase), it forms a brown precipitate stable for years. Combined with immunohistology, the technique allows a sensitive detection of targets of interest in histological sections, as it is possible to observe the tissue's structures without any supplementary dye. DAB staining was performed using the SuperVision 2 HRP Kit (Mouse/Rabbit) 2 steps polymer, peroxidase conjugated (PD000KIT, DCS Innovative Diagnostik-System, Germany), according to the fabricant's protocol. Following the staining steps, sections were dehydrated and mounted using the protocol Table 5:

***Table 5**: Mounting protocol for DAB staining.*

Dehydrating	Ethanol 70%, dip 3 times Ethanol 96%, dip 3 times Isopropanol 1, dip 3 times Isopropanol 2, dip 3 times Xylene 1, dip 3 times Xylene 2, dip 3 times
Mounting	1-2 drops of Entellan, Sigma Aldrich, REF 107960
Drying	Let dry overnight before taking pictures at the microscope

Immunofluorescence (IF)

Concerning immunofluorescence, sections were incubated with secondary antibodies – according to species of primary antibodies – for 45 minutes at room temperature. Table 6 shows secondary antibodies references:

***Table 6**: Secondary antibodies coupled with fluorophores, dilutions and references.*

Fluorophore	Target	Specie	Reference	Dilution
AlexaFluor 488	Mouse antibodies	Donkey	A31572, Invitrogen	1:400
AlexaFluor 555	Rabbit antibodies	Donkey	A21202, Invitrogen	1:400

Slides were then mounted using Fluoromount-G with DAPI (REF 00-4959-52, Invitrogen, ThermoFisher Scientific, Germany) then incubated for 3h at room temperature, or overnight at 4°C depending on scheduled plans. Pictures were taken with a Fluorescence microscope (All-In-One Fluorescence Microscope, BZ-X810, Keyence, Germany).

Alcian blue staining

Alcian blue staining, and in the next section Hematoxylin and Eosin staining, were used to observe the general structure of the tissue models for every donor.

Table 7 explicates the steps to perform the Alcian blue staining.

***Table 7**:Alcian blue staining*

Melting paraffin	60°C, 5-10 minutes
Paraffin removal	Xylol, 5 min, X2
Xylol removal	Ethanol 96%, dip 3 times, X2
Followed by ethanol removal	Ethanol 70%, dip 3 times
	Ethanol 50%, dip 3 times
Then rehydration	Deionized Water, until the next step
3% glacial acetic acid	3 minutes
Staining of the negatively charged proteoglycans	1% Alcian blue, 30 minutes
Rinses	Deionized wated
Staining of the nucleus	Nuclear fast red solution, 5 minutes
Dehydrating and mounting steps	As described for DAB staining

Hematoxylin and Eosin staining

Table 8 summarizes the steps to perform the Hematoxylin and Eosin staining

***Table 8**: Hematoxylin and Eosin staining*

Melting paraffin	60°C, 5-10 minutes
Paraffin removal	Xylol, 5 min, X2
Xylol removal	Ethanol 96%, dip 3 times, X2
Followed by ethanol removal	Ethanol 70%, dip 3 times
	Ethanol 50%, dip 3 times
Then rehydration	Deionized Water, until the next step
Staining of the nucleus	Hematoxylin, 6 minutes
Rinses until no color washes out	Deionized water
Staining the cytoplasm	Eosin, 3 minutes

Rinses until no color washes out	Deionized water
Dehydrating and mounting steps	As described for DAB staining

2.7.Odorant metabolism

As explained before, two methods were used: one using homogenates to verify the functionality of the target XME, and one fully embracing the 3D structure of the model by measuring compounds in the headspace of the tissue models. This second method is reffered as "Twister experiements" in this thesis, from the name TWISTER™ of the PDMS-coated magnetic rod commercialized by GERSTEL.

3D model homogenates

3D model homogenates were produced from whole tissue models dedicated to the experiment. After a PBS rinse, models were dismounted from the crowns and homogenized with 100 µL PBS per model using a Tissue Lyzer LT (Qiagen, Hilden, Germany) and tungsten beads for 3 minutes at 50 Hz. After a 5 minutes centrifugation step at 10,000 rpm, supernatants from 2 to 8 models from the same donor were pooled and kept at -80 °C until use, and sent to the Lehrstuhl für Aroma und Geruchsforschung (Chair of Aroma and Smell Research) for further analysis kindly performed by Nicole KORNBAUSCH, PhD student whose supervisor is Dr. Elene LOOS. There, the "full assays" were prepared by mixing 10 µL of the homogenate with 40 µL of freshly prepared odorant solutions and 50 µL of an NADPH-regenerating solution prepared according to the supplier's instruction. Full assays were incubated at 34.6 °C for 90 minutes to recreate the human nose conditions. A centrifugation step was then performed for 4 minutes at 13,500 rpm. The supernatants were extracted for 20 minutes with 3 mL of ice-cooled methanol (for the odorant benzaldehyde) or MTBE (for the odorant 3,4-hexanedione). The extracts were dried over Na_2SO_4 and filtrated. The volume was reduced to 100 µL using microdistillation (methanol: 75 °C, and MTBE: 65 °C). For each odorant, 3 different biological donors were tested in triplicate, meaning there were 9 measurements per odorants for full assays. Additional control experiments were performed, omitting either the odorant, the model's homogenate, or the NADPH-regenerating kit. Another control used heat-denaturized homogenates (100 °C for 10 minutes), or enzymatic inhibitors [DCXR: pentanoic acid (Nakagawa et al., 2002) CYP: KET (Back et al., 1989; Suzuki et al., 1987), ADH and AKR: NEM, (Christeller and Tolbert, 1978; Riggs, 1960), ALDH: citral (reversible inhibition), benomyl (irreversible inhibition) (Koppaka et al., 2012)]. Three technical replicates were performed per control

experiments, and served to assess the involvement of the mucosa and its enzymatic system in the formation of odorant metabolites. CG-MS analysis of the solvent extracts was done using an Agilent MSD quadrupole system (GC 7890 A, coupled to an MSD 5975C, Agilent Technologies) equipped with an MPS 2 autosampler and a cold injection system (CIS) 4 (both from Gerstel GmbH & Co. KG). Cold-on-column injection was performed using a 2 µL injection volume. The starting temperature of the GC oven was held at 40 °C for 2 minutes. The oven was equipped with a DB-FFAP column (Agilent J&W fused silica capillary 30 m x 0.32 mm, 0.25 µm; Agilent Technologies). The temperature was then increased for 10 °C per minutes until 240 °C, then hold for 5 minutes. During the analysis, the flow rate of the helium carrier gas was constantly 1.0 mL/min. The temperature of the ion source was held at 250 °C, and MS spectra were recorded within a mass by charge ratio (m/z) range of 20 – 400. The electron impact mode (EI-MS) at 70 eV was used to generate the mass spectra. The total ion chromatogram (TIC) was scan for metabolites for all experiments. Detected structures were taken into consideration when they had a structure related to the parent compound and were detected in the full assay but absent or reduced in the control experiments. They were then evaluated: if they could be formed through a certain enzyme-catalyzed reaction or other known reaction, they were included in the studies as potential metabolites. The metabolites were identified using reference compounds, considering they retention mass index and mass spectrum. Peaks were manually integrated using the following m/z value: 59 and 114 for 3,4-hexanedione, 59 and 116 for 4-Hydroxy-3-hexanone, 106 for benzaldehyde, 108 for benzyl alcohol, and 122 for benzoic acid. By doing so, odorant and corresponding metabolites could be detected. The peak areas were normalized to the overall peak are obtained by the respective extracted chromatogram that considered the m/z values of odorants and metabolites.

Twister experiments

The Twisters^{TM} exposed to the tissue model headspace were, as mentioned in the "direct liquid treatment – odorant metabolism part", sent to Nicole Kornbausch for further analysis. There, they were gently rinsed with distilled water, dried on a lint-free cloth, and transferred to a desorption tube. After having been sealed with a transport adapter, the desorption tubes were inserted into the thermal desorption unit (TDU) from Gerstel, using the Multi-Purpose MPS 2 XL autosampler from Gerstel, on splitless

mode. The program started at 40 °C from 2 minutes, then increased by 60 °C per minute until 240 °C. This last temperature was held for 5 minutes. The analytes were thermally desorbed in the TDU and immediately cryo concentrated at -120 °C in the cold injection system KAS 4 Injector from Gerstel (split mode, starting temperature -120 °C, then temperature increased by 12 °C every minute until 280 °C, which was held 5 minutes). This was followed by a chromatographic separation on a DB-FFAP capillary column (splitless mode, starting temperature held 2 minutes at 40 °C, then temperature increased by 10 °C every minute until 240 °C, which was held 5 minutes). This was followed by mass spectrometry using electron impact ionization (EI, 230 °C, 70 eV). The analyzed was a quadrupole (150 °C). Detection was performed in full-scan mode (total ion chromatogram TIC) in a range between 40 and 400 m/z. The system was checked for cleanliness before each measurement using a mixture of n-alkanes and to determine the retention indices of aroma metabolites signals.

RESULTS

1. Ex vivo rat experiments

This first part focuses on results obtained on rat olfactory explants. This *ex vivo* model was used at the beginning of the PhD program to test a proof of concept before moving to a human-based model. The aim was to investigate a potential early gene regulation of nasal xenobiotic metabolizing enzymes by short exposition time of volatile/odorant molecules at low concentration at the vicinity of olfactory receptors. The idea was, as explained before, to imitate an olfactory event.

The rat olfactory explant model, already known in Prof. Heydel's team at the Center for Taste and Feeding Behavior and used for odorant metabolism studies, seemed a safe start to test the hypothesis. By using explant, the structure and cell-types composing the olfactory mucosa are conserved. Experiments were first done on thawed rat olfactory explants, which have the advantage of being collected then frozen until use whenever rats were used for other purpose: this avoids animal waste. Experiments were then performed on freshly dissected explants, which corresponding results are presented the two following sub-parts. In a third hand, a short discussion part will then introduce the human tissue model.

3.4. Odorant exposure and gene regulation on thawed rat olfactory explants

Optimization of the protocol

Prior to any gene regulation experiments, it was necessary to optimize the RT-qPCR technique for the rat olfactory explants. As described in the material and method part, I chose the common based method described by Ganger's team (Ganger et al., 2017) which includes in the calculations as many reference genes as wanted, as well as PCR efficiencies of every primer pair used. Figure 13A shows PCR analysis of *Cyp2e1* in response to ethanol treatment depending on the reference genes used to normalize and calculate the fold change. Ethanol was chosen to establish a proof of concept to study XME gene regulation in response to a substrate, in a short exposure time at low concentrations to mimic an olfactory event. It is known that ethanol is metabolized by ADH1, ALDH2, and CYP2E1 in the liver. Each histogram presents the exact same data points; however, we can observe a bigger standard error of means and a fold change

almost 5 times higher when normalizing with a combination of *Cdkn1b*, *Rpl30*, and *B2m*, compared with normalization using a combination of *B2m* and *Rpl30*. In a similar manner, fold change calculated with *Actb* alone is 2.5 times higher than when normalizing with a combination of *Actb* and *B2m*. Hence, if one reference gene did not seem enough, neither was blindly using a combination of random potential reference genes. Choosing the best reference genes thus appeared to me a critical point to trust

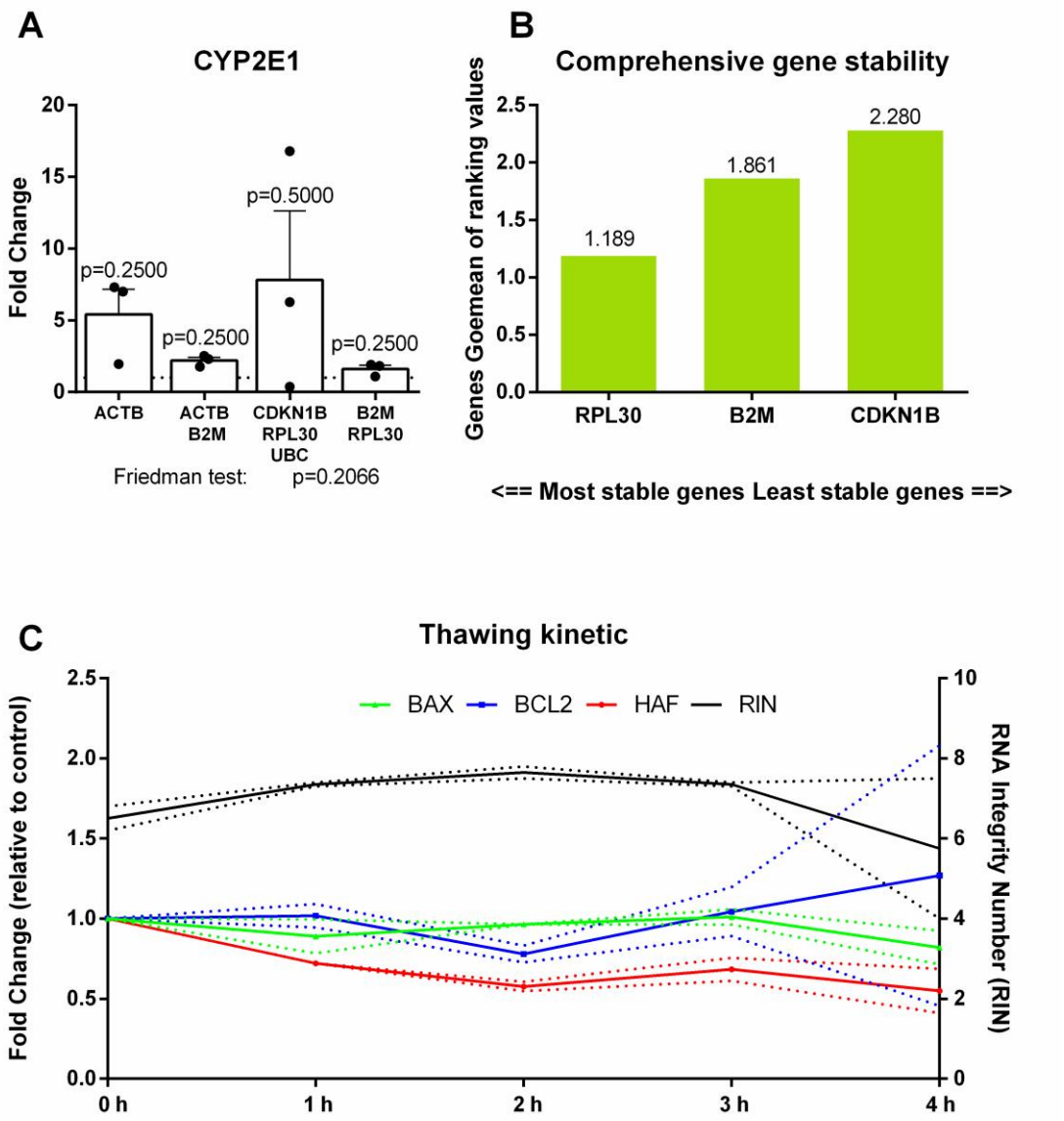

***Figure 13**: (A) Fold Change gene expression analysis of rat Cyp2E1 in response to headspace ethanol treatment, using RT-qPCR (n=3). Data are presented as fold change relative to untreated controls and represented as mean + SEM (represented by dotted lines of the same color). The common base method* (Ganger et al., 2017) *was used to calculate the fold change, each column presents the same data normalized by different reference genes. Statistical analysis was handled on GraphPad Prism 6.0. Each condition was tested against a theoretical mean of 1 using a Wilcoxon signed-rank test, and conditions were compared between them using a Friedman test. (B) Example of optimization of reference genes using RefFinder* (Xie et al., 2023, 2012)*, Rpl30 and B2m seems to be the most stable genes. (C) Thawing kinetic of frozen rat olfactory mucosa explant, mRNA abundance of tissue stress/death associated marker (Bax, Bcl2, Haf) and RNA integrity number (RIN), expressed in mean and SEM (n=2).*

any PCR results. Ideally, reference genes are ubiquitous and not affected by the conditions we want to compare. To verify this stability across all the samples, I used a web-based tool called RefFinder that Fuliang Xie's team developed (Xie et al., 2023, 2012), which integrate geNorm, Norm Finder, BestKeeper and the comparative ΔCT methods. Figure 13B is an example of the results than can be obtained from the tool. I used *B2m* and *Rpl30* for future RT-qPCR on the rat tissue, as they prove to be the most stable reference genes.

Since experiments started on frozen rat olfactory explants, a second critical step was to verify that rat olfactory explants could stand being thawed, exposed to a molecule, and analyzed with RT-qPCR. To do so, a thawing kinetic was designed from 0 hour to 4 hours, with n=2 per time point to start (Figure 13C). For each time point, RNA integrity number (RIN, in black) was measured: from 0 hour to 3 hours the RIN seems to be stable around 7 to 7.5, then decreases to around 6 when t=4 hours. Fold changes of *Bcl-2* (B cell lymphoma 2, in blue) and *Bax* (BCL-2 associated protein X, in green) seem to be stable around 1 from 0 hour to 3 hours, while the 4-hour time point shows higher variability. Lastly, fold change of *Haf* (Hypoxia Associated Factor, in red) seems to slowly decrease from 1 at t=0 hour, to around 0.5 at t=4 hours. Regarding these results, nothing seemed to indicate a degradation of the tissue.

Regulation of OMEs in response to ethanol treatment: thawed rat olfactory mucosa explants

Following these encouraging results, experiments on XME regulation by volatile/odorant molecules were started on thawed rat olfactory explants. Figure 14 shows expression of these three variants (Figure 14A: *Cyp2E1*; Figure 14B: *Adh1*; Figure 14C: *Aldh2*) in the rat olfactory explants in response to headspace ethanol treatment. During the ethanol exposure, explants were either incubated at 4°C or 30°C. *Cyp2E1* is not significantly upregulated in response to ethanol but show a similar trend between the 2 incubation temperatures. *Adh1* and *Aldh2* also are not significantly upregulated in response to ethanol. Unlike *Cyp2E1*, the trends seem to differ depending on the incubation temperature: for both *Adh1* and *Aldh2*, the fold change is below 1 for the

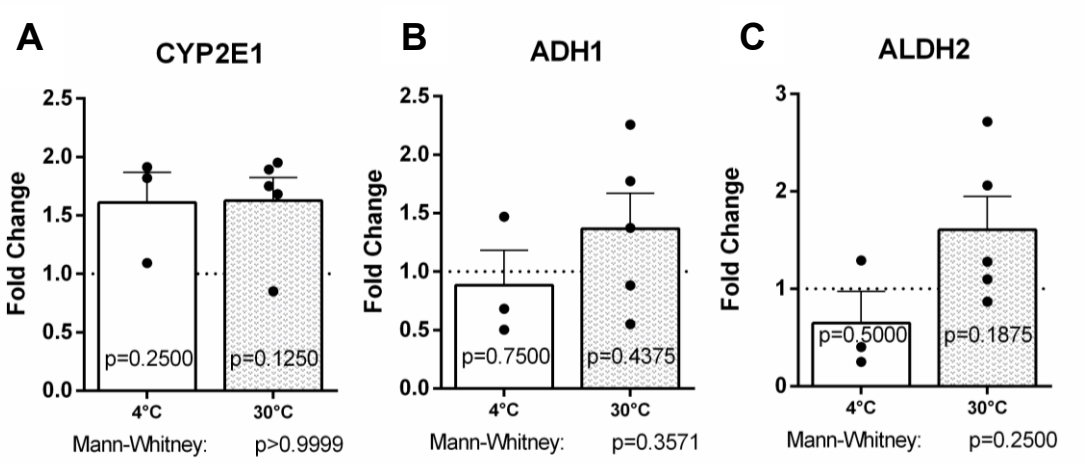

***Figure 14**: Fold Change gene expression analysis of rat Cyp2E1 (D), Adh1 (E), and Aldh2 (F) in response to gaseous ex vivo ethanol treatment and depending on the temperature of incubation, using RT-qPCR. Data are presented as mean + SEM, normalize by untreated control. Statistical analysis was performed on GraphPad Prism 6.0. Each condition was tested against a theoretical mean of 1 using a Wilcoxon signed-rank test, and conditions were compared using a Mann-Whitney test. In the graphs, each point represents a rat. 2 technical replicated were performed for PCR experiments.*

incubation at 4°C, and above 1 for the incubation at 30°C, although the difference is not statistically significant.

1.1. Odorant exposure and gene regulation in fresh rat olfactory explants

Experiments were then repeated on fresh explants with a four-time point kinetic from 0.5 hour to 2 hours. Aside ethanol, 2,3-pentanedione was also added in the headspace

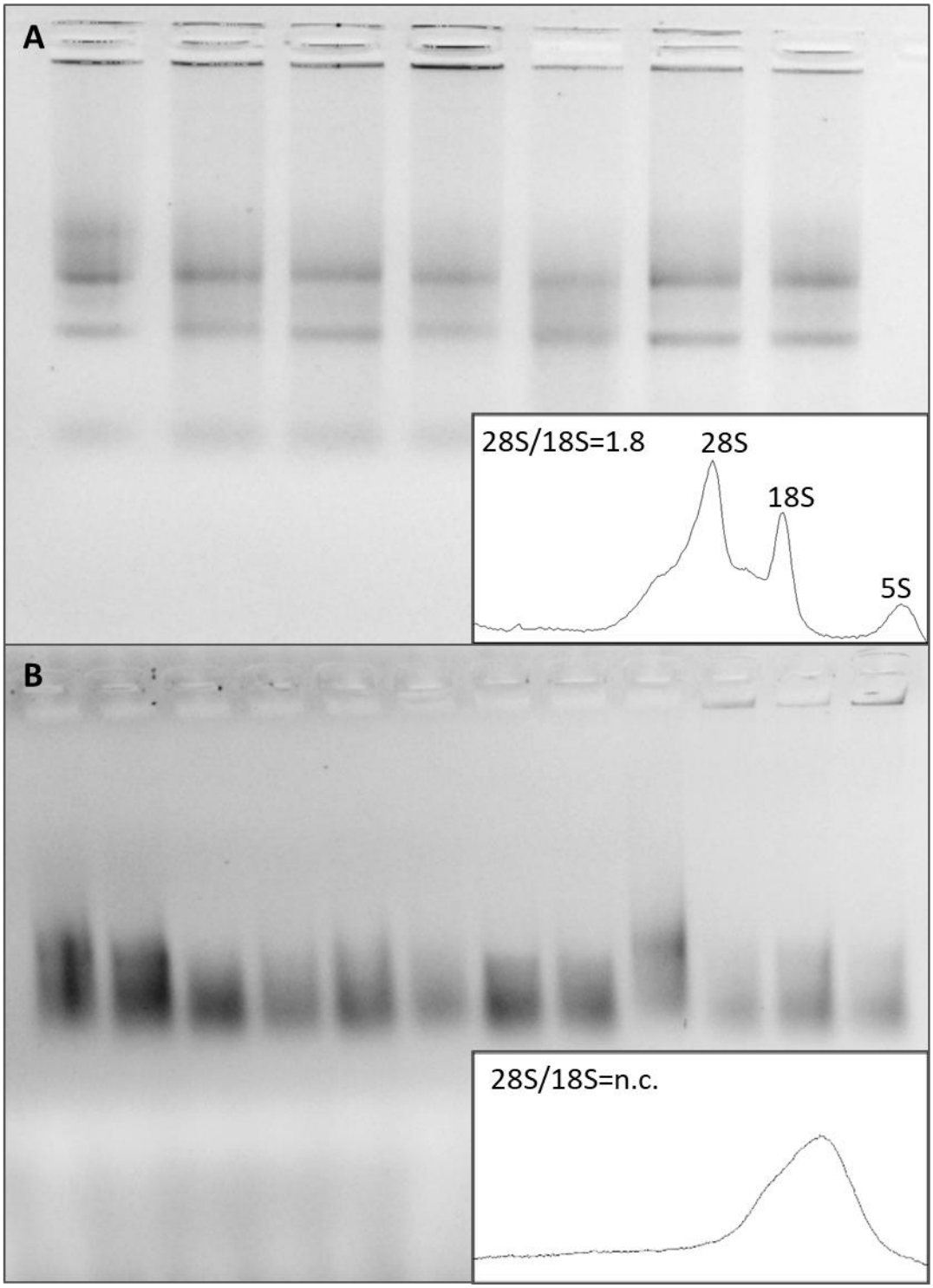

***Figure 15**: Representative gel electrophoresis and peaks of total RNAs extracted from (A) frozen rat olfactory explants, and from (B) freshly dissected rat olfactory explants, after odorant exposure. Peaks and areas were extracted from the gel pictures using ImageJ Gel Analysis tool. 28S/18S ratios were calculated when possible, n.c. means not calculated. Each band represent RNA extracted from one hemi-mucosa.*

treatment. At t= 0.5 hour, 1 hour, 1.5 hours and 2 hours, explants were snap frozen in liquid nitrogen and stored at -80°C until total RNAs were extracted, which was similar to what was performed on the frozen rat olfactory explants after odorant exposure.

Figure 15 shows that ribosomal RNAs 28S, 18S, and 5S bands were no longer present in the gel electrophoresis of freshly dissected rat olfactory explants (Figure 15B), compared to RNAs extracted from frozen rat olfactory explants (Figure 15A). The characteristic smears of degraded RNAs were visible on every samples and independently of the time point.

Figure 16 shows RT-qPCR results performed on the less degraded samples, although the dataset has a lot of missing values due to RNA degradation. There were enough samples with amplified mRNA for some time points to plot *Cyp2E1* (Figure 16A.), *Adh1* (Figure

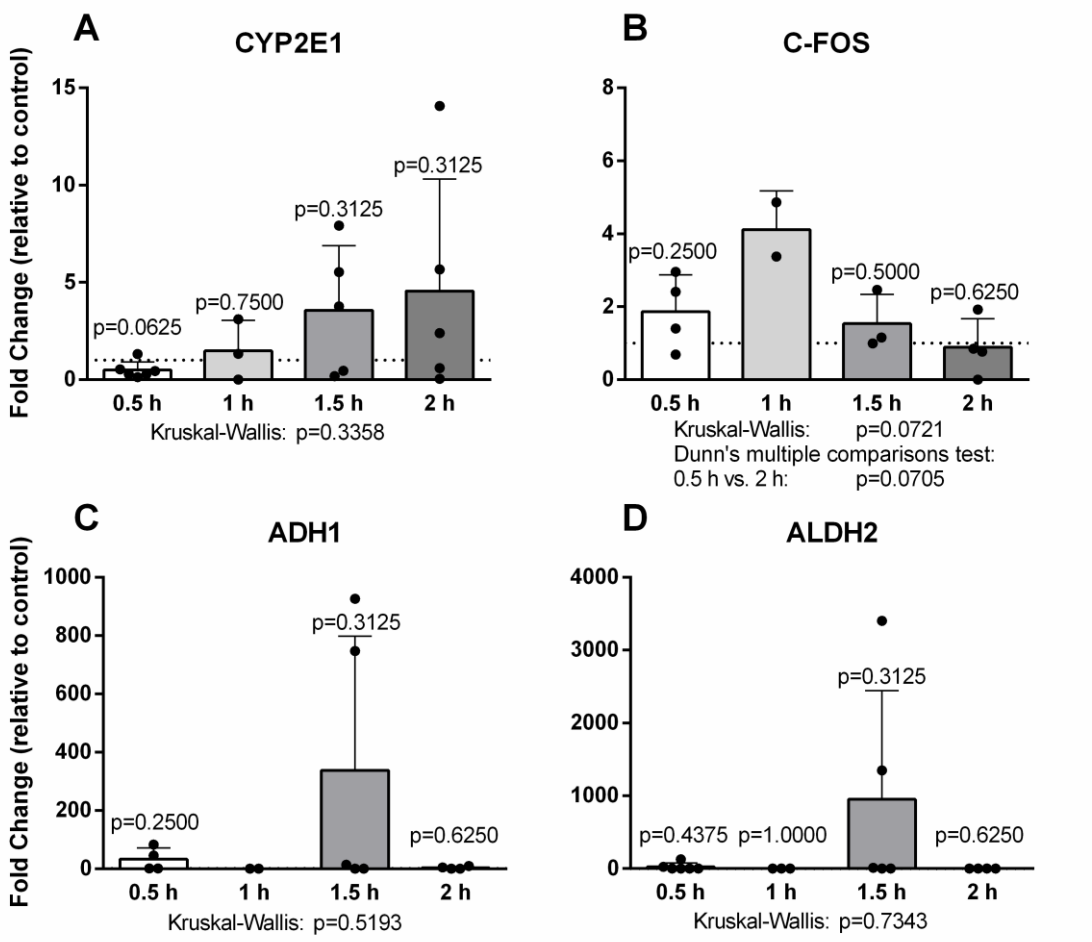

***Figure 16**: Fold Change gene expression analysis rat Cyp2E1 (A), c-fos (B), Adh1 (C), and Aldh2 (D) in response to headspace mix of ethanol (63 ppm) and 2,3-pentanedione (2 ppm), relative to an unexposed control. Data are presented as mean + SEM. Statistical analysis was performed on GraphPad Prism 6.0. Each time points were tested against a theoretical mean of 1 using a Wilcoxon signed-rank test, and time points were compared between them using Kruskal-Wallis tests followed by Dunn's multiple comparisons tests. In the graphs, each point represents a rat. 2 technical replicated were performed for PCR experiments.*

16C) and *Aldh2* (Figure 16D.). *C-fos* (Figure 16B.), a marker of neuronal activation, was also investigated. Cyp2E1 expression decreased after 30 minutes of incubation, then seemed to be upregulated as time of exposure increases. Neither *Adh1* nor *Aldh2* are significantly upregulated by the ethanol and 2,3-pentanedione treatment. However, for both enzyme a few data points raise the fold change to 13 and 26 at t=0.5 hour and to around 300 and 1000 at t=1.5 hours, for *Adh1* and *Aldh2*, respectively. Finally, I also investigated *c-fos* gene expression in response to the ethanol/2,3-pentanedione mixture. Figure 16B shows that *c-fos* is not significantly regulated by the treatment at 0.5 h, 1.5 h, and 2 h. At 1 h only 2 samples were exploitable, which is not enough to perform a statistical analysis. Overall, the fold change seems to increase around 1 hour before decreasing again.

1.2. Discussion on rat *ex vivo* experiments

Optimization of the odorant exposure protocol

Before starting any experiments on the rat olfactory mucosa explants, it was necessary to tailor the analytic methods used in further experiments to the model. I tested different reference genes and showed that they affected the RT-qPCR analysis outcomes (Figure 13A). I found *B2m* and *Rpl30* were the most stable genes among all the conditions tested and chose them for RT-qPCR experiments when using the rat olfactory explant model (Figure 13B). The search for best reference genes is definitely a good practice that was kept for human-based experiments – although not described in the next parts.

The second control I put in place before I started working with odorants on the explants was to verify that RNAs of the explant would survive a freezing/thawing procedure, since I started with frozen rat explants. I performed a thawing kinetic (Figure 13C) and chose different stress and death marker that would inform me of the state of the tissue during the procedure. The first marker was the RNA integrity number (RIN), which was globally stable up to 4 hours after the explants were left thawing on ice. RNA quality is generally linked with downstream analysis outcomes – including RT-qPCR (Schroeder et al., 2006). Usually, RNA integrity is observed using an electrophoresis, which allows to compare 28S and 18S bands intensity. Ideally, the ratio between them is 2:1. RIN calculation, in other hands, gives a scale between 1 and 10, the higher the number the better the RNA

quality, which is arguably more precise but demands a specific equipment that uses arrays. While a RIN from 8 to 10 is considered high quality and is usually demanded for some downstream application such as RNA sequencing, a RIN of 7 seems acceptable for RT-qPCR applications. One could argue the RNA quality of the 0-hour samples should have been the higher quality possible, while it could be expected to lower for the other time points as RNAs degrade with time. It was not the case, which could hint that (1): the tissue seems to be stable for around 3 hours after thawing started, and (2) steps of dissection, freeze, and RNA extraction are also critical point for RNA integrity and, despite careful execution of the protocol, contain risks of RNase contamination.

However, RNA degradation alone does not always reflect cellular stress or death. It has been shown for example that, for some cell lines, apoptosis and 28S RNA degradation is independent (Samali et al., 1997). I chose to investigate early actors of mitochondrial outer membrane permeation: BCL-2 and BAX (a pro-apoptotic factor). Mitochondrial outer membrane permeation is a marker common to caspase-dependent intrinsic apoptosis and caspase-independent intrinsic apoptosis, which are both induced by stress, bioenergetic and metabolic catastrophes (Galluzzi et al., 2012). By explanting the olfactory mucosa, the tissue is undergoing hypoxia and nutrient depletion, which leads to stress and bioenergetic catastrophes. In physiological conditions, BCL-2 inhibits BAX. When conditions become pro-apoptotic, BCL-2 decreases and BAX triggers the permeation of the outer mitochondrial membrane. In the present experiments, *Bcl-2* and *Bax* fold changes were mostly stable around 1, which means these markers neither decreased nor increased during the thawing process. At t=4 hours, *Bcl-2* fold change even seems to increase, which does not look like a pro-apoptotic pattern. However, the huge variability could also be a result of RNA being of a lesser quality at this time point. The last death-associated marker that was tested is HAF. HAF was found to be an interesting tool in forensic sciences to determine early *post mortem* intervals, which seems very fitting for tissue explants. According to Xiaogang Bai's team, *Haf* mRNAs decline between 0 hour and 4 hours *post mortem*, with a correlation coefficient R≈0.5 (Bai et al., 2017). Like the team's work, *Haf* mRNAs were amplified using RT-qPCR for each time point and normalized on caspase 3 DNA. Data showed a slowly but steady decrease of *Haf* between 0 and 4 hours of thawing, which would corroborate Bai's team

observation. To conclude on the thawing kinetic, frozen-thawed rat olfactory explants are early *post mortem* tissues, and chosen markers do not seem to indicate a fast degradation of the tissue in the window used to expose the explant to volatile/odorant molecules. However, these results have to be taken cautiously, as they are only preliminary. The small number of repetitions did not allow statistical analysis, and the analysis was not strengthened with further repetition as experiments on freshly dissected rat olfactory explants were later favored to the frozen ones, and thus, no longer of interest.

Regulation of XMEs/OMEs in response to ethanol treatment in thawed rat olfactory explants

Nonetheless, experiments on frozen rat olfactory explants were continued with odorant exposure assays to question whether nasal XME could be regulated by their one volatile/odorant substrate. I chose ethanol as volatile/odorant molecule, as I wanted to establish a proof of concept that nasal XME can be regulated by a substrate. In the liver, it is commonly accepted that CYP2E1, ADH1 and ALDH2 are the major enzymes involved in ethanol metabolism (Cederbaum, 2012).

I treated the headspace of rat olfactory explants for 2 hours with ethanol, and incubated the explants either at 4°C – on ice, as soon as thawing begins – or at 30°C, after one hour of gently thawing the explants at 4°C. I could not demonstrate a significant effect of a gaseous ethanol treatment on *Cyp2E1*, *Adh1* and *Aldh2* in the rat nasal olfactory explant (Figure 14). Nevertheless, the patterns for *Adh1* and *Aldh2* seem to indicate a relevance of temperature incubation, which dawned afterward since most cellular functions and enzymatic reactions demand an adequate temperature as close as possible to the body temperature. The air temperature in the nasal cavity fluctuates around 33 °C due to the heat exchange between air and the nasal mucosa (Bailey et al., 2017). When studying rhinovirus replication in nasal tissues and immune response, an incubation temperature of 33-35 °C is recommended instead of 37 °C (Foxman et al., 2014). For this exact reason, frozen rat olfactory explants were replaced by freshly dissected rat olfactory explants. There are protocols to revive cell lines after a freezing procedure, However, reviving a tissue is complex and the freezing procedure could have damaged the cellular function and thus, preventing a physiological response to a treatment.

Odorant exposure and gene regulation in fresh rat olfactory explants

I thus switched to freshly dissected rat olfactory explants and performed a four-time point odorant exposure kinetic from 0.5 hour to 4 hours. This time, a mixture of ethanol and 2,3-pentanedione was used. This odorant is a known substrate of DCXR. In a recent work on 2,3-pentanedione using rodent *ex-vivo* olfactory mucosa, two 2,3-pentanedione metabolites were identified in real-time in the headspace of tissue explants: 2-hydroxy-3-pentanone (truffle-like odor-type) and 3-hydroxy-2-pentanone (herbal-like odor-type). Synthesis of metabolites was inhibited by thermal enzymatic deactivation and by a specific competitor of DCXR (butyric acid, sour milk odor), which point again 2,3-pentanedione as a DCXR substrate. Not only were these metabolites associated with an odor, but they were detected in a time-scale relevant to olfactory perception, which could impact the overall odorant perception of 2,3-pentanedione via *in situ* metabolism. The release of metabolites in the headspace would also allow a clearance of the nasal cavity through the air flow (Robert-Hazotte et al., 2019b). These results were reproduced in human *in-vivo* with the same real-time technique and confirmed with assays on the recombinant protein (Robert-Hazotte et al., 2022). Nothing is known on the regulation of *DCXR* by 2,3-pentanedione. The only experiments done so far investigated the toxicity of the odorant molecules in rat models: the rat olfactory neuro epithelium expresses DCXR, mostly in sustentacular cells. Treatment with 360 ppm of 2,3-pentanedione changes its expression pattern and immune-histological experiments shows the enzyme gathering in vacuoles at the apical side of sustentacular cells, hypothetically to form a protective layer. Past a certain exposition time-point, the layer of DCXR is disrupted and tissues progressively get disorganized (Hubbs et al., 2012).

Unfortunately, the experimental setup I used was harsh on the explants. Gel electrophoresis on the total RNAs extracted from each sample at every time points showed a distinctive smear (Figure 15). Although I did not include a molecular ladder when performing the experiment, I analyzed the bands' profiles to search for their well-known peaks that usually serves to calculate the ratio between 28S and 18S: good quality RNAs should have a ratio approaching 2:1. Analysis of the bands showed that 28S, 18S and 5S units' respective bands obtained from freshly dissected mucosa were merged in a single smear, which is a telltale sign of RNA degradation. As stated before,

this could greatly impact RT-qPCR outcomes. The experiment was conducted twice, one during summer, and one during autumn 2021. When I obtained the results from the summer experiment, I thought the ambient heat might have had a negative impact on the tissues and RNAs as the laboratory is not equipped with air conditioner. Working in a cool environment indeed prove to be hard as the ice kept thawing very quickly during the RNA extraction. When the experiment was repeated in autumn, the mild temperatures allowed to keep the samples cool during RNA extraction. Samples were overall handled extra carefully, but it did not change the outcome: “autumn” samples were even in a worst state than the summer ones, and no PCR analysis could be done on them. Nevertheless, some “summer” samples were usable enough to perform a PCR analysis, although conclusions obtained on such degraded RNAs have to be taken cautiously. While *Dcxr* was one of the main targets, it could not be analyzed since most of the samples showed no amplification for this target. *Cyp2E1*, *Adh1*, and *Aldh2* had enough samples showing PCR amplification to calculate some gene expression ratios in response to ethanol (Figure 16). I also investigated a marker of neuronal activation, *c-fos*. The analysis of the samples that were the least degraded hints that an odorant treatment could affect the tissue in some ways,althoughthe statistical analysis did not show any significant effect. Concerning *Cyp2E1*, the gene expression ratio seems to increase with time,althoughnot significantly. This pattern could suggest a detoxification system that responds to an aggressive stimulus involving phase I enzymes activity. Time and dose make the poison; in this scenario, tissues were constantly exposed to 63 ppm of ethanol and 2 ppm of 2,3-pentanedione for 2 hours. In this experiment, I kept concentration and exposure time deliberately low to avoid a toxicological response and stay in the range of olfaction; perhaps these concentrations were already too high for the explants. Studies on CYP2E1 usually focus on physio pathological conditions, such as oxidative stress-related liver injuries after a 5 week *in vivo* treatment with ethanol (Lin et al., 2019). In another example in the rat nasal tissue, CYP2E1 was found to be upregulated on the mRNA level and the protein level after 48 h of treatment with acetone administrated with intragastrical injections. Interestingly, this study showed that only the rat nasal *Cyp2E1* responded to the treatment, which was not the case for its hepatic counterpart (Longo and Ingelman-Sundberg, 1993). This characteristic is not restricted to CYP2E1, as it was shown later on a panel of phase I, phase II and phase III

XME in response to various systemic drugs and inducers (Thiebaud et al., 2010). We can then hypothesize that the usual hepatic XME inducers might not have the same effect on their nasal homologues, hence the need to verify the regulation of XME in a specific tissue of interest like the nasal mucosa. Results on *Adh1* and *Aldh2* are less clear, some data points show a huge increase in the fold change especially at t=1.5 hour. ADH1 is the main ADH isoform that converts ethanol into the carcinogen acetaldehyde, and is known to be induced cyclically in ethanol-fed rats (Badger et al., 2000) and this induction depends on C/EBPs (CCAAT/enhancer-binding proteins) binding to a consensus C/EBP nucleotide sequence. This regulation mechanism differ from CYP2E1, which is not concerned by the C/EBP binding event (He et al., 2002). C/EBP are mostly expressed in differentiating cells and cells with high energy metabolism, especially adipocytes, hepatocytes, and monocytes/macrophages, but can also be found for example in fibroblasts or endothelial cells (Wedel and Lömsziegler-Heitbrock, 1995). C/EBP were shown to be important transcription factors for lung development and differentiation; in mature lungs, these transcription factors also play a role in lung gene expression, including *CYP2B1* (Cassel and Nord, 2003). With these clues in mind, the respiratory system seems to be equipped with the tools required for a regulation of *ADH1* by ethanol. However, until experimentally proven and confirmed with strong controls, the question remains.

ALDH2 is mostly known for its role in detoxifying the procarcinogen acetaldehyde into acetate in the liver. A regulation of the enzyme by ethanol in the liver has not been described to my knowledge. However, in endothelial cells, ALDH2 activity is induced very quickly by low concentration of ethanol via protein phosphorylation by εPKC (Chen et al., 2008) and deacetylation via SIRT3 (Xue et al., 2012), which has a protective effect against myocardial ischemia/reperfusion in rats (Kang et al., 2016). Li Xue's team describe that this effect enhances ALDH2 enzymatic activity, but this effect does not involve a change in transcripts or protein content. A treatment with low ethanol concentration might have produced enough acetaldehyde to enhance ADLH2 activity, which I did not verify, but might not have been enough to justify a change in gene expression. In our case, are these enzymes really highly upregulated in the olfactory

mucosa in a 2 hour-time range, or are these points outliers emerging from degraded RNAs?

Lastly, results on *c-fos* suggest a rapid upregulation; indeed, *c-fos* is known to be an immediate early gene expressed in neurons activated with acute stimulation, thus being a useful marker for neural activity (Chung, 2015; Krukoff, 1999). In some cell lines, this transcription factor can be induced within a few minutes and peak between 30 minutes to 1 hour after the stimulation (Kovács, 1998), which is coherent with the pattern we observe in the rat olfactory mucosa. This would hint that the treatment conditions are enough to stimulate the olfactory neurons. Rat olfactory mucosa explants were already used at the CSGA to perform electroolfactograms (Thiebaud et al., 2013); in theory, olfactory neurons in the explants that were used for this experiment could also have responded to the odorants. However, I did not perform any complementary experiments to verify it.

So far, we cannot conclude whether XME are regulated by their odorant substrates, or not. The first approach using frozen rat olfactory mucosa explants allowed to explore different variations of a protocol created to expose the tissue to odorants. However, this approach quickly proved to be limiting. Although freezing the tissue protected it against degradation during odorant exposure, this process might also prevent the tissue to have a physiological response to a stimulus. Shifting to freshly dissected rat olfactory explants solved this problem, but created another one: the tissue did not stand the treatment without RNAs being degraded. The RT-qPCR results also showed a high variation, as if some samples were upregulated and others did not. However, I could not identify which parameters triggered this response in some sample, nor if it is a genuine gene upregulation. Was it a technical variation due to my handling of the samples, a variation in the treatment, or an interindividual variation within the Wistar line? The experiments used the same tissues every time: when talking about the rat olfactory mucosa explant, I mean the olfactory recess and the ethmoturbinates that come in one piece when dissected. Theoretically, the exact same anatomical site was used so it should not be a source of variation. We can also imagine that the tissue explant could need a system regenerating the enzymatic co-factor,althoughthey were already used in odorant metabolism studies without it (e. g. Robert-Hazotte et al., 2019b).

Obviously, without better controls, a higher number of repetitions, and most importantly, a model that would allow an odorant treatment without the RNAs being degraded, most of these conclusions are speculative. Using rat olfactory explants prove to be a limiting factor,althoughit was a necessary step to imagine and question protocols to expose the tissue to odorants. This first step was also the occasion to question whether the rat olfactory mucosa explant model is a good fit to investigate XME regulation by short time exposure to lowly concentrated odorants, to reproduce the conditions of an olfactory event. Although the genetic stability that rat with a maintained lineage is advantageous to explore cellular mechanism, I could not obtain reliable and convincing results with this model.

At this stage, two options were presented to me: either pursuing on the rat model, but with more classic *in vivo* experiments, or I could seize the opportunity to explore the human-based tissue models developed by other partners of the NAOMI project, which is what I did. Results obtained on animal models do not always translate well to the human biology. In the olfactory context, the nasal apparatus of human differs from most rodent models used in laboratories by its architecture. While the human nose structure possesses three relatively simple turbinates, most non-primate animal models have a nasal cavity with intricated structures and folds that maximize the surface at the contact with the airflow. The structure also differs as most rodents are obligate nose breathers, which is not the case of humans. Most importantly for the topic of this thesis, only 3 % of the human nasal cavity is covered with olfactory epithelium, while 50 % of the rat nasal cavity is an olfactory tissue (Harkema et al., 2006). This means that in human, most the volatile compounds – including odorants – would be in contact with respiratory epithelium before reaching the olfactory region. On top of respiratory epithelium, the human nasal mucus was shown to contribute to odorant metabolism as well (Boichot et al., 2023; Ijichi et al., 2022). Thus, focusing only on the olfactory tissue might bring only partial answer to decipher the human nasal metabolism of odorant. Aside from human *in vivo* studies that cannot differentiate the involvement olfactory and respiratory tissue in odorant metabolism, and do not allow complex experiments to decipher XME gene regulation, no human-based models reproducing the human olfactory mucosa are available so far. In a study published in 2023, Shahbaz and coworkers claimed they

successfully created a tissue model reproducing the non-neuronal cells of the olfactory epithelium (Shahbaz et al., 2023). Although their work provides useful insights on the impact of Alzheimer's disease on nasal cells transcriptome, their arguments to prove the model mimics the olfactory epithelium are rather weak. Among the critical points of discussion, the use of neuropilin 1 (NRP-1) as a marker of olfactory tissue is not sufficient, as NRP-1 is expressed in the whole human nasopharynx according to the data of the human protein atlas[2]. In the study, CK18 was used to mark sustentacular cells, but CK18 marks other cell types including the multiciliated cells of the respiratory epithelium, which hints that the models are probably similar to the respiratory epithelium model I used in the second part of this thesis. Powerful *in vitro* tools already exist to mimic the human airways, including the human nasal respiratory mucosa (Maisonnasse et al., 2020; Mercier et al., 2019; Sivarajan et al., 2021), and can be used to study the release of volatile emissions in the headspace (Yamaguchi et al., 2018).

In this regard, I chose to investigate nasal XME in the human nasal respiratory mucosa developed at the Chair of Tissue Engineering and Regenerative Medicine of Würzburg by Dr. Maria Steinke. Under her supervision, I explored the XME expressed by the models, its response to odorant treatments, and its ability to metabolize odorant. These results are presented in the next part of this thesis.

[2] www.proteinatlas.org

2. In vitro human experiments

This second part explores the use of an *in vitro* human nasal respiratory mucosa model to study nasal XMEs and odorant metabolism. The results will be presented in 3 parts: (1) characterization of the model in terms of XME expression, (2) potential gene regulation of XME in response to their odorant substrate. Like the experiments performed on the rat olfactory explants, the odorant exposure imitated an olfactory even by being brief (2 hours maximum) and using low concentrations, and (3) verification of XME activity toward a selection of odorants.

2.1. Characterization of the human nasal respiratory mucosa model: nasal XMEs

This part will briefly go over the general structure of the model in terms of cell types and general structure, as a reminder to understand the characterization of the model in terms of nasal XMEs expression. Then we will explore the model's expression of phase I and phase II XME enzymes using single-cell RNA sequencing. The study will then focus on a list of enzymes of interest and investigate their presence at the transcriptional level using scRNA sequencing data and RT-qPCR to confirm it, as well as on the protein level using histology techniques.

Morphological characteristics of the human nasal respiratory mucosa model

We will first briefly go over the morphological characterization of the model to understand its structure. Figure 17 shows the general structure of the model. It is organized with a polarized pseudostratified columnar epithelium with kinocilia-like structures on the apical side, based on a biological scaffold made of porcine small intestinal submucosa (SIS) loaded with nasal fibroblasts, which is demonstrated with Haematoxylin & Eosin staining Figure 17A. Nuclei are stained in blue/violet by the Haematoxylin dye, while Eosin stains in pink other cellular components such as the cytoskeleton, cytoplasm, and connective tissue. Alcian blue staining (Figure 17B.) demonstrates the presence of mucin-producing goblet cells as it stains in blue acidic mucins. Figure 17C shows in detail the phenotypes of the epithelial cells. Sitting directly at the interface with the connective tissue are the basal cells (in green, marked with CK5 (Völkel et al., 2021)), that form a stem cells pools from which multiciliated epithelial cells (in red, marked with CK18) differentiate. As shown with the Alcian blue staining, some cells differentiate into goblet cells. Figure 17D explores the presence of two major mucin

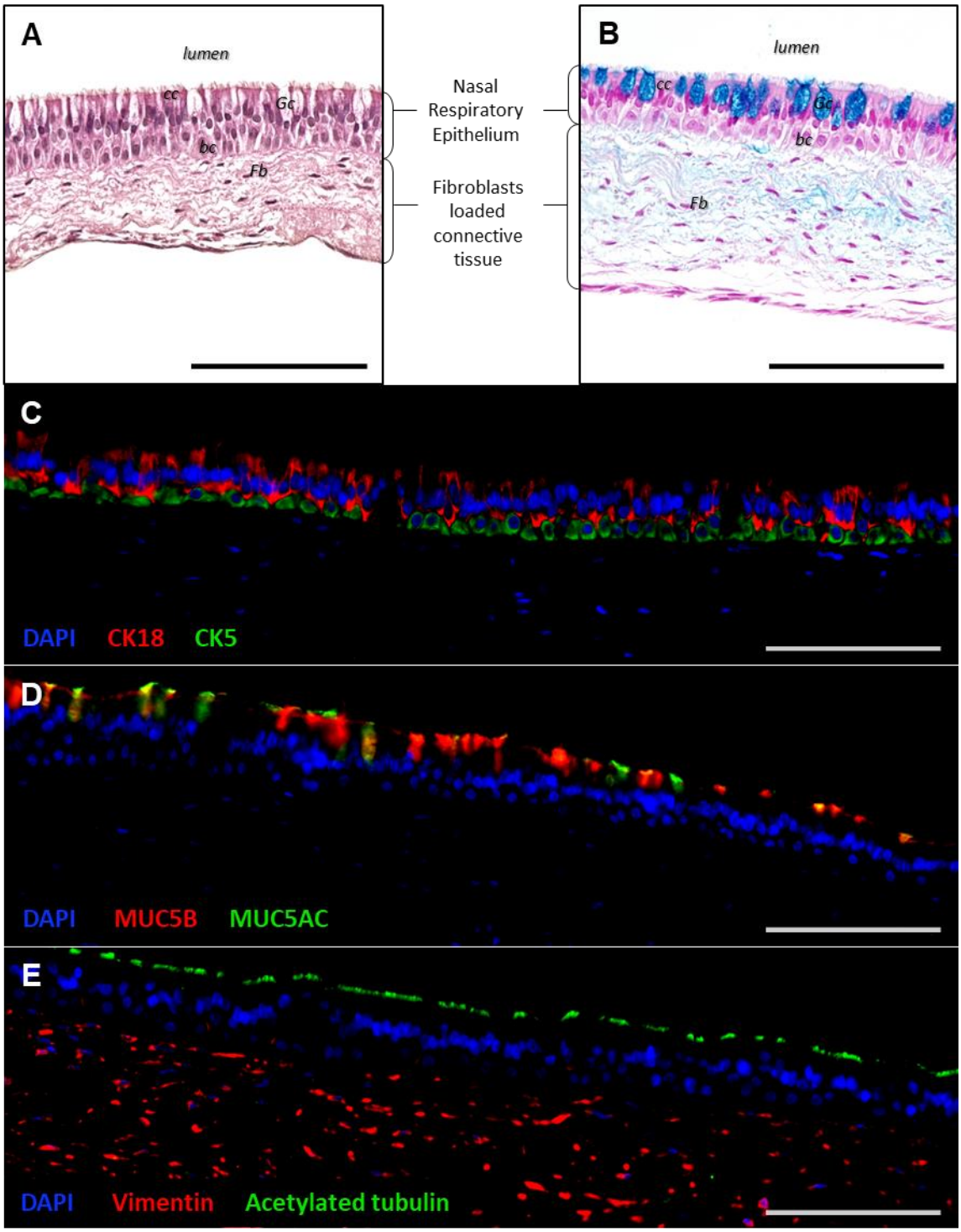

***Figure 17**: Structure of the human 3D nasal respiratory mucosa model. (A) Haematoxylin & Eosin stain nuclei and cytosol contents, respectively. (B) Alcian Blue staining showing in blue the acidic mucins contained in the goblet cells (blue bubbles), nuclei are stained with Nuclear Fast Red (Kernechtrot). (C) Immunofluorescent staining of multiciliated epithelial cells in red (marker: cytokeratin 18) and basal cells in green (marker: cytokeratin 5). (D) Immunofluorescent staining of mucins (goblet cells, markers: MUC5B in red and MUC5AC in green). (E) Immunofluorescent staining of fibroblasts in red (marker: vimentin) and cilia in green (marker: acetylated tubulin). Nuclei are stained in blue (DAPI) in immunofluorescence figures. Gc: goblet cells, cc: ciliated cells, bc: basal cells, Fb: fibroblasts. Scalebar = 100 µm.*

variants in the model: MUC5AC and MUC5B. The image shows define spots expressing either MUC5B (red) or MUC5AC (green) corresponding to goblet cells expressing preferentially one mucin over the other, and defined spots where MUC5B and MUC5AC

colocalize corresponding to goblet cells capable of expressing both variants. Lastly, Figure 17E shows in red the vimentin produced by fibroblasts in the scaffold, and in green the acetylated tubulin marking microtubules of cilia structures (Eshun-Wilson et al., 2019).

Cell types composing the human nasal respiratory mucosa model

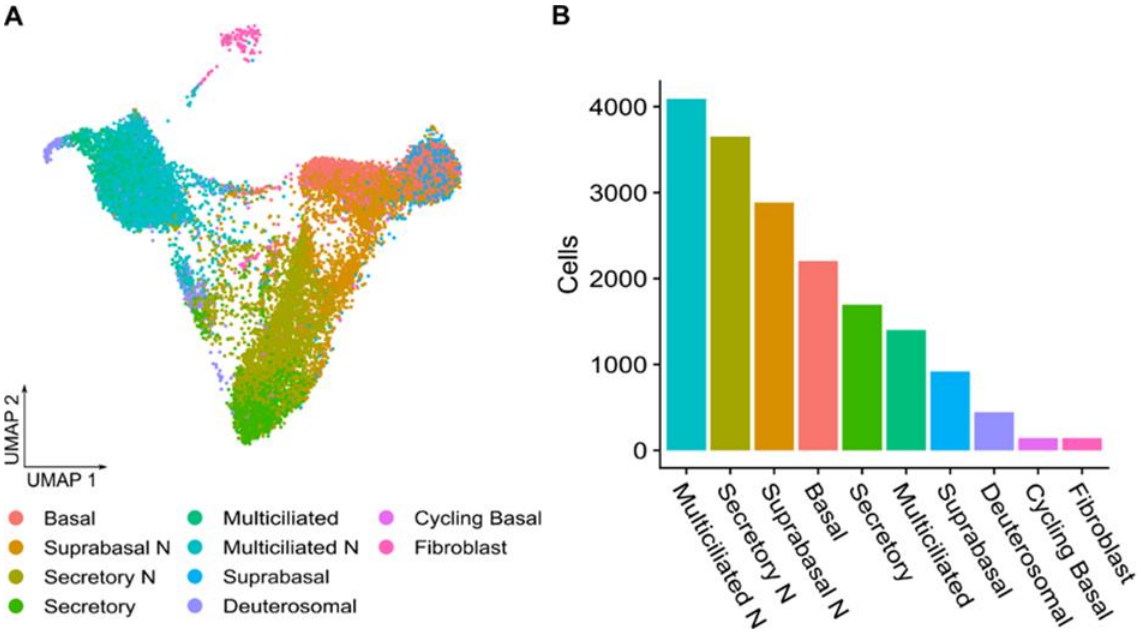

***Figure 18**: Single cell RNA sequencing of human mucosa tissue models. (A) UMAP projection showing cluster of cells assigned to different cell types. (B) frequencies of cell types identified in the tissue model (n=3). Experiments were performed by Rinu Sivarajan (Chair of Tissue Engineering and Regenerative Medicine, Würzburg). Cells were annotated to a single cell atlas of the human healthy airways using nasal and proximal airways samples* (Deprez et al., 2020) *by Prof. Florian Erhard and Kevin Berg (Institute of Virology and Immunobiology, Würzburg). Merignac-Lacombe, Kornbausch et al., under revision.*

Figure 18 shows scRNA-seq data from 3 donors mapped on a human cell atlas of healthy airways (Deprez et al., 2020). Clusters resulting from this analysis reveal several phenotypes associated with the sequenced cells (Figure 18A.), including basal cells, secretory cells, and multiciliated cells, which were already observed Figure 18. Interestingly, the mapping distinguishes subpopulations of these cell types that are associated with the nasal tissue specifically (noted N). Notably, these cells represent the major cells sequenced from the model (Figure 18B), which is expected given that this is a nasal model. Aside from these main cell types, the analysis revealed cellular subtypes such as suprabasal and deuterosomal cells. A small population of cycling basal cells was also observed, as well as fibroblasts.

Overall expression of nasal XMEs

Having a better view of the cellular population present in the model, I moved on to the characterization of the model in terms of XME expression. I decided to distinguish the different phases that classify the XMEs and to work in percentages. Figure 19 shows this analysis with pie charts presenting the different XME families found for each phase. ALDH (32.7 %), AKR (21.3 %), and CYP (19.7 %) are the main phase I families represented (Figure 19A), while GST members make 91.9 % of phase II XMEs (Figure 19B). I also had a look on phase III transporters out of curiosity,althoughthey are transport proteins and do not metabolize odorants *per se*. However, they are still relevant in odorant

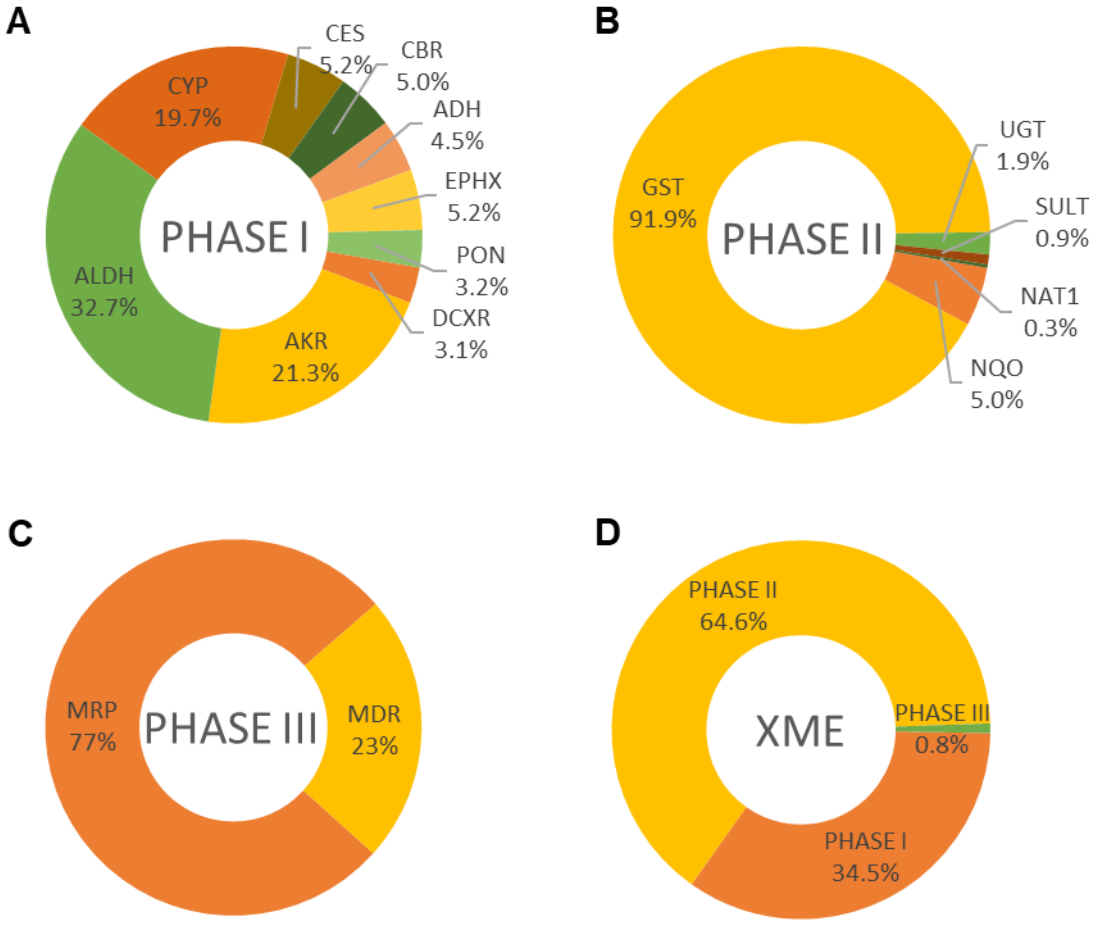

***Figure 19**: Analysis of the single-cell RNA sequencing data: proportion in % of (A) phase I XMEs families, (B) phase II XMEs families, (C) phase III efflux transporters, (D) phase I, II, and III genes families. Values were extracted from Rinu Sivarajan's single seq RNA sequencing data giving a mean expression value per RNA. Phase I, II and III variants were searched, classified and values were added per XME family, then normalized by the total sum to calculate a percentage.*

metabolism as they affect odorants and their metabolites availability for receptors, and thus their perception. 77 % of phase III transporters are MRP (Figure 19C). In total, phase

II enzymes are the most expressed with 64,6 %, followed by phase I (34.6 %). Phase III transporters only represent 0.8 % of XME in the model (Figure 19D).

The list of XME variants detected in the human nasal respiratory model is given in supplemental data Table 1 (cutoff: 0.0010).

Gene expression of phase I and phase II enzymes: focus on target variants

From this list a few phase I and phase II enzymes known for their role in odorant metabolism were selected for further investigations. Distribution of these enzymes among the different cell-types were explored using the scRNA-seq data, listed in Table 9. Expression of the enzymes was confirmed using RT-qPCR (Figure 20 for phase I and 21 for phase II).

***Table 9**: List of XMEs extracted from the human nasal model's scRNA-seq data.*

Gene	ID	Mean expression	Phase
DCXR	ENSG00000169738	0.182	phase I
AKR1A1	ENSG00000117448	0.34	phase I
AKR1B1	ENSG00000085662	0.043	phase I
AKR1B10	ENSG00000198074	0.074	phase I
AKR1C1	ENSG00000187134	0.199	phase I
AKR1C2	ENSG00000151632	0.182	phase I
AKR1C3	ENSG00000196139	0.282	phase I
AKR7A2	ENSG00000053371	0.137	phase I
ALDH16A1	ENSG00000161618	0.056	phase I
ALDH18A1	ENSG00000059573	0.029	phase I
ALDH1A1	ENSG00000165092	0.736	phase I
ALDH1A3	ENSG00000184254	0.12	phase I
ALDH1L1	ENSG00000144908	0.061	phase I
ALDH1L2	ENSG00000136010	0.01	phase I
ALDH2	ENSG00000111275	0.126	phase I
ALDH3A1	ENSG00000108602	0.267	phase I
ALDH3A2	ENSG00000072210	0.088	phase I
ALDH3B1	ENSG00000006534	0.219	phase I

ALDH3B2	ENSG00000132746	0.026	phase I
ALDH4A1	ENSG00000159423	0.019	phase I
ALDH5A1	ENSG00000112294	0.011	phase I
ALDH6A1	ENSG00000119711	0.02	phase I
ALDH7A1	ENSG00000164904	0.077	phase I
ALDH9A1	ENSG00000143149	0.065	phase I
CYP20A1	ENSG00000119004	0.04	phase I
CYP24A1	ENSG00000019186	0.028	phase I
CYP27A1	ENSG00000135929	0.021	phase I
CYP2A13	ENSG00000197838	0.011	phase I
CYP2F1	ENSG00000197446	0.072	phase I
CYP2J2	ENSG00000134716	0.035	phase I
CYP2S1	ENSG00000167600	0.028	phase I
CYP4B1	ENSG00000142973	0.62	phase I
CYP4V2	ENSG00000145476	0.023	phase I
CYP4X1	ENSG00000186377	0.057	phase I
CYP51A1	ENSG00000001630	0.226	phase I
CES1	ENSG00000198848	0.158	phase I
CES2	ENSG00000172831	0.117	phase I
CES4A	ENSG00000172824	0.033	phase I
CBR1	ENSG00000159228	0.263	phase I
CBR4	ENSG00000145439	0.033	phase I
ADH1C	ENSG00000248144	0.044	phase I
ADH5	ENSG00000197894	0.182	phase I
ADH7	ENSG00000196344	0.041	phase I
EPHX1	ENSG00000143819	0.282	phase I
EPHX2	ENSG00000120915	0.023	phase I
PON2	ENSG00000105854	0.189	phase I
GSTA1	ENSG00000243955	0.484	phase II
GSTA2	ENSG00000244067	0.067	phase II
GSTA3	ENSG00000174156	0.012	phase II

GSTA4	ENSG00000170899	0.024	phase II
GSTCD	ENSG00000138780	0.031	phase II
GSTK1	ENSG00000197448	0.263	phase II
GSTM3	ENSG00000134202	0.015	phase II
GSTO1	ENSG00000148834	0.223	phase II
GSTO2	ENSG00000065621	0.015	phase II
GSTP1	ENSG00000084207	7.374	phase II
GSTZ1	ENSG00000100577	0.059	phase II
MGST1	ENSG00000008394	0.775	phase II
MGST2	ENSG00000085871	0.222	phase II
MGST3	ENSG00000143198	0.578	phase II
NQO1	ENSG00000181019	0.506	phase II
NQO2	ENSG00000124588	0.051	phase II
SUGT1	ENSG00000165416	0.186	phase II
UGT2A1	ENSG00000173610	0.012	phase II
UGT2B7	ENSG00000171234	0.013	phase II
SULT1A1	ENSG00000196502	0.031	phase II
SULT1E1	ENSG00000109193	0.024	phase II
SULT2B1	ENSG00000088002	0.039	phase II
TPMT	ENSG00000137364	0.027	phase II
COMT	ENSG00000093010	0.314	phase II
NAT1	ENSG00000171428	0.031	phase II
ABCC1	ENSG00000103222	0.029	phase III
ABCC10	ENSG00000124574	0.012	phase III
ABCC3	ENSG00000108846	0.019	phase III
ABCC5	ENSG00000114770	0.033	phase III
ABCC6	ENSG00000091262	0.014	phase III
ABCB10	ENSG00000135776	0.011	phase III
ABCB7	ENSG00000131269	0.021	phase III

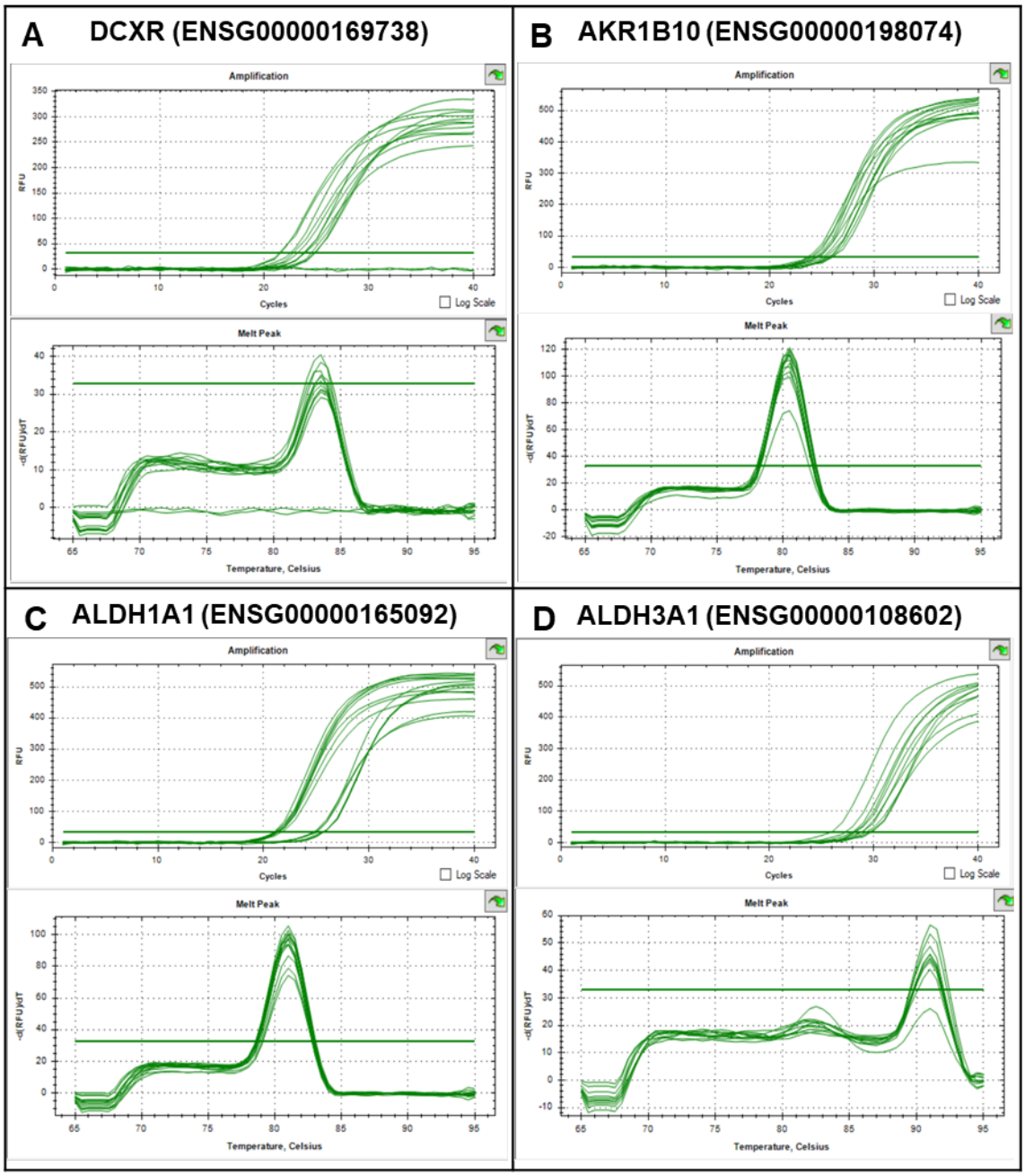

***Figure 20**: RT-qPCR confirming expression of A: DCXR (n=7), B: AKR1B10 (n=6), C: ALDH1A1 (n=7), D: ALDH3A1 (n=5). For each transcript amplification curves (top) and melting curves (bottom) are shown. Data come from 5 to 7 donors, 2 technical replicates per donor*

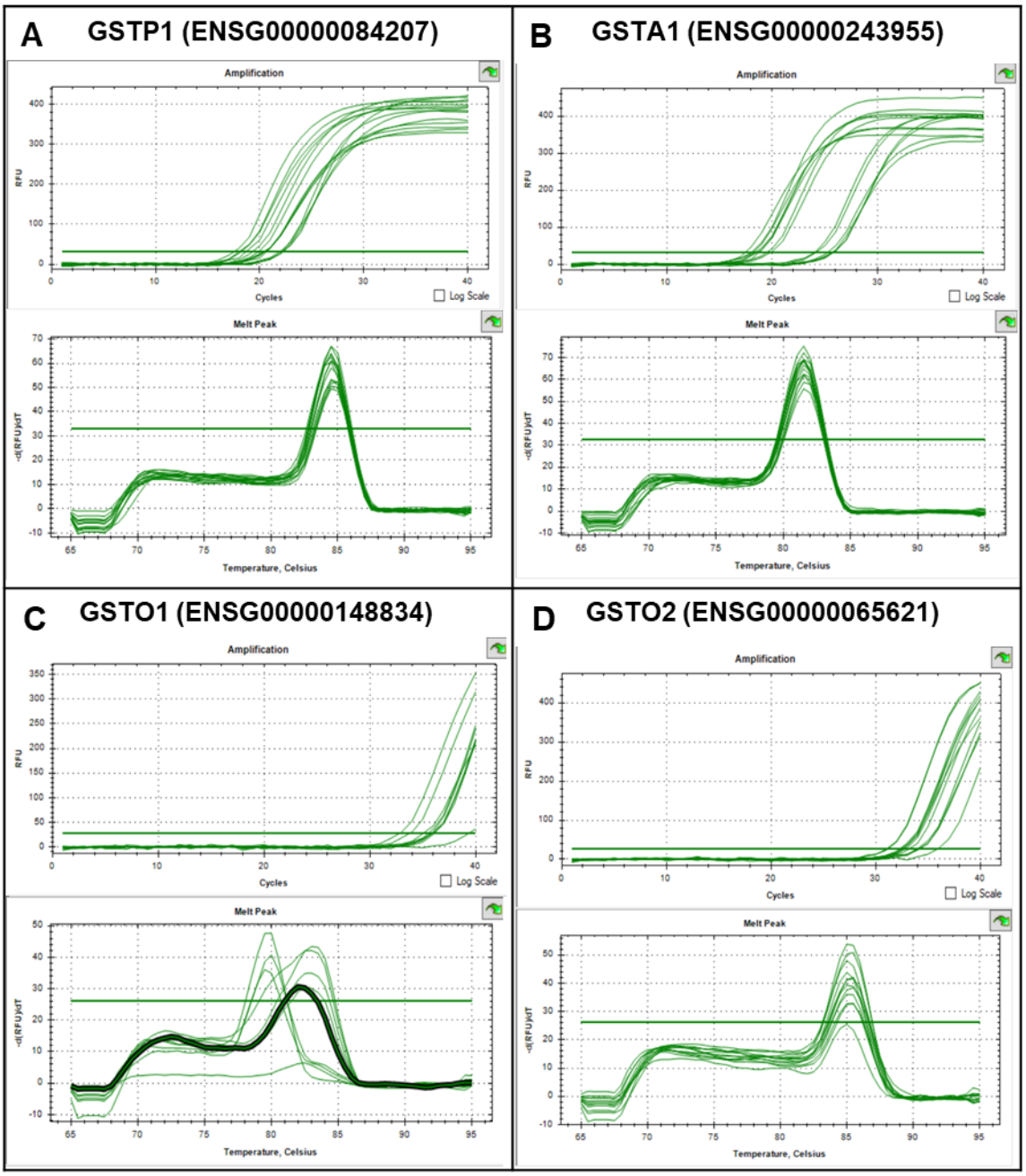

***Figure 21**: RT-qPCR confirming expression of A: GSTP1 (n=7), B: GSTA1 (n=7), C: GSTO1 (n=5), D: GSTO2 (n=7). For each transcript amplification curves (top) and melting curves (bottom) are shown. Data come from 5 to 7 donors, 2 technical replicates per donor.*

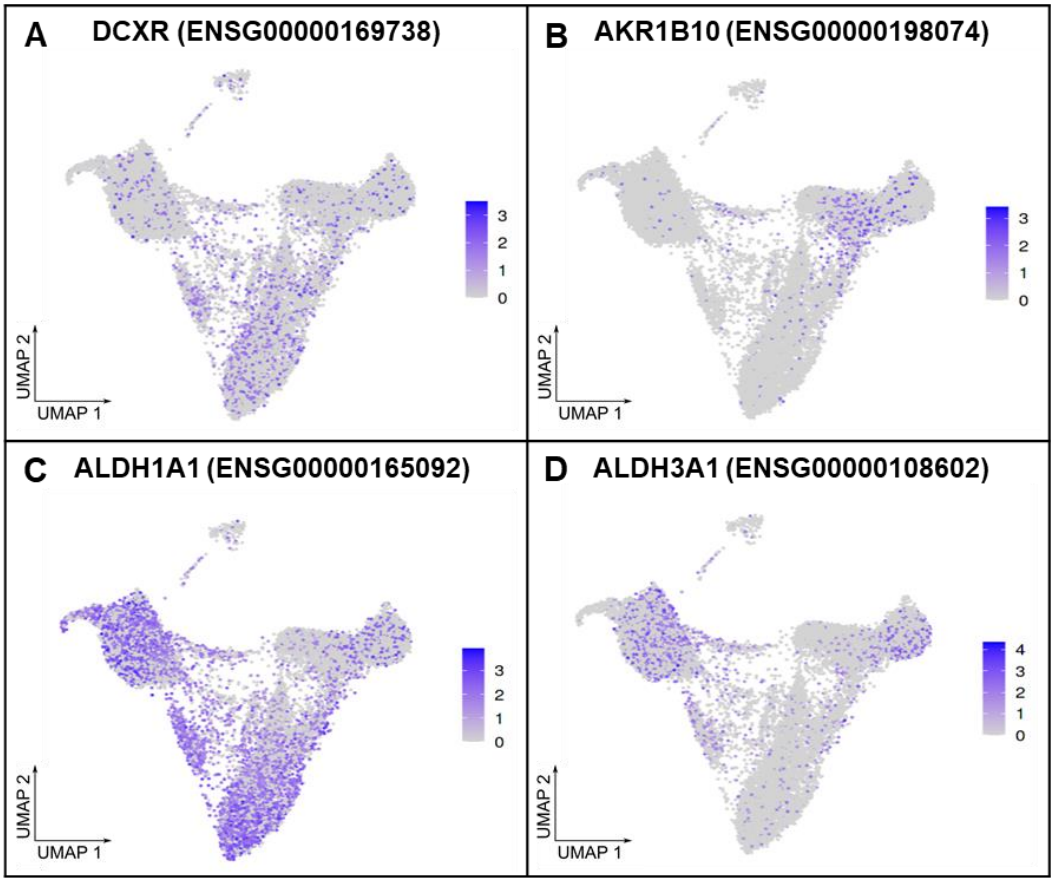

***Figure 22**: Distribution of phase I enzymes at the single-cell level for human nasal models. Cells expressing (A) DCXR; (B) AKR1B10; (C) ALDH1A1; (D) ALDH3A1, are noted as violet dots. Single-cell RNA sequencing as performed by Rinu Sivarajan (Chair of Tissue Engineering and Regenerative Medicine, Würzburg). UMAP were realized by Prof. Florian Erhard and Kevin Berg (Institute of Virology and Immunobiology, Würzburg). N=3*

Concerning phase I enzymes, *DCXR*, *AKR1B10*, *ALDH1A1* and *ALDH3A1* were investigated. Figure 22 shows the distribution of the phase I transcripts and Figure 23 the distribution of phase II transcripts among the cells sequenced for the scRNaseq, whose cell-type was attributed in Figure 18. Comparing Figure 18 with Figures 22 and 23 allows to have an idea of the cell types expressing the different XME variants investigated in Figure 22 and 23. *DCXR* gene seems to be moderately expressed within diverse cell populations present in the model (Figure 22A), while *AKR1B10* seems to have a low expression concentrated in the basal cells (Figure 22B). Regarding ALDH variants, *ALDH1A1* is ubiquitously expressed in the model, evenalthoughit seems slightly less present in basal cells (Figure 22C), while *ALDH3A1* seems to be slightly expressed in the model, mostly in ciliated cells and basal cells (Figure 22D). As stated before, expression of these phase I in the model was confirmed with RT-qPCR (Figure 20). However, PCR results concerning *ALDH3A1* should be handled carefully as the melting curve shows a second peak, meaning the primers may not be specific to one transcript,

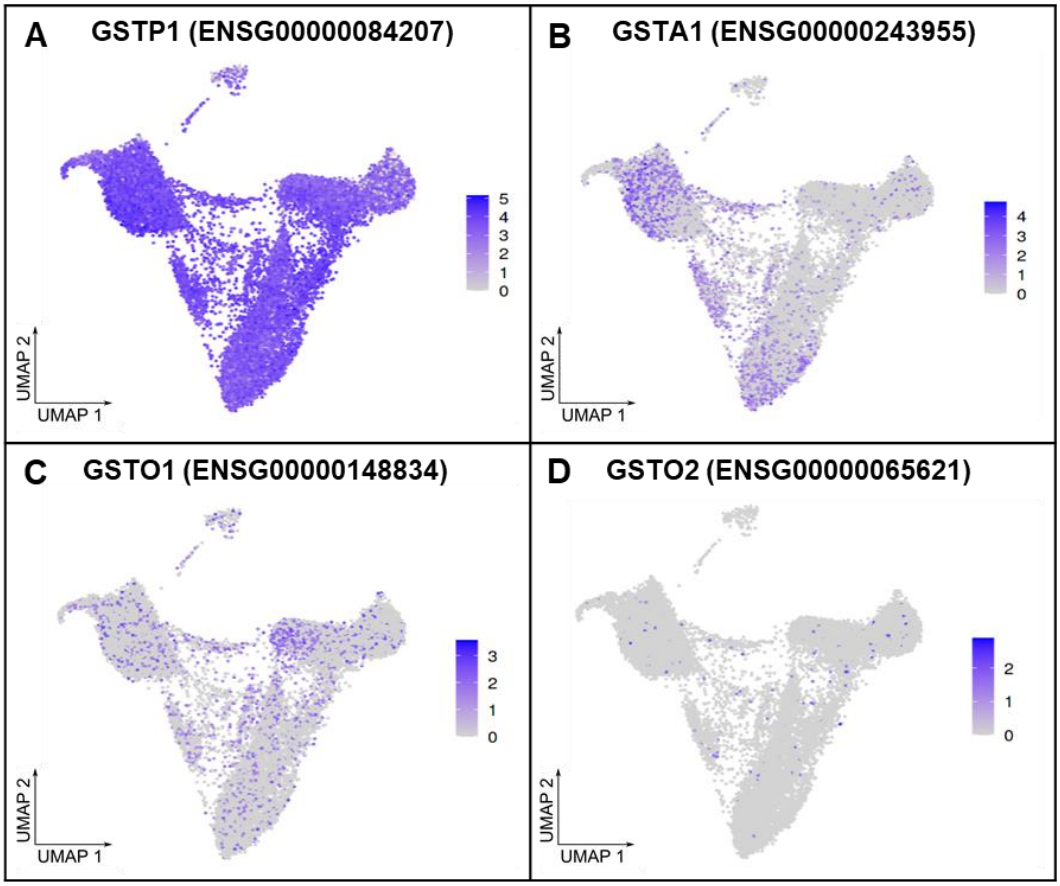

***Figure 23**: Distribution of phase I enzymes at the single-cell level for human nasal models. Cells expressing (A) GSTP1; (B) GSTA1; (C) GSTO1; (D) GSTO2, are noted as violet points. Single-cell RNA sequencing as performed by Rinu Sivarajan (Chair of Tissue Engineering and Regenerative Medicine, Würzburg). UMAP were realized by Prof. Florian Erhard and Kevin Berg (Institute of Virology and Immunobiology, Würzburg). N=3*

as *ALDH3A1* has 17 splice-variants transcripts[3]. Concerning phase II enzymes, three families of GST were investigated (Figure 23): pi GST (*GSTP1*), alpha GST (*GSTA1*), and omega GST (*GSTO1* and *GSTO2*). *GSTP1* is strongly and ubiquitously expressed in the model (Figure 23A), whereas *GSTA1* seems to be moderately expressed in multiciliated cells and secretory cells, but not so much in basal cells (Figure 23B). *GSTO1* seems to be moderately expressed in the model, with no particular preference for a cell type (Figure 23C), *GSTO2* is almost absent in the model (Figure 23D). Like phase I enzymes, expression was verified with RT-qPCR (Figure 21) for all the variants cited but *GSTO1*, for which the best primers melting curve shows two peaks, maybe due to potentially 7

[3] https://www.ensembl.org/Homo_sapiens/Gene/Splice?db=core;g=ENSG00000108602;r=17:19737984-19748943

splice-variants transcripts[4]; hence, PCR results should be handled carefully for this isoform.

[4] https://www.ensembl.org/Homo_sapiens/Gene/Splice?db=core;g=ENSG00000148834;r=10:104235356-104267459

Protein expression of phase I and phase II enzymes: focus on target variants

On the protein level, DCXR was found in an omnipresent manner within the model.

DAB staining and immunofluorescence staining (Figure 24A and 24B, respectively) show a strong presence of DCXR within the epithelium, but also a faint presence in the matrix were fibroblasts are. Figure 24C and 24C show colocalization of DCXR with CK5 (basal

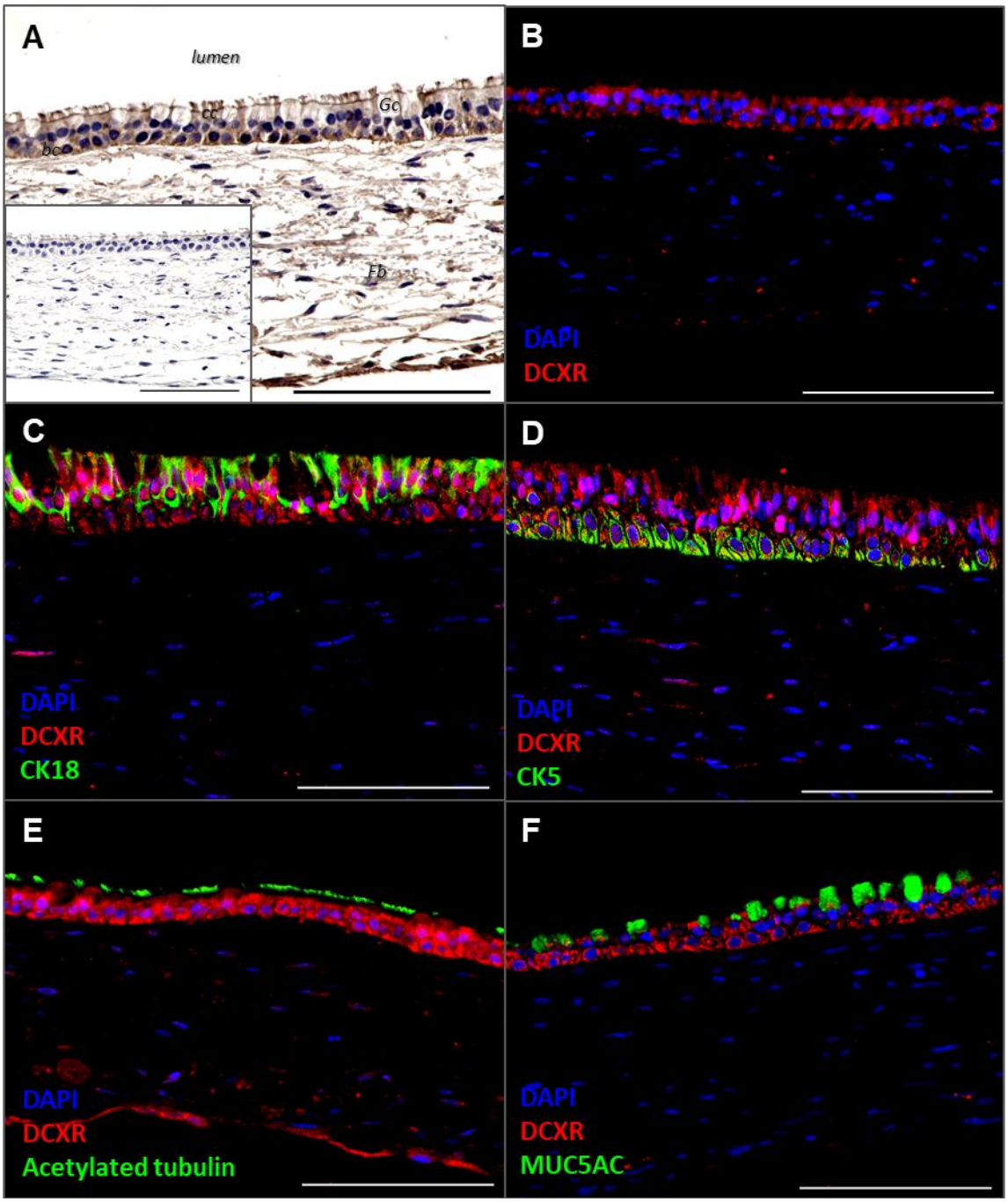

***Figure 24**: Localization of DCXR within the 3D human respiratory mucosa model. (A) DAB staining of DCXR in brown, the insert indicated the negative control. Immunofluorescence staining: co-localization is displayed via yellow color (red and green overlaying). (B) DCXR staining in red; (C) DCXR in red and epithelial cells in green (marker: CK18); (D) DCXR in red and basal cells in green (marker: CK5); (E) DCXR in red and cilia in green (marker: acetylated tubulin); (F) DCXR in red and MUC5AC in green. Nuclei are stained in blue (DAPI) in immunofluorescence figures. Gc: goblet cells, cc: ciliated cells, bc: basal cells, Fb: fibroblasts. Scalebar = 100 µm, N=7*

cells) and CK18 (differentiated epithelial cells), meaning the protein is present within these cell types, which is coherent with what has been described before (Robert-Hazotte et al., 2022). Figure 24E shows no colocalization of DCXR with acetylated tubulin. Figure 24F shows no colocalization of DCXR with MUC5AC.

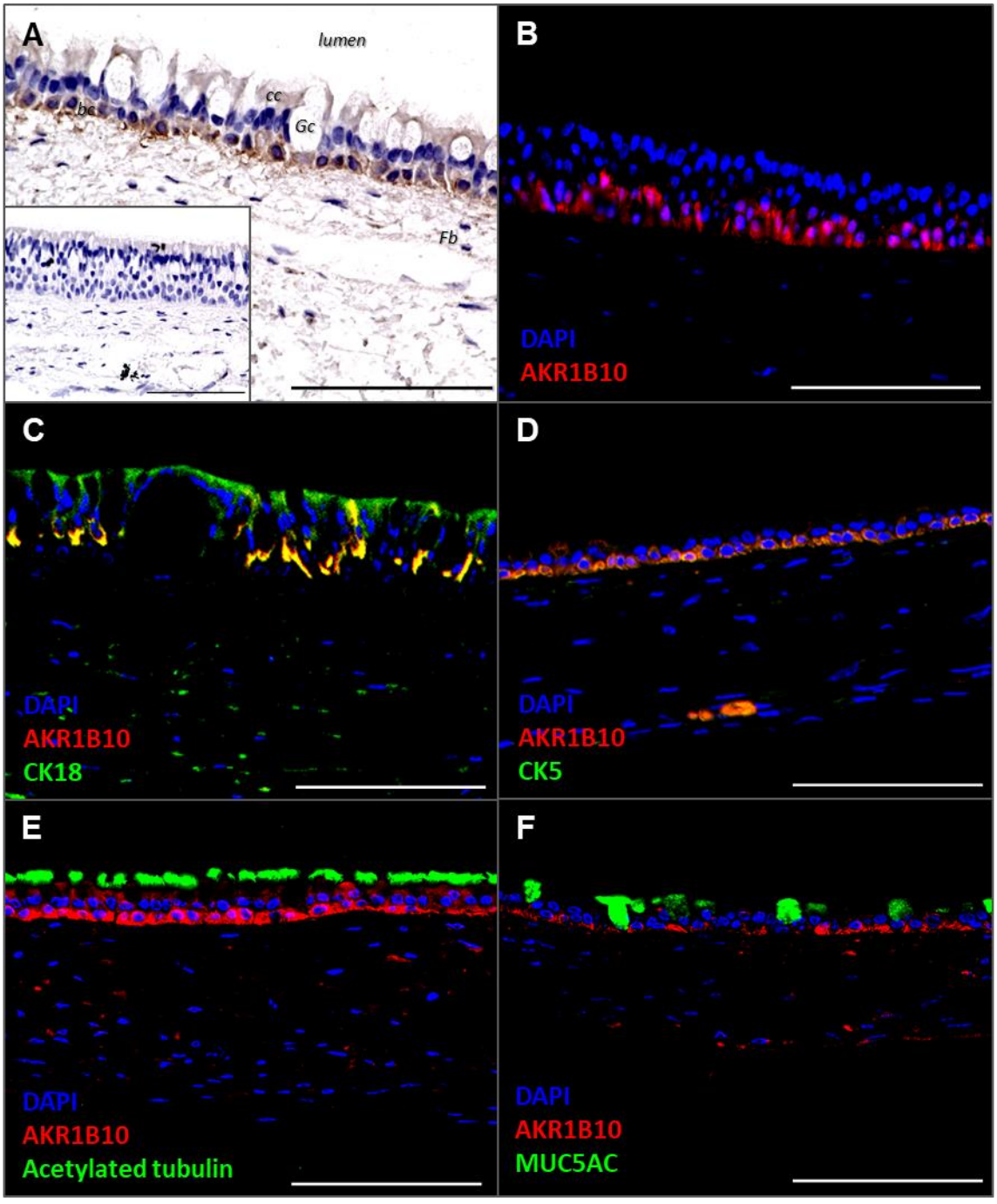

***Figure 25**: Localization of AKR1B10 within the 3D human respiratory mucosa model. (A) DAB staining of AKR1B10 in brown, the insert indicated the negative control. Immunofluorescence staining: co-localization is displayed via yellow color (red and green overlaying). (B) AKR1B10 staining in red; (C) AKR1B10 in red and epithelial cells in green (marker: CK18); (D) AKR1B10 in red and basal cells in green (marker: CK5); (E) AKR1B10 in red and cilia in green (marker: acetylated tubulin); (F) AKR1B10 in red and MUC5AC in green. Nuclei are stained in blue (DAPI) in immunofluorescence figures. Gc: goblet cells, cc: ciliated cells, bc: basal cells, Fb: fibroblasts. Scalebar = 100 µm, N=7*

AKR1B10 seems to be concentrated in cells at the basal side of the epithelial layer, which most probably are basal cells (Figure 25A and 25B). AKR1B10 and CK18 colocalization (yellow color, Figure 25C) is only present at the basal pole of differentiated epithelial cells (marked with CK18 in green). Figure 25D shows AKR1B10/CK5 colocalization, confirming the presence of AKR1B10 in basal cells. AKR1B10 does not colocalize with acetylated tubulin, supporting the restriction of the enzyme abundance to the basal compartment of the epithelial layer (Figure 25E). Similarly, there was no colocalization

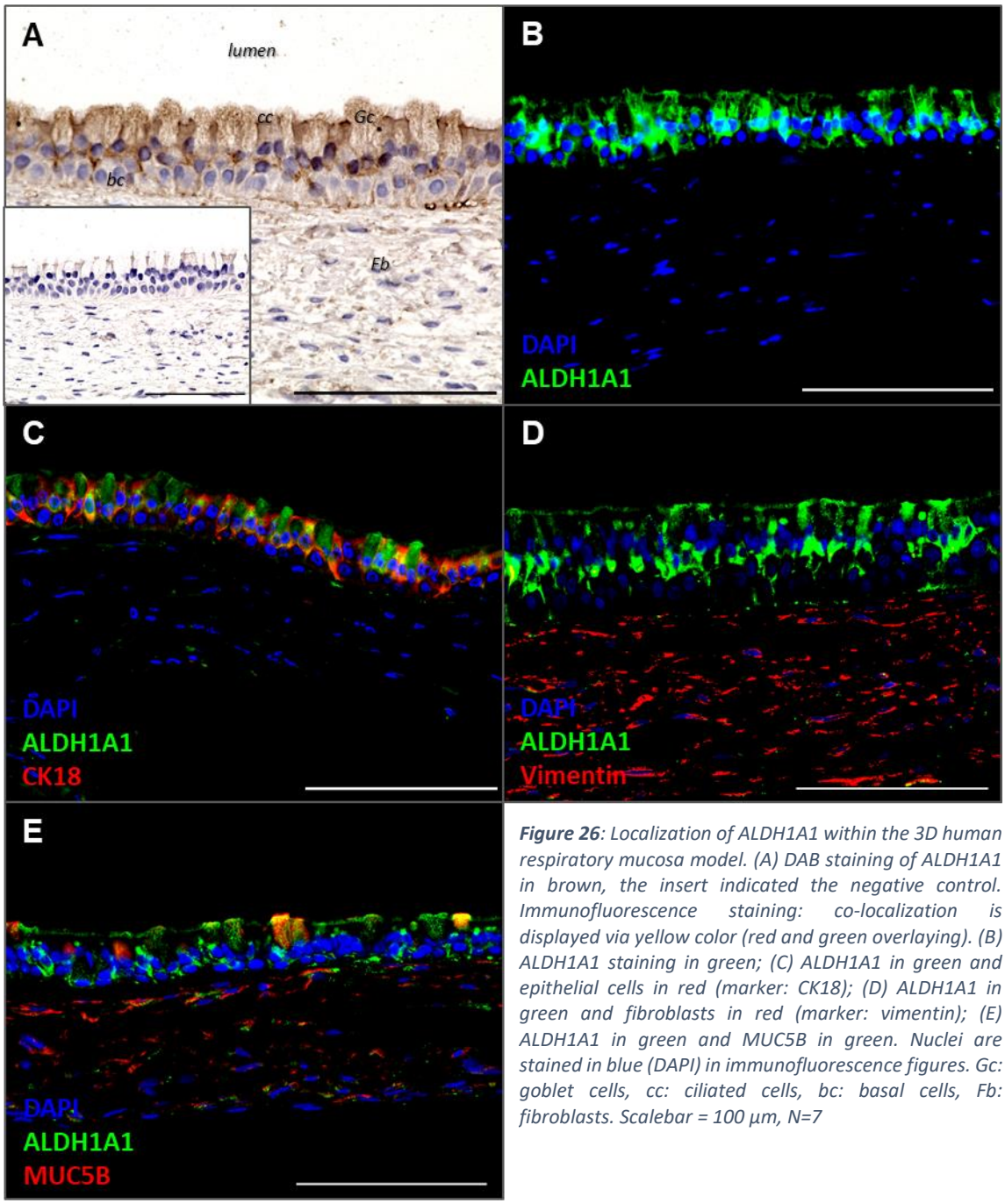

***Figure 26**: Localization of ALDH1A1 within the 3D human respiratory mucosa model. (A) DAB staining of ALDH1A1 in brown, the insert indicated the negative control. Immunofluorescence staining: co-localization is displayed via yellow color (red and green overlaying). (B) ALDH1A1 staining in green; (C) ALDH1A1 in green and epithelial cells in red (marker: CK18); (D) ALDH1A1 in green and fibroblasts in red (marker: vimentin); (E) ALDH1A1 in green and MUC5B in green. Nuclei are stained in blue (DAPI) in immunofluorescence figures. Gc: goblet cells, cc: ciliated cells, bc: basal cells, Fb: fibroblasts. Scalebar = 100 µm, N=7*

with MUC5AC, thus it appears not to be present in MUC5AC-expressing secretory cells or in secreted mucus (Figure 25F).

Immunofluorescence staining confirm the presence of ALDH1A1 spread throughout the whole epithelial layer (Figure 26A and 15B). Figure 26C shows colocalization of ALDH1A1 with differentiated epithelial cells (in yellow), as well as ALDH1A1 marked “bubbles” structures that could correspond to goblet cells. This is confirmed Figure 26E where ALDH1A1 colocalize with MUC5B, suggesting that this enzyme is present in MUC5B-secreting goblet cells. Finally, Figure 26D demonstrates a clear demarcation between the fibroblast-loaded scaffold (marked in red with vimentin) and the epithelial layer expressing ALDH1A1 (in green).

ALDH3A1 seems to be present at a lower lever throughout the entire model – epithelial layer and fibroblast-loaded scaffold,althoughit is only faintly present in the scaffold (Figure 27A and 27B). Moreover, ALDH3A1 and MUC5B do not colocalize.

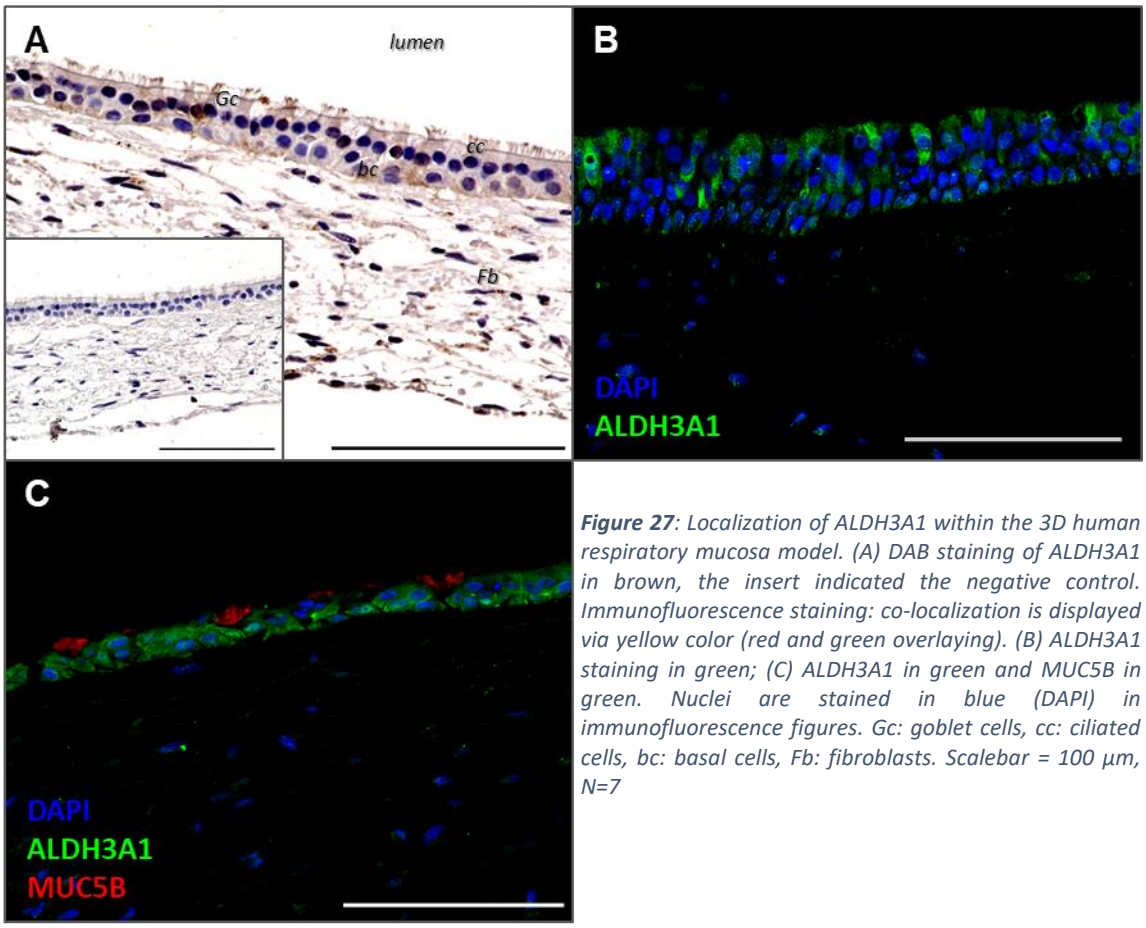

***Figure 27**: Localization of ALDH3A1 within the 3D human respiratory mucosa model. (A) DAB staining of ALDH3A1 in brown, the insert indicated the negative control. Immunofluorescence staining: co-localization is displayed via yellow color (red and green overlaying). (B) ALDH3A1 staining in green; (C) ALDH3A1 in green and MUC5B in green. Nuclei are stained in blue (DAPI) in immunofluorescence figures. Gc: goblet cells, cc: ciliated cells, bc: basal cells, Fb: fibroblasts. Scalebar = 100 µm, N=7*

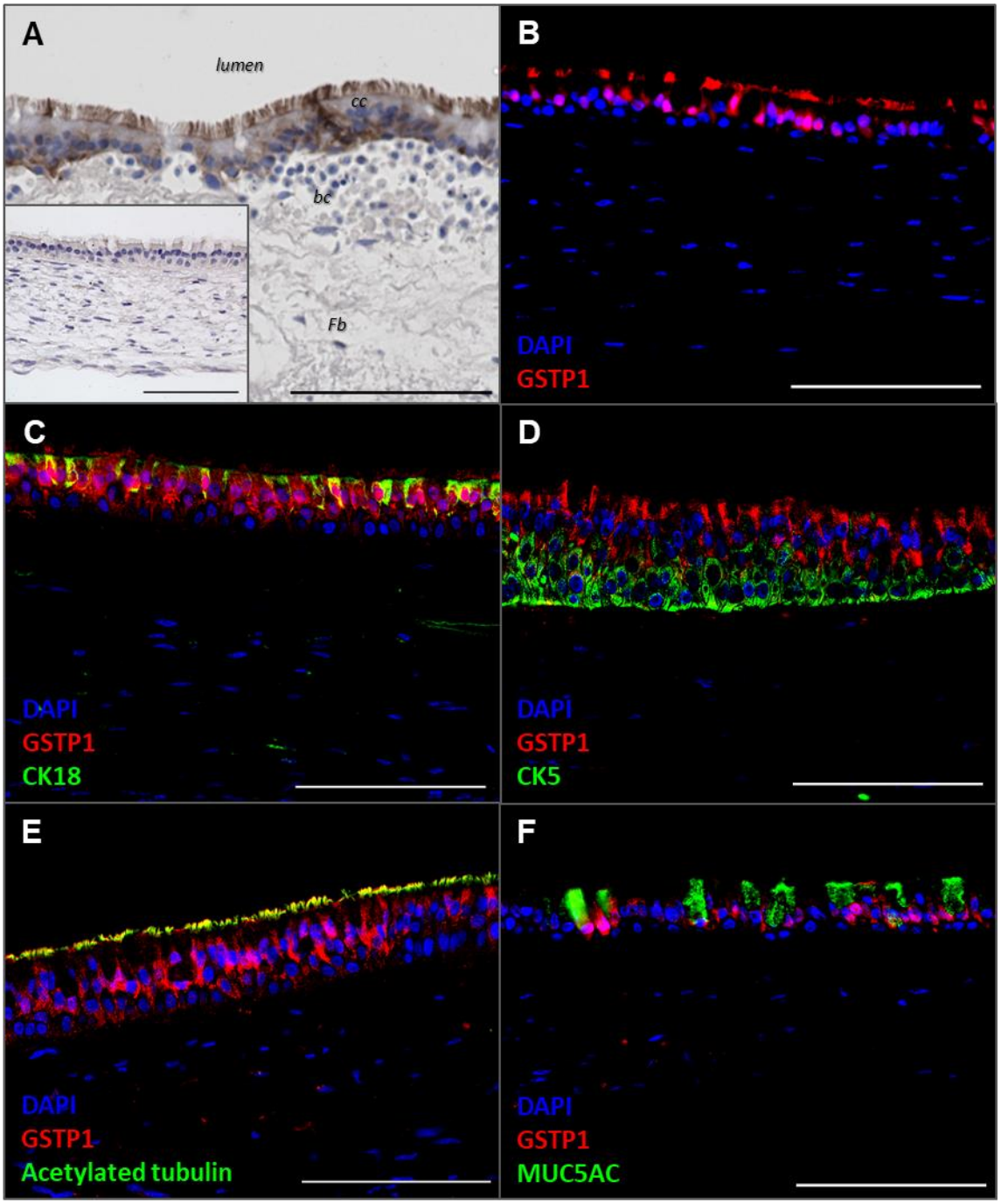

***Figure 28**: Localization of GSTP1 within the 3D human respiratory mucosa model. (A) DAB staining of GSTP1 in brown, the insert indicated the negative control. Immunofluorescence staining: co-localization is displayed via yellow color (red and green overlaying)l. (B) GSTP1 staining in red; (C) GSTP1 in red and epithelial cells in green (marker: CK18); (D) GSTP1 in red and basal cells in green (marker: CK5); (E) GSTP1 in red and cilia in green (marker: acetylated tubulin); (F) GSTP1 in red and MUC5AC in green. Nuclei are stained in blue (DAPI) in immunofluorescence figures; cc: ciliated cells, bc: basal cells, Fb: fibroblasts. Scalebar = 100 µm, N=7*

Concerning phase II enzymes, GSTP1 seems to be present strongly in punctual spots within the epithelium, mostly on the apical side (Figure 28A). Immunofluorescence pictures show presence of GSTP1 in the cytoplasm of these cells, but also in nuclei and in brush-like structures that most probably are cilia (Figure 28B). This was confirmed by GSTP1/acetylated tubulin nicely co-localizing in Figure 28E. GSTP1 colocalize with CK18,

confirming the presence of the protein in respiratory epithelial cells (Figure 28C). However, there was no colocalization with CK5-6, which means GSTP1 does not seems to be present in these cells (Figure 28E). Likewise, no colocalization was found with MUC5AC (Figure 28F), which means GSTP1 is not found in MUC5AC-expressing goblet cells.

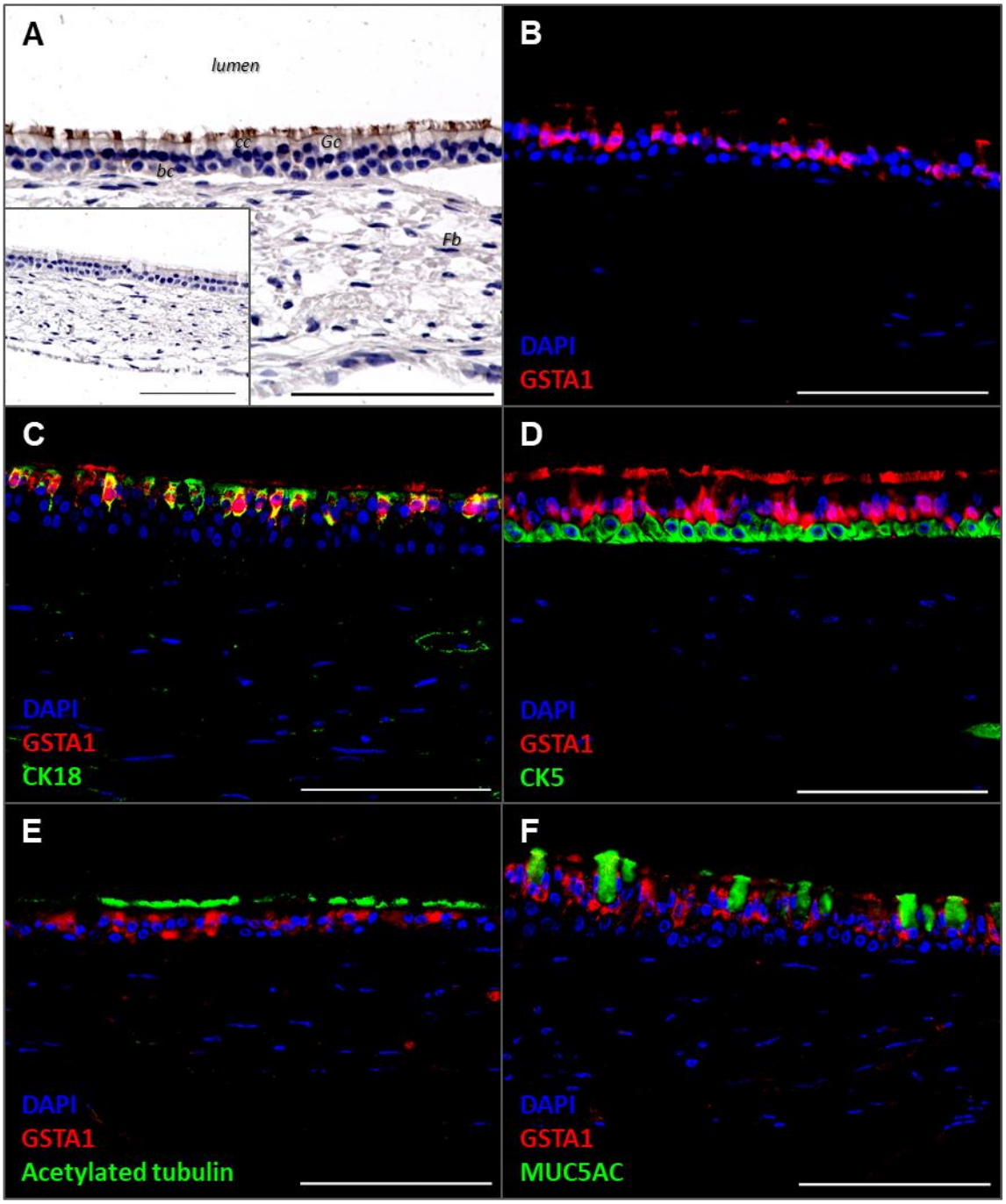

***Figure 29**: Localization of GSTA1 within the 3D human respiratory mucosa model. (A) DAB staining of GSTA1 in brown, the insert indicated the negative control. Immunofluorescence staining: co-localization is displayed via yellow color (red and green overlaying. (B) GSTA1 staining in red; (C) GSTA1 in red and epithelial cells in green (marker: CK18); (D) GSTA1 in red and basal cells in green (marker: CK5); (E) GSTA1 in red and cilia in green (marker: acetylated tubulin); (F) GSTA1 in red and MUC5AC in green. Nuclei are stained in blue (DAPI) in immunofluorescence figures. Gc: goblet cells, cc: ciliated cells, bc: basal cells, Fb: fibroblasts. Scalebar = 100 µm, N=7*

GSTA1 seems to be strongly present in some ciliated cells (Figure 29A). This is also shown in Figure 29B where the immunostaining lights up punctually what seems to be ciliated cells, with brush-like shapes on the apical pole. However, there seems to be no apparent colocalization of GSTA1 with acetylated tubulin (Figure 29E). In Figure 29E, the GSTA1 signal in the apical compartment is fainter than in Figure 29A and 29B, which could explain why we do not see a colocalization. Figure 29C shows colocalization of GSTA1 with CK18, which confirms expression of the protein in differentiated epithelial cells, while Figure 29D shows no colocalization with CK5-6, suggesting that GSTA1 is not

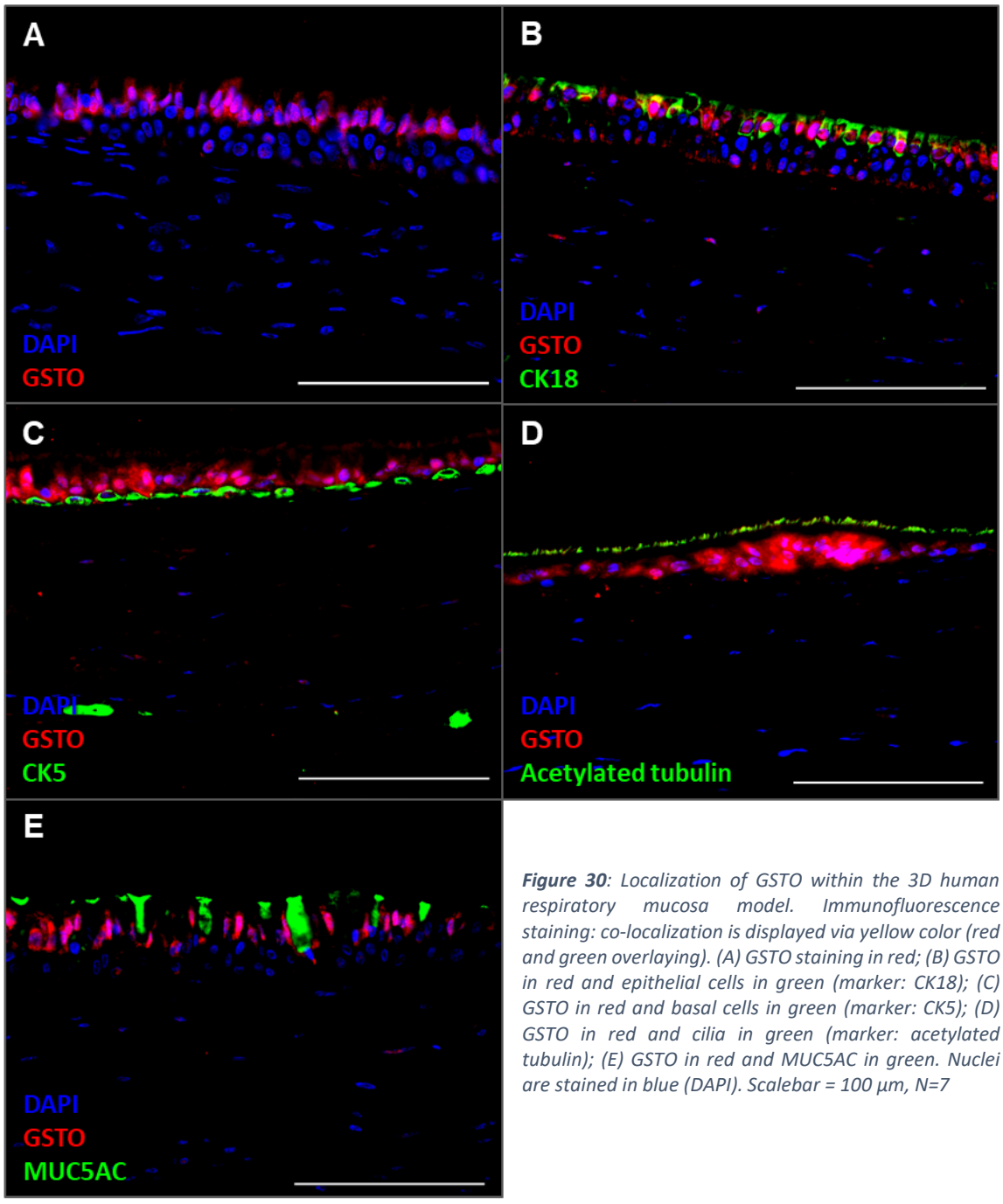

***Figure 30**: Localization of GSTO within the 3D human respiratory mucosa model. Immunofluorescence staining: co-localization is displayed via yellow color (red and green overlaying). (A) GSTO staining in red; (B) GSTO in red and epithelial cells in green (marker: CK18); (C) GSTO in red and basal cells in green (marker: CK5); (D) GSTO in red and cilia in green (marker: acetylated tubulin); (E) GSTO in red and MUC5AC in green. Nuclei are stained in blue (DAPI). Scalebar = 100 µm, N=7*

present in basal cells. Lastly, Figure 29F shows no apparent colocalization with MUC5AC, just like GSTP1.

Lastly, Figure 30A shows GSTO staining mostly on the apical side of the epithelial layer. Although GSTO staining is quite faint in Figure 30B, is seems to colocalize with epithelial cells (CK18), and it also seems to be localized in nuclei in the picture. Like GSTP1 and GSTA1, GSTO does not colocalize with basal cells (CK5, Figure 30C) and MUC5AC (Figure 30E). There is no colocalization of GSTO1 with acetylated tubulin (Figure 30D), meaning GSTO is probably not located in the cilia of multiciliated cells. Overall, GSTO localization pattern is very similar to what was found for GSTP1 and GSTA1.

2.2. Odorant exposure and gene regulation of XME in the human nasal respiratory mucosa model

Toxicity of the odorant treatments

Following the characterization of the human nasal respiratory mucosa model, I started to optimize the protocol to expose the model with odorants in a way as close as possible to the *in vivo* situation. Regarding my previous results on rat olfactory explants, I decided to first verify that the chosen conditions were not toxic nor damaged the tissue models. Figure 31 shows the MTT test results for different concentrations of 2,3-pentanedione

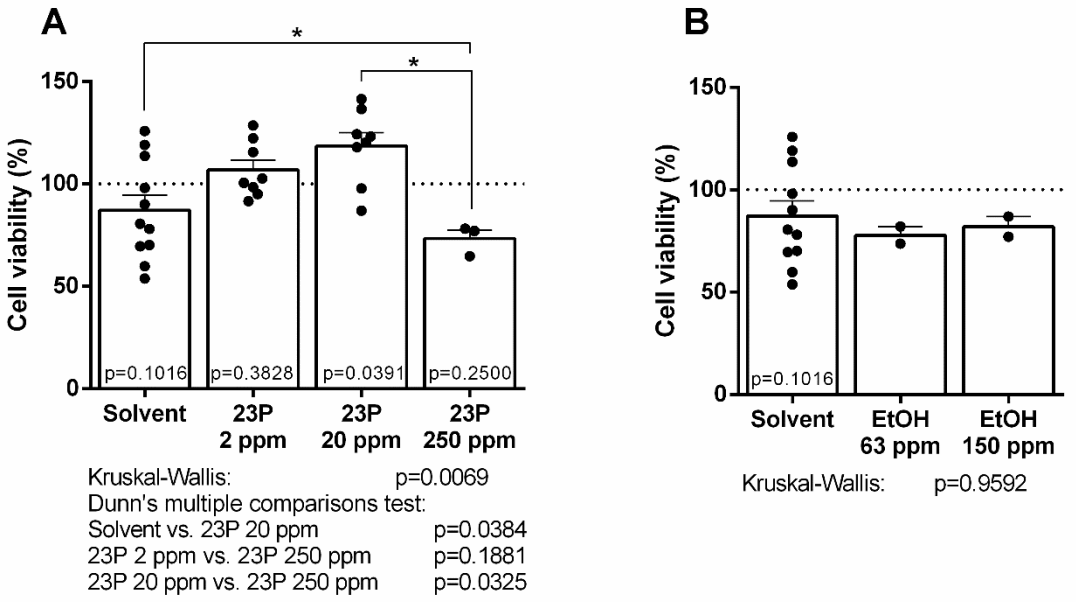

***Figure 31**: Cell viability tests of the human 3D respiratory tissue model in response to 2h incubation with: (A) 2,3-pentanedione (nebulized: 2 ppm and 20 ppm; liquid: 250 ppm), and (B) nebulized ethanol, using MTT assays. Data are presented in cellular viability (%) compared to untreated control. Statistical analysis was handled on GraphPad Prism 6.0. For each treatment, Wilcoxon signed rank tests against a theoretical mean of 100 were performed (p-values displayed in the bars), and treatments were compared between them using a Kruskal-Wallis test followed by Dunn's multiple comparisons tests (p-values inferior to p=0.2 are displayed below the graphs). Each point represents a different biological donor.*

(Figure 31A) and ethanol (Figure 31B) treatments. No treatment involving 2,3-pentanedione induced a cell viability significantly lower than 100 %, hence I considered all conditions tested non-toxic for the model. Concerning ethanol, there wasn't enough repetitions to perform statistic tests, as I later focused on 2,3-pentanedione and did not continue with ethanol. I chose to display the results nonetheless as I still kept ethanol exposed samples and included them in further experiments. Figure 32 shows haematoxylin and eosin staining of donor matched human nasal respiratory tissue models which were not treated as a control (Figure 32A), or incubated 2 hours with 250 ppm of 2,3-pentanedione (Figure 32B). In both pictures the tissue displays an organized

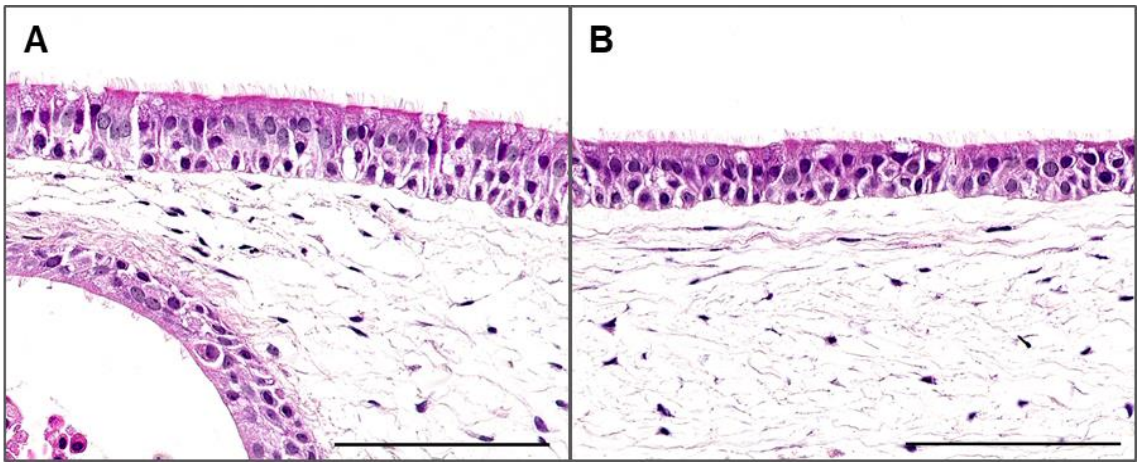

***Figure 32**: Haematoxylin and eosin staining of the human nasal respiratory mucosa, after (A) no treatment, and (B) 2 hours of incubation with 250 ppm of 2,3-pentanedione. Scalebar is equal to 100 µm. N=2*

and polarized pseudostratified columnar epithelium with kinocilia-like structures on the apical side, as described in Figure 17. No apparent deterioration of the structure of the tissue could be observed after a 2-hour treatment of 250 ppm of 2,3-pentanedione. In Figure 32A, part of a "bubble"-like structure can be observed in the left corner of the picture. These kinds of cyst-like inclusions were observed regularly among the models from different donors and not depending of the experimenter. A possible explanation for this phenomenon considers the fact that the porcine SIS scaffold present a huge variability in terms of thickness, and include blood vessels and a non-flat surface, which could explain why some epithelial cells migrated inside the scaffold to form these structures.

Regulation of XMEs in response to nebulized odorant treatments

I then proceeded with odorant exposure experiments. Odorant solutions were nebulized on top of the tissue models then incubated for 2 hours. This treatment method was chosen to mimic a punctual, physiological exposure to odorants. Results are compiled in Figure 33. Figure 33A shows gene expression of *DCXR* in response to ethanol and 2,3-pentanedione (2 ppm and 20 ppm). Ethanol is not a known substrate of DCXR, whereas 2,3-pentanedione is. Results show no significant effect of the treatment on *DCXR* gene expression,althoughthere seems to be a downward trend for the condition with 20 ppm of 2,3-pentanedione. I then investigated nuclear receptors within the models and only three could be amplified in a reliable manner using RT-qPCR. Figure 33B displays the gene expression of the aryl hydrocarbon receptor (*AhR*) in response to ethanol and 2,3-pentanedione (2 ppm and 20 ppm). No significant effect of either

molecule was found,althoughone donor seems to respond to ethanol treatment. Figure 22C shows nuclear factor erythroid 2 (NFE2)-related factor 2 (*Nrf2*) gene expression in response to ethanol and 2,3-pentanedione treatment. Like *AhR*, no significant effect was detected in these conditions, but one donor seems to respond to ethanol treatment.

Lastly, Figure 33D shows *PPARG* gene expression in response to ethanol and 2,3-pentanedione. Again, no significant effect of either molecule was shown, but models

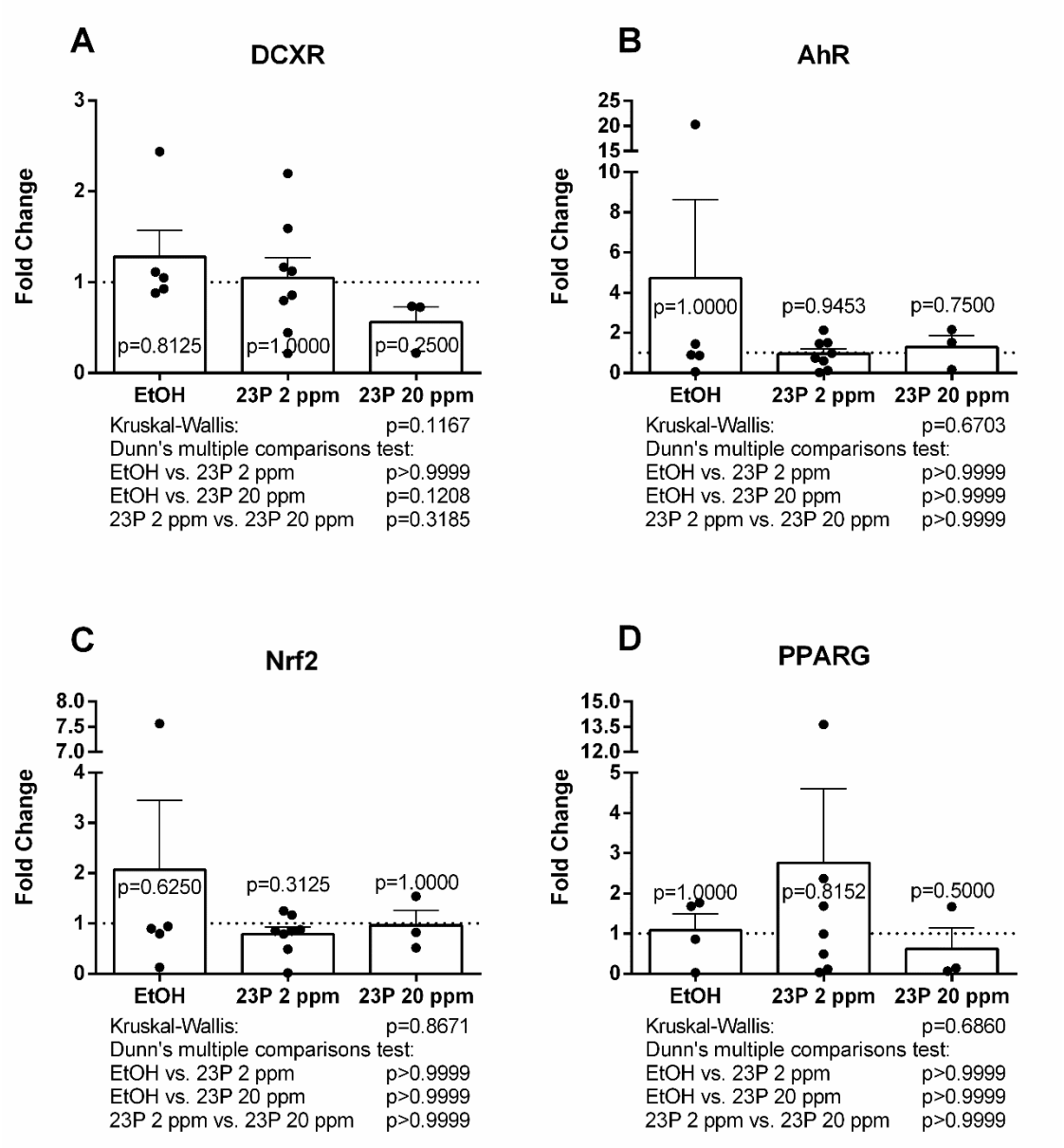

***Figure 33**: Fold Change gene expression analysis of (A) DCXR, (B) AhR, (C) Nrf2, and (D) PPARG in response to nebulized odorants (23P: 2,3-pentanedione) and ethanol (EtOH, 63 ppm) using RT-qPCR. For each biological donor, data are presented as fold change relative to solvent controls: gene expression ratios were calculated using the common base method (see Ganger et al., 2017) then normalized by the corresponding controls, and plotted as mean + SEM. Statistical analysis was handled on GraphPad Prism 6.0. For each treatment, Wilcoxon signed rank tests against a theoretical mean of 1 were performed (p-values displayed in the bars), and treatments were compared between them using a Kruskal-Wallis test followed by Dunn's multiple comparisons tests (p-values displayed below the graphs). Each point represents a different biological donor.*

treated with 2 ppm of 2,3-pentanedione seem to display a higher variability in the response.

Regulation of XME in response to a direct liquid odorant treatment

Following these results, I tried a stronger treatment by applying directly the odorant solution of the apical side of the models. I chose higher concentrations but kept a 2-hour incubation to limit the toxicity of the conditions. The aim was to keep conditions that could be encountered on a physiological, olfactory level, while trying a protocol that would allow other readouts (see Twister experiments page 115). Figure 34 summarizes gene expression of *DCXR* (Figure 34A), *GSTP1* (Figure 34B), *AhR* (Figure 34C), *Nrf2* (Figure 34D), and *PPARG* (Figure 34E), in response to 250 ppm of 2,3-pentanedione, 100 µM of dexamethasone, and 250 ppm of 3,4-hexanedione. While 2,3-pentanedione and 3,4-hexanedione are odorant substrates of DCXR, dexamethasone is a glucocorticoid known to induce GSTP1 in other tissue, in a dose dependent manner. The idea was to use it as a positive control: if dexamethasone can induce GSTP1 with a 2 h exposure time, but odorants do not, then the model can respond to a short treatment and 2,3-pentanedione and 3,4-hexanedione are simply not inducers of DCXR in conditions imitating an olfactory event. Concerning *DCXR*, the Wilcoxon statistical test could not detect a significant effect of any molecule on *DCXR* gene expression, and there is no difference between the treatments. On average, 2,3-pentanedione treatment seems to lower the gene expression of *DCXR*, while 3,4-hexanedione seems to increase it,althoughthe variability among the different donors does not allow to conclude anything with the use of statistics. None of the treatments had a significant effect on *GSTP1* gene expression. Like *DCXR*, conditions were also not significantly different between them, and displayed a high variability among the donors especially for the dexamethasone treatment.

Concerning the nuclear receptors, *AhR* gene expression was not significantly affected by any of the treatments, nor the treatments differed significantly between them. Likewise, *Nrf2* gene expression was not affected by the molecules,althoughfold changes between dexamethasone and 3,4-hexanedione are different enough for the p-value of the Dunn's test to approach 0.05. Finally, *PPARG* gene expression was also investigated,althoughresults were harder to obtain at a satisfying quality regarding this

nuclear receptor. Indeed, results for 2,3-pentanedione could not be properly calculated at all, and only two datapoints were exploitable for the dexamethasone treatment. 3,4-

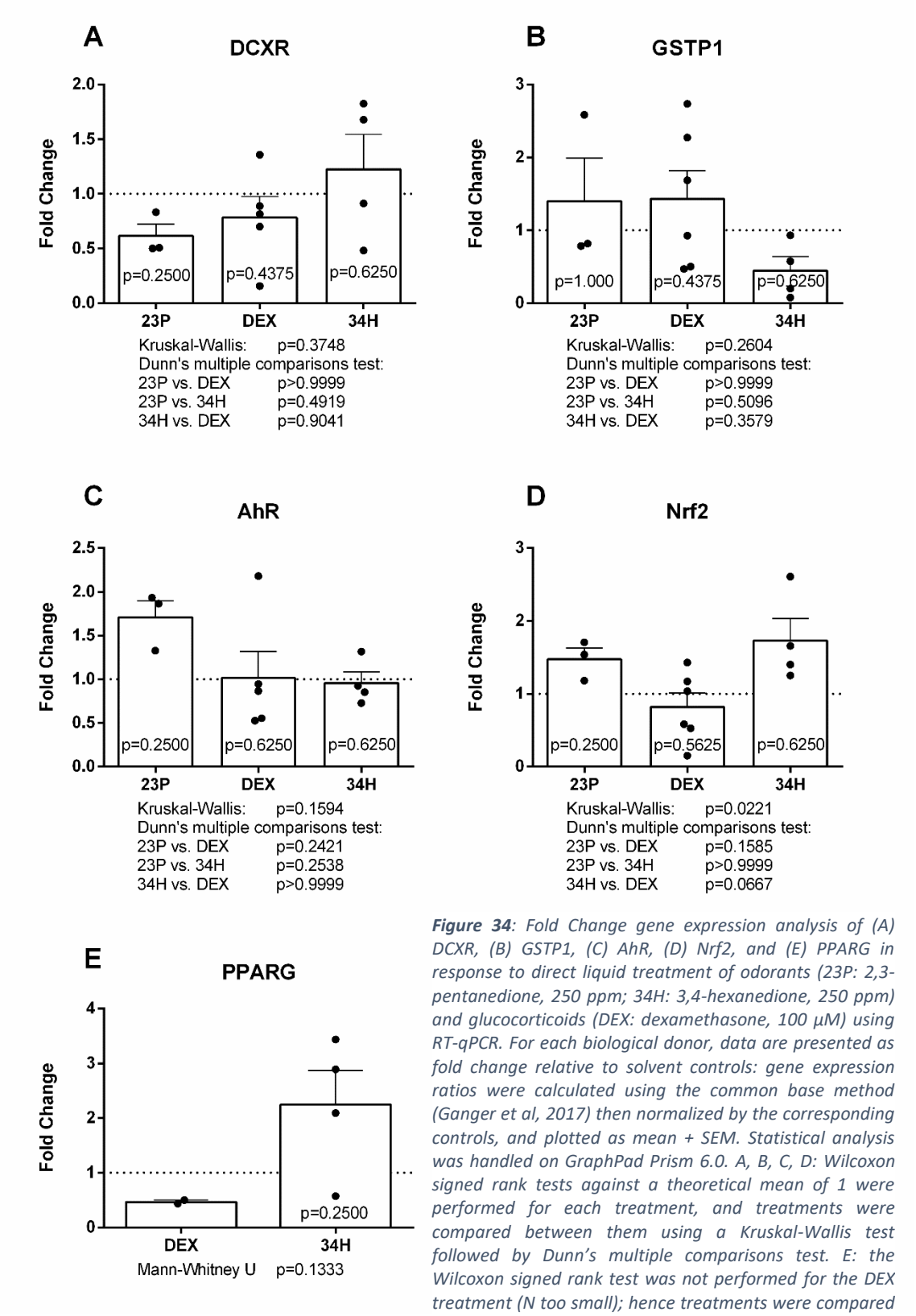

***Figure 34**: Fold Change gene expression analysis of (A) DCXR, (B) GSTP1, (C) AhR, (D) Nrf2, and (E) PPARG in response to direct liquid treatment of odorants (23P: 2,3-pentanedione, 250 ppm; 34H: 3,4-hexanedione, 250 ppm) and glucocorticoids (DEX: dexamethasone, 100 µM) using RT-qPCR. For each biological donor, data are presented as fold change relative to solvent controls: gene expression ratios were calculated using the common base method (Ganger et al, 2017) then normalized by the corresponding controls, and plotted as mean + SEM. Statistical analysis was handled on GraphPad Prism 6.0. A, B, C, D: Wilcoxon signed rank tests against a theoretical mean of 1 were performed for each treatment, and treatments were compared between them using a Kruskal-Wallis test followed by Dunn's multiple comparisons test. E: the Wilcoxon signed rank test was not performed for the DEX treatment (N too small); hence treatments were compared using a Mann-Whitney U test. Each point represents a different biological donor.*

hexanedione treatment did not cause *PPARG* gene expression to significantly differ from 1, and no statistical differences between dexamethasone and 3,4-hexanedione treatments could be calculated in these conditions.

2.3. Odorant metabolism

Odorant metabolism of human nasal respiratory mucosa model homogenates

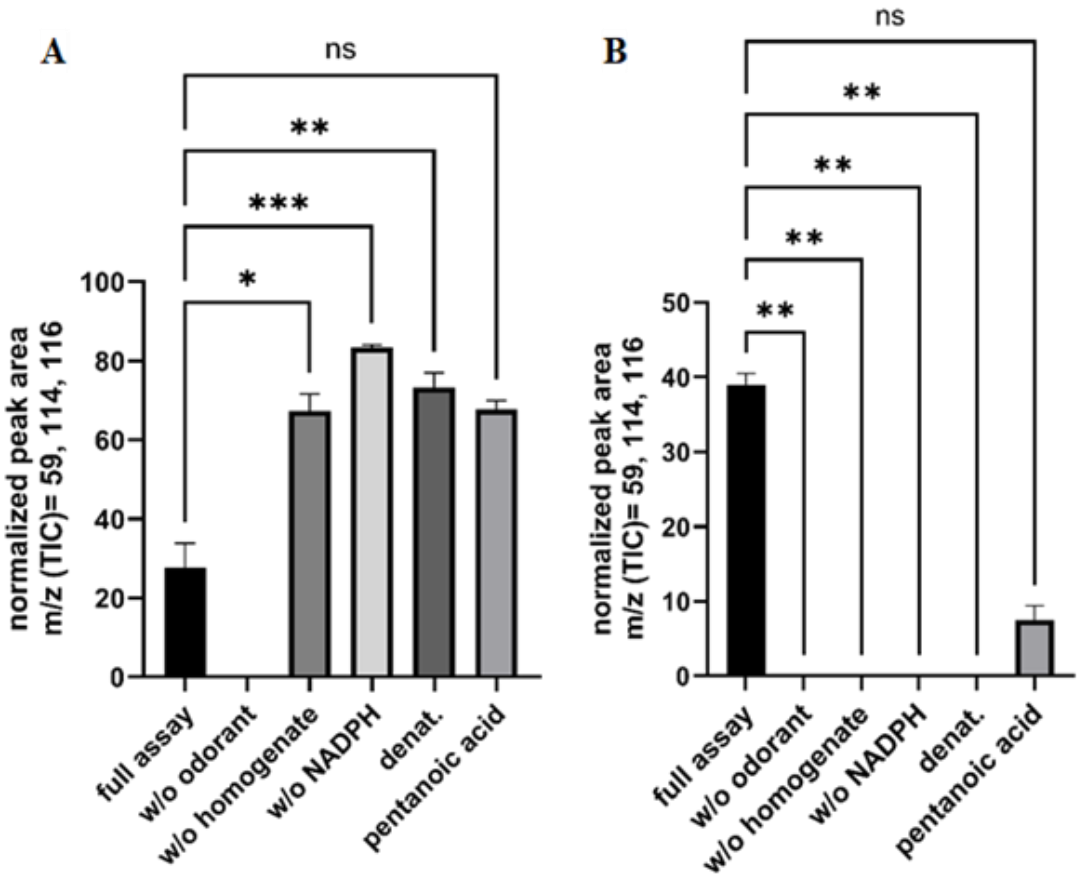

***Figure 35**: Metabolism of 3,4-hexanedione by tissue model homogenates. (A) Decrease in the amounts of the odorant 3,4-hexanedione. (B) Formation of the metabolite 4-hydroxy-3-hexanone. Technical triplicates were conducted for the full assays and control experiments. Odorant (w/o odorant), homogenate (w/o homogenate), or NADPH-regenerating system (w/o NADPH) was omitted; denaturized: mucosa was heated to 100 °C for 10 min before odorant application; pentanoic acid, NEM, KET, citral, and benomyl: incubation of the mucosa with a specific enzymatic inhibitor for 5 min before odorant application. Data are presented as means + SEM. Dunnett's posthoc tests were performed to compare the full assay with control conditions. n.d.= not detected, ns= not significant, *= p< 0.05; **= p< 0.01; ***= p< 0.001; ****= p<0.0001. N=3 biological donors.Merignac-Lacombe, Kornbausch et al., under revision*

After the detection of *DCXR* and several *ALDH* variants in the nasal respiratory mucosa model, we investigated the functionality of these XME families in the models, with the help of Nicole Kornbausch from the Chair of Aroma and Smell Research, Erlangen, Germany. Tissue models were homogenized, treated with defined compounds, and the corresponding metabolites were measured using GC-MS. Controls were also performed to verify that the peaks detected results of the enzymatic metabolism of the odorants: omission of the odorant (w/o odorant), replacement of the homogenate by human

albumin (w/o homogenate), omission of the NADPH regenerating-kit (w/o NADPH), or a heat-denaturation step of the homogenate before adding odorants. Additionally, several enzymatic inhibitors were added to investigate the contribution of different enzyme families in the odorant's metabolism. First, the metabolism of 3,4-hexanedione by DCXR was investigated (Figure 35). Figure 35A shows an expected decrease of the 3,4-hexanedione peak in the full assay, presumably due to its metabolism as it is restored in the controls. More precisely, there are statistically significant differences between the full assay and when the homogenate or the NADPH regenerating kit were

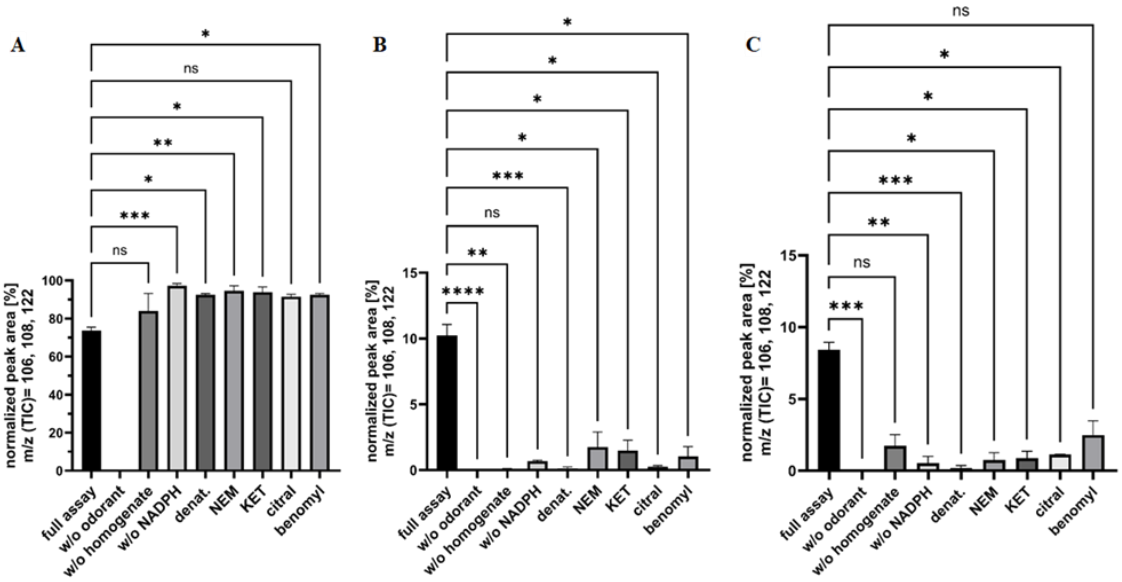

***Figure 36**: Metabolism of benzaldehyde by tissue model homogenates. (A) Decrease in the amounts of the odorant benzaldehyde. Formation of the metabolites (B) benzyl alcohol and (C) benzoic acid. Technical triplicates were conducted for the full assays and control experiments. Odorant (w/o odorant), homogenate (w/o homogenate), or NADPH-regenerating system (w/o NADPH) was omitted; denaturized: mucosa was heated to 100 °C for 10 min before odorant application; pentanoic acid, NEM, KET, citral, and benomyl: incubation of the mucosa with a specific enzymatic inhibitor for 5 min before odorant application. Data are presented as means + SEM. Dunnett's posthoc tests were performed to compare the full assay with control conditions. n.d.= not detected, ns= not significant, *= p< 0.05; **= p< 0.01; ***= p< 0.001; ****= p<0.0001. N=3 biological donors. Merignac-Lacombe, Kornbausch et al. under revision.*

absent, or when the homogenate was denaturized, underlying the involvement of enzymatic metabolism. In the control including pentanoic acid, an inhibitor of DCXR, the difference is smaller and no longer statistically significant. And as expected, 3,4-hexanedione was not detected in assays without odorant added, which confirm the odorant is not brought by any other parts constituting the assay. In Figure 35B, the metabolite 4-hydroxy-3-hexanone was detected in the full assay but not in the controls omitting the odorant, the homogenate, or the NADPH regenerating kit, or in the heat-

denaturized control. A smaller yet non-significant peak was detected in the assay containing the DCXR inhibitor.

The model's capacity to metabolize another odorant, benzaldehyde, was also investigated (Figure 36). Benzaldehyde is a substrate of ALDHs (Sołobodowska et al., 2012), but its metabolism is not restricted to this enzyme family. Like 3,4-hexanedione, benzaldehyde peak decreases in the full assay compared to controls (Figure 36A). This difference is only statistically significant when compared to the controls omitting the NADPH regenerating kit, when the homogenate is denaturized, and with some inhibitors, namely NEM, KET, and benomyl; however, controls omitting the homogenate or with citral as an inhibitor showed a smaller, non-statistically significant difference. Two metabolites were detected following the metabolism of benzaldehyde: benzyl alcohol (Figure 36B) and benzoic acid (Figure 36C). Peaks of benzyl alcohol and benzoic acid were significantly reduced in all controls, with the exception of the control without NADPH for benzyl alcohol, and the controls without homogenate or with the inhibitor benomyl for benzoic acid, which only show a visible downward trend.

Odorant metabolism of human nasal respiratory mucosa model headspace

In the meantime, I tried to optimize a protocol published by Yamaguchi and colleagues to detect odorant metabolites potentially released in the tissue model's headspace when treated with an odorant molecule. Figure 37 shows the only positive preliminary results obtained so far from these trials, obtained with the odorant 3-4-hexanedione. In Figure 37A, 3,4-hexanedione is detected in the headspace of the treated tissue models and the treated nasal fibroblasts-loaded scaffold, but not in the untreated controls. The

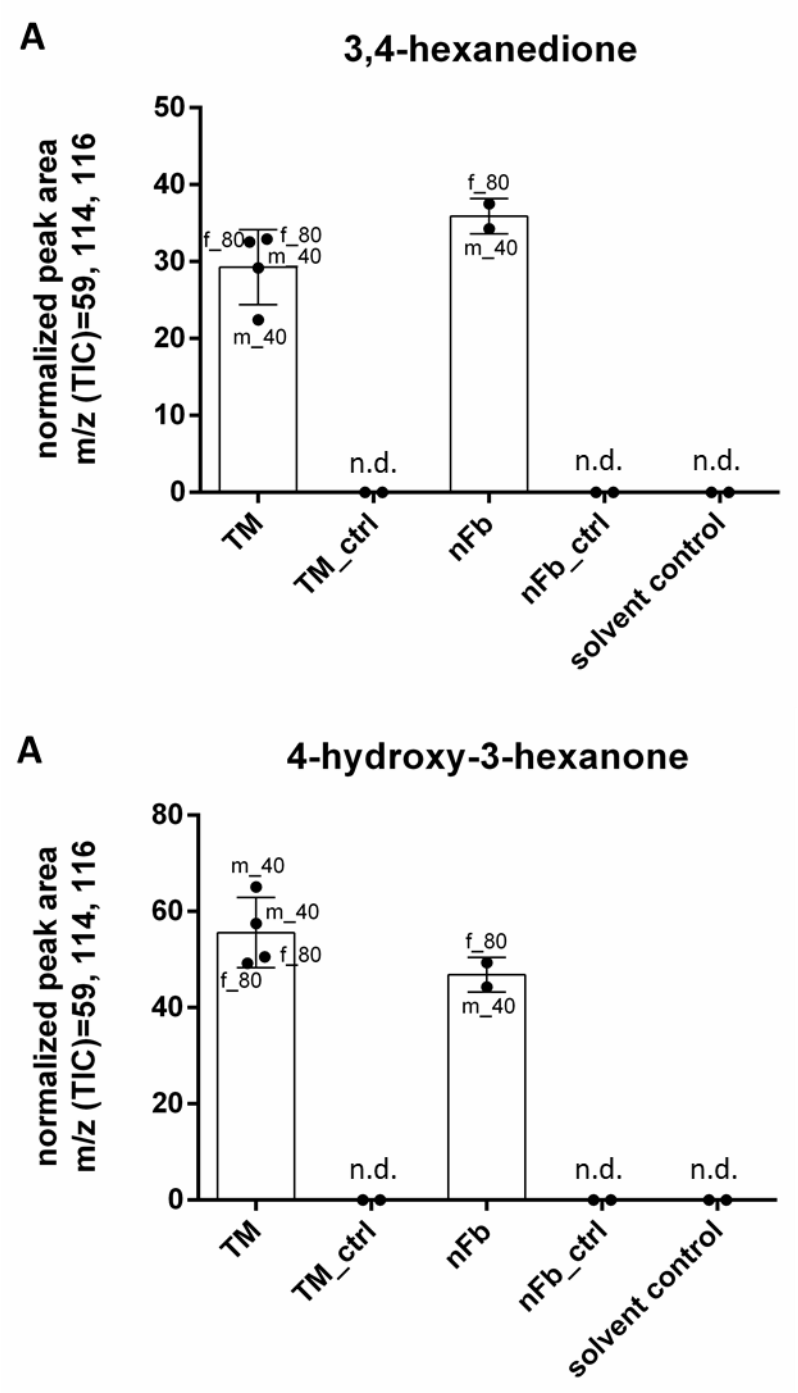

***Figure 37**: Metabolism of 3,4-hexanedione by tissue models. (A) Decrease in the amounts of the odorant 3,4-hexanedione when in presence of the tissue model (TM) compared to nasal fibroblasts-loaded scaffold (nFb). 3-4-hexanedioen was not detected in non-treated tissue models (TM_ctrl), nasal fibroblasts-loaded scaffolds (nFb_ctrl) and tissue models treated only treated with the solvent (solvent control). (B) Formation of the metabolite 4-hydroxy-3-hexanone in presence of the tissue model (TM) and the nasal fibroblasts-loaded scaffold (nFb), but not in the controls. Data are presented as means + SD. No statistic tests were performed as it is only preliminary data with N=2. n.d.= not detected. The two donors are labeled f_80 (female, 80 years old), and m_40 (male, 40 years old).*

amount of 3-4-hexanedione is found in lower amounts in the tissue models' headspace than in the fibroblasts-loaded scaffold, presumably because the tissue models metabolize it. In Figure 37B the metabolite 4-hydroxy-3-hexanone was identified in the headspace of tissue models, and seemingly in lower amounts in the headspace of the fibroblasts-loaded scaffolds, but not in the untreated controls. Only two biological donors were used to obtained these preliminary results, using two models per donor and two twisters per model. Only one model per donor was used in the controls and fibroblast loaded tissue.

2.4. Discussion on human *in vitro* experiments

Characterization of the human nasal respiratory mucosa model: nasal XMEs

In this part, I aimed to characterize a human nasal respiratory mucosa model in terms of XME expression and odorant metabolism. The model was developed by Dr. Maria Steinke's team at the Chair of Tissue Engineering and Regenerative Medicine (Würzburg, Germany), already characterized in terms of structure, morphology and cell types, and used for respiratory infection studies (Sivarajan et al., 2021). The purpose of such a model is generally to have an *in vivo*-like model relevant to human biology with the advantages of *in vitro* experimental conditions, which was exactly what I needed when the rat model proved to be limited for the use I needed. While I kept in mind the original question about nasal XME regulation by volatile substrates, it was necessary to first justify the suitability and relevance of the model to study human nasal XMEs. I first characterized the model and explored the XMEs families expressed in the tissue to compare it with *in vivo* data. Although it has already been done in a previous study, I explored first the morphological characterization of the tissue model using histology (Figure 17). The cell organization and structure of the tissue models show a polarized pseudostratified columnar epithelium with characteristic kinocilia on the apical side, which is comparable to what we see in human *in vivo* nasal respiratory tissue (Boichot et al., 2023; Robert-Hazotte et al., 2022). The Alcian blue staining brings out the mucins present in goblet cells;althoughit fails to show the mucus layer that is clearly visible with naked eye at the surface of the model. The protocol to fix and embed the models in paraffin probably gets rid of this layer. The model expresses cell types of a well differentiated epithelium, with basal cells on the basal side from which multiciliated epithelial cells and goblet cells differentiate. Two variants of mucins were explored and found in the model: MUC5B and MUC5AC, which are the major secreted variants of the nasal mucus. *In vivo*, MUC5AC is mostly secreted by goblet cells while MUC5B mostly comes from submucosal glands (Rubin, 2010); in mice, the depletion of MUC5B deplete the animals of Bowman's glands in the olfactory mucosa (Amini et al., 2019). This model does not possess these submucosal structures; However, its goblet cells are able to secrete them anyway and make them contribute to the mucus layer, probably because the primary epithelial cells are isolated from biopsies containing the nasal epithelium and glands. Further studies could tell whether the final composition of the model's

mucus resemble the *in vivo* mucus thank to this adaptation. We can also wonder if goblet cells adapt to secrete MUC5B in the model (as they are normally restricted to submucosal glands), or if MUC5B secreting cells come from glands of the biopsy samples, and that would be able to survive outside a submucosal gland. Immunofluorescent staining also highlighted the presence of acetylated tubulin structures on the apical side of the model. These structures form brushes at the surface of the epithelium and are in direct contact with the mucus layer. Previous studies showed that the ciliary beating phenotype is found in the model and that the beating is coordinated and able to move particles in a defined direction (Lodes et al., 2020). This ciliary beating is a physiological function that allows the movement of mucus towards the throat to remove impurities caught in the mucus layer and allows it to regenerate (Scherzad et al., 2019). The throat part is lacking in the *in vitro* model, which is why a weekly gentle mucus wash is performed to maintain a condition as physiological as possible. Overall the model expresses a mucociliary phenotype as described previously (Kessie et al., 2021; Lodes et al., 2020; Schweinlin et al., 2017; Sivarajan et al., 2021; Steinke et al., 2014). Specific cell-types were more deeply investigated using scRNA-seq performed by Rinu Sivarajan (Chair of Tissue Engineering and Regenerative Medicine, Würzburg) and Prof. Saliba, and annotated by Prof. Florian Erhard and Kevin Berg (Institute of Virology and Immunobiology, Würzburg (Sivarajan, 2023). The results were mapped on a cell atlas and showed the main epithelial cell-types described before (basal cells, ciliated epithelial cells, and secretory cells), but also revealed that a part of these cell populations was specific to the nasal tissue (Figure 18). Moreover, subpopulations were also discovered in the tissue models (subrabasal, deuterosomal), which are different stages of transition towards a differentiated/mature phenotype (Ha and Cho, 2023; Ruysseveldt et al., 2021). The analysis also revealed cycling basal cells showing the tissue might have the ability to renew the differentiated epithelial cells from a self-maintaining pool of stem cells, like an *in vivo* tissue (Ruysseveldt et al., 2021). Finally, a small population of fibroblasts was detected. During the analysis, we considered the fact that models are a coculture of epithelial cells and fibroblasts. Hence, some fibroblasts could have been detached as well when epithelial cells were dissociated from the scaffold. This is probably what happened since a small population of fibroblasts was also detected.

From this dataset, I investigated the overall XME expression of the models. I separated XME into phase I and phase II enzymes, and phase III transporters, and looked for expression of the different enzymatic families belonging to these phases (Figure 19). I

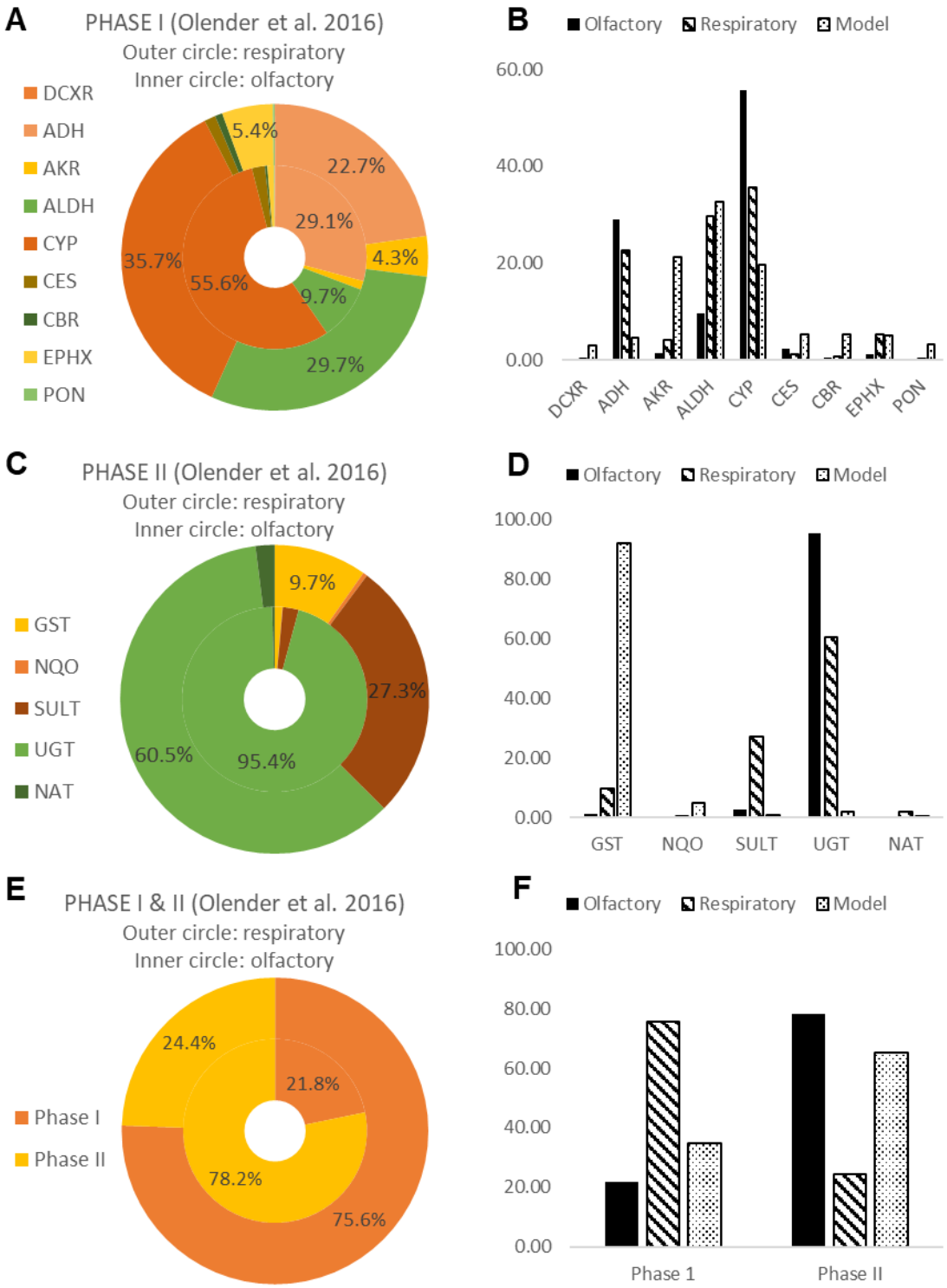

***Figure 38**: Proportion of XME families present in the human olfactory and respiratory tissues (data extracted from Olender et al., 2016). (A) and (B) show phase I enzymes, (C) and (D) show phase II enzymes, (E) and (F) show both phase I and phase II enzymes. A, C, and E compare respiratory and olfactory tissues (from Olender's data using pie charts. B, D, and F include Olender's data and our model using bar diagrams.*

chose to include phase III transporters in the analysis as they can be of interest for other research fields, like cancer research (Zhang et al., 2015). According to the dataset, phase I enzymes are mainly represented by CYP, ALDH, and AKR families, while GST represent around 90 % of phase II enzymes. Concerning phase III three-quarters are MRP. Overall, the majority of XME expressed in the models are phase II, followed by phase I. Phase III are less than 1 % of the XME expressed in the models. When compared with bulk RNA sequencing data performed on the human respiratory and olfactory tissues by Olender and colleagues (Olender et al., 2016), we can see that CYPs and ALDH (Figure 37A) are well represented in the respiratory mucosa (35.7 % and 29.7 %, respectively). However, data from Olender show a higher proportion of ADH (22.7 %) than AKR (4.3 %), which is the contrary of what we see in the tissue model (see Figure 37B). Concerning phase II XMEs (Figure 37C), the major enzyme family is UGTs in respiratory (60.5 %) and olfactory (95.4 %) tissues, which denote with what we observe in our model where GSTs are the main phase II enzymes. It is interesting to observe that there is a slightly higher variety of phase II XME in the respiratory tissue than in the olfactory tissue. In this regard, our model is similar to the olfactory tissue, as more than 90% of phase II enzymes are GSTs (Figure 37D). Lastly, I also wanted to compare the proportion of phase I and phase II in our model with the literature (Figure 37E). Phase I enzymes seem to be privileged in the respiratory mucosa (76.6 %), contrarily to the olfactory mucosa that contains more phase II enzymes (78.2 %), which is what we also observe in the models (Figure 37F).

In this regard, the human model not only shows a mucociliary phenotype similar to the *in vivo* tissue, but also harbors the same XME families found *in vivo*. Some differences between the tissues sequenced can be noted, However, they can also be attributed to the fact that different techniques were used to sequence the model and the human in vivo tissue. There could also be differences between the *in vivo* tissue and the model. To verify it, it would be interesting to sequence matching donor biopsies and models.

Phase I and phase II target enzymes

To continue with the general overview of XME expression within the model, I then focused on some phase I and phase II variants, namely *DCXR*, *AKR1B10*, *ALDH1A1*, and *ALDH3A1* for phase I enzymes, and four variants of GST for phase II (*GSTP1*, *GSTA1*, *GSTO1* and *GSTO2*). I used the scRNA-seq data set to investigate expression of these

variants in the different cell populations (Figures 22 and 23), confirmed their expression using RT-qPCR (Figures 20 and 21), then searched for the subsequent protein via immunofluorescent staining (Figures 24 to 30).

Concerning phase I, *DCXR* was expressed ubiquitously in the model, and the immunofluorescent staining revealed the localization of the protein in the epithelial layer (basal cells, and multiciliated cells) as well as in the matrix. In some cells, DCXR also seems to be present in the nuclei, although it could be due to the thickness of the cut. Curiously, *DCXR* transcript, but not the protein, was detected in secretory cells. The enzyme has been previously detected in the human respiratory mucosa, where it is present in the whole epithelium layer except in secretory cells (Robert-Hazotte et al., 2022). Data of the Human Protein Atlas[5] suggest that overall *DCXR* has a low expression in the respiratory tract, but that the protein is found at a relatively high level within these tissues. In the nasopharynx, high levels of DCXR protein have notably been found in basal cells and ciliated cells. According to the database, DCXR protein had also been found at a low level inside fibroblasts, which can explain the staining in the matrix. DCXR has been described intracellularly at the vicinity of microtubule within the cytoplasm and in the nucleoli before (Uhlén et al., 2015). *AKR1B10* gene expression and protein were restricted mainly to the basal cells,althoughthere was a faint staining in the basal pole of multiciliated cells as well. In the immunofluorescent staining, the protein was absent from secretory cells and faintly present in ciliated cells. Overall, these results were new considering AKR1B10 was not detected in the nasopharynx of donors used to build the Human Protein Atlas[1] (Uhlén et al., 2015). Low levels of the AKR1B10 protein were previously detected in the human turbinate and olfactory cleft,althoughthe signal is not restricted to basal cells at all. However, AKR1B10 is absent from goblet cells, which confirms our results here (Boichot et al., 2023). Like DCXR, ALDH1A1 is present ubiquitously in the model. Gene expression of ALDH1A1 was not restricted to a particular cell population, and the protein was found in multiciliated cells, basal cells, but also secretory cells. This staining is coherent with the human *in vivo* situation, where ALDH1A1 was found to be strongly expressed in human turbinate,althoughin these *in vivo* tissues it is absent from goblet cells. The authors concluded that ALDH1A1, which is

[5] www.proteinatlas.org

found in the nasal mucus, must be secreted by nasal glands (Boichot et al., 2023). These structures are absent from the human 3D respiratory mucosa model, However, we identified MUC5B goblet cells in the model, which are probably derived from glands present in the biopsies. Likewise, ALDH3A1 expression is not restricted to a particular cell population, and the protein is present in the whole epithelial layer except in secretory cells. *In vivo*, the enzyme is found throughout the epithelium but is absent from goblet cells, similarly to ALDH1A1 (Boichot et al., 2023).

Concerning phase II enzymes, GSTP1 is strongly expressed in the model,althoughthe protein seems restricted to multiciliated cells, in the cytoplasm, some nuclei, and particularly near the kinocilia. This is coherent with previous work and staining on *in vivo* tissues showing strong staining of GSTP1 in human nasal samples (Schwartz et al., 2020) and in the human nasopharynx[6] (Uhlén et al., 2015). GSTP1, However, was not found in MUC5AC-sectreting cells. Either GSTP1 is not secreted in the mucus in this model, or it does not come from Muc5AC-expressin secretory cells. Overall, these results confirm what was already known on GSTP1 expression pattern in the nasal respiratory mucosa, showing the 3D model can reproduce with high fidelity the *in vivo* situation, at least concerning GSTP1 cell-type expression. GSTA1 shows a similar patternalthoughit is expressed at a much lower lever than GSTP1. The protein is found in multiciliated epithelial cells, and sometimes seems to be present in the nuclei. GSTA1 seems to be present on the apical pole of these cells, near the kinocilia, but the protein did not colocalized with kinocilia marker. The enzyme was also absent from secretory cells. GSTA was previously detected in human nasal mucosa at the apical side of ciliated epithelial cells (Schwartz et al., 2020), and in the nasopharynx in what appears to be multiciliated epithelial cells[6] (Uhlén et al., 2015). Lastly, GSTO protein was found in a similar pattern than its homologues GSTA1 and GSTP1. On the gene level, two variants can be differentiated: *GSTO1* and *GSTO2*. Of the two variants, *GSTO1* seems to be the one preferentially expressed in the models. This is new, as so far GSTO was found in the oral cavity (Schwartz et al., 2021b) and the lung (Yin et al., 2001), and GSTO2 isoform was discovered *in vivo* in the nasopharynx[6] (Uhlén et al., 2015).

[6] www.proteinatlas.org

Globally, all three variants were found in multiciliated epithelial cells but not in secretory cells,althoughGSTs were previously detected in nasal mucus: GSTP1 in rats (Heydel et al., 2019b), GST activity in new-born rabbits (Robert-Hazotte et al., 2019a), GSTA1 in human olfactory cleft mucus (Débat et al., 2007). GSTs must be secreted in the mucus by other means than secretory cells; it would be interesting to verify their presence in the mucus secreted by the human respiratory model with proteomics. In the pictures presented it seems that some variants are also present in brush-like structures corresponding to cilia of multiciliated epithelial cells, meaning these variants would be directly at the contact with odorants diluted in the mucus, at the vicinity of cilia, and on the apical side of the epithelium. GSTs were found to be important in the clearance of odorants so that the olfactory system remains responsive to new stimuli (Legendre et al., 2014) and several odorants were shown to be GST substrates (Schwartz et al., 2020).

Toxicity of odorants for the human nasal respiratory model

After the characterization of the models, I started exposing them to potential inducers of some target XMEs. Remembering the effect of odorants treatments on the rat olfactory explants, I also checked whether such conditions have an impact on the model's viability. In parallel of odorant exposure experiments, I performed MTT tests and looked for an effect of different concentrations of 2,3-pentanedione and ethanol (Figure 31). Cell viability for every condition was not significantly different from the untreated controls. Interestingly, 20 ppm of 2,3-pentanedione seems to increase cell-viability significantly compared to the solvent control. This amount of 2,3-pentanedione was not expected to trigger any toxicological response, as cell culture models have already been exposed to similar amount for a longer exposure time (Zaccone et al., 2015). As mentioned before in the material and method, MTT test uses colorimetry to investigate cell metabolism and especially NADP(H)-dependent oxidoreductases activity, which is then extrapolated as cell viability. 2,3-pentanedione is a known substrate of DCXR (Nakagawa et al., 2002), which is a NAPD(H) dependent oxidoreductase. 2,3-pentanedione treatment may enhance the enzymatic activity of DCXR at 2 ppm and 20 ppm, but not at 250 ppm, which percentage of "cell viability" is significantly lower than at 20 ppm, but not significantly different from the untreated controls. This effect could be due to the concentration either inhibiting the enzyme or stressing the cell models. Such hypothetical stress is nevertheless not translated by

damages in the tissue structure, as demonstrated in Figure 32. As for ethanol, it was first chosen for exposure experiments to try to translate results obtained on the rat olfactory explants models. However, the first difference I could observe in terms of XME expression between the rat olfactory explant model and the human nasal respiratory mucosa model was the very low expression of ethanol metabolizing enzymes in the human model, compared to the rat model. For instance, *CYP2E1* was not detected in the scRNA-seq data, and *ADH1* (more precisely *ADH1C* isoform) and *ALDH2* were detected but at low levels. In RT-qPCR experiments, I could not amplify in reliable manners these enzymes; hence, I did not pursue with the investigation of the potential gene regulation of *CYP2E1*, *ADH1*, and *ALDH2* in response to ethanol treatment.

Regulation of XMEs in response to nebulized odorant treatments

I then proceeded with gene regulation experiments in response to odorant treatments. Odorants were first nebulized on top of the tissue models to mimic an exposure of the airways to volatile compounds in aerosols (Figure 33). Neither 2,3-pentanedione (2 ppm and 20 ppm) nor ethanol (63 ppm) had a significant effect on DCXR gene expression. DCXR activity toward 2,3-pentanedione has been shown *ex vivo* in rat (Robert-Hazotte et al., 2019b) and *in vivo* in humans (Robert-Hazotte et al., 2022). While competitive inhibition of the enzyme by other substrates such as butyric acid was shown (Nakagawa et al., 2002; Robert-Hazotte et al., 2022), nothing about *DCXR* gene expression in response to a substrate is known so far. 2,3-pentanedione has been previously studied for potential toxicity toward the airways, as it was linked to pulmonary diseases developed by popcorn workers that were chronically exposed to popcorn flavoring agents including 2,3-pentanedione (Kreiss, 2017; Van Rooy et al., 2007). Toxicity was tested at high concentrations (up to 360 ppm) in rats, and showed that airways tissue started showing apoptosis and necrosis signs after 17 hours of exposure (318 ppm), but before disruption of the epithelial barrier DCXR seems to accumulate in vacuoles at the apical pole of the epithelium (Hubbs et al., 2012). We could imagine a secretion of the enzyme, or that the enzyme accumulates at the surface to create a protective barrier, or a potential inactivation of DCXR leading to the protein degradation. Following these results, I hypothesized that 2 hours might not be sufficient to trigger a response from the XME at the gene expression level, but might be enough for the nuclear receptor gene expression to change. Among all the nuclear receptors I searched for in the human nasal

respiratory mucosa model, only three appeared to be expressed enough to be detected with RT-qPCR: *Nrf2*, *AhR*, and *PPARG*. Like for *DCXR*, 2,3-pentanedione and ethanol did not induce any significant difference in the gene expression of the three nuclear receptors. Nrf2 is known for its role in the resistance of tissues to oxidative stress. It regulates notably XMEs involved in oxidation (CYP2A5, ALDH3A1, ADH7), in reduction (NQO1, AKR1B3), conjugation (UGT1A1, SULT3A1), and nucleophilic trapping (GSTA1/A2/A3, MGST1, EPHX1, ES-10) (Ma, 2013). Nrf2 is also involved in the resistance to oxidative stress due to ethanol (Wu et al., 2012), so we could expect an effect of ethanol on the gene expression of *Nrf2*. However, mRNAs of *Nrf2* were shown to be present on a high basal level and independently of inducers, which means post-transcriptional regulation of Nrf2 is most likely (Ma, 2013). Concerning the other two nuclear receptors, AhR binds numerous ligands including hydrocarbons, but also natural compounds in food such as flavonoids or indoles. AhR is known to regulate the expression of cytochrome P450 family 1 (Larigot et al., 2018), which were not the enzymes originally targeted by ethanol and 2,3-pentanedione. A potential effect on *AhR* fold change was hence not expected, However, it does not exclude ethanol and 2,3-pentanedione from being potential substrates of other CYPs. As previously mentioned, ethanol is a known substrate of CYP2E1, and CYPs are suspected to be able to reduce ketones groups,althoughnot specifically α-diketone (Lehr et al., 2015). PPARG is one isotype of a peroxisome proliferator-activated receptor with a pleiotropic function and plays a major role in the regulation of the metabolism, especially in the adipose tissue. Among its ligands can be cited natural lipid-derived metabolites such as prostaglandins, and arachidonic acid, as well as anti-inflammatory drugs, and the list goes on. *PPARG* was shown to be increased by moderate plasma ethanol concentration in rat adipose tissue and sera, which led to a decrease in insulin resistance due to a high-fat diet. This effect was only seen in moderate ethanol levels; higher concentrations of ethanol were damaging and only increased ethanol resistance in the study (Feng et al., 2012). In our conditions, *PPARG* is not in adipose tissue but in respiratory mucosa, and the concentration of ethanol might be too low to be relevant for cell energetic metabolism.

Regulation of XMEs in response to a direct liquid odorant treatment

I then switched toward direct liquid treatments instead of nebulization, as it allowed me to have odorant metabolism readouts that I'll present later in this manuscript. I exposed

the models to 2,3-pentanedione (250 ppm), as well as 3,4-hexanedione (250 ppm), and dexamethasone (100 µM), see Figure 34. Such conditions did not have any significant impact on *DCXR*, *GSTP1*, *Nrf2*, *AhR*, or *PPARG*. Like 2,3-pentanedione, 3,4-hexanedione is a substrate of the human DCXR. The enzyme has even more affinity for 3,4-hexanedione (K_m=0.014 mM) than 2,3-pentanedione (K_m=0.028 mM) (Nakagawa et al., 2002), which makes 3,4-hexanedione a great competitor of 2,3-pentanedione for DCXR (Robert-Hazotte et al., 2022). Like 2,3-pentanedione, it was detected in air samples of factory using buttermilk flavoring agents with its isomer 2,3-hexanedione (Day et al., 2011),althoughtoxicity assays of butter flavoring agents mostly focused on diacetyl and 2,3-pentanedione so far, as previously mentioned. A study investigating proapoptotic effects of 2,3-hexanedione and 3,4-hexanedione found effects on neuroblastoma cell viability at concentrations around the millimolar and exposure over several days (Zilz et al., 2007), However, I chose for this thesis short exposure times and low concentrations to imitate an olfactory event, which also avoids such toxic effect. We could argue that 3,4-hexanedione, like 2,3-pentanedione, could have post translational regulation on DCXR, but no effect on the gene expression could be demonstrated in the present conditions. I was expecting an effect of 2,3-pentanedione and 3,4-hexanedione on *Nrf2* at this concentration (250 ppm) as it gets close to the concentrations used in toxicity studies (Hubbs et al., 2012; Zaccone et al., 2015, 2013).

Concerning *GSTP1*, neither 2,3-pentanedione nor 3,4-hexanedione were expected to upregulate the enzyme's gene expression. However, dexamethasone was shown to induce *GSTP1* expression in some esophagus precancerous lesions in a dose-dependent manner (Compton et al., 1999), and downregulated in rat hepatoma cells (de Waziers et al., 1992). Knowing this, and because I could not show any change in the fold change of my target genes so far, I tried to reproduce this effect on the model to have a positive control that would validate the "negative" ones obtained so far with odorant molecules. However, I could not impact *GSTP1* fold change with dexamethasone treatment in the model, which could be due to (1) the nature of the tissue model that might not respond like a precancerous human esophagus model or a rat liver model, or (2) the conditions of the treatment that may not be ideal to impact *GSTP1* gene fold change. Indeed, studies using dexamethasone usually indicate a treatment of minimum 24 hours and up

to several days (Compton et al., 1999; de Waziers et al., 1992; Thiebaud et al., 2010; Zhao et al., 2015). The amount used could also be not ideal: in the studies cited just above, the concentrations of dexamethasone ranged from the nanomolar up to 10 micromolar. Some effects shown in these papers showed a dose-dependent response, which is why I tried to put all chances on my side by using 100 µM of dexamethasone. Upon later reflections, that might not have been the best strategy, as dexamethasone mimics corticoids, which are hormones and thus, trigger their effect at very low doses (Hiller-Sturmhöfel and Bartke, 1998).

Though not supported by statistical analysis, the fold change of *Nrf2* seems to nevertheless increase in response to 2,3-pentanedione and 3,4-hexanedione, unlike the *Nrf2* fold change of models treated with dexamethasone, which is an anti-inflammatory corticosteroid acting in a dose-dependent manner (Abraham et al., 2006) and was previously not impacted by a systemic dexamethasone treatment in the rat olfactory mucosa (Thiebaud et al., 2010). Perhaps 250 ppm of α-diketones for 2 hours induce an oxidative stress requiring Nrf2 involvement.

As mentioned before, neither AhR nor PPARG were expected to be impacted by 2,3-pentanedione, nor by 3,4-hexanedione. Dexamethasone is not expected to impact *AhR* as well (Thiebaud et al., 2010). However, it was previously shown that the molecule is able to impact *PPARG* expression in several tissues. For example, dexamethasone decreased *PPARG* expression in transfected mouse cells, but its effect was reversed by adiponectin (She et al., 2007); *PPARG* was induced by dexamethasone in human eosinophils, and the authors supposed this effect might play a role in the anti-inflammatory effect of dexamethasone (Usami et al., 2006). Rats exposed to dexamethasone *in utero* and nursed by female rats treated with dexamethasone had a lower expression of *PPAGR* in the jejunum (de Souza et al., 2021). During my thesis, I could amplify *PPARG* in the human nasal respiratory model using RT-qPCR. Dexamethasone seems to decrease *PPARG* expression by half, however, as only two datapoints could be exploited, no statistical analysis was performed. *PPARG* is weakly expressed in the model, which is translated by very high CT. If dexamethasone truly decreases *PPARG* expression in the tissue model, it could explain why I had so much difficulty to extract data points for this condition. 3,4-hexanedione, on the contrary,

seems to increase *PPARG* gene expression, but the variability is so high it is not statistically significant. PPARG is particularly involved in energy metabolism, especially via its role in the adipose tissue, and impact of food extracts on PPAR including PPARG has already been widely investigated (Domínguez-Avila et al., 2016). However, it mostly focuses on polyphenols like epigallocatechin gallate or resveratrol, and I could not find a link between butter flavoring agents and PPARG in the literature. We could imagine that flavoring agents like α-diketone might be interesting cues for the energetic metabolism and thus might impact nuclear receptors of the PPAR family, but this is a far-fetch theory that needs a lot more investigations.

A last remark on the absence of response to chosen odorants points that, as mentioned in the rat olfactory explant part, odorants partition between the liquid and the air above it. This could mean that the untreated controls might not be that untreated if the odorant contaminated the whole incubator, which was not verified. However, if that may have been true for models exposed in 6-well plates, which were not sealed, it is not the case of models treated in jars, whose readouts included odorant metabolism that needed a sealed space. This critical point should be considered for future experiments.

Odorant metabolism

The last part of this discussion is dedicated to the functionality of the human nasal respiratory tissue models, demonstrated by the metabolic capacity of the tissue models toward odorant substrates. I aimed to demonstrate the functionality of the phase I enzymes I detected in the models, by using two different methods to study odorant metabolism: models' homogenates, and headspace measurements using Stir Bar Sorptive Extraction (more commonly called TWISTER™ from Gerstel).

Odorant metabolism of human nasal respiratory mucosa model homogenates

First, enzymatic activity of models' homogenates was tested using 3,4-hexanedione and benzaldehyde. The involvement of a functional enzymatic system capable of metabolizing these odorants was first shown in Figures 35A and 36A, where the odorant peak is almost always significantly lower in the full assay than in the different controls, supposedly because parts of the original odorants were metabolized. We then detected the corresponding metabolites in the full assay (Figure 35B for the 3,4-hexanedione metabolite 4-hydroxy-3-hexanone, and Figures 36B and 36C for the benzaldehyde

metabolites benzyl alcohol and benzoic acid, respectively). These metabolites were detected at a much lower level – and sometimes not even detected – in the controls, which underlines again a functional enzymatic system. More precisely, the heat-denaturation control aims to inactivate any enzymatic activity by disrupting the 3D structure of enzymes (Berg et al., 2013). Controls omitting the odorant or replacing the homogenates by human albumin allowed to confirm the absence of contaminants and impurities of the different parts composing the assays. In other words, it verifies that odorants or enzymatic activity seen in the full assay are only coming from the odorants deliberately added and the models' homogenates. Control without the NADPH regenerating system highlight the involvement of the enzymatic co-factor NADPH in the chosen odorants' metabolism; DCXR and the ALDH family notably depend on this co-factor. While intact tissue models possess a functional NADPH regenerating system, homogenization disrupt a lot of cellular functions and can decrease NADPH levels below detection thresholds (Fomenko et al., 2022). Experiment of the metabolism of benzaldehyde into benzyl alcohol and benzoic acid showed low levels of metabolites produced even in the absence of NADPH-regenerating system, which could be due to traces of NAPDH remaining in the homogenates.

Concerning the metabolism of 3-4-hexanedione, the involvement of DCXR was tested by applying 9 mM of pentanoic acid before exposure to the odorant. Pentanoic acid is an irreversible inhibitor of DCXR, with an IC50 from 0.15 mM (Nakagawa et al., 2002) to 4.4 mM (Yang et al., 2017), depending on the study. When applied to the assay, a lower amount of the metabolite 4-hydroxy-3-hexanone was observed, confirming the DCXR enzymatic activity toward the odorant in the models' homogenates. However, some metabolites still formed despite DCXR inhibition. Several hypotheses can be considered: in response to xenobiotic exposure, other alternative enzymes could assure the metabolism of the molecule if the main enzyme is no longer able to do it. Candidates for this role could be AKR as they are able to reduce ketones (Bachur, 1976), and some variants were detected in the models. AKR1B10 isoform was confirmed on the protein level as well. To confirm this hypothesis, a supplementary control could be done using sorbinil, an AKR inhibitor (Barski et al., 2008).

Regarding benzaldehyde metabolism into benzyl alcohol and benzoic acid, several inhibitors were used. N-Ethylmaleimide (NEM) is a broad irreversible inhibitor that impact enzymes with the sulfhydryl group of cysteines in their active center, which is the case for CYP (Meunier et al., 2004), ALDH (Koppaka et al., 2012; Shortall et al., 2021), and potentially CR (Bateman et al., 2008) enzyme families. These enzymes could be involved in the metabolism of benzaldehyde as some metabolites were found after treatment with NEM. Ketoconazole (KET) is a CYP3A inhibitor via a mix of competitive and non-competitive mechanisms. Controls including this inhibitor show a significantly lower level of metabolites than the full assay, meaning this enzyme subfamily is likely involved in the metabolism of benzaldehyde in the models' homogenates; several variants of CYP were detected in the single-cell RNA sequencing data. The next inhibitors applied were citral and benomyl, which are reversible and irreversible inhibitors of ALDH, respectively (Koppaka et al., 2012). As expected, application of citral and benomyl decreases benzoic acid levels,althoughnot significantly with benomyl, confirming involvement of ALDHs in the metabolism of benzaldehyde. Surprisingly, it also lowered the levels of benzyl alcohol, which is not an expected product of ALDH (Shortall et al., 2021). We hypothesize that, in the case of citral, the inhibitor could compete with benzaldehyde for similar enzymes producing benzyl alcohol. Like benzaldehyde, citral is also an odorant and they share a similar structure. To validate this hypothesis, experiments with citral as an odorant would need to be conducted, with inhibitors of the supposed enzymes as controls. We suppose ADH (inhibitors: ethanol, methanol (Puetz et al., 2020), fomepizole (Hall, 2002)), CYP (inhibitor : ketoconazole (Deodhar et al., 2020)) and aldehyde oxidase (AOX, inhibitor : ketoconazole, raloxifene (Obach et al., 2004)) would be involved. In the case of benomyl, the non-significant reduction of benzoic acid formation could be due to the fact that the inhibitor affects differentially variants of ALDH and was originally used to target low-Km microsomal ALDH (mALDH), such as ALDH2 (Staub et al., 1998). Other ALDH variants, such as ALDH1A1 and ALDH3A1 that were confirmed on the protein level in the models, could be still active enough to produce benzoic acid. Interestingly, benomyl inhibitory action is maximal after a six-step bioactivation by other XMEs. Among these XMEs are CYPs, which convert MeSC(O)NHBu (MBT) into MeSC(O)N(OH)Bu (N-OH-MBT) and MeS(O)C(O)NHBu (MBT-SO), which are the ultimate mALDH inhibitors (Staub et al., 1998). CYPs are potential candidates for the

metabolism benzaldehyde into benzyl alcohol, thus benzaldehyde and MBT could compete for CYP, which would lead to a competitive inhibition of CYP to metabolize benzaldehyde into benzyl alcohol. We can also imagine an inhibition of CYP or AKR by one of the benomyl metabolites, which would also reduce the formation of benzyl alcohol. This hypothesis could be tested by using these benomyl metabolites with purified enzymes in enzymatic assays.

In any case, the fact that inhibitors could not completely abolish the formation of metabolites suggests that more than one enzyme are involved in the odorants' metabolism. Unravelling these pathways would request the use of other enzyme inhibitors, such as sorbinil for AKR, as stated before. Such experiments could be done with the human nasal respiratory mucosa model, and could be complemented with enzymatic assays on purified protein to verify the inhibition of some enzymes by potential inhibitors, such as benomyl metabolites on CYP family, for example.

Odorant metabolism of human nasal respiratory mucosa model headspace

Meanwhile, I tested several setups to measure odorant metabolism from the headspace of intact tissue models, as the main advantage of these models it that they present a structure and cell-types very close to the *in vivo*-like situation, while being a cellular model that can be handled in an *in vitro* experiment. Such model notably allows to know exactly the dosage of odorant molecules it is exposed to, but also the usage of potentially toxic molecules that could not be used with human volunteers.

As the generation of tissue models can take time and that human nasal biopsies are precious, I also wanted to include more readouts from this setup, notably by using the treated models for RT-qPCR experiments (some readouts were presented in the "Regulation of XMEs in response to a direct liquid odorant treatment"). I gradually increased the concentration of 2,3-pentanedione from 2 ppm to 250 ppm until I realized that maybe 2,3-pentanedione in particular was not very well detected by the GC-MS we used to analyze the TWISTER^{TM}. Nicole and I had indeed a lot of difficulty to even identify the faint peak of the odorant that I knew was present at 250 ppm, let alone identify even fainter potential metabolites.

The results presented in Figure 37 were obtained using 3,4-hexanedione as the odorant, as we knew we identified the metabolites with the tissue model homogenates. The

absence of 3,4-hexanedione and its metabolite 4-hydroxy-3-hexanone in the untreated control shows that the odorant was not initially present in the tissue models, in the solvent I used to dilute the 3,4-hexanedione, nor in the culture media that was incubated with the tissue models. Although I did not perform a statistical analysis as technically N equals only 2, there seems to be less 3,4-hexanedione detected in the headspace of the tissue models than in the headspace of fibroblasts-loaded scaffold, which could hint that the odorant is metabolized by the tissue models. However, as the metabolite 4-hydroxy-3-hexanone was detected in the headspace of fibroblasts-loaded scaffold, the metabolism seen with tissue models is not entirely due to the respiratory epithelial cells. This observation is quite logical as for example DCXR protein was also identified in the scaffold in histological experiments. Is seems that more metabolites were produced with the tissue models than with the fibroblast-loaded scaffold, which could attest for the involvement of the respiratory epithelial cells in the metabolism of 3,4-hexanedione.

In my opinion, at least two controls are missing in this experiment: a treated control with only the scaffold, to attribute or not odorant metabolism to the different cell-types of the tissue model and not on the scaffold purely and to measure the real disappearance of 3,4-hexanedione when metabolized by the cells, and a heated control to inactivate the enzymatic activity of the model, to attribute this metabolism to an enzymatic activity. Additional control with inhibitors could allow to discuss in more depths the enzyme families involved. Nonetheless, it was the first occurrence where odorant metabolites were identified in the headspace of the tissue models, widening the future experimental possibilities using this model in the odorant metabolism field.

CONCLUSION AND PERSPECTIVES

During my thesis, I aimed to understand XMEs roles and regulation in the context of olfaction. I first tried to establish a protocol that would allow the detection of a change in XME gene expression in response to odorant substrates and started using the rat olfactory explant as a biological model of the olfactory system. With the conditions I chose, that is to say low odorant substrate concentrations and a short exposure time that would mimic a simple olfactory event, I could not show any impact of ethanol and 2,3-pentanedione on CYP2E1, ADH1, ALDH2, and DCXR. Although it is no proof that odorant substrates regulate XME in the olfactory context, my results do not condemn this hypothesis either. Indeed, I may not have chosen the most suitable odorants and XME targets to demonstrate that, and the rat olfactory explant proved to be a very limited model for this specific application. Although I started with frozen/thawed rat olfactory explants, which is an established and stable model to study odorant metabolism in Pr. Jean-Marie Heydel's team, our experiments showed that the freezing process was an obstacle to study gene expression. I switched to freshly dissected rat olfactory explants but RNAs in the explants were quickly degraded during odorant exposure, even at the first time-points. I used the exact same RNA extraction protocol for fresh explants than for the frozen ones, and performed the experiment at different times of the year to rule out a potential effect of the ambient temperature on the RNA integrity. Regarding XME fold changes for the different targets in response to ethanol and 2,3-pentanedione I had a hunch that (1) a long odorant exposure could trigger the regulation of some XME, if only to prevent the tissue to being damaged by a toxic and prolonged exposure with (odorant) volatile substances, and (2) a short exposure to volatile odorant could be sufficient to trigger a gene expression response of neuronal activation markers like *c-fos*, if not XME. Answering the first question would require to dive in the pharmacotoxicology world, while the second would require access to a neuroepithelium that does not degrade during the experiment, and thus involve *in vivo* animal experiment. Thanks to this experience, I had the pleasure to wander for a while in the world of forensic sciences which notably seeks markers to assess *post-mortem* intervals. Having experiences the different behaviors of frozen and fresh tissue explants around 2 to 4 hours *post-mortem*, I do believe there are interesting RNA markers to

exploit for the assessment of short *post-mortem* intervals, and parts of me regret no having analyzed *Haf*, *Bax*, and *Bcl-2* mRNA in the "fresh" explants to compare it with the "frozen" ones. It was sadly way beyond the scope of my original research.

Enriched by this first experience, I had the opportunity to use another biological model that reproduces the human nasal respiratory mucosa, developed by Dr. Maria Steinke's team. The model has the advantage of recreating the 3D structure of a nasal tissue, but also allows *in vitro* conditions that bring the stress of the tissue to a minimum: namely, the presence of a culture media bringing nutrients, and the absence of hypoxia. While the question on XME regulation in an olfactory context remained a priority, it was necessary to establish the model as relevant for the olfaction field. Indeed, the model is not a neuroepithelium, while most studies in the olfactory field focus on the olfactory epithelium and its olfactory neurons. However, the model is human based and thus, highly relevant for human health and peripheral olfactory functions. There are currently no *in vitro* model of the human olfactory neuroepithelium available. However, human respiratory models have potentials to understand the human olfaction. The main argument behind the use of this model to study XME in the olfactory context is that the human nasal cavity is mainly lined with this respiratory tissue, while most of the laboratory animal models possess a much more invasive olfactory epithelium in their nasal cavity. In humans, this tissue could participate in odorant metabolism as well. I first characterized the model in terms of XME expression, using a scRNA-seq dataset generated by my colleague Dr. Rinu Sivarajan on the tissue model for another use, and was able to demonstrate the presence of roughly 80 variants of phase I and II XME, and III transporters in the human nasal respiratory model. I confirmed the expression of some variants (*DCXR*, *AKR1B10*, *ALDH1A1*, *ADLH3A1*, *GSTA1*, *GSTP1*, *GSTO1*, and *GSTO2*) using RT-qPCR and also investigated their protein localization in the tissue model using immunofluorescence. While DCXR, ALDH1A1, and ALDH3A1 were present throughout the whole tissue layer, AKR1B10 protein was mostly localized in the basal cells, and GST variants were predominantly in multiciliated cells. Finding XME in a nasal tissue was not surprising as it is directly at the contact with the external volatile environment and thus exposed to a lot of potentially toxic compounds. A functional detoxifying system seems then crucial to protect the nasal mucosa, and it is not a new concept (Watelet et al.,

2009). Despite a very low expression of some variants predominant in the olfactory mucosa (Neiers et al., 2021; Su et al., 2000) (*UGT2A1*, *CYP2A13*, see Table 9), which was not a surprise as it is a respiratory mucosa model, these results encouraged me to think that the human nasal respiratory mucosa had the potential to participate in odorant metabolism. In accordance with the original aim of my work, I exposed the models to different odorant molecules to look for a potential up or down regulation of target XME. I tried to induce *CYP2A13* expression with its odorant substrate 2-methoxyacetophenone, and despite scRNA-seq data list showing its faint expression, I could not amplify the gene in a reliable manner. I used two different modes to expose the human nasal respiratory model for 2 hours to 2,3-pentanedione, ethanol, 3,4-hexanedione, or dexamethasone: a gentle aerosol exposure the *in vivo* tissue is susceptible to encounter in the everyday life, and a direct liquid treatment on top of the tissue model, harsher, but that allowed me to include other readouts. Neither of the methods were able to impact significantly the target enzymes *DCXR*, *GSTP1*, or the nuclear receptors *AhR*, *Nrf2*, and *PPARG*. Different hypotheses rise from these results: either there is (1) indeed no impact of the molecules tested on the targets gene expression, (2) the conditions used do not allow to perceive these effects, or (3) the model is simply not able to respond to a treatment. While the dexamethasone treatment was intended to be a positive control to validate the experimental setup – that is to say, a 2-hour incubation at 37°C that could trigger a fold change in gene expression – the results did not prove this theory right. In the absence of a positive control, I cannot rule-out the tested odorants as potential up or down regulators of the target XME gene expression. The third option is not likely since the model has been previously used in infectious studies showing how human nasal models respond to *Bordetella pertussis* virulence factor (Sivarajan et al., 2021). Shahbaz's model was also responsive to infection, and scRNA-seq data showed some XME variants expressed in the model are differentially regulated depending on the health status of the donors (Alzheimer vs non-Alzeheimer's disease), including variants of the GST, CYP, and ALDH families, as well as some transporters like OAT (Shahbaz et al., 2023).

While a reflex would be to increase the odorant's concentrations and the exposure time to get a response on the gene expression level, it would most likely fall into the scope of

a toxicological response, as it has been previously done with butter flavoring agents (Hubbs et al., 2012; Zaccone et al., 2015, 2013). It could be interesting to test whether a long exposure time at very low concentrations could impact gene expression, which would be answer to the impact of a chronic, environmental exposure to odorant molecules on the nasal xenobiotic metabolism. While a short odorant exposure might not impact gene expression, there could be consequences of a short odorant exposure on the protein level: we could imagine a heightened protein translation, which could be verified using Western blot on models dedicated to this readout, or an enhanced enzymatic activity due to post-translational modifications, which could be more difficult to tackle. Finally, we should not forget that these models come from human primary epithelial cells, which were isolated from biopsies from different patients of all age, sex and health – and probably different ethnicity,althoughthat information was not disclosed to us. This means a higher inter-individual variability might mask any effect of odorants on XME gene expression, and it would need a higher number of repetitions to decipher a potential pattern depending on age, sex, health, and eventually ethnicity of the donors. Based on experience, it would have been safer to start on a cell-line to exclude inter-individual variability and allow a higher number of repetitions to be done. Creating the models is a long process that only allows a limited number of trials in a limited time, but it does not mean that the model is doomed. It simply fills different needs as it is higher up in the scale of complexity, and seems more suited for experiments requiring that complexity, such as odorant metabolism.

Odorant metabolism was investigated using two methods: tissue model homogenates, and headspace sorptive extraction-gas chromatography-mass spectrometry. Tissue model homogenates allowed to explore the functionality of XME such as DCXR, but also ALDH or CYPs to only cite them, with the used of specific inhibitors. This method is powerful to screen a rather large range of odorants as it only consumes a small amount of the homogenates for each trial, which makes repeating the experience less expensive in tissue models. This method also allows the use of different inhibitors without having to worry about a potential toxicity for the model. Now that the method is established with an α-diketone and an aldehyde, other odorant class can be tested. The metabolic activity of the models' homogenates can also be compared to tissue homogenates of

other origin: with *ex vivo* human nasal tissue, to further validate the fidelity of the tissue model to the *in vivo* tissue on the odorant metabolism level, with the liver tissue to compare tissue differences as they do not express the same variants, or with nasal tissue of animal model to compare inter-species odorant metabolism variation. It could also be interesting to compare the metabolism capacity of the model's homogenates with the models' mucus fraction to investigate the participation of the mucus to odorant metabolism. Model's mucus metabolic activity can also be compared with *in vivo* mucus. Although this method is powerful, it completely erases the 3D structure that makes the tissue models so attractive. Hence, in parallel, headspace sorptive extraction-gas chromatography-mass spectrometry was performed. Only preliminary results were obtained regarding this last point during my thesis. However, they are very promising as we could identify 3,4-hexanedione metabolites in the headspace of the models, which would confirm the involvement of the respiratory tissue in odorant metabolism in humans.

Overall, this work explored the hypothesis that XME could be regulated when an odorant event happens, and results so far do not tend to that direction. However, different models were used to reach this conclusion, and especially a human nasal tissue model that shifts the focus of odorant metabolism studies on the human biology. Although establishing the relevance of the model to study olfaction and odorant metabolism took some time, there are now numerous opportunities to derive the methods described in this manuscript. This model does not only express nasal XME and is functional to study odorant metabolism, it is also relevant to the human biology, and has the advantage of complying with the 3R principle by offering an alternative to animal olfactory explants, which have been used as the gold standard in the research field to obtain most of the odorant metabolism results so far. However, the tissue models used in the present study still imply some animal-based components. For instance, the connective tissue used as a scaffold for the model is derived from the porcine gut, the fibroblast growth medium is supplemented with fetal calf serum, and the antibodies used for immunofluorescent staining are animal-derived. There are strategies in place to replace animal-derived components that involves switching from porcine gut material to synthetic fibers already used in other *in vitro* models (Weigel et al., 2022). Current

research addresses the transition toward an FCS-free growth medium and reproduces immunofluorescent staining data using engineered recombinant antibodies. These steps, encouraged notably by the PETA Science Consortium International through grants, can allow future work in the odorant metabolism field as much as possible toward non-animal research.

BIBLIOGRAPHY

Abraham, S.M., Lawrence, T., Kleiman, A., Warden, P., Medghalchi, M., Tuckermann, J., Saklatvala, J., Clark, A.R., 2006. Antiinflammatory effects of dexamethasone are partly dependent on induction of dual specificity phosphatase 1. J. Exp. Med. 203, 1883–1889. https://doi.org/10.1084/jem.20060336

Ache, B.W., Young, J.M., 2005. Olfaction: diverse species, conserved principles. Neuron 48, 417–430. https://doi.org/10.1016/j.neuron.2005.10.022

Adams, D.R., 1992. Fine structure of the vomeronasal and septal olfactory epithelia and of glandular structures. Microsc. Res. Tech. 23, 86–97. https://doi.org/10.1002/jemt.1070230108

Alvites, R.D., Caseiro, A.R., Pedrosa, S.S., Branquinho, M.E., Varejão, A.S.P., Maurício, A.C., 2018. The Nasal Cavity of the Rat and Mouse-Source of Mesenchymal Stem Cells for Treatment of Peripheral Nerve Injury. Anat. Rec. (Hoboken). 301, 1678–1689. https://doi.org/10.1002/ar.23844

Amatngalim, G.D., Rodenburg, L.W., Aalbers, B.L., Raeven, H.H.M., Aarts, E.M., Sarhane, D., Spelier, S., Lefferts, J.W., Silva, I.A.L., Nijenhuis, W., Vrendenbarg, S., Kruisselbrink, E., Brunsveld, J.E., van Drunen, C.M., Michel, S., de Winter-De Groot, K.M., Heijerman, H.G., Kapitein, L.C., Amaral, M.D., van der Ent, C.K., Beekman, J.M., 2022. Measuring cystic fibrosis drug responses in organoids derived from 2D differentiated nasal epithelia. Life Sci. Alliance 5, e202101320. https://doi.org/10.26508/LSA.202101320

Amini, S.E., Gouyer, V., Portal, C., Gottrand, F., Desseyn, J.L., 2019. Muc5b is mainly expressed and sialylated in the nasal olfactory epithelium whereas Muc5ac is exclusively expressed and fucosylated in the nasal respiratory epithelium. Histochem. Cell Biol. 152, 167–174.

Aruci, E., 2023. Implication of an odorant-binding protein in precopulatory behaviour and interaction with the bacterial microbiota. University of Burgundy.

Asakawa, M., Fukutani, Y., Savangsuksa, A., Noguchi, K., Matsunami, H., Yohda, M., 2017. Modification of the response of olfactory receptors to acetophenone by CYP1a2. Sci. Reports 2017 71 7, 1–9. https://doi.org/10.1038/s41598-017-10862-5

Bachur, N.R., 1976. Cytoplasmic Aldo-Keto Reductases: A Class of Drug Metabolizing Enzymes. Science (80-.). 193, 595–597. https://doi.org/10.1126/SCIENCE.959821

Back, D., Stevenson, P., Tjia, J., 1989. Comparative effects of two antimycotic agents, ketoconazole and terbinafine on the metabolism of tolbutamide, ethinyloestradiol, cyclosporin and ethoxycoumarin by human liver microsomes in vitro. Br. J. Clin. Pharmacol. 28, 166–170. https://doi.org/10.1111/J.1365-2125.1989.TB05410.X

Badger, T.M., Hoog, J.O., Svensson, S., McGehee, R.E., Fang, C., Ronis, M.J.J., Ingelman-Sundberg, M., 2000. Cyclic Expression of Class I Alcohol Dehydrogenase in Male Rats Treated with Ethanol. Biochem. Biophys. Res. Commun. 274, 684–688. https://doi.org/10.1006/BBRC.2000.3186

Bai, X., Peng, D., Li, Z., Tian, H., Zhang, L., Yang, D., Bai, P., Liang, W., 2017. Postmortem interval (PMI) determination by profiling of HAF mRNA degradation using RT-qPCR. Forensic Sci. Int. Genet. Suppl. Ser. 6, e182–e183. https://doi.org/10.1016/j.fsigss.2017.09.072

Bailey, R.S., Casey, K.P., Pawar, S.S., Garcia, J.M., 2017. Correlation of Nasal Mucosal Temperature With Subjective Nasal Patency in Healthy Individuals. JAMA Facial Plast.

Surg. 19, 46–52. https://doi.org/10.1001/jamafacial.2016.1445

Barski, O.A., Tipparaju, S.M., Bhatnagar, A., 2008. The aldo-keto reductase superfamily and its role in drug metabolism and detoxification. Drug Metab. Rev. 40, 553–624. https://doi.org/10.1080/03602530802431439

Bateman, R.L., Rauh, D., Tavshanjian, B., Shokat, K.M., 2008. Human carbonyl reductase 1 is an S-nitrosoglutathione reductase. J. Biol. Chem. 283, 35756–35762. https://doi.org/10.1074/JBC.M807125200

Bathla, G., Hegde, A.N., 2013. The trigeminal nerve: an illustrated review of its imaging anatomy and pathology. Clin. Radiol. 68, 203–213. https://doi.org/10.1016/j.crad.2012.05.019

Bauer, S., Rasika, S., Han, J., Mauduit, C., Raccurt, M., Morel, G., Jourdan, F., Benahmed, M., Moyse, E., Patterson, P.H., 2003. Leukemia Inhibitory Factor Is a Key Signal for Injury-Induced Neurogenesis in the Adult Mouse Olfactory Epithelium. J. Neurosci. 23, 1792–1803. https://doi.org/10.1523/JNEUROSCI.23-05-01792.2003

Ben-Arie, N., Khen, M., Lancet, D., 1993. Glutathione S-transferases in rat olfactory epithelium: purification, molecular properties and odorant biotransformation. Biochem. J. 292 (Pt 2, 379–384. https://doi.org/10.1042/BJ2920379

Ben-Arie, Nissim, Khen, M., Lancet, D., 1993. Glutathione S-transferases in rat olfactory epithelium: purification, molecular properties and odorant biotransformation. Biochem. J 292, 379–384.

Bensafi, M., Iannilli, E., Gerber, J., Hummel, T., 2008. Neural coding of stimulus concentration in the human olfactory and intranasal trigeminal systems. Neuroscience 154, 832–838. https://doi.org/10.1016/j.neuroscience.2008.03.079

Berg, J.M., Tymoczko, J.L., Stryer, L., 2013. Zusammensetzung und Struktur der Proteine. Stryer Biochem. 25–65. https://doi.org/10.1007/978-3-8274-2989-6_2

Bianchi, M., Sivarajan, R., Walles, T., Hackenberg, S., Steinke, M., 2021. Susceptibility of primary human airway epithelial cells to Bordetella pertussis adenylate cyclase toxin in two- and three-dimensional culture conditions. Innate Immun. 27, 89–98. https://doi.org/10.1177/1753425920979354/ASSET/IMAGES/LARGE/10.1177_1753425920979354-FIG2.JPEG

Bignetti, E., Cavaggioni, A., Pelosi, P., Persaud, K.C., Sorbi, R.T., Tirindelli, R., 1985. Purification and characterisation of an odorant-binding protein from cow nasal tissue. Eur. J. Biochem. 149, 227–231. https://doi.org/10.1111/j.1432-1033.1985.tb08916.x

Blazing, R.M., Franks, K.M., 2020. Odor coding in piriform cortex: mechanistic insights into distributed coding. Curr. Opin. Neurobiol. 64, 96–102. https://doi.org/10.1016/j.conb.2020.03.001

Block, E., Jang, S., Matsunami, H., Sekharan, S., Dethier, B., Ertem, M.Z., Gundala, S., Pan, Y., Li, S., Li, Z., Lodge, S.N., Ozbil, M., Jiang, H., Penalba, S.F., Batista, V.S., Zhuang, H., 2015. Implausibility of the vibrational theory of olfaction. Proc. Natl. Acad. Sci. U. S. A. 112, E2766–E2774. https://doi.org/10.1073/pnas.1503054112

Board, P.G., Menon, D., 2013. Glutathione transferases, regulators of cellular metabolism and physiology. Biochim. Biophys. Acta 1830, 3267–3288. https://doi.org/10.1016/j.bbagen.2012.11.019

Bogdanffy, M.S., 1990. Biotransformation enzymes in the rodent nasal mucosa: the value of a histochemical approach. Environ. Health Perspect. 85, 177–186. https://doi.org/10.1289/ehp.85-1568341

Boichot, V., Menetrier, F., Saliou, J.M., Lirussi, F., Canon, F., Folia, M., Heydel, J.M., Hummel, T., Menzel, S., Steinke, M., Hackenberg, S., Schwartz, M., Neiers, F., 2023. Characterization of human oxidoreductases involved in aldehyde odorant metabolism. Sci. Rep. 13, 4876. https://doi.org/10.1038/S41598-023-31769-4

Bojanowski, V., Hummel, T., 2012. Retronasal perception of odors. Physiol. Behav. 107, 484–487. https://doi.org/10.1016/j.physbeh.2012.03.001

Bovard, D., Giralt, A., Trivedi, K., Neau, L., Kanellos, P., Iskandar, A., Kondylis, A., Luettich, K., Frentzel, S., Hoeng, J., Peitsch, M.C., 2020. Comparison of the basic morphology and function of 3D lung epithelial cultures derived from several donors. Curr. Res. Toxicol. 1, 56–69. https://doi.org/10.1016/j.crtox.2020.08.002

Brain, J.D., 1970. The Uptake of Inhaled Gases by the Nose. Ann. Otol. Rhinol. Laryngol. 79, 529–539. https://doi.org/10.1177/000348947007900315/ASSET/000348947007900315.FP.PNG_V03

Brechbühl, J., Klaey, M., Moine, F., Bovay, E., Hurni, N., Nenniger-Tosato, M., Broillet, M.C., 2014. Morphological and physiological species-dependent characteristics of the rodent Grueneberg ganglion. Front. Neuroanat. 8, 87. https://doi.org/10.3389/fnana.2014.00087

Brechbühl, J., Moine, F., Klaey, M., Nenniger-Tosato, M., Hurni, N., Sporkert, F., Giroud, C., Broillet, M.C., 2013. Mouse alarm pheromone shares structural similarity with predator scents. Proc. Natl. Acad. Sci. U. S. A. 110, 4762–4767. https://doi.org/10.1073/pnas.1214249110

Briand, L., Eloit, C., Nespoulous, C., Bézirard, V., Huet, J.C., Henry, C., Blon, F., Trotier, D., Pernollet, J.C., 2002. Evidence of an odorant-binding protein in the human olfactory mucus: location, structural characterization, and odorant-binding properties. Biochemistry 41, 7241–7252. https://doi.org/10.1021/bi015916c

Briand, L., Nespoulous, C., Perez, V., Rémy, J.J., Huet, J.C., Pernollet, J.C., 2000. Ligand-binding properties and structural characterization of a novel rat odorant-binding protein variant. Eur. J. Biochem. 267, 3079–3089. https://doi.org/10.1046/j.1432-1033.2000.01340.x

Brito, N.F., Moreira, M.F., Melo, A.C., 2016. A look inside odorant-binding proteins in insect chemoreception. J. Insect Physiol. 95, 51–65. https://doi.org/10.1016/j.jinsphys.2016.09.008

Brunjes, P.C., Illig, K.R., Meyer, E.A., 2005. A field guide to the anterior olfactory nucleus (cortex). Brain Res. Brain Res. Rev. 50, 305–335. https://doi.org/10.1016/j.brainresrev.2005.08.005

Bryche, B., Baly, C., Meunier, N., 2021. Modulation of olfactory signal detection in the olfactory epithelium: focus on the internal and external environment, and the emerging role of the immune system. Cell Tissue Res. 384, 589–605. https://doi.org/10.1007/s00441-021-03467-y

Bryche, B., St Albin, A., Murri, S., Lacôte, S., Pulido, C., Ar Gouilh, M., Lesellier, S., Servat, A., Wasniewski, M., Picard-Meyer, E., Monchatre-Leroy, E., Volmer, R., Rampin, O., Le Goffic,

R., Marianneau, P., Meunier, N., 2020. Massive transient damage of the olfactory epithelium associated with infection of sustentacular cells by SARS-CoV-2 in golden Syrian hamsters. Brain. Behav. Immun. 89, 579–586. https://doi.org/10.1016/j.bbi.2020.06.032

Buck, L., Axel, R., 1991. A novel multigene family may encode odorant receptors: A molecular basis for odor recognition. Cell 65, 175–187. https://doi.org/10.1016/0092-8674(91)90418-X

Butler, A., Hoffman, P., Smibert, P., Papalexi, E., Satija, R., 2018. Integrating single-cell transcriptomic data across different conditions, technologies, and species. Nat. Biotechnol. 2018 365 36, 411–420. https://doi.org/10.1038/nbt.4096

Caggiano, M., Kauer, J.S., Hunter, D.D., 1994. Globose basal cells are neuronal progenitors in the olfactory epithelium: a lineage analysis using a replication-incompetent retrovirus. Neuron 13, 339–352. https://doi.org/10.1016/0896-6273(94)90351-4

Candau, J., 2015. L'anthropologie des odeurs : un état des lieux.

Cassel, T.N., Nord, M., 2003. C/EBP transcription factors in the lung epithelium. Am. J. Physiol. - Lung Cell. Mol. Physiol. https://doi.org/10.1152/ajplung.00023.2003

Catani, M., Dell'acqua, F., Thiebaut de Schotten, M., 2013. A revised limbic system model for memory, emotion and behaviour. Neurosci. Biobehav. Rev. 37, 1724–1737. https://doi.org/10.1016/j.neubiorev.2013.07.001

Cederbaum, A.I., 2012. Alcohol Metabolism. Clin. Liver Dis. 16, 667–685. https://doi.org/10.1016/j.cld.2012.08.002

Chen, C.H., Budas, G.R., Churchill, E.N., Disatnik, M.H., Hurley, T.D., Mochly-Rosen, D., 2008. An Activator of Mutant and Wildtype Aldehyde Dehydrogenase Reduces Ischemic Damage to the Heart. Science 321, 1493. https://doi.org/10.1126/SCIENCE.1158554

Chen, Y., Getchell, M.L., Ding, X., Getchell, T. V., 1992. Immunolocalization of two cytochrome P450 isozymes in rat nasal chemosensory tissue. Neuroreport 3, 749–752. https://doi.org/10.1097/00001756-199209000-00007

Chertemps, T., François, A., Durand, N., Rosell, G., Dekker, T., Lucas, P., Maïbèche-Coisne, M., 2012. A carboxylesterase, Esterase-6, modulates sensory physiological and behavioral response dynamics to pheromone in Drosophila. BMC Biol. 10, 56. https://doi.org/10.1186/1741-7007-10-56

Chertemps, T., Younus, F., Steiner, C., Durand, N., Coppin, C.W., Pandey, G., Oakeshott, J.G., Maïbèche, M., 2015. An antennal carboxylesterase from Drosophila melanogaster, esterase 6, is a candidate odorant-degrading enzyme toward food odorants. Front. Physiol. 6, 316. https://doi.org/10.3389/fphys.2015.00315

Chiu, M.C., Li, C., Liu, X., Song, W., Wan, Z., Yu, Y., Huang, J., Xiao, D., Chu, H., Cai, J.P., To, K.K.W., Yuen, K.Y., Zhou, J., 2022. Human Nasal Organoids Model SARS-CoV-2 Upper Respiratory Infection and Recapitulate the Differential Infectivity of Emerging Variants. MBio 13, e0194422. https://doi.org/10.1128/mbio.01944-22

Christeller, J.T., Tolbert, N.E., 1978. Mechanism of Phosphoglycolate Phosphatase: STUDIES OF HYDROLYSIS AND TRANSPHOSPHORYLATION, SUBSTRATE ANALOGS, AND SULFHYDRYL INHIBITION. J. Biol. Chem. 253, 1791–1798. https://doi.org/10.1016/S0021-9258(19)62323-9

Chung, L., 2015. A Brief Introduction to the Transduction of Neural Activity into Fos Signal. Dev.

Reprod. 19, 61–67. https://doi.org/10.12717/dr.2015.19.2.061

Cleland, T.A., Linster, C., 2019. Central olfactory structures. Handb. Clin. Neurol. 164, 79–96. https://doi.org/10.1016/B978-0-444-63855-7.00006-X

Compton, K.R., Orringer, M.B., Beer, D.G., 1999. Induction of Glutathione S-Transferase-p in Barrett's Metaplasia and Barrett's Adenocarcinoma Cell Lines. Mol. Carcinog. 24, 128–136. https://doi.org/10.1002/(sici)1098-2744(199902)24:2<128::aid-mc7>3.0.co;2-f

Contreras-Zentella, M.L., Villalobos-García, D., Hernández-Muñoz, R., 2022. Ethanol Metabolism in the Liver, the Induction of Oxidant Stress, and the Antioxidant Defense System Ethanol Metabolism in the Liver, the Induction of Oxidant Stress, and the Antioxidant Defense System. Antioxidants. https://doi.org/10.3390/antiox11071258

Crews, L., Hunter, D., 1994. Neurogenesis in the olfactory epithelium. Perspect. Dev. Neurobiol. 2, 151–161.

Dahl, A.R., Hadley, W.M., Hahn, F.F., Benson, J.M., McClellan, R.O., 1982. Cytochrome P-450-dependent monooxygenases in olfactory epithelium of dogs: possible role in tumorigenicity. Science 216, 57–59. https://doi.org/10.1126/science.7063870

Dahl, A.R., Miller, S.C., Petridou-Fischer, J., 1987. Carboxylesterases in the respiratory tracts of rabbits, rats and Syrian hamsters. Toxicol. Lett. 36, 129–136. https://doi.org/10.1016/0378-4274(87)90176-7

Day, G., LeBouf, R., Grote, A., Pendergrass, S., Cummings, K., Kreiss, K., Kullman, G., 2011. Identification and measurement of diacetyl substitutes in dry bakery mix production. J Occup Env. Hyg. 8, 93–103. https://doi.org/doi: 10.1080/15459624.2011.547148

de Bruijn, M.J., Bender, M., 2018. Olfactory cues are more effective than visual cues in experimentally triggering autobiographical memories. Memory 26, 547–558. https://doi.org/10.1080/09658211.2017.1381744

de Lorenzo, A.J., 1957. ELECTRON MICROSCOPIC OBSERVATIONS OF THE OLFACTORY MUCOSA AND OLFACTORY NERVE. J. Biophys. Biochem. Cytol. 3, 839–850. https://doi.org/10.1083/jcb.3.6.839

de Souza, D.N., Teixeira, C.J., Veronesi, V.B., Murata, G.M., Santos-Silva, J.C., Hecht, F.B., Vicente, J.M., Bordin, S., Anhê, G.F., 2021. Dexamethasone programs lower fatty acid absorption and reduced PPAR-γ and fat/CD36 expression in the jejunum of the adult rat offspring. Life Sci. 265, 118765. https://doi.org/10.1016/j.lfs.2020.118765

de Waziers, I., Bouguet, J., Beaune, P.H., Gonzalez, F.J., Ketterer, B., Barouki, R., 1992. Effects of ethanol, dexamethasone and RU 486 on expression of cytochromes P450 2B, 2E, 3A and glutathione transferase pi in a rat hepatoma cell line (Fao). Pharmacogenetics 2, 12–18. https://doi.org/10.1097/00008571-199202000-00003

Débat, H., Eloit, C., Blon, F., Sarazin, B., Henry, C., Huet, J.C., Trotier, D., Pernollet, J.C., 2007. Identification of human olfactory cleft mucus proteins using proteomic analysis. J. Proteome Res. 6, 1985–1996.

Dénes, L., Pap, Z., Szántó, A., Gergely, I., Pop, T.S., 2015. Human vomeronasal epithelium development: An immunohistochemical overview. Acta Microbiol. Immunol. Hung. 62, 167–181. https://doi.org/10.1556/030.62.2015.2.7

Deodhar, M., Al Rihani, S.B., Arwood, M.J., Darakjian, L., Dow, P., Turgeon, J., Michaud, V., 2020. Mechanisms of CYP450 Inhibition: Understanding Drug-Drug Interactions Due to

Mechanism-Based Inhibition in Clinical Practice. Pharm. 2020, Vol. 12, Page 846 12, 846. https://doi.org/10.3390/PHARMACEUTICS12090846

Deprez, M., Zaragosi, L.E., Truchi, M., Becavin, C., García, S.R., Arguel, M.J., Plaisant, M., Magnone, V., Lebrigand, K., Abelanet, S., Brau, F., Paquet, A., Pe'er, D., Marquette, C.H., Leroy, S., Barbry, P., 2020. A Single-Cell Atlas of the Human Healthy Airways. Am. J. Respir. Crit. Care Med. 202, 1636–1645. https://doi.org/10.1164/RCCM.201911-2199OC

Derakhshani, S., Kurz, A., Japtok, L., Schumacher, F., Pilgram, L., Steinke, M., Kleuser, B., Sauer, M., Schneider-Schaulies, S., Avota, E., 2019. Measles virus infection fosters dendritic cell motility in a 3d environment to enhance transmission to target cells in the respiratory epithelium. Front. Immunol. 10, 1294. https://doi.org/10.3389/fimmu.2019.01294

Domínguez-Avila, J.A., González-Aguilar, G.A., Alvarez-Parrilla, E., de la Rosa, L.A., 2016. Modulation of PPAR Expression and Activity in Response to Polyphenolic Compounds in High Fat Diets. Int. J. Mol. Sci. 17, 1002. https://doi.org/https://doi.org/10.3390/ijms17071002

Doty, R.L., Brugger, W.E., Jurs, P.C., Orndorff, M.A., Snyder, P.J., Lowry, L.D., 1978. Intranasal trigeminal stimulation from odorous volatiles: psychometric responses from anosmic and normal humans. Physiol. Behav. 20, 175–185. https://doi.org/10.1016/0031-9384(78)90070-7

Durand, N., Chertemps, T., Maïbèche-Coisne, M., 2012. Antennal carboxylesterases in a moth, structural and functional diversity. Commun. Integr. Biol. 5, 284–286. https://doi.org/https://doi.org/10.4161/cib.19701

Ehlers, A., These, A., Hessel, S., Preiss-Weigert, A., Lampen, A., 2014. Active elimination of the marine biotoxin okadaic acid by P-glycoprotein through an in vitro gastrointestinal barrier. Toxicol. Lett. 225, 311–317. https://doi.org/10.1016/j.toxlet.2013.12.019

Elsaesser, R., Paysan, J., 2005. Morituri te salutant? Olfactory signal transduction and the role of phosphoinositides. J. Neurocytol. 34, 97–116. https://doi.org/10.1007/s11068-005-5050-z

Eshun-Wilson, L., Zhang, R., Portran, D., Nachury, M. V., Toso, D.B., Löhr, T., Vendruscolo, M., Bonomi, M., Fraser, J.S., Nogales, E., 2019. Effects of α-tubulin acetylation on microtubule structure and stability. Proc. Natl. Acad. Sci. U. S. A. 116, 10366–10371. https://doi.org/10.1073/PNAS.1900441116/SUPPL_FILE/PNAS.1900441116.SAPP.PDF

Esteves, F., Rueff, J., Kranendonk, M., 2021. The central role of cytochrome p450 in xenobiotic metabolism—a brief review on a fascinating enzyme family. J. Xenobiotics. https://doi.org/10.3390/jox11030007

Faure, P., Legendre, A., Hanser, H.-I., Andriot, I., Artur, Y., Guichard, E., Coureaud, G., Heydel, J.-M., 2016. Odorant Metabolism Analysis by an Automated Ex Vivo Headspace Gas-Chromatography Method. Chem. Senses 41, 15–23. https://doi.org/10.1093/chemse/bjv055

Feng, L., Han, B., Wang, R., Li, Q., Bian, D., Ma, C., Song, G., Gao, L., Zhao, J., 2012. The frequency of daily ethanol consumption influences the effect of ethanol on insulin sensitivity in rats fed a high-fat diet. Br. J. Nutr. 107, 850–857. https://doi.org/10.1017/S0007114511003722

Filiou, R.P., Lepore, F., Bryant, B., Lundström, J.N., Frasnelli, J., 2015. Perception of trigeminal mixtures. Chem. Senses 40, 61–69. https://doi.org/10.1093/chemse/bju064

Fomenko, M. V., Yanshole, L. V., Tsentalovich, Y.P., 2022. Stability of Metabolomic Content during Sample Preparation: Blood and Brain Tissues. Metabolites 12, 811. https://doi.org/10.3390/METABO12090811/S1

Foxman, E.F., Storer, J.A., Fitzgerald, M.E., Wasik, B.R., Hou, L., Zhao, H., Turner, P.E., Pyle, A.M., Iwasaki, A., 2014. Temperature-dependent innate defense against the common cold virus limits viral replication at warm temperature in mouse airway cells. Proc. Natl. Acad. Sci. U. S. A. 112, 827–832. https://doi.org/10.1073/pnas.1411030112

Frasnelli, J., Albrecht, J., Bryant, B., Lundström, J.N., 2011. Perception of specific trigeminal chemosensory agonists. Neuroscience 189, 377–383. https://doi.org/10.1016/j.neuroscience.2011.04.065

Gadziola, M.A., Tylicki, K.A., Christian, D.L., Wesson, D.W., 2015. The olfactory tubercle encodes odor valence in behaving mice. J. Neurosci. 35, 4515–4527. https://doi.org/10.1523/JNEUROSCI.4750-14.2015

Galluzzi, L., Vitale, I., Abrams, J.M., Alnemri, E.S., Baehrecke, E.H., Blagosklonny, M. V., Dawson, T.M., Dawson, V.L., El-Deiry, W.S., Fulda, S., Gottlieb, E., Green, D.R., Hengartner, M.O., Kepp, O., Knight, R.A., Kumar, S., Lipton, S.A., Lu, X., Madeo, F., Malorni, W., Mehlen, P., Nũez, G., Peter, M.E., Piacentini, M., Rubinsztein, D.C., Shi, Y., Simon, H.U., Vandenabeele, P., White, E., Yuan, J., Zhivotovsky, B., Melino, G., Kroemer, G., 2012. Molecular definitions of cell death subroutines: Recommendations of the Nomenclature Committee on Cell Death 2012. Cell Death Differ. 19, 107–120. https://doi.org/10.1038/cdd.2011.96

Gamage, N., Barnett, A., Hempel, N., Duggleby, R.G., Windmill, K.F., Martin, J.L., McManus, M.E., 2006. Human sulfotransferases and their role in chemical metabolism. Toxicol. Sci. 90, 5–22. https://doi.org/10.1093/toxsci/kfj061

Gan, J., Ma, S., Zhang, D., 2016. Non-cytochrome P450-mediated bioactivation and its toxicological relevance. Drug Metab. Rev. 48, 473–501. https://doi.org/10.1080/03602532.2016.1225756

Ganger, M.T., Dietz, G.D., Ewing, S.J., 2017. A common base method for analysis of qPCR data and the application of simple blocking in qPCR experiments. BMC Bioinformatics 18, 1–11. https://doi.org/10.1186/s12859-017-1949-5

Gascuel, J., Lemoine, A., Rigault, C., Datiche, F., Benani, A., Penicaud, L., Lopez-Mascaraque, L., 2012. Hypothalamus-Olfactory System Crosstalk: Orexin A Immunostaining in Mice. Front. Neuroanat. 6, 44. https://doi.org/Hypothalamus-Olfactory System Crosstalk: Orexin A Immunostaining in Mice

Gautam, S.H., Verhagen, J. V., 2012. Direct Behavioral Evidence for Retronasal Olfaction in Rats. PLoS One 7, e44781. https://doi.org/10.1371/journal.pone.0044781

Gervasi, P.G., Longo, V., Naldi, F., Panattoni, G., Ursino, F., 1991. Xenobiotic-metabolizing enzymes in human respiratory nasal mucosa. Biochem. Pharmacol. 41, 177–184. https://doi.org/10.1016/0006-2952(91)90474-J

Getchell, M.L., Chen, Y., Getchell, T. V., Getchell, M.L., Sparks, D.L., Getchell, T. V., Getchell, T. V., Sparks, D.L., Ding, X., 1993. Immunohistochemical localization of a cytochrome p-450 isozyme in human nasal mucosa: Age-related trends. Ann. Otol. Rhinol. Laryngol. 102, 368–374. https://doi.org/10.1177/000348949310200509

Getchell, T. V., Getchell, M.L., 1990. Regulatory factors in the vertebrate olfactory mucosa.

Chem. Senses 15, 223–231. https://doi.org/10.1093/Chemse/15.2.223

Getchell, T. V., Margolis, F.L., Getchell, M.L., 1984. Perireceptor and receptor events in vertebrate olfaction. Prog. Neurobiol. 23, 317–345. https://doi.org/10.1016/0301-0082(84)90008-x

Gholizadeh, H., Ong, H.X., Bradbury, P., Kourmatzis, A., Traini, D., Young, P., Li, M., Cheng, S., 2021. Real-time quantitative monitoring of in vitro nasal drug delivery by a nasal epithelial mucosa-on-a-chip model. Expert Opin. Drug Deliv. 18, 803–818. https://doi.org/10.1080/17425247.2021.1873274

Giannetti, N., Pellier, V., Oestreicher, A.B., Astic, L., 1995. Immunocytochemical study of the differentiation process of the septal organ of Masera in developing rats. Brain Res. Dev. Brain Res. 84, 287–293. https://doi.org/10.1016/0165-3806(94)00195-6

Girard, S.D., Devéze, A., Nivet, E., Gepner, B., Roman, F.S., Féron, F., 2011. Isolating Nasal Olfactory Stem Cells from Rodents or Humans. J. Vis. Exp. 2762. https://doi.org/10.3791/2762

Glezer, I., Malnic, B., 2019. Olfactory receptor function. Handb. Clin. Neurol. 164, 67–78. https://doi.org/10.1016/B978-0-444-63855-7.00005-8

Goldstein, B.J., Schwob, J.E., 1996. Analysis of the Globose Basal Cell Compartment in Rat Olfactory Epithelium Using GBC-1, a New Monoclonal Antibody against Globose Basal Cells. J. Neurosci. 16, 4005–4016. https://doi.org/10.1523/JNEUROSCI.16-12-04005.1996

Grant, D.M., 1991. Detoxification pathways in the liver. J. Inherit. Metab. Dis. 14, 421–430. https://doi.org/10.1007/BF01797915

Graziadei, P.P., 1973. Cell dynamics in the olfactory mucosa. Tissue Cell 5, 113–131. https://doi.org/10.1016/s0040-8166(73)80010-2

Graziadei, P.P.C., Graziadei, G.A.M., 1985. Neurogenesis and plasticity of the olfactory sensory neurons. Ann. N. Y. Acad. Sci. 457, 127–142. https://doi.org/10.1111/j.1749-6632.1985.tb20802.x

Ha, J.G., Cho, H.J., 2023. Unraveling the Role of Epithelial Cells in the Development of Chronic Rhinosinusitis. Int. J. Mol. Sci. https://doi.org/10.3390/ijms241814229

Haberly, L.B., Bower, J.M., 1989. Olfactory cortex: model circuit for study of associative memory? Trends Neurosci. 12, 258–264. https://doi.org/10.1016/0166-2236(89)90025-8

Hadley, W.M., Dahl, A.R., 1982. Cytochrome P-450 dependent monooxygenase activity in rat nasal epithelial membranes. Toxicol. Lett. 10, 417–422. https://doi.org/10.1016/0378-4274(82)90240-5

Hall, T.L., 2002. Fomepizole in the treatment of ethylene glycol poisoning. CJEM 4, 199–204. https://doi.org/10.1017/S1481803500006382

Halldin, C.N., Suarthana, E., Fedan, K.B., Lo, Y.-C.C., Turabelidze, G., Kreiss, K., 2013. Increased respiratory disease mortality at a microwave popcorn production facility with worker risk of bronchiolitis obliterans. PLoS One 8, e57935. https://doi.org/10.1371/JOURNAL.PONE.0057935

Han, P., Mann, S., Raue, C., Warr, J., Hummel, T., 2018. Pepper with and without a sting: Brain processing of intranasal trigeminal and olfactory stimuli from the same source. Brain Res. 1700, 41–46. https://doi.org/10.1016/j.brainres.2018.07.010

Hanser, H.-I., Faure, P., Robert-Hazotte, A., Arthur, Y., Duchamp-Viret, P., Coureaud, G., Heydel, J.-M., 2017. Odorant-odorant metabolic interaction, a novel actor in olfactory perception and behavioral responsiveness. Sci. Rep. 7, 10219. https://doi.org/10.1038/S41598-017-10080-Z

Hao, Y., Hao, S., Andersen-Nissen, E., Mauck, W.M., Zheng, S., Butler, A., Lee, M.J., Wilk, A.J., Darby, C., Zager, M., Hoffman, P., Stoeckius, M., Papalexi, E., Mimitou, E.P., Jain, J., Srivastava, A., Stuart, T., Fleming, L.M., Yeung, B., Rogers, A.J., McElrath, J.M., Blish, C.A., Gottardo, R., Smibert, P., Satija, R., 2021. Integrated analysis of multimodal single-cell data. Cell 184, 3573-3587.e29. https://doi.org/10.1016/J.CELL.2021.04.048

Hao, Y., Stuart, T., Kowalski, M.H., Choudhary, S., Hoffman, P., Hartman, A., Srivastava, A., Molla, G., Madad, S., Fernandez-Granda, C., Satija, R., 2023. Dictionary learning for integrative, multimodal and scalable single-cell analysis. Nat. Biotechnol. 2023 1–12. https://doi.org/10.1038/s41587-023-01767-y

Harkema, J., Morgan, K., 1996. Normal morphology of the nasal passages in laboratory rodents, in: Jones, T., Dungworth, D., Mohr, U. (Eds.), Respiratory System. Springer, Berlin Heidelberg, pp. 3–17.

Harkema, J.R., Carey, S.A., Wagner, J.G., 2006. The nose revisited: a brief review of the comparative structure, function, and toxicologic pathology of the nasal epithelium. Toxicol. Pathol. 34, 252–269. https://doi.org/10.1080/01926230600713475

Haseba, T., Ohno, Y., 2010. A new view of alcohol metabolism and alcoholism-Role of the high-Km class III alcohol dehydrogenase (ADH3). Int. J. Environ. Res. Public Health 7, 1076–1092. https://doi.org/10.3390/ijerph7031076

He, L., Ronis, M.J.J., Badger, T.M., 2002. Ethanol Induction of Class I Alcohol Dehydrogenase Expression in the Rat Occurs through Alterations in CCAAT/Enhancer Binding Proteins β and γ. J. Biol. Chem. 277, 43572–43577. https://doi.org/10.1074/JBC.M204535200

Heming, C.P., Muriithi, W., Macharia, L.W., Filho, P.N., Moura-Neto, V., Aran, V., 2022. P-glycoprotein and cancer: what do we currently know? Heliyon 8, e11171. https://doi.org/10.1016/j.heliyon.2022.e11171

Herman, T.F., Santos, C., 2023. First-Pass Effect, in: StatPearls. StatPearls Publishing.

Heydarian, M., Yang, T., Schweinlin, M., Steinke, M., Walles, H., Rudel, T., Kozjak-Pavlovic, V., 2019. Biomimetic human tissue model for long-term study of Neisseria gonorrhoeae infection. Front. Microbiol. 10. https://doi.org/10.3389/FMICB.2019.01740/PDF

Heydel, J.M., Coelho, A., Thiebaud, N., Legendre, A., Bon, A.M. Le, Faure, P., Neiers, F., Artur, Y., Golebiowski, J., Briand, L., 2013. Odorant-binding proteins and xenobiotic metabolizing enzymes: Implications in olfactory perireceptor events. Anat. Rec. 296, 1333–1345. https://doi.org/10.1002/AR.22735

Heydel, J.M., Faure, P., Neiers, F., 2019a. Nasal odorant metabolism: enzymes, activity and function in olfaction. Drug Metab. Rev. 51, 224–245. https://doi.org/10.1080/03602532.2019.1632890

Heydel, J.M., Holsztynska, E.J., Legendre, A., Thiebaud, N., Artur, Y., Le Bon, A.M., 2010. UDP-glucuronosyltransferases (UGTs) in neuro-olfactory tissues: Expression, regulation, and function. Drug Metab. Rev. 42, 74–97. https://doi.org/10.3109/03602530903208363

Heydel, J.M., Leclerc, S., Bernard, P., Pelczar, H., Gradinaru, D., Magdalou, J., Minn, A., Artur, Y., Goudonnet, H., 2001. Rat olfactory bulb and epithelium UDP-glucuronosyltransferase

2A1 (UGT2A1) expression: In situ mRNA localization and quantitative analysis. Mol. Brain Res. 90, 83–92. https://doi.org/https://doi.org/10.1016/s0169-328x(01)00080-8

Heydel, J.M., Menetrier, F., Belloir, C., Canon, F., Faure, P., Lirussi, F., Chavanne, E., Saliou, J.M., Artur, Y., Canivenc-Lavier, M.C., Briand, L., Neiers, F., 2019b. Characterization of rat glutathione transferases in olfactory epithelium and mucus. PLoS One 14. https://doi.org/10.1371/JOURNAL.PONE.0220259

Hill, R.W., Wyse, G.A., Anderson, M., Anderson, M., 2004. Animal physiology, First edit. ed. Sinauer Associates Inc.

Hiller-Sturmhöfel, S., Bartke, A., 1998. The Endocrine System. Alcohol Health Res. World 22, 153–164.

Hodgson, E., 2010. Introduction to Biotransformation (Metabolism). Hayes' Handb. Pestic. Toxicol. 865–875. https://doi.org/10.1016/B978-0-12-374367-1.00036-7

Hornung, D.E., Mozell, M.M., 1977. Factors influencing the differential sorption of odorant molecules across the olfactory mucosa. J. Gen. Physiol. 69, 343–361. https://doi.org/10.1085/jgp.69.3.343

Hosokawa, M., Furihata, T., Yaginuma, Y., Yamamoto, N., Watanabe, N., Tsukada, E., Ohhata, Y., Kobayashi, K., Satoh, T., Chiba, K., 2008. Structural organization and characterization of the regulatory element of the human carboxylesterase (CES1A1 and CES1A2) genes. Drug Metab. Pharmacokinet. 23, 73–84. https://doi.org/10.2133/dmpk.23.73

Hosokawa, M., Maki, T., Satoh, T., 1990. Characterization of molecular species of liver microsomal carboxylesterases of several animal species and humans. Arch. Biochem. Biophys. 277, 219–227. https://doi.org/10.1016/0003-9861(90)90572-g

Howell, J., Costanzo, R.M., Reiter, E.R., 2018. Head trauma and olfactory function. J. Otorhinolaryngol. - Head Neck Surg. 4, 39–45. https://doi.org/10.1016/j.wjorl.2018.02.001

Huard, J.M., Schwob, J.E., 1995. Cell cycle of globose basal cells in rat olfactory epithelium. Dev. Dyn. 203, 17–26. https://doi.org/10.1002/aja.1002030103

Hubbs, A.F., Cumpston, A.M., Goldsmith, W.T., Battelli, L.A., Kashon, M.L., Jackson, M.C., Frazer, D.G., Fedan, J.S., Goravanahally, M.P., Castranova, V., Kreiss, K., Willard, P.A., Friend, S., Schwegler-Berry, D., Fluharty, K.L., Sriram, K., 2012. Respiratory and Olfactory Cytotoxicity of Inhaled 2,3-Pentanedione in Sprague-Dawley Rats. Am. J. Pathol. 181, 829–844. https://doi.org/10.1016/J.AJPATH.2012.05.021

Hubrecht, R.C., Carter, E., 2019. The 3Rs and Humane Experimental Technique: Implementing Change. Anim. An Open Access J. From MDPI 9, 754. https://doi.org/10.3390/ani9100754

Hummel, T., Livermore, A., 2002. Intranasal chemosensory function of the trigeminal nerve and aspects of its relation to olfaction. Int. Arch. Occup. Environ. Health 75, 305–313. https://doi.org/10.1007/s00420-002-0315-7

Ijichi, C., Wakabayashi, H., Sugiyama, S., Hayashi, K., Ihara, Y., Nishijima, H., Touhara, K., Kondo, K., 2022. Odorant metabolism of the olfactory cleft mucus in idiopathic olfactory impairment patients and healthy volunteers. Int. Forum Allergy Rhinol. 12, 293–301. https://doi.org/10.1002/ALR.22897

Ijichi, C., Wakabayashi, H., Sugiyama, S., Ihara, Y., Nogi, Y., Nagashima, A., Ihara, S., Niimura, Y.,

Shimizu, Y., Kondo, K., Touhara, K., 2019. Metabolism of odorant molecules in human nasal/oral cavity affects the odorant perception. Chem. Senses 44, 465–481. https://doi.org/10.1093/chemse/bjz041

Ishikawa, S., Nakayama, T., Watanabe, M., Matsuzawa, T., 2009. Flow mechanisms in the human olfactory groove: numerical simulation of nasal physiological respiration during inspiration, expiration, and sniffing. Arch. Otolaryngol. Head. Neck Surg. 135, 156–162. https://doi.org/10.1001/archoto.2008.530

Iwai, N., Zhou, Z., Roop, D.R., Behringer, R.R., 2008. Horizontal basal cells are multipotent progenitors in normal and injured adult olfactory epithelium. Stem Cells 26, 1298–1306. https://doi.org/10.1634/stemcells.2007-0891

Jacobson, L., 1813. Anatomisk. Beskrivelse over et nyt Organ i Huusdyrenes Næse. Veterinær Selsk. Skr. 2, 209–246.

Jancova, P., Anzenbacher, P., Anzenbacherova, E., 2010. Phase II drug metabolizing enzymes. Biomed. Pap. Med. Fac. Univ. Palacky. Olomouc. Czech. Repub. 154, 103–116. https://doi.org/10.5507/BP.2010.017

Jedlitschky, G., Cassidy, A.J., Sales, M., Pratt, N., Burchell, B., 1999. Cloning and characterization of a novel human olfactory UDP-glucuronosyltransferase. Biochem. J 340, 837–843.

Kang, P.F., Wu, W.J., Tang, Y., Xuan, L., Guan, S.D., Tang, B., Zhang, H., Gao, Q., Wang, H.J., 2016. Activation of ALDH2 with Low Concentration of Ethanol Attenuates Myocardial Ischemia/Reperfusion Injury in Diabetes Rat Model. Oxid. Med. Cell. Longev. 2016. https://doi.org/10.1155/2016/6190504

Kannan, K., Galizia, C.G., Nouvian, M., 2022. Olfactory Strategies in the Defensive Behaviour of Insects. Insects 13, 470. https://doi.org/10.3390/insects13050470

Kao, S.S.T., Bassiouni, A., Ramezanpour, M., Finnie, J., Chegeni, N., Colella, A.D., Chataway, T.K., Wormald, P.J., Vreugde, S., Psaltis, A.J., 2021. Proteomic analysis of nasal mucus samples of healthy patients and patients with chronic rhinosinusitis. J. Allergy Clin. Immunol. 147, 168–178. https://doi.org/10.1016/j.jaci.2020.06.037

Kessie, D.K., Lodes, N., Oberwinkler, H., Goldman, W.E., Walles, T., Steinke, M., Gross, R., 2021. Activity of Tracheal Cytotoxin of Bordetella pertussis in a Human Tracheobronchial 3D Tissue Model. Front. Cell. Infect. Microbiol. 10, 853. https://doi.org/10.3389/FCIMB.2020.614994/BIBTEX

Kia'i, N., Bajaj, T., 2022. Histology, Respiratory Epithelium. StatPearls.

Kim, M.S., Smith, D.P., 2001. The invertebrate odorant-binding protein LUSH is required for normal olfactory behavior in Drosophila. Chem. Senses 26, 195–199. https://doi.org/10.1093/chemse/26.2.195

Kistiakowsky, G.B., 1950. On the Theory of Odors. Science (80-.). 112, 154–155. https://doi.org/10.1126/science.112.2901.154-a

Kleemann, A.M., Albrecht, J., Schöpf, V., Haegler, K., Kopietz, R., Hempel, J.M., Linn, J., Flanagin, V.L., Fesl, G., Wiesmann, M., 2009. Trigeminal perception is necessary to localize odors. Physiol. Behav. 97, 401–405. https://doi.org/10.1016/j.physbeh.2009.03.013

Knecht, M., Hummel, T., 2004. Recording of the human electro-olfactogram. Physiol. Behav.

83, 13–9. https://doi.org/10.1016/j.physbeh.2004.07.024

Koppaka, V., Thompson, D.C., Chen, Y., Ellermann, M., Nicolaou, K.C., Juvonen, R.O., Petersen, D., Deitrich, R.A., Hurley, T.D., Vasiliou Dr., V., 2012. Aldehyde dehydrogenase inhibitors: a comprehensive review of the pharmacology, mechanism of action, substrate specificity, and clinical application. Pharmacol. Rev. 64, 520–539. https://doi.org/10.1124/PR.111.005538

Kornbausch, N., Mérignac-Lacombe, J., Neiers, F., Thomas-Danguin, T., Heydel, J.-M., Steinke, M., Hackenberg, S., Loos, H.M., 2023. Perspectives on Nasal Odorant Metabolism Research. J. Agric. Food Chem. 71, 16488–16492. https://doi.org/10.1021/ACS.JAFC.3C04662

Kovács, K.J., 1998. Invited review c-Fos as a transcription factor: a stressful (re)view from a functional map. Neurochem. Int. 33, 287–297. https://doi.org/10.1016/S0197-0186(98)00023-0

Kreiss, K., 2017. Recognizing occupational effects of diacetyl: What can we learn from this history? Toxicology 388, 48–54. https://doi.org/10.1016/j.tox.2016.06.009

Kreiss, K., Gomaa, A., Kullman, G., Fedan, K., Simoes, E.J., Enright, P.L., 2002. Clinical Bronchiolitis Obliterans in Workers at a Microwave-Popcorn Plant. N. Engl. J. Med. 347, 330–338. https://doi.org/10.1056/nejmoa020300

Krukoff, T.L., 1999. c-fos Expression as a Marker of Functional Activity in the Brain. Cell Neurobiol. Tech. 213–230. https://doi.org/10.1385/0-89603-510-7:213

Kuntová, B., Stopková, R., Stopka, P., 2018. Transcriptomic and Proteomic Profiling Revealed High Proportions of Odorant Binding and Antimicrobial Defense Proteins in Olfactory Tissues of the House Mouse. Front. Genet. 9, 26. https://doi.org/10.3389/fgene.2018.00026

Kurian, S.M., Naressi, R.G., Manoel, D., Barwich, A.S., Malnic, B., Saraiva, L.R., 2021. Odor coding in the mammalian olfactory epithelium. Cell Tissue Res. https://doi.org/10.1007/s00441-020-03327-1

Lacazette, E., Gachon, A.M., Pitiot, G., 2000. A novel human odorant-binding protein gene family resulting from genomic duplicons at 9q34: differential expression in the oral and genital spheres. Hum. Mol. Genet. 9, 289–301. https://doi.org/10.1093/hmg/9.2.289

Larigot, L., Juricek, L., Dairou, J., Coumoul, X., 2018. AhR signaling pathways and regulatory functions. Biochim. Open 7, 1. https://doi.org/10.1016/J.BIOPEN.2018.05.001

Laska, M., Distel, H., Hudson, R., 1997. Trigeminal perception of odorant quality in congenitally anosmic subjects. Chem. Senses 22, 447–456. https://doi.org/10.1093/chemse/22.4.447

Lazard, D., Zupko, K., Poria, Y., Nef, P., Lazarovits, J., Horn, S., Khen, M., Lancet, D., 1991a. Odorant Signal termination by olfactory UDP glucuronosyltransferase. 16. Semenza, C. Zettin, M. Nat. 27, 587–601.

Lazard, D., Zupko, K., Poria, Y., Net, P., Lazarovits, J., Horn, S., Khen, M., Lancet, D., 1991b. Odorant signal termination by olfactory UDP glucuronosyl transferase. Nature 349, 790–793. https://doi.org/10.1038/349790A0

Le Guérer, A., 2017. Évolution de notre perception de l'odorat [WWW Document]. Pollut. atmosphérique [online] N°234. URL http://lodel.irevues.inist.fr/pollution-atmospherique/index.php?id=6225 (accessed 1.24.24).

Le Magnen, J., 1944. Étude des facteurs dynamiques de l'excitation olfactive. Annee. Psychol. 45–46, 77–89. https://doi.org/10.3406/psy.1944.8156

Le Visage, C., Dunham, B., Flint, P., Leong, K.W., 2004. Coculture of Mesenchymal Stem Cells and Respiratory Epithelial Cells to Engineer a Human Composite Respiratory Mucosa. https://home.liebertpub.com/ten 10, 1426–1435. https://doi.org/10.1089/TEN.2004.10.1426

Leclerc, S., Heydel, J.M., Amossé, V., Gradinaru, D., Cattarelli, M., Artur, Y., Goudonnet, H., Magdalou, J., Netter, P., Pelczar, H., Minn, A., 2002. Glucuronidation of odorant molecules in the rat olfactory system. Activity, expression and age-linked modifications of UDP-glucuronosyltransferase isoforms, UGT1A6 and UGT2A1, and relation to mitral cell activity. Mol. Brain Res. 107, 201–213. https://doi.org/https://doi.org/10.1016/s0169-328x(02)00455-2

Lee, S.K., Son, L.T., Choi, H.J., Ahnn, J., 2013. Dicarbonyl/l-xylulose reductase (DCXR): The multifunctional pentosuria enzyme. Int. J. Biochem. Cell Biol. 45, 2563–2567. https://doi.org/10.1016/j.biocel.2013.08.010

Legendre, A., Faure, P., Tiesset, H., Potin, C., Jakob, I., Sicard, G., Schaal, B., Arthur, Y., Coureaud, G., Heydel, J.-M., 2014. When the nose must remain responsive: glutathione conjugation of the mammary pheromone in the newborn rabbit. Chem. Senses 39, 425–437. https://doi.org/10.1093/CHEMSE/BJU013

Lehr, M., Jörg, F., Walburga, H., 2015. Involvement of microsomal NADPH-cytochrome P450 reductase in metabolic reduction of drug ketones. Biopharm. Drug Dispos. 36, 398–404. https://doi.org/10.1002/bdd.1946

Leijon, S.C.M., Neves, A.F., Breza, J.M., Simon, S.A., Chaudhari, N., Roper, S.D., 2019. Oral thermosensing by murine trigeminal neurons: modulation by capsaicin, menthol and mustard oil. J. Physiol. 597, 2045–2061. https://doi.org/10.1113/JP277385

Leitner, F.C., Melzer, S., Lütcke, H., Pinna, R., Seeburg, P.H., Helmchen, F., Monyer, H., 2016. Spatially segregated feedforward and feedback neurons support differential odor processing in the lateral entorhinal cortex. Nat. Neurosci. 19, 935–944. https://doi.org/10.1038/nn.4303

Lewis, J.L., Nikula, K.J., Novak, R., Dahl, A.R., 1994. Comparative localization of carboxylesterase in F344 rat, beagle dog, and human nasal tissue. Anat. Rec. 239, 55–64. https://doi.org/https://doi.org/10.1002/ar.1092390107

Liberles, S.D., 2015. Trace amine-associated receptors: ligands, neural circuits, and behaviors. Curr. Opin. Neurobiol. 34, 1–7. https://doi.org/10.1016/j.conb.2015.01.001

Liberles, S.D., Horowitz, L.F., Kuang, D., Contos, J.J., Wilson, K.L., Siltberg-Liberles, J., Liberles, D.A., Buck, L.B., 2009. Formyl peptide receptors are candidate chemosensory receptors in the vomeronasal organ. Proc. Natl. Acad. Sci. U. S. A. 106, 9842–9847. https://doi.org/10.1073/pnas.0904464106

Lin, Q., Kang, X., Li, X., Wang, T., Liu, F., Jia, J., Jin, Z., Xue, Y., 2019. NF-κB-mediated regulation of rat CYP2E1 by two independent signaling pathways. PLoS One 14, e0225531. https://doi.org/10.1371/journal.pone.0225531

Listowsky, I., Abramovitz, M., Homma, H., Niitsu, Y., 1988. Intracellular binding and transport of hormones and xenobiotics by glutathione-S-transferases. Drug Metab. Rev. 19, 305–318. https://doi.org/10.3109/03602538808994138

Liu, Z., Anderson, J.D., Deng, L., Mackay, S., Bailey, J., Kersh, L., Rowe, S.M., Guimbellot, J.S., 2020. Human Nasal Epithelial Organoids for Therapeutic Development in Cystic Fibrosis. Genes 2020, Vol. 11, Page 603 11, 603. https://doi.org/10.3390/GENES11060603

Lledo, P.M., Gheusi, G., Vincent, J.D., 2005. Information processing in the mammalian olfactory system. Physiol. Rev. 85, 281–317. https://doi.org/10.1152/physrev.00008.2004

Löbel, D., Jacob, M., Völkner, M., Breer, H., 2002. Odorants of different chemical classes interact with distinct odorant binding protein subtypes. Chem. Senses 27, 39–44. https://doi.org/10.1093/chemse/27.1.39

Lodes, N., Seidensticker, K., Perniss, A., Nietzer, S., Oberwinkler, H., May, T., Walles, T., Hebestreit, H., Hackenberg, S., Steinke, M., 2020. Investigation on Ciliary Functionality of Different Airway Epithelial Cell Lines in Three-Dimensional Cell Culture. Tissue Eng. Part A 26, 432. https://doi.org/10.1089/TEN.TEA.2019.0188

Longo, V., Ingelman-Sundberg, M., 1993. Acetone-dependent regulation of cytochromes P4502E1 and P4502B1 in rat nasal mucosa. Biochem. Pharmacol. 46, 1945–1951. https://doi.org/10.1016/0006-2952(93)90635-A

Longo, V., Mazzaccaro, A., Naldi, F., Gervasi, P.G., 1991. Drug-metabolizing enzymes in liver, olfactory, and respiratory epithelium of cattle. J. Biochem. Toxicol. 6, 123–128. https://doi.org/10.1002/JBT.2570060206

Ma, Q., 2013. Role of Nrf2 in Oxidative Stress and Toxicity. Annu. Rev. Pharmacol. Toxicol. 53, 401. https://doi.org/10.1146/ANNUREV-PHARMTOX-011112-140320

Mainland, J., Sobel, N., 2006. The sniff is part of the olfactory percept. Chem. Senses 31, 181–196. https://doi.org/10.1093/chemse/bjj012

Maisonnasse, P., Guedj, J., Contreras, V., Behillil, S., Solas, C., Marlin, R., Naninck, T., Pizzorno, A., Lemaitre, J., Gonçalves, A., Kahlaoui, N., Terrier, O., Fang, R.H.T., Enouf, V., Dereuddre-Bosquet, N., Brisebarre, A., Touret, F., Chapon, C., Hoen, B., Lina, B., Calatrava, M.R., van der Werf, S., de Lamballerie, X., Le Grand, R., 2020. Hydroxychloroquine use against SARS-CoV-2 infection in non-human primates. Nat. 2020 5857826 585, 584–587. https://doi.org/10.1038/s41586-020-2558-4

Malnic, B., Hirono, J., Sato, T., Buck, L.B., 1999. Combinatorial receptor codes for odors. Cells 96, 713–723. https://doi.org/10.1016/s0092-8674(00)80581-4

Mannervik, B., Danielson, U.H., 1988. Glutathione transferases--structure and catalytic activity. CRC Crit. Rev. Biochem. 23, 283–337. https://doi.org/10.3109/10409238809088226

Mao, Q., Unadkat, J.D., 2014. Role of the Breast Cancer Resistance Protein (BCRP/ABCG2) in Drug Transport—an Update. AAPS J. 17, 67–82. https://doi.org/10.1208/s12248-014-9668-6

Maresh, A., Rodriguez Gil, D., Whitman, M.C., Greer, C.A., 2008. Principles of glomerular organization in the human olfactory bulb--implications for odor processing. PLoS One 3, e2640. https://doi.org/10.1371/journal.pone.0002640

Mayer, U., Küller, A., Daiber, P.C., Neudorf, I., Warnken, U., Schnölzer, M., Frings, S., Möhrlen, F., 2009. The proteome of rat olfactory sensory cilia. Proteomics 9, 322–334. https://doi.org/10.1002/pmic.200800149

Mayer, U., Ungerer, N., Klimmeck, D., Warnken, U., Schnolzer, M., Frings, S. et, Mohrlen, F., 2007. Proteomic Analysis of a Membrane Preparation from Rat Olfactory Sensory Cilia.

Chem. Senses 33, 145–162. https://doi.org/10.1093/chemse/bjm073

McGill, M.R., Hinson, J.A., 2020. The development and hepatotoxicity of acetaminophen: reviewing over a century of progress. Drug Metab. Rev. 52, 472–500. https://doi.org/10.1080/03602532.2020.1832112

Menco, B.P., 1980. Qualitative and quantitative freeze-fracture studies on olfactory and nasal respiratory epithelial surfaces of frog, ox, rat, and dog. II. Cell apices, cilia, and microvilli. Cell Tissue Res. 211, 5–29. https://doi.org/10.1007/BF00233719

Menco, B.P.M., Bruch, R.C., Dau, B., Danho, W., 1992. Ultrastructural localization of olfactory transduction components: the G protein subunit Golfα and type III adenylyl cyclase. Neuron 8, 441–453. https://doi.org/10.1016/0896-6273(92)90272-F

Mercier, C., Jacqueroux, E., He, Z., Hodin, S., Constant, S., Perek, N., Boudard, D., Delavenne, X., 2019. Pharmacological characterization of the 3D MucilAir^{TM} nasal model. Eur. J. Pharm. Biopharm. 139, 186–196. https://doi.org/10.1016/J.EJPB.2019.04.002

Meredith, M., 2001. Human vomeronasal organ function: A critical review of best and worst cases. Chem. Senses. https://doi.org/10.1093/chemse/26.4.433

Meunier, B., de Visser, S.P., Shaik, S., 2004. Mechanism of oxidation reactions catalyzed by cytochrome P450 enzymes. Chem. Rev. 104, 3947–3980. https://doi.org/10.1021/CR020443G/ASSET/IMAGES/LARGE/CR020443GF00040.JPEG

Meunier, N., Raynaud, A., Le Bourhis, M., Grébert, D., Dewaele, A., Acquistapace, A., Bombail, V., 2020. The olfactory mucosa, first actor of olfactory detection, is sensitive to glucocorticoid hormone. Eur. J. Neurosci. 51, 1403–1418. https://doi.org/10.1111/EJN.14564

Minn, A.-L., Pelczar, H., Denizot, C., Martinet, M., Heydel, J.-M., Walther, B., Minn, A., Goudonnet, H., Artur, Y., 2005. CHARACTERIZATION OF MICROSOMAL CYTOCHROME P450-DEPENDENT MONOOXYGENASES IN THE RAT OLFACTORY MUCOSA. Drug Metab. Dispos. 33, 1229–1237. https://doi.org/10.1124/dmd.105.004085

Minn, A., Leclerc, S., Heydel, J.M., Minn, A.L., Denizcot, C., Cattarelli, M., Netter, P., Gradinaru, D., 2002. Drug transport into the mammalian brain: the nasal pathway and its specific metabolic barrier. J. Drug Target. 10, 285–296. https://doi.org/10.1080/713714452

Miragall, F., Breipohl, W., Naguro, T., Voss-Wermbter, G., 1984. Freeze-fracture study of the plasma membranes of the septal olfactory organ of Masera. J. Neurocytol. 13, 111–125. https://doi.org/10.1007/BF01148321

Mohana, K., Achary, A., 2017. Human cytosolic glutathione-S-transferases: quantitative analysis of expression, comparative analysis of structures and inhibition strategies of isozymes involved in drug resistance. Drug Metab. Rev. 49, 318–337. https://doi.org/10.1080/03602532.2017.1343343

Monti Graziadei, G.A., Graziadei, P.P.C., 1979. Neurogenesis and neuron regeneration in the olfactory system of mammals. II. Degeneration and reconstitution of the olfactory sensory neurons after axotomy. J. Neurocytol. 8, 197–213. https://doi.org/10.1007/BF01175561

Moran, D.T., Rowley, J.C. 3rd, Jafek, B.W., 1982. Electron microscopy of human olfactory epithelium reveals a new cell type: the microvillar cell. Brain Res. 253, 39–46. https://doi.org/10.1016/0006-8993(82)90671-0

Mori, K., Sakano, H., 2021. Olfactory Circuitry and Behavioral Decisions. Annu. Rev. Physiol. 83, 231–256. https://doi.org/10.1146/annurev-physiol-031820-092824

Morrison, E.E., Costanzo, R.M., 1992. Morphology of olfactory epithelium in humans and other vertebrates. Microsc. Res. Tech. 23, 49–61. https://doi.org/10.1002/jemt.1070230105

Muñoz-González, C., Feron, G., Brulé, M., Canon, F., 2018. Understanding the release and metabolism of aroma compounds using micro-volume saliva samples by ex vivo approaches. Food Chem. 240, 275–285. https://doi.org/10.1016/J.FOODCHEM.2017.07.060

Nagashima, A., Touhara, K., 2010. Enzymatic conversion of odorants in nasal mucus affects olfactory glomerular activation patterns and odor perception. J. Neurosci. 30, 16391–16398. https://doi.org/10.1523/JNEUROSCI.2527-10.2010

Nakagawa, J., Ishikura, S., Asami, J., Isaji, T., Usami, N., Hara, A., Sakurai, T., Tsuritani, K., Oda, K., Takahashi, M., Yoshimoto, M., Otsuka, N., Kitamura, K., 2002. Molecular Characterization of Mammalian Dicarbonyl/l-Xylulose Reductase and Its Localization in Kidney. J. Biol. Chem. 277, 17883–17891. https://doi.org/10.1074/JBC.M110703200

Nef, P., Heldman, J., Lazard, D., Margalit, T., Jaye, M., Hanukoglu, I., Lancet, D., 1989. Olfactory-specific cytochrome P-450. cDNA cloning of a novel neuroepithelial enzyme possibly involved in chemoreception. J. Biol. Chem. 264, 6780–6785. https://doi.org/10.1016/S0021-9258(18)83497-4

Negoias, S., Visschers, R.W., Boelrijk, A., Hummel, T., 2008. New ways to understand aroma perception. Food Chem. 108, 1247–1254. https://doi.org/10.1016/j.foodchem.2007.08.030

Neiers, F., Jarriault, D., Menetrier, F., Briand, L., Heydel, J.-M.M., Neiers Id, F., Jarriault, D., Menetrier, F., Briand, L., Heydel, J.-M.M., 2021. The odorant metabolizing enzyme UGT2A1: Immunolocalization and impact of the modulation of its activity on the olfactory response. PLoS One 16, e0249029. https://doi.org/10.1371/JOURNAL.PONE.0249029

Neiers, F., Mérignac-Lacombe, J., Heydel, J.-M., 2022. Odorant metabolizing enzymes in the peripheral olfactory process, in: Guichard, Elisabeth; Salles, C. (Ed.), Flavor: From Food to Behaviors, Wellbeing and Health. Elsevier Science, pp. 127–147.

Niimura, Y., 2009. Evolutionary dynamics of olfactory receptor genes in chordates: interaction between environments and genomic contents. Hum. Genomics 4, 107–118. https://doi.org/10.1186/1479-7364-4-2-107

Niimura, Y., Matsui, A., Touhara, K., 2014. Extreme expansion of the olfactory receptor gene repertoire in African elephants and evolutionary dynamics of orthologous gene groups in 13 placental mammals. Genome Res. 24, 1485–1496.

Obach, R.S., Huynh, P., Allen, M.C., Beedham, C., 2004. Human liver aldehyde oxidase: inhibition by 239 drugs. J. Clin. Pharmacol. 44, 7–19. https://doi.org/10.1177/0091270003260336

Oka, Y., Omura, M., Kataoka, H., Touhara, K., 2004. Olfactory receptor antagonism between odorants. EMBO J. 23, 120–126. https://doi.org/10.1038/sj.emboj.7600032

Olender, T., Keydar, I., Pinto, J.M., Tatarskyy, P., Alkelai, A., Chien, M.S., Fishilevich, S., Restrepo, D., Matsunami, H., Gilad, Y., Lancet, D., 2016. The human olfactory transcriptome. BMC Genomics 17, 1–18. https://doi.org/10.1186/S12864-016-2960-3/FIGURES/9

Oliveira, P., Fortuna, A., Alves, G., Falcao, A., 2016. Drug-metabolizing Enzymes and Efflux Transporters in Nasal Epithelium: Influence on the Bioavailability of Intranasally Administered Drugs. Curr. Drug Metab. 17, 628–647. https://doi.org/10.2174/1389200217666160406120509

Ozturk, A.B., Damadoglu, E., Karakaya, G., Kalyoncu, A.F., 2011. Does nasal hair (vibrissae) density affect the risk of developing asthma in patients with seasonal rhinitis? Int. Arch. Allergy Immunol. 156, 75–80. https://doi.org/10.1159/000321912

Patel, R.M., Pinto, J.M., 2014. Olfaction: Anatomy, physiology, and disease. Clin. Anat. https://doi.org/10.1002/ca.22338

Pelosi, P., 1996. Perireceptor events in olfaction. J. Neurobiol. 30, 3–19. https://doi.org/10.1002/(SICI)1097-4695(199605)30:1<3::AID-NEU2>3.0.CO;2-A

Pelosi, P., 1994. Odorant-binding proteins. Crit. Rev. Biochem. Mol. Biol. 29, 199–228. https://doi.org/10.3109/10409239409086801

Pelosi, P., Baldaccini, N.E., Pisanelli, A.M., 1982. Identification of a specific olfactory receptor for 2-isobutyl-3-methoxypyrazine. Biochem. J. 201, 245–248. https://doi.org/10.1042/bj2010245

Pérez-Jiménez, M., Muñoz-González, C., Pozo-Bayón, M.Á., 2021. Specificity of Saliva Esterases by Wine Carboxylic Esters and Inhibition by Wine Phenolic Compounds Under Simulated Oral Conditions. Front. Nutr. 8. https://doi.org/10.3389/FNUT.2021.761830/PDF

Pérez-Mota, J., Solorio-Ordaz, F., Cervantes-de Gortari, J., 2018. Flow and air conditioning simulations of computer turbinectomized nose models. Med. Biol. Eng. Comput. 56, 1899–1910. https://doi.org/10.1007/s11517-018-1823-2

Pfister, P., Smith, B.C., Evans, B.J., Brann, J.H., Trimmer, C., Sheikh, M., Arroyave, R., Reddy, G., Jeong, H.Y., Raps, D.A., Peterlin, Z., Vergassola, M., Rogers, M.E., 2020. Odorant Receptor Inhibition Is Fundamental to Odor Encoding. Curr. Biol. 30, 2574-2587.e6. https://doi.org/10.1016/J.CUB.2020.04.086

Pinching, A.J., Powell, T.P., 1971. The neuron types of the glomerular layer of the olfactory bulb. J. Cell Sci. 9, 305–345. https://doi.org/10.1242/jcs.9.2.305

Pollara, L., Sottile, V., Valente, E.M., 2022. Patient-derived cellular models of primary ciliopathies. J. Med. Genet. 59, 517–527. https://doi.org/10.1136/jmedgenet-2021-108315

Pourmorady, A.D., Bashkirova, E. V., Chiariello, A.M., Belagzhal, H., Kodra, A., Duffié, R., Kahiapo, J., Monahan, K., Pulupa, J., Schieren, I., Osterhoudt, A., Dekker, J., Nicodemi, M., Lomvardas, S., 2024. RNA-mediated symmetry breaking enables singular olfactory receptor choice. Nature 625, 181–188. https://doi.org/10.1038/s41586-023-06845-4

Puetz, H., Puchl'ová, E., Vranková, K., Hollmann, F., 2020. Biocatalytic Oxidation of Alcohols. Catal. 2020, Vol. 10, Page 952 10, 952. https://doi.org/10.3390/CATAL10090952

R Core Team, 2018. R: A Language and Environment for Statistical Computing.

Ramezanpour, M., Bolt, H., Hon, K., Shaghayegh, G., Rastin, H., Fenix, K.A., Alkis, J.P., Wormald, P.J., Vreugde, S., 2022. Characterization of human nasal organoids from chronic rhinosinusitis patients. Biol. Open 11, bio059267. https://doi.org/10.1242/bio.059267

Riggs, A., 1960. The Nature and Significance of the Bohr Effect in Mammalian Hemoglobins. J. Gen. Physiol. 43, 737–752. https://doi.org/10.1085/JGP.43.4.737

Robert-Hazotte, A., Faure, P., Ménétrier, F., Folia, M., Schwartz, M., Le Quéré, J.L., Neiers, F., Thomas-Danguin, T., Heydel, J.M., 2022. Nasal Odorant Competitive Metabolism Is Involved in the Human Olfactory Process. J. Agric. Food Chem. 70, 8385–8394. https://doi.org/10.1021/acs.jafc.2c02720

Robert-Hazotte, A., Faure, P., Neiers, F., Potin, C., Yves, A., Coureaud, G., Heydel, J.-M., 2019a. Nasal mucus glutathione transferase activity and impact on olfactory perception and neonatal behavior. Sci. Rep. 9. https://doi.org/10.1038/S41598-019-39495-6

Robert-Hazotte, A., Schoumacker, R., Semon, E., Briand, L., Guichard, E., Le Quéré, J.-L., Faure, P., Heydel, J.-M., 2019b. Ex vivo real-time monitoring of volatile metabolites resulting from nasal odorant metabolism. Sci. Rep. 9, 2492. https://doi.org/10.1038/S41598-019-39404-X

Robinson, D.A., Bogdanffy, M.S., Reed, C.J., 2002. Histochemical localisation of carboxylesterase activity in rat and mouse oral cavity mucosa. Toxicology 180, 209–220. https://doi.org/10.1016/s0300-483x(02)00375-x

Rodriguez, I., Greer, C.A., Mok, M.Y., Mombaerts, P., 2000. A putative pheromone receptor gene expressed in human olfactory mucosa. Nat. Genet. 26, 18–19. https://doi.org/10.1038/79124

Rolls, E.T., 2019. Taste and smell processing in the brain. Handb. Clin. Neurol. 164, 97–118. https://doi.org/10.1016/B978-0-444-63855-7.00007-1

Royet, J.P., Distel, H., Hudson, R., Gervais, R., 1998. A re-estimation of the number of glomeruli and mitral cells in the olfactory bulb of rabbit. Brain Res. 788, 35–42. https://doi.org/10.1016/s0006-8993(97)01504-7

Rozin, P., 1982. "Taste-smell confusions" and the duality of the olfactory sense. Percept. Psychophys. 31, 397–401. https://doi.org/10.3758/bf03202667

Rubin, B.K., 2010. Mucus and Mucins. Otolaryngol. Clin. North Am. 43, 27–34. https://doi.org/10.1016/J.OTC.2009.11.002

Ruysseveldt, E., Martens, K., Steelant, B., 2021. Airway Basal Cells, Protectors of Epithelial Walls in Health and Respiratory Diseases. Front. Allergy 2, 787128. https://doi.org/10.3389/FALGY.2021.787128/BIBTEX

Salazar, I., Sanchez-Quinteiro, P., Barrios, A.W., López Amado, M., Vega, J.A., 2019. Anatomy of the olfactory mucosa, in: Handbook of Clinical Neurology. Elsevier B.V., pp. 47–65. https://doi.org/10.1016/B978-0-444-63855-7.00004-6

Samali, A., Gilje, B., Døskeland, S.O., Cotter, T.G., Houge, G., 1997. The ability to cleave 28S ribosomal RNA during apoptosis is a cell-type dependent trait unrelated to DNA fragmentation. Cell Death Differ. 4, 289–293. https://doi.org/10.1038/sj.cdd.4400246

Sankaran, S., Khot, L.R., Panigrahi, S., 2012. Biology and applications of olfactory sensing system: A review. Sensors Actuators B Chem. 171–172, 1–17.

Sarkar, M.A., 1992. Drug metabolism in the nasal mucosa. Pharm. Res. 9, 1–9. https://doi.org/10.1023/a:1018911206646

Satija, R., Farrell, J.A., Gennert, D., Schier, A.F., Regev, A., 2015. Spatial reconstruction of single-cell gene expression data. Nat. Biotechnol. 2015 335 33, 495–502. https://doi.org/10.1038/nbt.3192

Satoh, T., 2002. Current Progress on Esterases: From Molecular Structure to Function. Drug

Metab. Dispos. 30, 488–493. https://doi.org/10.1124/dmd.30.5.488

Scherzad, A., Hagen, R., Hackenberg, S., 2019. Current Understanding of Nasal Epithelial Cell Mis-Differentiation. J. Inflamm. Res. 12, 309. https://doi.org/10.2147/JIR.S180853

Schilling, B., 2009. Method to identify or evaluate compounds useful in the field of fragrances and aromas.

Schilling, B., Kaiser, R., Natsch, A., Gautschi, M., 2010. Investigation of odors in the fragrance industry. Chemoecology 20, 135–147.

Schivo, M., Aksenov, A.A., Linderholm, A.L., McCartney, M.M., Simmons, J., Harper, R.W., Davis, C.E., 2014. Volatile emanations from in vitro airway cells infected with human rhinovirus. J. Breath Res. 8, 037110. https://doi.org/10.1088/1752-7155/8/3/037110

Schoumacker, R., Robert-Hazotte, A., Heydel, J.M., Faure, P., Le Quéré, J.L., 2016. Real-time monitoring of the metabolic capacity of ex vivo rat olfactory mucosa by proton transfer reaction mass spectrometry (PTR-MS). Anal. Bioanal. Chem. 408, 1539–1543. https://doi.org/10.1007/s00216-015-9289-7

Schroeder, A., Mueller, O., Stocker, S., Salowsky, R., Leiber, M., Gassmann, M., Lightfoot, S., Menzel, W., Granzow, M., Ragg, T., 2006. The RIN: An RNA integrity number for assigning integrity values to RNA measurements. BMC Mol. Biol. 7, 1–14. https://doi.org/10.1186/1471-2199-7-3/FIGURES/8

Schwab, J.A., Zenkel, M., 1998. Filtration of particulates in the human nose. Laryngoscope 108, 120–124. https://doi.org/10.1097/00005537-199801000-00023

Schwarcz, J., 2017. The Story of Perfume. Off. Sci. Soc.

Schwartz, M., Canon, F., Feron, G., Neiers, F., Gamero, A., 2021a. Impact of Oral Microbiota on Flavor Perception: From Food Processing to In-Mouth Metabolization. Foods 10. https://doi.org/10.3390/FOODS10092006

Schwartz, M., Menetrier, F., Heydel, J.-M., Chavanne, E., Faure, P., Labrousse, M., Lirussi, F., Canon, F., Mannervik, B., Briand, L., Neiers, F., 2020. Interactions Between Odorants and Glutathione Transferases in the Human Olfactory Cleft. Chem. Senses 45, 645–654. https://doi.org/10.1093/chemse/bjaa055

Schwartz, M., Neiers, F., Charles, J.P., Heydel, J.M., Muñoz-González, C., Feron, G., Canon, F., 2021b. Oral enzymatic detoxification system: Insights obtained from proteome analysis to understand its potential impact on aroma metabolization. Compr. Rev. Food Sci. Food Saf. 20, 5516–5547. https://doi.org/10.1111/1541-4337.12857

Schweinlin, M., Rossi, A., Lodes, N., Lotz, C., Hackenberg, S., Steinke, M., Walles, H., Groeber, F., 2017. Human barrier models for the in vitro assessment of drug delivery. Drug Deliv. Transl. Res. 7, 217–227. https://doi.org/10.1007/S13346-016-0316-9

Schwob, J.E., 2002. Neural regeneration and the peripheral olfactory system. Anat. Rec. 269, 33–49. https://doi.org/10.1002/ar.10047

Scott, J.W., Scott-Johnson, P.E., 2002. The electroolfactogram: a review of its history and uses. Microsc. Res. Tech. 58, 152–160. https://doi.org/10.1002/jemt.10133

Scott, W.R., Taulbee, D.B., Yu, C.P., 1978. Theoretical study of nasal deposition. Bull. Math. Biol. 40, 581–604. https://doi.org/10.1007/BF02460732

Sell, C.S., 2007. On the unpredictability of odor. Angew. Chem. Int. Ed. Engl. 45, 6254–6261.

https://doi.org/10.1002/anie.200600782

Sette, G., Cicero, S. Lo, Blaconà, G., Pierandrei, S., Bruno, S.M., Salvati, V., Castelli, G., Falchi, M., Fabrizzi, B., Cimino, G., De Maria, R., Biffoni, M., Eramo, A., Lucarelli, M., 2021. Theratyping cystic fibrosis in vitro in ALI culture and organoid models generated from patient-derived nasal epithelial conditionally reprogrammed stem cells. Eur. Respir. J. 58. https://doi.org/10.1183/13993003.00908-2021

Shahbaz, M.A., Kuivanen, S., Lampinen, R., Mussalo, L., Hron, T., Závodná, T., Ojha, R., Krejčík, Z., Saveleva, L., Tahir, N.A., Kalapudas, J., Koivisto, A.M., Penttilä, E., Löppönen, H., Singh, P., Topinka, J., Vapalahti, O., Chew, S., Balistreri, G., Kanninen, K.M., 2023. Human-derived air–liquid interface cultures decipher Alzheimer's disease–SARS-CoV-2 crosstalk in the olfactory mucosa. J. Neuroinflammation 20, 299. https://doi.org/10.1186/s12974-023-02979-4

Sharma, A., Kumar, R., Aier, I., Semwal, R., Tyagi, P., Varadwaj, P., 2018. Sense of Smell: Structural, Functional, Mechanistic Advancements and Challenges in Human Olfactory Research, Current Neuropharmacology. Bentham Science Publishers Ltd. https://doi.org/10.2174/1570159x17666181206095626

She, Q.M., Zhao, J., Wang, X.L., Zhou, C.M., Shi, X.Z., 2007. Effect of dexamethasone on peroxisome proliferator activated receptor-gamma mRNA expression in 3T3-L1 adipocytes with the human recombinant adiponectin. Chin. Med. J. (Engl). 120, 155–158.

Shepherd, G.M., 2010. New Perspectives on Olfactory Processing and Human Smell, in: Menini, A. (Ed.), The Neurobiology of Olfaction. Fronties in Neuroscience, Boca Raton (FL).

Shortall, K., Djeghader, A., Magner, E., Soulimane, T., 2021. Insights into Aldehyde Dehydrogenase Enzymes: A Structural Perspective. Front. Mol. Biosci. 8, 659550. https://doi.org/10.3389/FMOLB.2021.659550/BIBTEX

Shorter, J.R., Dembeck, L.M., Everett, L.J., Morozova, T. V., Arya, G.H., Turlapati, L., St Armour, G.E., Schal, C., Mackay, T.F., Anholt, R.R., 2016. Obp56h Modulates Mating Behavior in Drosophila melanogaster. G3 (Bethesda). 6, 3335–3342. https://doi.org/10.1534/g3.116.034595

Sicard, R.M., Frank-Ito, D.O., 2021. Role of nasal vestibule morphological variations on olfactory airflow dynamics. Clin. Biomech. (Bristol, Avon) 82, 105282. https://doi.org/10.1016/j.clinbiomech.2021.105282

Sivarajan, R., 2023. Engineered Human Airway Mucosa for Modelling Respiratory Infections: Characterisation and Applications. Julius-Maximilians-Universität Würzburg.

Sivarajan, R., Kessie, D.K., Oberwinkler, H., Pallmann, N., Walles, T., Scherzad, A., Hackenberg, S., Steinke, M., 2021. Susceptibility of Human Airway Tissue Models Derived From Different Anatomical Sites to Bordetella pertussis and Its Virulence Factor Adenylate Cyclase Toxin. Front. Cell. Infect. Microbiol. 11. https://doi.org/10.3389/FCIMB.2021.797491/PDF

Smith, T.D., Bhatnagar, K.P., 2019. Anatomy of the olfactory system. Handb. Clin. Neurol. 164, 17–28. https://doi.org/10.1016/B978-0-444-63855-7.00002-2

Sołobodowska, S., Giebułtowicz, J., Wolinowska, R., Wroczyński, P., 2012. Contribution of ALDH1A1 isozyme to detoxification of aldehydes present in food products. Acta Pol. Pharm. 69, 1380–3.

Sozansky, J., Houser, S.M., 2014. The physiological mechanism for sensing nasal airflow: a

literature review. Int. Forum Allergy Rhinol. 4, 834–838. https://doi.org/10.1002/alr.21368

Spencer, T.L., Clark, A., Fonollosa, J., Virot, E., Hu, D.L., 2021. Sniffing speeds up chemical detection by controlling air-flows near sensors. Nat. Commun. 12, 1232. https://doi.org/10.1038/s41467-021-21405-y

Sreerama, L., Hedge, M.W., Sladek, N.E., 1995. Identification of a class 3 aldehyde dehydrogenase in human saliva and increased levels of this enzyme, glutathione S-transferases, and DT-diaphorase in the saliva of subjects who continually ingest large quantities of coffee or broccoli. Clin. Cancer Res. 1, 1153–1163.

Staub, R.E., Quistad, G.B., Casida, J.E., 1998. Mechanism for benomyl action as a mitochondrial aldehyde dehydrogenase inhibitor in mice. Chem. Res. Toxicol. 11, 535–543. https://doi.org/10.1021/TX980002L/ASSET/IMAGES/LARGE/TX980002LF00013.JPEG

Steiner, C., Bozzolan, F., Montagné, N., Maïbèche, M., Chertemps, T., 2017. Neofunctionalization of "Juvenile Hormone Esterase Duplication" in Drosophila as an odorant-degrading enzyme towards food odorants. Sci. Rep. 7, 12629. https://doi.org/10.1038/s41598-017-13015-w

Steinke, M., Gross, R., Walles, H., Gangnus, R., Schütze, K., Walles, T., 2014. An engineered 3D human airway mucosa model based on an SIS scaffold. Biomaterials 35, 7355–7362. https://doi.org/10.1016/J.BIOMATERIALS.2014.05.031

Storan, M.J., Key, B., 2006. Septal organ of Grüneberg is part of the olfactory system. J. Comp. Neurol. 494, 834–844. https://doi.org/10.1002/cne.20858

Stoyanov, G.S., Matev, B.K., Valchanov, P., Sapundzhiev, N., Young, J.R., 2018. The Human Vomeronasal (Jacobson's) Organ: A Short Review of Current Conceptions, With an English Translation of Potiquet's Original Text. Cureus 10, e2643. https://doi.org/10.7759/cureus.2643

Strauss, J.F., FitzGerald, G.A., 2018. Steroid Hormones and Other Lipid Molecules Involved in Human Reproduction, in: Jaffe, Y. and (Ed.), Reproductive Endocrinology. pp. 75–114. https://doi.org/10.1016/B978-0-323-47912-7.00004-4

Stuart, T., Butler, A., Hoffman, P., Hafemeister, C., Papalexi, E., Mauck, W.M., Hao, Y., Stoeckius, M., Smibert, P., Satija, R., 2019. Comprehensive Integration of Single-Cell Data. Cell 177, 1888-1902.e21. https://doi.org/10.1016/J.CELL.2019.05.031

Su, T., Bao, Z., Zhang, Q.Y., Smith, T.J., Hong, J.Y., Ding, X., 2000. Human cytochrome P450 CYP2A13: predominant expression in the respiratory tract and its high efficiency metabolic activation of a tobacco-specific carcinogen, 4-(methylnitrosamino)-1-(3-pyridyl)-1-butanone. Cancer Res. 60, 5074–5079.

Suzuki, K., Inano, H., Omura, M., Higashi, Y., Oshima, H., 1987. Ketoconazole as a Possible Universal Inhibitor of Cytochrome P-450 Dependent Enzymes: Its Mode of Inhibition1. Endocrinol. Jpn. 34, 105–115. https://doi.org/10.1507/endocrj1954.34.105

Suzuki, Y., Schafer, J., Farbman, A.I., 1995. Phagocytic cells in the rat olfactory epithelium after bulbectomy. Exp. Neurol. 136, 225–233. https://doi.org/10.1006/exnr.1995.1099

Swaney, W.T., Keverne, E.B., 2009. The evolution of pheromonal communication. Behav. Brain Res. 200, 239–247. https://doi.org/10.1016/j.bbr.2008.09.039

Swift, D.L., Kesavanathan, J., 1996. The anterior human nasal passage as a fibrous filter for

particles. Chem. Eng. Commun. 151, 65–78. https://doi.org/10.1080/00986449608936542

Tang, J., Tang, J., Ling, E.A., Wu, Y., Liang, F., 2009. Juxtanodin in the rat olfactory epithelium: specific expression in sustentacular cells and preferential subcellular positioning at the apical junctional belt. Neuroscience 161, 249–258. https://doi.org/10.1016/j.neuroscience.2009.03.051

Tcatchoff, L., Nespoulous, C., Pernollet, J.C., Briand, L., 2006. A single lysyl residue defines the binding specificity of a human odorant-binding protein for aldehydes. FEBS Lett. 580, 2102–2108. https://doi.org/10.1016/j.febslet.2006.03.017

Tegoni, M., Campanacci, V., Cambillau, C., 2004. Structural aspects of sexual attraction and chemical communication in insects. Trends Biochem. Sci. 29, 257–264. https://doi.org/10.1016/j.tibs.2004.03.003

Tegoni, M., Pelosi, P., Vincent, F., Spinelli, S., Campanacci, V., Grolli, S., Ramoni, R., Cambillau, C., 2000. Mammalian odorant binding proteins. Biochim. Biophys. Acta 1482, 229–240. https://doi.org/10.1016/s0167-4838(00)00167-9

Testa, B., 2005. Principles of Drug Metabolism 2: Hydrolysis and Conjugation Reactions. Chem. Mol. Sci. Chem. Eng. 5, 133–166. https://doi.org/10.1016/B0-08-045044-X/00120-6

Thiebaud, N., Menetrier, F., Belloir, C., Minn, A.L., Neiers, F., Artur, Y., Le Bon, A.M., Heydel, J.M., 2011. Expression and differential localization of xenobiotic transporters in the rat olfactory neuro-epithelium. Neurosci. Lett. 505, 180–185. https://doi.org/10.1016/J.NEULET.2011.10.018

Thiebaud, N., Sigoillot, M., Chevalier, J., Artur, Y., Heydel, J.M., Le Bon, A.M., 2010. Effects of typical inducers on olfactory xenobiotic-metabolizing enzyme, transporter, and transcription factor expression in rats. Drug Metab. Dispos. 38, 1865–1875. https://doi.org/10.1124/DMD.110.035014

Thiebaud, N., Silva, V. Da, Sicard, J.I., Chevalier, G., Veloso Da Silva, S., Jakob, I., Sicard, G., Chevalier, J., Ménétrier, F., Berdeaux, O., Artur, Y., Heydel, J.M., Le Bon, A.M., 2013. Odorant Metabolism Catalyzed by Olfactory Mucosal Enzymes Influences Peripheral Olfactory Responses in Rats. PLoS One 8, 59547. https://doi.org/10.1371/journal.pone.0059547

Tirindelli, R., 2021. Coding of pheromones by vomeronasal receptors. Cell Tissue Res. 383, 367–386. https://doi.org/10.1007/s00441-020-03376-6

Tomassini Barbarossa, I., Ozdener, M.H., Melania, Love-Gregory, L., Mitreva, M., Abumrad, N.A., Pepino, M.Y., 2017. Variant in a common odorant-binding protein gene is associated with bitter sensitivity in people. Behav. Brain Res. 329, 200–204. https://doi.org/10.1016/j.bbr.2017.05.015

Touhara, K., 2002. Odor discrimination by G protein-coupled olfactory receptors. Microsc. Res. Tech. 58, 135–141. https://doi.org/10.1002/jemt.10131

Turin, L., 2002. A method for the calculation of odor character from molecular structure. J. Theor. Biol. 216, 367–385.

Turin, L., Yoshii, F., 2003. Structure-Odor Relations: a modern perspective in Handbook of Olfaction and Gustation Second Edition. New York Marcel Dekker.

Uhlén, M., Fagerberg, L., Hallström, B.M., Lindskog, C., Oksvold, P., Mardinoglu, A., Sivertsson,

Å., Kampf, C., Sjöstedt, E., Asplund, A., Olsson, I.M., Edlund, K., Lundberg, E., Navani, S., Szigyarto, C.A.K., Odeberg, J., Djureinovic, D., Takanen, J.O., Hober, S., Alm, T., Edqvist, P.H., Berling, H., Tegel, H., Mulder, J., Rockberg, J., Nilsson, P., Schwenk, J.M., Hamsten, M., Von Feilitzen, K., Forsberg, M., Persson, L., Johansson, F., Zwahlen, M., Von Heijne, G., Nielsen, J., Pontén, F., 2015. Tissue-based map of the human proteome. Science (80-.). 347. https://doi.org/10.1126/SCIENCE.1260419

Uraih, L.C., Maronpot, R.R., 1990. Normal histology of the nasal cavity and application of special techniques. Environ. Health Perspect. 85, 187–208. https://doi.org/10.1289/ehp.85-1568325

Usami, A., Ueki, S., Ito, W., Kobayashi, Y., Chiba, T., Mahemuti, G., Oyamada, H., Kamada, Y., Fujita, M., Kato, H., Saito, N., Kayaba, H., Chihara, J., 2006. Theophylline and dexamethasone induce peroxisome proliferator-activated receptor-gamma expression in human eosinophils. Pharmacology 77, 33–37. https://doi.org/10.1159/000092376

Van Rooy, F.G.B.G.J., Rooyackers, J.M., Prokop, M., Houba, R., Smit, L.A.M., Heederik, D.J.J., 2007. Bronchiolitis obliterans syndrome in chemical workers producing diacetyl for food flavorings. Am. J. Respir. Crit. Care Med. 176, 498–504. https://doi.org/10.1164/rccm.200611-1620OC

Vidic, J.., Grosclaude, J.., Monnerie, R. ég. ., Persuy, M.-A.M.-A.., Badonnel, K.., Baly, C.., Caillol, M.., Briand, L. ïc. ., Salesse, R.., Pajot-Augy, E., 2008. On a chip demonstration of a functional role for Odorant Binding Protein in the preservation of olfactory receptor activity at high odorant concentration. Lab Chip 8, 678–688. https://doi.org/10.1039/b717724k

Völkel, C., De Wispelaere, N., Weidemann, S., Gorbokon, N., Lennartz, · Maximilian, Luebke, A.M., Hube-Magg, C., Kluth, M., Fraune, C., Möller, K., Christian Bernreuther, ·, Lebok, · Patrick, Till, ·, Clauditz, S., Jacobsen, · Frank, Sauter, G., Uhlig, R., Wilczak, W., Steurer, S., Minner, S., Krech, R.H., Dum, D., Krech, · Till, Marx, A.H., Simon, R., Eike Burandt, ·, Menz, A., 2021. Cytokeratin 5 and cytokeratin 6 expressions are unconnected in normal and cancerous tissues and have separate diagnostic implications. Virchows Arch. 480, 433–437. https://doi.org/10.1007/s00428-021-03204-4

Wang, W., Yan, Y., Li, C.W., Xia, H.M., Chao, S.S., Wang, D.Y., Wang, Z.P., 2014. Live human nasal epithelial cells (hNECs) on chip for in vitro testing of gaseous formaldehyde toxicity via airway delivery. Lab Chip 14, 677–680. https://doi.org/10.1039/C3LC51208H

Watelet, J.B., Strolin-Benedetti, M., Whomsley, R., 2009. Defence mechanisms of olfactory neuro-epithelium: mucosa regeneration, metabolising enzymes and transporters. B-ENT.

Wedel, A., Lömsziegler-Heitbrock, H.W., 1995. The C/EBP Family of Transcription Factors. Immunobiology 193, 171–185. https://doi.org/10.1016/S0171-2985(11)80541-3

Weigel, T., Malkmus, C., Weigel, V., Wußmann, M., Berger, C., Brennecke, J., Groeber-Becker, F., Hansmann, J., 2022. Fully Synthetic 3D Fibrous Scaffolds for Stromal Tissues-Replacement of Animal-Derived Scaffold Materials Demonstrated by Multilayered Skin. Adv. Mater. 34. https://doi.org/10.1002/ADMA.202106780

Wu, B., Dong, D., 2012. Human cytosolic glutathione transferases: structure, function, and drug discovery. Trends Pharmacol. Sci. 33, 656–668. https://doi.org/10.1016/j.tips.2012.09.007

Wu, K.C., Liu, J., Klaassen, C.D., 2012. Role of Nrf2 in preventing ethanol-induced oxidative stress and lipid accumulation. Toxicol. Appl. Pharmacol. 262, 321–329.

https://doi.org/10.1016/J.TAAP.2012.05.010

Xie, F., Wang, J., Zhang, B., 2023. RefFinder: a web-based tool for comprehensively analyzing and identifying reference genes. Funct. Integr. Genomics 23. https://doi.org/10.1007/S10142-023-01055-7

Xie, F., Xiao, P., Chen, D., Xu, L., Zhang, B., 2012. miRDeepFinder: A miRNA analysis tool for deep sequencing of plant small RNAs. Plant Mol. Biol. 80, 75–84. https://doi.org/10.1007/s11103-012-9885-2

Xue, L., Xu, F., Meng, L., Wei, S., Wang, J., Hao, P., Bian, Y., Zhang, Y., Chen, Y., 2012. Acetylation-dependent regulation of mitochondrial ALDH2 activation by SIRT3 mediates acute ethanol-induced eNOS activation. FEBS Lett. 586, 137–142. https://doi.org/10.1016/J.FEBSLET.2011.11.031

Yabuki, M., Scott, D.J., Briand, L., Taylor, A.J., 2011. Dynamics of odorant binding to thin aqueous films of rat-OBP3. Chem. Senses 36, 659–671. https://doi.org/10.1093/chemse/bjr037

Yamaguchi, M.S., McCartney, M.M., Linderholm, A.L., Ebeler, S.E., Schivo, M., Davis, C.E., 2018. Headspace sorptive extraction-gas chromatography-mass spectrometry method to measure volatile emissions from human airway cell cultures. J. Chromatogr. B. Analyt. Technol. Biomed. Life Sci. 1090, 36–42. https://doi.org/10.1016/J.JCHROMB.2018.05.009

Yang, S., Jan, Y.H., Mishin, V., Heck, D.E., Laskin, D.L., Laskin, J.D., 2017. Diacetyl/ l -Xylulose Reductase Mediates Chemical Redox Cycling in Lung Epithelial Cells. Chem. Res. Toxicol. 30, 1406–1418. https://doi.org/10.1021/ACS.CHEMRESTOX.7B00052/ASSET/IMAGES/MEDIUM/TX-2017-00052V_0011.GIF

Yaqub, N., Wayne, G., Birchall, M., Song, W., 2022. Recent advances in human respiratory epithelium models for drug discovery. Biotechnol. Adv. 54, 107832. https://doi.org/10.1016/j.biotechadv.2021.107832

Yin, Z.-L., Dahlstrom, J.E., Le Couteur, D.G., Board, P.G., 2001. Immunohistochemistry of Omega Class Glutathione S-Transferase in Human Tissues. J. Histochem. Cytochem. 49, 983–987.

Young, J.M., Kambere, M., Trask, B.J., Lane, R.P., 2005. Divergent V1R repertoires in five species: Amplification in rodents, decimation in primates, and a surprisingly small repertoire in dogs. Genome Res. 15, 231–240. https://doi.org/10.1101/gr.3339905

Yousem, D.M., Geckle, R.J., Bilker, W.B., McKeown, D.A., Doty, R.L., 1996. Posttraumatic olfactory dysfunction: MR and clinical evaluation. Am. J. Neuroradiol. 17, 1171–1179.

Zaccone, E.J., Goldsmith, W.T., Shimko, M.J., Wells, J.R., Schwegler-Berry, D., Willard, P.A., Case, S.L., Thompson, J.A., Fedan, J.S., 2015. Diacetyl and 2,3-pentanedione exposure of human cultured airway epithelial cells: Ion transport effects and metabolism of butter flavoring agents. Toxicol. Appl. Pharmacol. 289, 542–549. https://doi.org/10.1016/j.taap.2015.10.004

Zaccone, E.J., Thompson, J.A., Ponnoth, D.S., Cumpston, A.M., Goldsmith, W.T., Jackson, M.C., Kashon, M.L., Frazer, D.G., Hubbs, A.F., Shimko, M.J., Fedan, J.S., 2013. Popcorn flavoring effects on reactivity of rat airways in vivo and in vitro. J. Toxicol. Environ. Health. A 76, 669. https://doi.org/10.1080/15287394.2013.796302

Zhang, Y.-K., Wang, Y.-J., Gupta, P., Chen, Z.-S., 2015. Multidrug Resistance Proteins (MRPs)

and Cancer Therapy. AAPS J. 17, 802–812. https://doi.org/10.1208/s12248-015-9757-1

Zhao, B., Xie, G., Li, R., Chen, Q., Zhang, X., 2015. Dexamethasone protects normal human liver cells from apoptosis induced by tumor necrosis factor-related apoptosis-inducing ligand by upregulating the expression of P-glycoproteins. Mol. Med. Rep. 12, 8093–8100.

Zhao, K., Scherer, P.W., Hajiloo, S.A., Dalton, P., 2004. Effect of anatomy on human nasal air flow and odorant transport patterns: implications for olfaction. Chem. Senses 29, 365–379. https://doi.org/10.1093/chemse/bjh033

Zilz, T.R., Griffiths, H.R., Coleman, M.D., 2007. Apoptotic and necrotic effects of hexanedione derivatives on the human neuroblastoma line SK-N-SH. Toxicology 231, 210–214. https://doi.org/10.1016/J.TOX.2006.12.002

Zjacic, N., Scholz, M., 2022. The role of food odor in invertebrate foraging. Genes. Brain. Behav. 21, e12793. https://doi.org/10.1111/gbb.12793

Zucker, S.D., Goessling, W., Ransil, B.J., Gollan, J.L., 1995. Influence of glutathione S-transferase B (ligandin) on the intermembrane transfer of bilirubin. Implications for the intracellular transport of nonsubstrate ligands in hepatocytes. J. Clin. Invest. 96, 1927–1935. https://doi.org/10.1172/JCI118238

RÉSUMÉ EN FRANÇAIS

Introduction

Physiologie de l'olfaction

Le nez est l'organe de l'odorat. C'est dans la cavité nasale cachée derrière les narines que se trouve le tissu sensible aux signaux olfactifs. L'épithélium olfactif contenant les neurones olfactifs se situe chez l'humain au fond de la cavité nasale, en dessous de l'os ethmoïde (aussi appelé lame criblée). Chez le rat, l'os ethmoïde forme des circonvolutions complexes appelées volutes ethmoïdales, majoritairement recouvertes par l'épithélium olfactif qui en conséquence tapisse environ 50 % de la cavité nasale du rat. En comparaison, seulement 3 % de la cavité nasale humaine est recouverte d'épithélium olfactif, le reste étant en grande majorité de l'épithélium nasal respiratoire. Les neurones olfactifs dits bipolaires ont la particularité d'être en contact à la fois avec le mucus qui tapisse l'ensemble de la muqueuse nasale, et avec les cellules mitrales du bulbe olfactif, la première structure cérébrale participant au traitement du signal olfactif conduit par les neurones olfactifs. Dans le mucus, les neurones olfactifs projettent leurs dendrites appelées cils olfactifs, qui portent les récepteurs olfactifs. Lorsque ces récepteurs sont stimulés par les molécules odorantes, une cascade de signalisation intracellulaire engendre un potentiel d'action dans le neurone olfactif. Le signal est alors transmis via l'axone des neurones olfactifs jusque dans le bulbe olfactif, puis vers d'autres régions du cerveau afin d'être intégré. Le cerveau peut discriminer les molécules olfactives en fonction des combinaisons de récepteurs olfactifs que l'odorant active : c'est le code combinatoire. L'humain possède dans son génome 380 à 400 gènes codant pour des récepteurs olfactifs ; le rat en possède environ 1430, soit presque 4 fois plus. A proximité des récepteurs olfactifs, dans les neurones, le mucus mais aussi dans les cellules de soutien qui entourent les neurones olfactifs, se trouvent des protéines ayant la capacité d'influer sur la disponibilité des molécules odorantes pour les récepteurs. On appelle cela les événements péri-récepteurs, qui agissent sur la disponibilité du signal olfactif. Parmi ces protéines sont retrouvées les protéines liant les odorants (Odorant Binding Proteins, OBP), et les enzymes du métabolisme des xénobiotiques (EMX). Ces dernières sont l'objet d'étude de ces travaux de thèse.

Les enzymes du métabolisme des xénobiotiques

La présence des EMX n'est pas restreinte au tissu nasal, on les trouve dans presque tous les tissus du corps. Parmi la diversité de leurs fonctions, leur rôle de détoxification est celui sur lequel cette thèse s'articule. La détoxification a pour but de rendre les composés xénobiotiques, généralement hydrophobes, plus hydrophiles afin de les éliminer facilement par la suite, par exemple dans les urines ou les selles. Dans le foie, elles sont très connues pour ce rôle, et elles sont classées en deux catégories : les enzymes de phase I et les enzymes de phase II. Les enzymes de phase I vont fonctionnaliser les xénobiotiques, c'est-à-dire les rendre capables de réagir avec d'autres composés, en ajoutant ou démasquant des groupements électrophiles ou nucléophiles (par exemple un groupement alcool -OH). Parfois, l'action des enzymes de phase I va rendre le composé xénobiotique actif. Par exemple l'acétaminophène (plus connu sous le nom de paracétamol en France), n'est pas le principe actif à proprement parler : c'est le métabolite para-aminophénol qui possède des propriétés analgésiques et antipyrétiques. Cependant, en cas de surdose, certaines enzymes de phase I appelées cytochromes P450 (CYP), convertissent l'acétaminophène en N-acétyl-p-benzoquinone (NAPQI) qui est très toxique pour le foie. Les enzymes de phase II vont conjuguer à ces groupes de gros composés hydrophiles (par exemple, le glutathion), ce qui va rendre le xénobiotique très hydrophile tout en inactivant sa potentielle activité. Une troisième phase de transport en dehors des cellules complète l'action des EMX, car les métabolites hydrophiles ne peuvent plus retraverser la membrane cellulaire pour être évacués de l'organisme.

Dans le tissu nasal, les EMX ont aussi un rôle de détoxification qui va protéger la muqueuse nasale, et particulièrement la muqueuse olfactive, des xénobiotiques volatiles transportés dans l'air. Cependant, les molécules odorantes sont aussi des xénobiotiques volatiles, et sont donc impactées par l'activité enzymatique des EMX avant même d'atteindre les récepteurs olfactifs. Dans le cadre des événements périrécepteurs, on attribue à ce jour 2 rôles principaux aux EMX :

(1) En dégradant les odorants, les EMX nasales permettent au tissu nasal d'évacuer au fur et à mesure les molécules odorantes pour laisser la place à de nouvelles molécules odorantes, qui pourront à leur tour interagir avec les récepteurs

olfactifs. Par exemple, les métabolites glucurono-conjugués ou glutathion-conjugués perdent leur capacité à induire un signal olfactif. C'est le cas de la phéromone mammaire qui est inactivée par conjugaison avec le glutathion par les glutathiontransférases (GST) du mucus nasal des lapereaux. Ainsi, il a été montré qu'après un simple lavage nasal enlevant temporairement une partie du mucus nasal, le seuil de perception des lapereaux pour la phéromone mammaire diminue. En d'autres termes, ils détectent la molécule à de plus faibles concentrations car la dégradation de la phéromone est temporairement inhibée, elle s'accumule et active plus de récepteurs.

(2) Les EMX nasales peuvent aussi produire des métabolites qui possèdent des propriétés olfactives. Par exemple le 2-furfurylthiol est décrit comme ayant une forte odeur de café brûlé et d'ail. Pourtant, une étude récente a montré que c'est le métabolite furfurylméthylsulfide qui sent l'ail. L'odeur de café brûlé et d'ail vient donc de la détection conjointe par les récepteurs olfactifs du 2-furfurylthiol originellement inhalé et du furfurylméthylsulfide métabolisé *in situ*.

Ces enzymes peuvent être sujettes à des mécanismes d'inhibition par compétition : la compétition entre odorants pour une même enzyme peut modifier leur métabolisme. Ainsi, un compétiteur empêchant la dégradation d'un odorant peut modifier son seuil de perception, comme cela a été montré pour la 2,3-pentanedione. Cet odorant entre en compétition avec l'acide butyrique pour une enzyme appelée Dicarbonyl and L-Xylulose Réductase (DCXR). En présence d'acide butyrique, pour lequel la DCXR a plus d'affinité, le seuil de détection de la 2,3-pentanedione diminue.

Objectifs des travaux de thèse

Le but de ce travail de thèse est de caractériser l'expression, la régulation et la fonction des EMX nasales par le biais de modèles innovants.

Jusqu'à présent, l'étude des événements périrécepteurs a été permise grâce à l'utilisation de modèles animaux vivants, ou d'explants de tissus olfactifs de ces animaux. Certaines expériences autorisent leur réalisation sur des sujets humains volontaires ou sur des biopsies de tissus humains. Néanmoins les lois éthiques limitent la portée de ces expériences humaines *in vivo* et les biopsies humaines sont

relativement précieuses comparées à la disponibilité des tissus olfactifs d'origine animale. Récemment, le développement de modèles tissulaires humains *in vitro* connait un bond tant par leur nouveauté que par les utilisations qu'ils permettent. D'origine humaine, ces modèles tissulaires ont pour but de mieux refléter la biologie humaine ; et de par leur nature *in vitro*, ils permettent l'usage et l'étude de composés interdits pour l'usage *in vivo* chez l'humain.

Dans ce travail de thèse, le choix a été fait de se détacher progressivement du modèle animal pour favoriser un modèle alternatif reproduisant la structure et les types cellulaires de la muqueuse respiratoire humaine. Dans un premier temps, la régulation des EMX exprimées dans la muqueuse olfactive de rat a été explorée via l'utilisation d'explants prélevés immédiatement après la mise à mort des rongeurs. Bien que ce modèle soit très bien connu et déjà utilisé pour étudier le métabolisme des odorants au sein de l'équipe du Pr. Jean-Marie Heydel au Centre des Sciences du Goût et de l'Alimentation (CSGA, Dijon, France), il s'avère très vite limité lorsque la cible étudiée sont les ARN messagers et l'expression génique en réponse à des odorants. Dans un second temps, les EMX exprimées dans le modèle tissulaire de muqueuse respiratoire humaine développée par le Dr. Maria Steinke au sein de la Chaire d'Ingénierie Tissulaire et de Médecine Régénérative (TERM, Wurtzbourg, Allemagne) ont été caractérisées. L'étude des deux modèles a été placée dans un contexte olfactif : pour recréer un événement olfactif, les molécules odorantes ont été utilisées à des concentrations faibles et des temps d'exposition courts (environ 2 heures). Ce sont donc des événements se produisant à court terme qui ont été étudiés (que ce soit la régulation des EMX ou le métabolisme des odorants).

Partie 1 : explants de muqueuse olfactive de rat

Le début des travaux de thèse a porté sur l'étude de la régulation des EMX nasales de la muqueuse olfactive du rat en réponse à des odorants. Pour se faire, des explants de muqueuses nasales de rat Wistar ont été disséqués *post-mortem*, exposés à des odorants, puis les ARN messagers ont été isolés et analysés par RT-qPCR (reverse transcription – quantitative polymerase chain reaction). Après avoir mis au point la technique de RT-qPCR sur ce tissu particulier, plusieurs protocoles ont été testés (Figure 13). En premier lieu, j'ai utilisé des explants congelés pour leur conservation, que j'ai

décongelés avant de les exposer à des odorants et d'analyser les ARN messagers. Ces explants congelés étaient déjà utilisés au sein du CSGA pour étudier le métabolisme des odorants, les EMX étant protégées et conservées par l'étape de congélation. J'ai essayé plusieurs protocoles pour décongeler ces explants et les incuber avec des odorants, tout en vérifiant au passage que cette étape n'endommageait pas les ARN messagers au sein du tissu olfactif. J'ai pu observer que l'étape de décongélation n'induisait pas de dégradation des ARN messagers, en observant notamment l'évolution de certains facteurs en différents points d'une cinétique de décongélation :

- Le RIN (RNA Integrity Number), allant de 1 à 10, 10 étant la meilleure qualité d'ARN, varie entre 6 et 7,5 entre 0 et 4 heures de décongélation, ce qui est acceptable pour effectuer par la suite des RT-qPCR.

- Le fold-change de HAF (Hypoxia-Associated Factor) a été décrit dans la littérature comme diminuant entre 0 et 4 heures post mortem, ce qui semble être le cas dans les explants olfactifs de rat.

- BCL-2 (B cell lymphoma 2, un facteur anti-apoptotique) et BAX (BCL-2 associated protein X, un facteur pro-apoptotique) ont des effets antagonistes et régulent les processus d'apoptose. Aucune variation notable dans leur expression génique n'a pu être démontrée lors de la cinétique de décongélation des explants olfactifs de rat.

Les tissus ne montrant aucun signe de stress, je les ai ensuite exposés à de l'éthanol sous forme peu concentrée et volatile, dans le but de réaliser une preuve de concept : est-ce qu'un événement olfactif (molécules peu concentrée, temps d'exposition très court) entraine la régulation d'EMX métabolisant la molécule odorante ? L'éthanol est connu pour être métabolisé dans le foie par l'alcool déshydrogénase 1 (ADH1), l'aldéhyde déshydrogénase 2 (ALDH2) et CYP2E1, toutes les trois étant exprimées dans la muqueuse olfactive du rat. Les explants ont été incubés avec l'éthanol à 4 °C et à 30 °C (Figure 14), dans le but d'optimiser le protocole en testant plusieurs modalités. Dans les deux cas, aucun impact statistiquement significatif n'a pu être montré sur le fold-change d'*Adh1*, *Aldh2*, et *Cyp2E1*. Cependant l'incubation à 4 °C semble faire baisser l'expression d'*Adh1* et *Aldh2*, alors que celle à 30 °C semble l'augmenter, tandis

qu'aucun changement n'est montré pour *Cyp2E1* entre les deux températures d'incubation.

A ce moment-là, j'ai réalisé qu'utiliser des tissus préalablement congelés n'était certes pas un problème pour étudier l'activité de certaines enzymes, mais pouvait être un point limitant pour étudier l'expression de gènes. Il est possible de conserver des cellules à l'état congelé et de les raviver via des protocoles spécifiques, mais c'est autrement plus compliqué de faire de même avec des tissus entiers. J'ai donc par la suite tenté d'utiliser des explants olfactifs de rats fraîchement disséqués. Les tissus ont tout de suite été exposés à un mélange d'odorants (éthanol et 2,3-pentanedione), en de faibles quantités volatiles ayant pour but d'imiter une perception olfactive. Les ARN messagers ont été extraits en 4 points d'une cinétique entre 30 minutes et 2 heures, afin d'étudier une potentielle réponse précoce des gènes d'EMX en réponse à un stimulus olfactif.

Malheureusement ces tissus frais se sont révélés beaucoup plus fragiles que leurs homologues congelés : exposés ou non à des odorants, au bout de deux heures la majorité des ARN messagers étaient détruits (Figures 15). La Figure 16 montre les résultats qui ont pu être obtenus :

- *Cyp2E1* semble augmenter dans le temps entre 30 minutes et 2 heures, ce qui pourrait ressembler à la réponse d'une EMX à un stimulus toxique devant être éliminé.

- *Adh1* et *Aldh2* semblent répondre au stimulus odorant le plus fortement après 1 heure 30 d'incubation, néanmoins ces résultats montrent énormément de variabilité et sont les plus difficiles à interpréter.

- Enfin, le marqueur précoce d'activité neuronale *c-fos* a aussi été investigué. *C-fos* semble répondre au stimulus odorant le plus fortement après 1 heure d'incubation. Les explants « frais » ayant déjà été utilisés pour réaliser des électro-olfactogrammes dans d'autres études, il semble cohérent qu'un marqueur d'activité neuronal réponde à un stimulus olfactif.

Néanmoins, l'état de dégradation avancée des ARN messagers incite à prendre ces résultats avec beaucoup de précaution. L'usage d'un modèle animal vivant à ce stade

semblait être la seule solution pour pallier à cette dégradation, néanmoins, j'ai choisi de prendre le risque de transitionner vers un modèle *in vitro* d'épithélium respiratoire humain, et de continuer l'étude des EMX dans ce modèle dans le laboratoire du TERM. La poursuite des travaux chez le rat est toujours une possibilité au sein du CSGA, d'autant plus que ce modèle est bien établi. D'un autre côté, l'opportunité de transférer les connaissances acquises sur les EMX chez le rat à un modèle issu de l'ingénierie tissulaire humaine était une occasion unique rendue possible grâce à la collaboration internationale qu'était le consortium NAOMI (Nasal Odorant Metabolites). L'étude de la contribution des EMX de la muqueuse nasale respiratoire humaine dans l'olfaction est notamment intéressante car ce tissu constitue presque 97 % de la muqueuse nasale, or cela n'avait jusqu'alors pas été investigué. C'est donc sur ce second modèle que la suite de mes travaux s'est portée.

Partie 2 : modèles tissulaires de la muqueuse respiratoire humaine

Le modèle tissulaire de muqueuse respiratoire humaine est construit à partir de cellules épithéliales nasales et de fibroblastes isolés à partir de biopsies nasales humaines, que des chirurgiens otorhinolaryngologistes transmettent au laboratoire avec le consentement des patients. Les cellules sont ensemencées sur une matrice extracellulaire (de la sous-muqueuse décellularisée d'intestin grêle de porc) tendue comme un tambour entre deux petites couronnes emboitées d'environ 1,5 cm de diamètre. La Figure 17 montre que le modèle reproduit la structure d'une muqueuse respiratoire, avec en surface un épithélium différencié constitué de cellules ciliées et de cellules sécrétrices du mucus, ainsi que des cellules basales (cellules souches de l'épithélium) vers le pôle basal de l'épithélium. L'épithélium repose sur la matrice extracellulaire colonisée et entretenue par les fibroblastes.

Avant de pouvoir utiliser le modèle tissulaire de muqueuse respiratoire humaine dans un contexte olfactif, il a été nécessaire de caractériser le modèle. Exprime-t-il les enzymes que je souhaite étudier ? Pour répondre à cette question, je me suis servie d'un jeu de données de single-cell RNA sequencing (scRNA-seq) obtenues à partir du modèle par ma collègue Dr. Rinu Sivarajan pour son propre projet : la Figure 18 montre les différents types cellulaires identifiés grâce à ses données. Parmi les gènes exprimés par le modèle se trouvent 71 isoformes d'EMX de phase I et II, ainsi que 8 transporteurs

d'efflux (Figure 19 et Tableau 9). L'expression de certaines EMX a été ensuite confirmée par RT-qPCR : DCXR, ALDH1A1 et ALDH3A1 pour les enzymes de phase I (Figure 20), ainsi que GSTA1, GSTP1, et GSTO (GSTO1 et GSTO2 ont été investigués) pour les enzymes de phase II (Figure 21). Les données de scRNA-seq ont aussi permis de visualiser l'expression de ces isoformes au sein des populations cellulaires identifiées (Figures 22 et 23). Cependant l'expression d'un gène n'est pas toujours corrélée avec la présence de la protéine qu'il code, c'est pourquoi j'ai vérifié leur présence au niveau protéique dans le modèle grâce à l'immunofluorescence (Figures 24 à 30). Dans l'ensemble ces résultats montrent que ces isoformes sont bien présentes au niveau protéique dans le modèle, et confirme ce qui avait déjà été observé *in vivo*.

Les EMX sont donc présentes dans le modèle tissulaire de la muqueuse respiratoire humaine, mais sont-elles fonctionnelles et peuvent-elles métaboliser les odorants ? Pour répondre à cette question, il a fallu trouver un moyen d'observer l'activité enzymatique des EMX du modèle envers des substrats odorants. Pour cela, dans le cadre du consortium NAOMI, j'ai effectué un partenariat avec Nicole Kornbausch, doctorante du Dr. Helene Loos dans la chaire de recherche sur les arômes et sur l'odeur d'Erlangen (Chair of Aroma and Smell Research), dirigée par le Pr. Andrea Büttner. Nicole avait déjà travaillé sur un protocole permettant de mesurer le métabolisme des odorants par des homogénats de tissus olfactifs de rat, en partenariat avec le CSGA. Nous avons donc adapté le protocole pour mesurer la même chose avec des homogénats de modèles tissulaires ; nous avons pu détecter des métabolites lorsque les homogénats sont mis en contact avec des odorants. Plus particulièrement, l'odorant 3,4-hexanedione donne le métabolite 4-hydroxy-3-hexanone (Figure 35), et l'odorant benzaldéhyde donne deux métabolites : l'alcool benzylique et l'acide benzoïque (Figure 36). L'implication des EMX dans ces réactions a été montrée grâce à différents contrôles : sans homogénat, ou lorsque l'homogénat est chauffé pour dénaturer les enzymes, il n'y a plus de métabolites formés. Lorsque le kit permettant de régénérer le NADPH est omis, la formation des métabolites est très fortement inhibée voire complètement abolie, mettant en lumière que ce sont des enzymes ayant besoin de ce cofacteur qui sont impliquées. D'autres contrôles incluant divers inhibiteurs permettent d'investiguer plus précisément les familles d'enzymes qui contribuent au métabolisme des odorants choisis. Parmi les EMX

candidates, DCXR semble être l'enzyme majoritairement impliquée dans la conversion du 3,4-hexanedione en 4-hydroxy-3-hexanone, bien que des ADH semblent être aussi impliquées. L'acide benzoïque semblerait être majoritairement un produit des ALDH, mais il semblerait qu'une partie de ce métabolite soit aussi synthétisée par des ADH, des CYP, et des aldéhydes oxydases (AOX). Quant à l'alcool benzylique, les ADH seraient majoritaires, bien que les CYP et les AOX puissent aussi participer.

Le protocole utilisant des homogénats permet de montrer la fonctionnalité de ces enzymes, mais l'intérêt du modèle tissulaire utilisé ici est qu'il présente une structure proche d'un tissu *in vivo*, avec notamment une interface air-liquide. En d'autres termes, la surface du tissu n'est séparée de l'air ambiant que par une couche de mucus que le modèle sécrète, exactement comme dans la cavité nasale. Les enzymes retrouvées dans l'homogénat peuvent métaboliser les enzymes, mais est-ce toujours le cas quand celles-ci sont dans le mucus ou à l'intérieur des cellules ? Pour évaluer cela, j'ai enfermé des modèles « vivants » dans des petites jarres hermétiques et les ai exposés à la 3,4-hexanedione pendant 2 heures. En les enfermant dans un milieu relativement petit, j'espérais concentrer les molécules volatiles dans un petit espace de tête au-dessus des modèles. Des petites barres magnétiques recouvertes de polydimethylsiloxane (PDMS), un matériau capable de piéger des molécules, et que nous appellerons « Twister », sont fixées dans le couvercle par magnétisme. Toujours en collaboration avec Nicole Kornbausch, qui a ensuite procédé à l'analyse des molécules piégées dans les Twisters, nous avons pu montrer que les modèles, en présence de 3,4-hexanedione, rejettent dans l'espace de tête le métabolite 4-hydroxy-3-hexanone (Figure 37). La muqueuse respiratoire humaine contribuerait donc aussi au métabolisme des odorants, observé jusqu'alors *ex vivo* seulement avec la muqueuse olfactive, ou *in vivo* sur l'ensemble de la cavité nasale. Ces résultats doivent être confirmés en répétant l'expérience plusieurs fois avec des modèles produits à partir d'autres donneurs, mais aussi en incluant plus de contrôles et peut être d'autres odorants.

Enfin, la question initiale sur la régulation des EMX par des odorants n'a pas été oubliée, toujours en gardant des conditions se rapprochant le plus d'un événement olfactif (molécules odorantes peu concentrées, temps d'exposition court). Deux modalités ont été tentées : une première utilisant une machine permettant de nébuliser une solution

odorante, afin d'imiter au mieux l'exposition à des aérosols (Figure 33), et une deuxième, en traitant directement la surface des modèles avec une solution odorante (Figure 34). Dans les deux cas, je n'ai pu démontrer un effet des traitements sur la régulation des gènes testés. Plus en détail, je m'attendais à ce que la 2,3-pentanedione et la 3,4-hexanedione influent l'expression de *DCXR*, et à ce que la dexaméthasone induise l'expression de *GSTP1*, mais les résultats ne sont statistiquement pas significatifs. Ni la 2,3-pentanedione, la 3,4-hexanedione, l'éthanol et la dexaméthasone n'ont impacté l'expression des seuls trois récepteurs nucléaires détectés par RT-qPCR. L'éthanol n'a aucun effet sur Nrf2, qui est pourtant connu pour réagir au stress oxydant. Il est possible que les EMX ne soient tout simplement pas régulées au niveau de l'expression de leurs gènes par un stimulus de seulement 2 heures, ou que le modèle tissulaire, bien qu'utile pour beaucoup d'autres applications, ne soit pas le bon modèle pour étudier la régulation des EMX. Enfin, il est aussi possible que la variabilité entre tous les donneurs ne permette pas d'observer de différences statistiques avec le nombre de répétitions à ma disposition : en effet, et contrairement aux rats Wistar qui sont syngéniques, les biopsies proviennent de différentes personnes de tout âge et des deux sexes, et surtout ayant des parcours de vie différents et potentiellement des traitements médicamenteux différents. Construire des modèles avec des lignées cellulaires stables pourrait peut-être permettre d'effacer ce biais.

Conclusion et perspectives

La conclusion de ces trois ans de recherche se résume en plusieurs points :

- L'explant olfactif de rat n'a pas permis d'obtenir des résultats probants sur la régulation génique dans nos conditions expérimentales. Le modèle tissulaire a l'avantage de supporter les expositions aux odorants sans que les ARNs se dégradent et de pouvoir servir pour étudier le métabolisme des odorants. Cependant la variabilité génétique introduite par les différents patients rend possiblement la lecture des résultats plus compliquée.

- Aucun des résultats obtenus n'a pu démontrer que les EMX pouvaient être régulées par leur substrat odorant, que ce soit en utilisant les explants olfactifs de rat ou le modèle tissulaire de muqueuse respiratoire humaine, dans les

conditions testées. Pour autant, cette hypothèse ne peut pas non plus être complètement écartée : les explants comme le modèle ne sont pas des tissus *in vivo*, bien qu'ils s'en rapprochent beaucoup. Il est toujours possible qu'ils ne se comportent pas de la même manière qu'un tissu *in vivo* connecté à son organisme d'origine. De plus, les conditions testées ne sont peut-être tout simplement pas celles qui induisent un changement d'expression pour ces gènes cibles.

- Enfin, il a été montré que les modèles tissulaires de muqueuse respiratoire humaine non seulement expriment des EMX, mais que les EMX sont aussi retrouvées au niveau protéique dans les différents types cellulaires du modèle et qu'elles sont fonctionnelles. Jusqu'à présent, le métabolisme des odorants a surtout été étudié dans des tissus olfactifs car c'est dans ces derniers que se trouvent les récepteurs olfactifs. Néanmoins chez l'humain une grosse majorité du tissu nasal est en contact avec le tissu respiratoire avant d'atteindre l'épithélium olfactif ; les travaux présentés dans cette thèse suggèrent que le tissu respiratoire contribue au métabolisme des odorants.

Le modèle a de l'avenir dans le milieu du métabolisme des odorants : il serait possible d'évaluer un potentiel impact d'une maladie dans le métabolisme des odorants ou dans l'expression des EMX, en utilisant des biopsies issues de patients malades pour générer des modèles et les comparer à des modèles issus de personnes saines. Ce serait envisageable pour étudier les anosmies dues à des maladies neurodégénératives telles qu'Alzheimer, dont la perte de l'odorat peut être un des premiers signes. Des modèles tissulaires d'épithélium respiratoires ont déjà été générés à partir de personnes atteintes d'Alzheimer pour étudier leur propension à être infectées par le SARS-CoV-2. Il serait tout à fait possible d'utiliser ces modèles dans un contexte olfactif, d'autant plus que le tissu respiratoire semble contribuer au métabolisme des odorants.

Lorsqu'il peut se substituer à des modèles animaux, le modèle tissulaire de muqueuse respiratoire humaine offre une alternative intéressante à l'expérimentation animale. Pour autant il n'est pas dénué de matériaux et composés issus d'animaux. La matrice extracellulaire est constituée de la sous-muqueuse décellularisée d'intestin grêle de porc, qui sont élevés et abattus pour l'expérimentation animale. Le milieu de culture des

cellules contient du sérum de veau fœtal, et les anticorps utilisés en histologie proviennent d'animaux. Néanmoins des solutions se présentent à court terme pour remplacer ces composants : le TERM transitionne vers l'utilisation d'une matrice synthétique pour remplacer l'intestin de porc. Le protocole doit être adapté car les fibroblastes doivent coloniser la matrice et produire le collagène nécessaire, mais jusqu'à présent les modèles construits sont prometteurs. Des milieux de culture sans sérum de veau fœtal voient le jour, et il est possible de produire des anticorps recombinants par ingénierie. Ces transitions sont notamment encouragées par le PETA Science Consortium International à travers des bourses, et devraient rendre l'accès à des modèles alternatifs et basés sur la biologie humaine plus attractifs auprès des jeunes chercheurs.